

# Development of Electrodes for the NASA Iron/Chromium Redox System and Factors Affecting Their Performance

(NASA-CR-174724) DEVELOPMENT OF ELECTRODES  
FOR THE NASA IRON/CHROMIUM Final Report  
(Giner, Inc., Waltham, Mass.) 285 p  
HC A13/MF A51

N85-35471

CSSL 10A

Unclas  
22268

33/44

Larry Swette and Vinod Jalan  
GINER, INC.

June 1984



Prepared for  
NATIONAL AERONAUTICS AND SPACE ADMINISTRATION  
Lewis Research Center  
Under Contract DEN 3-262

for  
**U.S. DEPARTMENT OF ENERGY**  
**Conservation and Renewable Energy**  
**Division of Energy Storage Systems**

DOE/NASA/0262-1  
NASA CR-174724

**Development of Electrodes for the  
NASA Iron/Chromium Redox  
System and Factors Affecting  
Their Performance**

Larry Swette and Vinod Jalan  
GINER, INC.  
Waltham, Massachusetts 02154

June 1984

Prepared for  
NATIONAL AERONAUTICS AND SPACE ADMINISTRATION  
Lewis Research Center  
Cleveland, Ohio 44135  
Under Contract DEN 3-262

for  
U.S. DEPARTMENT OF ENERGY  
Conservation and Renewable Energy  
Division of Energy Storage Systems  
Washington, D.C. 20545  
Under Interagency Agreement DE-AI04-80AL12726

CONTENTS —

	Page .....
I. INTRODUCTION AND SUMMARY	1
II. ELECTROCHEMICAL TESTING PROCEDURES	12
A. Electrode Mounting Procedures	12
B. Electrochemical Test Cell	13
C. Corrections for Resistance	13
D. Testing Procedures	14
E. Data Reduction Methods	17
III. GOLD CATALYZATION METHODS	27
A. Double Immersion Process	27
B. Standard NASA Process (NASA-1)	29
C. Modified NASA Process (NASA-11)	30
IV. CARBON FELT PROCESSING FACTORS	32
A. Sample Descriptions	32
B. Experimental Procedures	32
C. Results	34
D. Conclusions and Recommendations	36
V. OPTIMIZATION OF GOLD CATALYZATION	66
A. Effects of Process Variations	66
B. Controlled Variations of Catalyzing Procedures	99
C. Effects of Pre-Catalyzation State and Catalyzation Temperature	104
D. Reproducibility of Electrochemical Performance	117
E. Study of Lead Distribution on Electrode	126
F. Conclusions and Recommendations	156
VI. EFFECTS OF REACTANT CROSS-MIXING	158
A. Effects of $Fe^{2+}$ in Negative Electrode Solution	158
B. Effects of $Cr^{3+}$ in Positive Electrode Solution	160
VII. EFFECTS OF ACIDITY LEVEL ON Fe/Cr REDOX REACTIONS	172
A. Acidity Level Effects on the Positive Electrode Solution	172
B. Acidity Level Effects on the Negative Electrode Solution	174
VIII. TEMPERATURE DEPENDENCE	179
A. Positive Electrode Studies	179
B. Negative Electrode Studies	182
IX. PERFORMANCE IN SYSTEMS HARDWARE	189

	Page
X. REFERENCES.....	197
APPENDIX I - Carbon Felt Processing Factors.....	199
APPENDIX II - Effect of Process Variations on Gold Catalyzation	203
APPENDIX III - Controlled Variations of Catalyzing Procedure	210
APPENDIX IV - Effects of Pre-Catalyzation State and Catalyzation Temperature	217
APPENDIX V - Reproducibility of Electrochemical Performance	226
APPENDIX VI - Study of Lead Distribution on Electrodes	227
APPENDIX VII - Effects of Acidity Level	230
APPENDIX VIII - Temperature Dependence	245

LIST OF TABLES

<u>Number</u>	<u>Title</u>	<u>Page</u>
<b>SECTION IV. CARBON FELT PROCESSING FACTORS</b>		
I.	Phase I Characterization Study - Unscoured Felts: Carbon Felt Thickness Measurements	40
II.	Phase I Characterization Study - Scoured Felts: Weight and Thickness Measurements of 49 cm <sup>2</sup> Samples	41
III.	Phase II Characterization Study: Weight and Thickness Measurements of 49 cm <sup>2</sup> Samples	42
IV.	Phase I Characterization Study (Unscoured Felts): Compari- son of Quantities of Reactants Reduced or Oxidized to Quantities of Reactants Theoretically Available	43
V.	Phase I Characterization Study (Scoured Felts): Comparison of Quantities of Reactants Reduced or Oxidized to Quantities of Reactants Theoretically Available	44
VI.	Phase I Characterization Study (Scoured Felts): Comparison of Peak and Trailing Cr <sup>2+</sup> Oxidation Charges	45
VII.	NASA-I versus NASA-II Catalyzation Methods: Comparison of Quantities of Reactants Reduced or Oxidized to Quantities of Reactants Theoretically Available	50
VIII.	NASA-I versus NASA-II Catalyzation Methods: Comparison of Peak and Trailing Cr <sup>2+</sup> Oxidation Charges	51
IX.	Phase II Characterization Study: Comparison of Quantities of Reactants Theoretically Available	60
<b>SECTION V. OPTIMIZATION OF GOLD CATALYZATION</b>		
X.	Phase II Characterization Study: Comparison of Peak and Trailing Cr <sup>2+</sup> Oxidation Charges	61
XI.	Catalyzation Parameter Variation: Comparison of Quantities of Reactants Reduced or Oxidized to Quantities of Reactants Theoretically Available	103
XII.	Catalyzation Optimization Study: Comparison of Quantities of Reactants Reduced or Oxidized to Quantities of Reactants Theoretically Available	112
XIII.	Reproducibility Study: Summary of Quantities of Reactants Reduced or Oxidized and Quantities of Reactants Theoretically Available	122

List of Tables (con't)

XIV.	Reproducibility Study: Summary of Charge Segments and Ratios	124
XV.	Charges Recorded for Pb Oxidation and $Pb^{2+}$ Reduction (Integrated Peak Areas)	136

**SECTION VII. EFFECTS OF ACIDITY LEVEL ON Fe/Cr REDOX REACTIONS**

XVI.	Peak Separation for $Fe^{3+}/Fe^{2+}$ Redox Reaction as a Function of HCl Concentration	177
XVII.	$Fe^{3+}$ Reduction and $Fe^{2+}$ Oxidation Charges as a Function of HCl Concentration	178

**APPENDICES**

AI-I.	Phase I Characterization Study (Unscoured Felts): Summary of Electrochemical Features versus Felt Processing Temp.	199
AI-II.	Phase I Characterization Study (Scoured Felts): Summary of Electrochemical Features versus Felt Processing Temp.	200
AI-III.	NASA-I versus NASA-II. Catalyzation Methods: Summary of Electrochemical Features versus Felt Processing Temp.	201
AI-IV.	Phase II Characterization Study: Summary of Selected Current-Data Points	202
AIII-1.	Catalyzation Parameter Variation: Summary of Selected Current-Data Points	210
AIV-1.	Catalyzation Optimization Study: Summary of Selected Current-Data Points	217
AV-1.	Reproducibility Study: Summary of Selected Current-Data Points	226

## LIST OF FIGURES

Figure No.	Title	Page
<b>SECTION II. ELECTROCHEMICAL TESTING PROCEDURES</b>		
1.	Waxed Clip Electrode Holder; Waxing Procedure	22
2.	Cell Configuration with Waxed Clip Holder	23
3.	Representative Voltammogram Showing $Pb^{2+}/Pb$ Data Points Summarized in Tables	24
4.	Representative Voltammogram Showing $Cr^{3+}/Cr^{2+}$ Data Points Summarized in Tables	25
5.	Definition of Anodic and Cathodic Charge Segments	26
<b>SECTION IV. CARBON FELT PROCESSING FACTORS</b>		
6.	Cutting Plan for Phase I Carbon Felt	37
7.	Total Anodic Chromium Charge versus Felt Processing Temp.	38
8.	Ratio $Q_aCr^{2+}/Q_cH^+$ Versus Felt Processing Temperature	39
9.	$H^+$ Reduction Charge ( $Q_cH^+$ ) versus Felt Processing Temp.	46
10.	Lead Loading as Measured by the Anodic Lead Charge ( $Q_aPb$ ) versus Felt Processing Temperature	47
10a.	Total Anodic Chromium Charge versus Felt Processing Temp.	48
11.	Ratio $Q_aCr^{2+}/Q_cH^+$ versus Felt Processing Temperature	49
12.	$H^+$ Reduction Charge ( $Q_cH^+$ ) versus Felt Processing Temp.	52
13.	Lead Loading as Measured by the Anodic Lead Charge ( $Q_aPb$ ) versus Felt Processing Temperature	53
14.	Total Anodic Chromium Charge versus Felt Processing Temp.	54
15.	Ratio $Q_aCr^{2+}/Q_cH^+$ versus Felt Processing Temperature	55
16.	$H^+$ Reduction Charge ( $Q_cH^+$ ) on Pb/Au versus Felt Processing Temperature	56
17.	Lead Loading as Measured by the Anodic Lead Charge ( $Q_aPb$ ) versus Felt Processing Temperature	57
18.	Total Anodic Chromium Charge versus Felt Processing Temp.	58
19.	Ratio $Q_aCr^{2+}/Q_cH^+$ versus Felt Processing Temperature	59

List of Figures (con't)

20.	H <sup>+</sup> Reduction Charge ( $Q_C H^+$ ) on Pb/Au versus Felt Processing Temperature	62
21.	Lead Loading as Measured by the Anodic Lead Charge ( $Q_a Pb$ ) versus Felt Processing Temperature	63
22.	Total Anodic Chromium Charge versus Felt Processing Temp.	64
23.	Negative Electrode Charging Efficiency versus Felt Processing Temperature; Phase I and Phase II Tests	65

**SECTION V. OPTIMIZATION OF GOLD CATALYZATION**

24.	H <sup>+</sup> Reduction Charge ( $Q_C H^+$ ) versus Felt Processing Temp.	75
25.	Lead Loading as Measured by the Anodic Lead Charge ( $Q_a Pb$ ) versus Felt Processing Temperature	76
26.	Percentage of Available Lead Deposited versus Felt Processing Temperature	77
27.	Total Anodic Chromium Charge versus Felt Processing Temp.	78
28.	Fraction of Available Chromic Ion Reduced (%) versus Felt Processing Temperature	79
29.	Quantity of Cr <sup>2+</sup> Oxidized as a Fraction of Available Cr <sup>3+</sup> (%) versus Felt Processing Temperature	80
30.	Ratio of Anodic Chromium Charge (Peak) to Anodic Chromium Charge (Trailing) versus Felt Processing Temperature	81
31.	$Q_a Cr^{2+}/Q_C Cr^{3+}$ (%) versus Felt Processing Temperature	82
32.	Total Anodic Chromium versus Anodic Lead Charge	83
33.	Ratio of Chromium Charge to Anodic Lead Charge versus Felt Processing Temperature	84
34.	Ratio $Q_a Cr^{2+}/Q_C H^+$ versus Felt Processing Temperature	85
35.	H <sup>+</sup> Reduction Current at -950 mV on Pb/Au in HCl versus Felt Processing Temperature	86
36.	H <sup>+</sup> Reduction Charge ( $Q_C H^+$ ) on Pb/Au versus Felt Processing Temperature	87
37.	Lead Loading as Measured by the Anodic Lead Charge ( $Q_a Pb$ ) versus Felt Processing Temperature	88
38.	Percentage of Available Lead Deposited versus Felt Processing Temperature	89

List of Figures (con't)

39.	Total Anodic Chromium Charge versus Felt Processing Temp.	90
40.	Cathodic Chromium Charge versus Felt Processing Temperature	91
41.	Fraction of Available Chromic Ion Reduced versus Felt Processing Temperature	92
42.	Quantity of $\text{Cr}^{2+}$ Oxidized as a Fraction of Available $\text{Cr}^{3+}$ (%) versus Felt Processing Temperature	93
43.	$Q_a\text{Cr}^{2+}/Q_c\text{Cr}^{3+}$ (%) versus Felt Processing Temperature	94
44.	Ratio of Anodic Chromium Charge (Peak) to Anodic Chromium Charge (Trailing) versus Felt Processing Temperature	95
45.	Total Anodic Chromium Charge versus Anodic Lead Charge	96
46.	Ratio of Anodic Chromium Charge to Anodic lead Charge versus Felt Processing Temperature	97
47. ---	Ratio $Q_a\text{Cr}^{2+}/Q_c\text{H}^+$ versus Felt Processing Temperature	98.
48.	Total Anodic Chromium Charge versus Anodic Lead Charge (Catalyzation Optimization Study)	113
49.	Anodic Charge versus Test Temperature and Precatalyzation Felt pH	114
50.	Relative Hydrogen Evolution Rate versus Test Temperature and Precatalyzation Felt pH	115
51.	$\text{Cr}^{2+}$ Oxidation Charge versus Pb Loading (Pb Oxidation Charge) at $25^\circ\text{C}$	116
52.	Comparison of Reproducibility Study Data Points to Previous Test Data; $\text{Cr}^{2+}$ Oxidation Charge versus Felt Processing Temperature	123
53.	Comparison of Reproducibility Study Data Points to Previous Data: Charging Efficiency versus Felt Processing Temp.	125
54.	Steady-State Pb/Pb $^{2+}$ Voltammogram before Removal and Drying of Electrode (pH7 Felt; Control Sample)	134
55.	Steady-State Pb/Pb $^{2+}$ Voltammogram before Removal and Drying of Electrode (pH7 Felt; SEM Sample)	135
56.	Pb/Pb $^{2+}$ Voltammograms after 5 minute Hold at -950 mV versus SCE (pH7 Felt)	137
57.	Steady-State Pb/Pb $^{2+}$ Voltammogram after 5 Minute Hold at -950 mV versus SCE (pH7 Felt)	138

List of Figures (con't)

58.	Pb/Pb <sup>2+</sup> Voltammograms Immediately After Reimmersion of Dried Electrode (pH5 Felt)	139
59.	Pb/Pb <sup>2+</sup> Voltammogram Immediately after Reimmersion of Dried Electrode (pH7 Felt)	140
60.	Pb/Pb <sup>2+</sup> Voltammograms Immediately after Reimmersion of Dried Electrode (pH9 Felt)	141
61.	Steady-State Pb/Pb <sup>2+</sup> Voltammogram after Reimmersion of Dried Electrode (pH7 Felt)	142
62.	Voltammograms Recorded after Reimmersion of Dried Electrode in 1 N HCl with no PbCl <sub>2</sub> .	143
63.	STEM Photograph of Carbon Fiber Surface ("pH 5" Pb/Au sample) showing Gold Particles (bright spots); X6400.	144
64.	Same View as Figure 63, at 25,000X. The Particle Indicated was Identified as Gold by EDAX	144
65.	Energy Dispersive Analysis by X-ray of Particle shown in Figure 64	145
66.	STEM Photograph of Carbon Fiber Surface ("pH 7" Pb/Au sample) showing Gold Particles X25,000	146
67.	Same View as Figure 66 at 100,000X. The Large Bright Particle was Identified as Gold by EDAX	146
68.	Energy Dispersive Analysis by X-ray of Particle Shown in Figure 67	147
69.	Gold X-ray Dot Map at 25,000X Magnification of the Same Area shown in Figure 66.	148
70.	Gold X-ray Dot Map at 100,000 Magnification of the same Approximate Area shown in Figure 67. Note differentiation over Gold Particle	148
71.	STEM Photograph of Carbon Fiber Surface ("pH 5" Pb/Au sample) 3200X	149
72.	Pb X-ray Dot Map of the Carbon Fiber Surface shown in Figure 71; 3200X	149
73.	STEM Photograph of Carbon Fibers ("pH 7" Pb/Au sample) 3200X	150
74.	Pb X-ray Dot map of the Carbon Fibers shown in Figure 73 3200X	150

List of Figures (con't)

75.	STEM Photograph of Carbon Fibers ("PbCl <sub>2</sub> " No-Gold sample) 6400X	151
76.	Pb X-ray Dot Map Corresponding to Carbon Fibers in Figure 75; 6400X	151
77.	Pb X-ray Dot Map of Carbon Fiber ("PbCl <sub>2</sub> " No-Gold sample) 1600X	152
78.	STEM Photograph of the Carbon Fiber Shown in Figure 77. Note Differentiation in Dot Map Corresponding to Deposits of PbCl <sub>2</sub> in Flutes of Fiber	152
79.	Energy Dispersive Analysis by X-ray of PbCl <sub>2</sub> Deposits on Carbon Fiber shown in Figure 78	153
80.	Raw, Untreated and Uncatalyzed Carbon Fiber; STEM 25,000X	154
81.	Same Fiber Surface Shown in Figure 80; STEM 100,000X	154
82.	Uncatalyzed Carbon Fiber after Standard Pretreatment in Hot Potassium Hydroxide; STEM 25,000X	155
83.	Same Carbon Fiber as shown in Figure 82; STEM 100,000X	155

**SECTION VI. EFFECTS OF REACTANT CROSS-MIXING**

84.	Crossover Effects; Increasing Fe <sup>2+</sup> in Negative Electrode Solution (HCl, Pb <sup>2+</sup> , No Cr <sup>3+</sup> )	165
85.	Crossover Effects: Extended Cycling with 500 mM Fe <sup>2+</sup> in Negative Electrode Solution (HCl, Pb <sup>2+</sup> , No Cr <sup>3+</sup> )	166
86.	Crossover Effects; Increasing Fe <sup>2+</sup> in Negative Electrode Solution (HCl, Pb <sup>2+</sup> , 50 mM Cr <sup>3+</sup> )	167
87.	Crossover Effects: Extended Cycling with 500 mM Fe <sup>2+</sup> in Negative Electrode Solution (HCl, Pb <sup>2+</sup> , 50 mM Cr <sup>3+</sup> )	168
88.	Crossover Effects: Effect of Added Cr <sup>3+</sup> in Positive Electrode Solution, "Fe <sup>3+</sup> First"	169
89.	Crossover Effects: Extended Cycling with 500 mM Cr <sup>3+</sup> in Positive Electrode Solution, "Cr <sup>3+</sup> First"	170
90.	Crossover Effects: Extended Cycling with 500 mM Cr <sup>3+</sup> in Positive Electrode Solution, "Fe <sup>3+</sup> First"	171

**SECTION VIII. TEMPERATURE DEPENDENCE**

91.	Fe <sup>3+</sup> /Fe <sup>2+</sup> Reaction at 25°C. in 0.050M FeCl <sub>3</sub>	185
-----	--	-----

List of Figures (con't)

92.	Fe <sup>3+</sup> /Fe <sup>2+</sup> Reaction at 45°C. in 0.050M FeCl <sub>3</sub>	186
93.	Fe <sup>3+</sup> /Fe <sup>2+</sup> Reaction at 55°C. in 0.050M FeCl <sub>3</sub>	187
94.	Fe <sup>3+</sup> /Fe <sup>2+</sup> Reaction at 65°C. in 0.050M FeCl <sub>3</sub>	188

**SECTION IX. PERFORMANCE IN SYSTEM HARDWARE**

95.	1/3 Square Foot Redox Flow Cell Run #3; Initial Performance	191.
96.	1/3 Square Foot Redox Flow Cell Run #3; Performance After 200 Rapid Cycles	192
97.	Fe/Cr Redox Flow Cell; 1/3 Sq. Ft.; Run #3. Polarization	193
98.	1/3 Square Foot Redox Flow Cell Run #4; Initial Performance	194
99.	1/3 Square Foot Redox Flow Cell Run #4; Performance After 223 Rapid Cycles	19;
100.	Fe/Cr Redox Flow Cell; 1/3 Sq. Ft.; Run #4. Polarization	196

**APPENDICES**

AII-1.	Transmission Electron Micrograph of 1500°C Felt Sample Catalyzed by Double Immersion Method, 12.5 μg Au/cm <sup>2</sup> . (90,000 X Magnification; 1 mm = 11 nm).	203
AII-2.	TEM Photograph of 1500°C Felt Sample Catalyzed by NASA-I Method, 12.5 μg/Au/cm <sup>2</sup> . (90,000 X Magnification; 1 mm = 11 nm.)	204
AII-3.	TEM Photograph of 1500°C Felt Sample Catalyzed by NASA-II Method, 12.5 μg Au/cm <sup>2</sup> . (90,000 X Magnification; 1 mm = 11 nm)	205
AII-4.	TEM Photograph of 1800°C Felt Sample Catalyzed by Double Immersion-Method, 12.5 μg Au/cm <sup>2</sup> . (90,000 X Magnification; 1 mm = 11 nm)	206
AII-5.	TEM Photograph of 1800°C Felt Sample Catalyzed by NASA-I Method, 12.5 μg Au/cm <sup>2</sup> . (90,000 X Magnification; 1 mm = 11 nm)	207
AII-6.	TEM Photograph of 1800°C Felt Sample Catalyzed by NASA-II Method, 12.5 μg Au/cm <sup>2</sup> . (90,000 X Magnification; 1 mm = 11 nm)	208
AII-7.	TEM Photograph of 2300°C Felt sample Catalyzed by NASA-I Method, 12.5 μg Au/cm <sup>2</sup> . (90,000 X Magnification; 1 mm = 11 nm)	209

List of Figures (con't)

AIII-1.	Sample EVF-16; "Exact Volume", 16 Hours "Closed" Exposure	211
AIII-2.	Sample DVP-16; "Double Volume", 16 Hours "Closed" Exposure	212
AIII-3.	Sample EVA-5B; "Exact Volume", 5 Minutes "Open" Exposure	213
AIII-4.	Sample EVA 30B; "Exact Volume", 30 Minutes "Open" Exposure	214.
AIII-5.	Sample EVA-180B; "Exact Volume", 180 Minutes "Open" Exposure	215
AIII-6.	Sample EVA-180; "Exact Volume", 180 Minutes "Open" Exposure	216
AIV-1.	Gold Particles on Carbon Fiber; Precatalyzation pH of Felt was 5, Sample A. Catalyzed at 25°C by NASA-I Method	218
AIV-2.	Gold Particles on Carbon Fiber; Precatalyzation pH of Felt was 5, Sample B. Catalyzed at 25°C by NASA-I Method	219
AIV-3.	Gold Particles on Carbon Fiber; Precatalyzation pH of Felt was 9, Sample A. Catalyzed at 25°C by NASA-I Method	220
AIV-4.	Gold Particles on Carbon Fiber; Precatalyzation pH of Felt was 9, Sample B. Catalyzed at 25°C by NASA-I Method	221
AIV-5.	Gold Particles on Carbon Fiber; Precatalyzation pH of Felt was 7, Sample A. Catalyzed at 25°C by NASA-I Method	222
AIV-6.	Gold Particles on Carbon Fiber; Precatalyzation pH of Felt was 7, Sample B. Catalyzed at 25°C by NASA-I Method	223
AIV-7.	Gold Particles on Carbon Fiber; Precatalyzation pH of Felt was 7; Catalyzed at 0°C by NASA-I Method	224
AIV-8.	Gold Particles on Carbon Fiber; Precatalyzation pH of Felt was 7; Catalyzed at 50°C by NASA-I Method	225
AVI-1.	Lead Plated Sample; Gold Particles on Carbon Fiber. Catalyzed from pH 5 Felt at 25°C by NASA-I Method	227
AVI-2.	Lead Plated Sample; Gold Particles on Carbon Fiber. Catalyzed from pH 7 Felt at 25°C by NASA-I Method	228
AVI-3.	Lead Plated Sample; Gold Particles on Carbon Fiber. Catalyzed from pH 9 Felt at 25°C by NASA-I Method	229
AVII-1.	Effect of Acidity Level: Fe <sup>3+</sup> in 0.1N HCl	230
AVII-2.	Effect of Acidity Level: Fe <sup>3+</sup> in 0.5N HCl	231
AVII-3.	Effect of Acidity Level: Fe <sup>3+</sup> in 1.0N HCl	232
AVII-4.	Effect of Acidity Level: Fe <sup>3+</sup> in 2.0N HCl	233

List of Figures (con't)

AVII-5.	Effect of Acidity Level: $\text{Fe}^{3+}$ in 4.0N HCl	234
AVII-6.	Effect of Acidity Level: $\text{Fe}^{2+}$ in 0.1N HCl	235
AVII-7.	Effect of Acidity Level: $\text{Fe}^{2+}$ in 0.5N HCl	236
AVII-8.	Effect of Acidity Level: $\text{Fe}^{2+}$ in 1.0N HCl	237
AVII-9.	Effect of Acidity Level: $\text{Fe}^{2+}$ in 2.0N HCl	238
AVII-10.	Effect of Acidity Level: $\text{Fe}^{2+}$ in 4.0N HCl	239
AVII-11.	Acidity Level Effects: Electrochemical Performance in 50 mM $\text{CrCl}_3$ in 4.0N HCl (aged)	240
AVII-12.	Acidity Level Effects: Electrochemical Performance in 50 mM $\text{CrCl}_3$ in 2.0N HCl (aged)	241
AVII-13.	Acidity Level Effects: Electrochemical Performance in 50 mM $\text{CrCl}_3$ in 1.0N HCl (aged)	242
AVII-14.	Acidity Level Effects: Electrochemical Performance in 50 mM $\text{CrCl}_3$ in 0.5N HCl	243
AVII-15.	Acidity Level Effects: Electrochemical Performance in 50 mM $\text{CrCl}_3$ in 0.1N HCl (aged)	244
AVIII-1.	$\text{Fe}^{3+}/\text{Fe}^{2+}$ Reaction at 25°C in 1.0M $\text{FeCl}_3$	245
AVIII-2.	$\text{Fe}^{3+}/\text{Fe}^{2+}$ Reaction at 45°C in 1.0M $\text{FeCl}_3$	246
AVIII-3.	$\text{Fe}^{3+}/\text{Fe}^{2+}$ Reaction at 55°C in 1.0M $\text{FeCl}_3$	247
AVIII-4.	$\text{Fe}^{3+}/\text{Fe}^{2+}$ Reaction at 65°C in 1.0M $\text{FeCl}_3$	248
AVIII-5.	$\text{Fe}^{3+}/\text{Fe}^{2+}$ Reaction at 25°C in 1.5M $\text{FeCl}_3$	249
AVIII-6.	$\text{Fe}^{3+}/\text{Fe}^{2+}$ Reaction at 45°C in 1.5M $\text{FeCl}_3$	250
AVIII-7.	$\text{Fe}^{3+}/\text{Fe}^{2+}$ Reaction at 55°C in 1.5M $\text{FeCl}_3$	251
AVIII-8.	$\text{Fe}^{3+}/\text{Fe}^{2+}$ Reaction at 65°C in 1.5M $\text{FeCl}_3$	252
AVIII-9.	$\text{Fe}^{3+}/\text{Fe}^{2+}$ Reaction at 25°C in 2.0M $\text{FeCl}_3$	253
AVIII-10.	$\text{Fe}^{3+}/\text{Fe}^{2+}$ Reaction at 45°C in 2.0M $\text{FeCl}_3$	254
AVIII-11.	$\text{Fe}^{3+}/\text{Fe}^{2+}$ Reaction at 55°C in 2.0M $\text{FeCl}_3$	255
AVIII-12.	$\text{Fe}^{3+}/\text{Fe}^{2+}$ Reaction at 65°C in 2.0M $\text{FeCl}_3$	256
AVIII-13.	$\text{Cr}^{3+}/\text{Cr}^{2+}$ Reaction at 25°C in 1.0M $\text{CrCl}_3$	257

List of Figures (con't)

AVIII-14. $\text{Cr}^{3+}/\text{Cr}^{2+}$ Reaction at $45^{\circ}\text{C}$ in 1.0M $\text{CrCl}_3$	258
AVIII-15. $\text{Cr}^{3+}/\text{Cr}^{2+}$ Reaction at $55^{\circ}\text{C}$ in 1.0M $\text{CrCl}_3$	259
AVIII-16. $\text{Cr}^{3+}/\text{Cr}^{2+}$ Reaction at $65^{\circ}\text{C}$ in 1.0M $\text{CrCl}_3$	260
AVIII-17. $\text{Cr}^{3+}/\text{Cr}^{2+}$ Reaction at $25^{\circ}\text{C}$ in 1.5M $\text{CrCl}_3$	261
AVIII-18. $\text{Cr}^{3+}/\text{Cr}^{2+}$ Reaction at $45^{\circ}\text{C}$ in 1.5M $\text{CrCl}_3$	262
AVIII-19. $\text{Cr}^{3+}/\text{Cr}^{2+}$ Reaction at $55^{\circ}\text{C}$ in 1.5M $\text{CrCl}_3$	263
AVIII-20. $\text{Cr}^{3+}/\text{Cr}^{2+}$ Reaction at $65^{\circ}\text{C}$ in 1.5M $\text{CrCl}_3$	264
AVIII-21. $\text{Cr}^{3+}/\text{Cr}^{2+}$ Reaction at $25^{\circ}\text{C}$ in 2.0M $\text{CrCl}_3$	265
AVIII-22. $\text{Cr}^{3+}/\text{Cr}^{2+}$ Reaction at $45^{\circ}\text{C}$ in 2.0M $\text{CrCl}_3$	266
AVIII-23. $\text{Cr}^{3+}/\text{Cr}^{2+}$ Reaction at $55^{\circ}\text{C}$ in 2.0M $\text{CrCl}_3$	267
AVIII-24. $\text{Cr}^{3+}/\text{Cr}^{2+}$ Reaction at $65^{\circ}\text{C}$ in 2.0M $\text{CrCl}_3$	268

## I. INTRODUCTION AND SUMMARY

### A. Background

The iron/chromium redox energy storage system has the capability of providing inexpensive, reliable bulk energy storage suitable for the efficient capture of energy from intermittent sources such as solar or wind energy, and it has, with recent developments in higher temperature operation at NASA-Lewis Research Center (1), the potential for meeting the requirements of electric utility applications such as load leveling and peak shaving. All of the reactant species in the system are soluble in hydrochloric acid at practical concentrations, a feature which permits scaling of the energy section of the system independently of the power section (2). The negative electrode couple is  $\text{Cr}^{3+}/\text{Cr}^{2+}$  and the positive electrode couple is  $\text{Fe}^{3+}/\text{Fe}^{2+}$ ; both couples are in the form of chlorides dissolved in hydrochloric acid. The electrochemical conversion reactions take place on inert carbon felts. The solutions may be separated by an ion-selective membrane, which permits charge transfer with little cross-mixing of the reactive species (3).

During discharge of this system,  $\text{Cr}^{2+}$  is oxidized to  $\text{Cr}^{3+}$  at the negative electrode, and  $\text{Fe}^{3+}$  is reduced to  $\text{Fe}^{2+}$  at the positive electrode. In one configuration, using a two-tank system, the solutions are pumped continuously through the reactor generating energy and gradually reducing the state-of-charge of the bulk solutions. During charging of the system, energy is delivered from an external source and stored by reversing the electrode reactions and gradually raising the state-of-charge of the bulk solutions.

This system has been under development since 1974 with the direction

and active participation of the Lewis Research Center of the National Aeronautics and Space Administration (NASA-LeRC) with Funding from both NASA and the Department of Energy (1-11). Semi-permeable membranes have been developed by Ionics, Inc. that are sufficiently conductive and selective to meet the requirements for solar and wind energy applications (12). The system has been scaled up to a 1kW, 11 kWh size without difficulty and many system features such as flow, shunt currents, electrochemical balance, mixed reactants, temperature effects and catalyst systems have been studied.

Giner, Inc. has been involved in the development of this system since 1975, with emphasis on the negative electrode (13-16). Early in the project it was observed that the bare carbon felt was adequate to support the  $\text{Fe}^{3+}/\text{Fe}^{2+}$  reactions but the  $\text{Cr}^{3+}/\text{Cr}^{2+}$  reactions required catalyzation to proceed at reasonable polarization and efficiency. Gold at a very low loading (12-15 micrograms/cm<sup>2</sup>) was found to be a suitable catalyst for the negative electrode but with the disadvantage that it simultaneously lowered the overvoltage for hydrogen evolution accelerating this parasitic co-reaction to unacceptable levels.

This problem was surmounted by adding lead chloride to the electrolyte and electrodepositing lead, in situ, over the gold-activated carbon felt (14-20). The lead has a high overvoltage for hydrogen evolution and is also an excellent catalyst for the  $\text{Cr}^{3+}/\text{Cr}^{2+}$  reactions. With this catalyst system the negative electrode can be cycled at moderate rates with low polarization and little interference from hydrogen evolution.

During extensive testing of the negative electrode, both at NASA-LeRC and at Giner, Inc., it was observed that the performance of the negative electrode could be somewhat variable both in terms of reactivity for the

$\text{Cr}^{3+}/\text{Cr}^{2+}$  redox reaction as well as the level of hydrogen evolution on charge. In the previous program (16), it was determined that a component of this variability could be attributed to the carbon felt substrate, specifically the heat treatment temperature (1250-2300°C, following pyrolysis of the rayon felt at 750°C). The effects of this factor were found to be mitigated by an acid or alkaline treatment preceding the gold catalyzation process. Beyond this it was observed that increasing the gold loading was not beneficial and that the lead loading, measured by anodic stripping during cyclic voltammetry, showed a consistent correlation with reactivity. At this point the investigation turned to physical surface analysis methods in an attempt to clarify the observations gathered by electrochemical testing, and to attempt to optimize the catalyzation process.

Using transmission electron microscopy (TEM) and scanning transmission electron microscopy (STEM), uncatalyzed carbon felt fibers were found to be fluted resembling a bundle of smaller fibers but otherwise smooth and generally free of particles. Gold-catalyzed felts exhibited opaque particles in the range of 10-500nm scattered over the surfaces. Energy dispersive analysis by X-ray (EDAX) showed these particles to be gold. Estimates of the gold surface area also showed direct correlation with reactivity and the observed lead loadings.

These two lines of investigation, the effects of the carbon felt substrate and optimization of the gold/lead catalyst system, were continued in this phase of the program, as well as new areas of investigation as summarized below.

## **B. Program Summary**

The research and development work presented in this report was directed to two broad tasks as outlined below. The first task, Electrode Development, represents an extension of the previous work, and the second task was addressed to performance factors of significance to advanced development of the iron/chromium redox system.

### **TASK I. ELECTRODE DEVELOPMENT**

- A. Characterization of Carbon Felt Substrates
- B. Catalyzation Procedure Optimization
- C. Performance in System Hardware
- D. Specifications for Substrate and Catalyzation

### **TASK II. ELECTRODE PERFORMANCE VARIABLES**

- A. Temperature Dependence
- B. Crossover Effects
- C. Acidity Level

The characterization of carbon felts was initiated with a broad range sampling of temperatures for the heat treatment, from 1250° to 2300°C. These were carefully controlled preparations purchased from Fiber Materials, Inc., in contrast to the random sampling of commercially available materials examined in the previous program. The samples included a set that was "scoured" (solvent washed to remove sizing before pyrolysis).

The initial test results, in concert with the results of the previous program, suggested a processing temperature of 1650°C for optimum electrochemical performance. On this basis, a second set of carbon felts was ordered in a narrower band around 1650°C. Before these samples were received, it was discovered that there were several discrepancies in the gold catalyzation procedure as practiced at Giner, Inc. compared to that used at NASA-LeRC (8). A preliminary investigation of catalyzation procedures indicated considerable performance variations associated with

processing parameters. As a consequence, the carbon felt characterization study, which was originally anticipated to yield a single sample for use in further studies, was extended to partially overlap the catalyzation optimization study (TASKI-B), in order to generate a broader base of information. The general conclusions and recommendations derived from this study regarding carbon felt processing factors are that the starting material should be unscoured and the optimum heat treatment temperature is in the range of 1650° to 1750°C. A broader temperature selection, 1500° to 1800°C, would probably be acceptable if used in similar narrow bands, e.g. 1500° to 1600°C or 1700° to 1800°C, etc.

A variety of gold catalyzation parameters were studied over the course of the program as outlined below:

PRECATALYZATION TREATMENT

KOH 1 N 80°C 0.5 hours  
45% 90°C 2.0 hours

PRECATALYZATION STATE

Dried: After rinsing to pH 7  
Damp: After rinsing to pH 7  
Damp: After pH 5 pre-soak  
After pH 7 pre-soak  
After pH 9 pre-soak

CATALYZATION PROCESS

Solvent/Wetting Agent  
Water/Methanol  
Water/Acetone

Solution

Temperature: 0°, 25°, 50°C

Volume: Saturation, small excess, large excess

Exposure

5 minutes to 16 hours  
open or closed container

POST-CATALYZATION TREATMENT

Heating Time and Temperature

Drying at 100°C for 1-2 hours

Drying and baking at 250-270°C for 2 hours

Both electrochemical measurements and surface analysis techniques were used to evaluate catalyzation parameters. The recommended process centers on the published NASA procedure (8) with the imposition of some additional controls (see Section V-F).

Initially, three variations of a basic methanolic/gold deposition process were used to catalyze carbon felt samples (Section V-A); other factors, such as processing temperatures, were examined later. The catalyzation methods were 1) the Double Immersion method, a set of procedures developed in the previous program for rigorous control of the total gold loading, 2) the NASA-I method, a standard method used at NASA-LeRC, and 3) the NASA-II method, a modification of the standard method in which the gold chloride concentration was reduced by half and the volume doubled.

The standard NASA catalyzation process (NASA-I), and more particularly the modified process (NASA-II), presented an opportunity to observe the solutions "in process" by way of the excess solution volume, in contrast to the Double Immersion method in which the solution was designed to be totally absorbed by the carbon felt sample. For NASA-II electrodes, it was immediately noticed that the excess gold chloride solution had a faint blue color. For NASA-I electrodes, the excess gold chloride solution looked clear and colorless at first. After two hours, however, it changed to purple. The next day the solution was still purple and had become noticeably cloudy. These colors are reported to be due to suspended gold particles, the formation of which is initiated by contact of gold chloride solution with the felt (21). Based on the blue color, observed in the NASA-II preparation, the particles were anticipated to be very small, on the

order of 1.0 nm diameter (nucleates). The actual gold crystallites on the carbon fiber, observed by transmission electron microscopy, were larger than 1 nm, ranging from 10 to 25 nm. The purple color seen for NASA-I electrodes was reported to indicate larger particles, on the order of 100 nm diameter. The actual gold crystallites deposited on the carbon fibers were observed to be on average smaller than 100 nm (20-60 nm), but larger than the gold particles deposited by the NASA-II method. The gold crystallites deposited by the Double Immersion method were within the same range as the particles deposited by the NASA-I method (25-35 nm). These observations also suggested that metallic gold is formed when the methanolic gold solution contacts the carbon felt. Previously it had been assumed that gold chloride was deposited, requiring thermal decomposition to gold. Similar results, in terms of particle size, were obtained in a study of controlled procedural variations (Section V-B), but the correlation with electrochemical performance was less obvious.

The smaller and more uniform gold particles deposited by the NASA-II method resulted in higher electrochemical activity, including a higher level of hydrogen evolution, a combination that would lead to low charging efficiency. These same electrodes exhibited high lead deposits which may be consistent with higher gold surface areas. The values for lead deposition consistently exceeded the theoretical quantity of lead available, however, which may have resulted in some unplated gold leading to higher hydrogen evolution rates. Such a condition would not be expected in a flow cell which may suggest that the NASA-II modification is worth further study under flow conditions.

ORIGINAL PAGE IS  
OF POOR QUALITY .

The NASA-I catalyzation procedure, yielding larger, less uniform particles, resulted in lower electrochemical activity but higher charging efficiency values. The Double Immersion method, yielding gold particle sizes within the same range as the NASA-I method, resulted in electrochemical performance which was quite different (low activity, low charging efficiency) suggesting the influence of factors in addition to gold particle size, or non-representative microscopy samplings.

In the course of catalyzing electrodes over a period of many months, other process variables that could affect the gold deposit were noted. Some of these are related to the precatalyzation state of the carbon felt such as its moisture content, damp or dry, and its residual pH. Other factors are the wetting agent used (methanol or acetone), and the temperature of the catalyzing process. The work done to determine the effects of these factors is discussed in Section V-C.

With regard to the selection of a wetting agent and a damp versus dry precatalyzation state for the carbon felt, the small sample of test data was not sufficient to clearly differentiate the factors tested. Both wetting agents have been used successfully at NASA-LeRC. It was also concluded that the damp/dry condition of the felt per se, prior to catalyzation, was not a significant factor. A related factor, the residual pH of the felt after pretreatment in KOH, was considered to have more potential influence on the subsequent catalyzation; pH values of 5, 7 and 9 were studied. The mean particle size was fairly consistent in all cases, but the range of sizes for the pH 9 samples was much larger. Again, the data do not permit any clear selection of conditions but suggest rather that 1) a pH range of 5 to 9 is

an acceptable precatalyzation condition for the carbon felt, and 2) still other factors influence the catalyzation or testing process.

Three catalyzation temperatures were studied, 0, 25 and 50°C. It was found that there was a progressive increase in gold particle size with increasing catalyzation temperature, as anticipated. The range of particle sizes also increased with increasing temperature. The electrochemical performance data was quite scattered but the values for relative charging efficiency improved somewhat with increasing catalyzation temperature. This data suggests that, although catalyzation temperature affects gold particle size in an expected manner, here again there are other factors influencing electrochemical performance.

In the above studies directed to defining the critical factors in the gold catalyzation process, the electrochemical performance observed, as noted, was frequently erratic suggesting that some influential factors were not being controlled. One such factor is the carbon felt substrate, which can exhibit variations in physical and chemical properties and has been found to influence performance, as discussed earlier. The KOH pretreatment process is directed to neutralizing some of the chemical properties of the felt, but it is obviously not completely effective and does not address variations in physical properties such as density, thickness and surface area. Thus the carbon felt remains as a potentially influential factor that is probably not completely controllable. Another factor is the cyclic voltammetry testing procedures used. A study of reproducibility (Section V-D) was directed to the latter, assuming that the carbon felt substrate over a small area would be sufficiently uniform in properties. A concerted

effort was then made to control all other factors in the catalyzation and testing processes. For this purpose, three felt samples (from a small section of one lot of felt) were catalyzed in three separate operations using the same catalyzation method (NASA-I). Each sample was then cut into three strips to provide a total of nine samples for electrochemical testing. Examination of the resulting set of test data in the context of a selection of previous test data showed that the data points nearly span the full range of the previous data and thus could mask any differences between catalyzation by the Double Immersion method through the NASA-II method. There was a definite grouping of points around values characteristic of NASA-I preparations but it is apparent that a large number of data points might be needed to obtain a statistically significant value.

At the completion of the catalyst procedure optimization study, it was concluded that 1) there are factors influencing the gold catalyzation process that were not determined or sufficiently controlled for closely predictable results in terms of gold particle size or performance, 2) the cyclic voltammetry testing methods are only suitable for qualitative analysis and broad distinctions in performance; the results may be best interpreted on a statistical basis over many samples for the present state of refinement in cyclic voltammetry, catalyzation, electrode preparation and handling.

In an extension of the catalyst optimization task, an attempt was made to define the physical character of the lead deposit i.e., particles versus a continuous layer, and on-the-gold versus on-the-carbon fibers or evenly distributed on all surfaces (Section V-E). Transmission and scanning

transmission electron microscopy techniques were used to examine the surface for particles, and both EDAX and X-ray dot mapping techniques were used for material analysis. Lead in particulate form was not observed in any case; the lead that was detected appeared rather to cover the entire fiber with a thin layer. The disposition of the lead in specific relation to the gold could not be clearly established.

The effects of reactant crossover were examined briefly using cyclic voltametry. From these studies it was concluded that there were no significant effects associated with crossover, i.e.  $\text{Fe}^{2+}$  in the chromium solution and  $\text{Cr}^{3+}$  in the iron solution. [In studies at NASA-LeRC,  $\text{Fe}^{3+}$  in the chromium solution, a situation which can be avoided, was found to be detrimental, however (10)].

Minor investigations of the effects of temperature and acidity level were also performed. The results were generally as anticipated e.g. greater reversibility with higher temperature and acidity level. The effects of temperature, especially with regard to the shift in the chromium complex equilibrium ("open-circuit voltage hysteresis" phenomenon), were addressed more specifically by work done at NASA-LeRC (1,10,11).

Finally, optimized negative electrodes were tested in system hardware, a 1/3 square foot flow cell, with generally good results.

## II. ELECTROCHEMICAL TESTING PROCEDURES

All of the electrochemical testing performed on this program was done by cyclic voltammetry in a three electrode cell. The details of the electrode mounting, cell configuration, solutions, standard sweep sequences and data reduction, are described below. Individual variations, such as the use of  $\text{FeCl}_3$  and higher concentrations and temperatures, are described separately.

### A. Electrode Mounting Procedures

The "waxed-clip" electrode holder was used to mount all test samples studied in this program. This type of electrode holder was developed at NASA-LeRC to reduce contact resistance problems and the undesirable compression of the carbon felt associated with the tantalum wire electrode holder used earlier (15). The holder, shown in Figure 1, consists of a binder clip with added copper contact surfaces and a heavy threaded brass connector rod. A 1.5 cm wide strip of felt was clamped between the copper contacts and 1.3 cm of its length isolated by means of pressure from the stop-off clamp. The entire binder clip assembly was then submerged momentarily in hot ( $130^\circ\text{C}$ ) Ceresin wax, allowing the melted wax to wick up the felt as far as the end of the stop-off clamp, as depicted in Figure 1. To provide an external electrical contact, a length of the connector rod was masked with Teflon tape prior to dipping. The stop-off clamp and masking were removed once the wax had hardened. Thus, only the unwaxed 1.5 x 1.3 cm ( $2\text{cm}^2/\text{side}$ ) felt section was exposed to the solution for testing.

### B. Electrochemical Test Cell

The test cell, illustrated in Figure 2, consisted of a 75 ml glass vessel threaded to accept a plastic screw cap provided with five standard taper ports (ECO Model 494). The center port contained a specially designed Teflon plug with threaded contacts to which the waxed-clip electrode was attached. Counter electrodes, consisting of graphite rods (Ultra-Carbon "F") contained in fritted glass tubes, were placed on either side of the working electrode. A saturated calomel reference electrode (SCE) and nitrogen gas bubbler occupied the remaining ports. The gas bubbler was equipped with a two-way stopcock so that nitrogen could be bubbled through the solution or over the surface. A small Teflon-covered magnetic stirring bar was generally provided for in situ mixing of reactants. During testing, the stirring was stopped and nitrogen bubbling was switched to a surface flow.

### C. Corrections for Resistance

Electrical contact problems, particularly with regard to variability, can be reduced substantially through the use of the waxed-clip holder. However, the actual potentials, especially at the switching points, remain somewhat undefined. Consequently, electronic compensation for  $iR$  loss was used for all tests in this program.

The device used measures the current flowing to or from the working electrode and feeds back a proportional voltage in series with the input signal to the potentiostat. The triangular linear potential sweep signal, rather than the working-to-reference voltage, is used as the input for the

potential axis of the voltammogram. The iR compensation point is determined by monitoring the working-to-reference potential on an oscilloscope while increasing the level of compensation; the onset of oscillation represents the beginning of over-compensation. It appeared that being within 1/4 to 1/2 of a turn (on a ten turn potentiometer) of the oscillation point was adequate compensation in most cases, i.e., the effect of closer correction was negligibly small. .

#### D. Testing Procedures

All measurements were made versus a saturated calomel electrode (SCE). The felt test electrode was always saturated with solution by evacuating the cell after immersion of the electrode, and the solution was deaerated with nitrogen before each run. Pairs of counter electrodes in fritted glass tubes were designated for each solution composition to reduce cross-contamination between tests. For routine negative electrode testing, the three compositions examined in sequence were 1) HCl, 2) HCl, PbCl<sub>2</sub>, and 3) HCl, PbCl<sub>2</sub>, CrCl<sub>3</sub>.

A Wenking potentiostat was used to control the electrode potential in response to a cyclic linear potential sweep signal provided by a Hewlett-Packard function generator (Model 3310B). The cell working-to-reference potential was used to drive the Y-axis and the resulting current (as voltage drop across a 1.0 ohm precision resistor) was recorded on the X-axis of a Linseis X-Y recorder (Model 1700). When electronic iR compensation was used, the triangular sweep signal rather than cell working-to-reference potential was used to drive the potential axis, as discussed in Section C above.

On the previous program (16), the negative potential region was explored using a gold-activated carbon felt in 1.0 N hydrochloric acid. The negative electrode test region was initially set at 0.0 to -1.0 v vs. SCE. It was observed that no reactions other than  $H^+$  reduction (hydrogen evolution) occurred over a wide potential region in hydrochloric acid. It was also demonstrated that the sweep rate could be changed from 10 mV/s to 100 mV/s without effect on the observed current. Since this was the case, a sweep rate of 100 mV/sec was selected for this particular test,  $H^+$  reduction on gold-activated felt in HCl, to avoid excessive hydrogen evolution. For most other tests the sweep rate was kept at 10 mV/s. An exception was the high concentration solution testing where the sweep rate had to be reduced considerably to stay within instrumental limits.

When iR compensation was introduced, it was found that in many cases the current became almost asymptotic at -1000 mV which sometimes induced irreversible oscillation in the potentiostat. For this reason, the negative electrode test region was shifted 50 mV more positive, i.e. +50 mV to -950 mV vs. SCE. The potential was always applied at approximately 0.0 V.

A routine negative electrode test procedure then consisted of recording cyclic voltammograms in the following sequence (as a composite figure):

- 1)  $H^+$  Reduction in 1.0 N HCl. The hydrogen evolution characteristics of the gold-activated felt were initially examined in 1.0 N HCl only. The hydrogen evolution rate on gold was generally five to ten times greater than other reaction levels. Consequently, the  $H^+$  reduction curve on gold/carbon felt (Au/C) is frequently shown with a current scale multiplier in the composite voltammograms.

2) Pb<sup>2+</sup>/Pb and H<sup>+</sup>/H<sub>2</sub>-on-Pb Redox Reactions. At the completion of the first test, the counter electrode set was exchanged and lead chloride was introduced. The lead chloride concentration was 10<sup>-3</sup> M (which is close to the saturation level in hydrochloric acid). In order to achieve this concentration it was necessary to add lead chloride crystals to the 50 ml cell volume of hydrochloric acid to avoid a volume change. This procedure was found to be somewhat undesirable in the previous program both because of the small quantity of material involved and the difficulty in achieving complete dissolution. Consequently, instead of adding lead chloride to the solution, a large volume of 1.0 N HCl was premixed with 10<sup>-3</sup> M PbCl<sub>2</sub> and a 50 ml quantity of this solution was substituted for the HCl-only solution used in the previous test. The solution was stirred and deaerated again for 20 minutes.

Cyclic voltammograms were then recorded over the same potential range, at 10 mV/s starting at 0.0 V, to measure lead plating (Pb<sup>2+</sup> reduction; -550 mV vs. SCE), the subsequent hydrogen evolution on the lead-on-gold (-800 to -950 mV vs. SCE); and lead deplating (Pb oxidation; -500 mV vs. SCE) on the return sweep. A voltammogram was typically recorded after the third or fourth cycle. Later in the program this was extended to 10 or more cycles.

3) Cr<sup>3+</sup>/Cr<sup>2+</sup> Redox Reaction. After completion of the testing with lead chloride, the counter electrode set was again exchanged and chromic chloride (CrCl<sub>3</sub>.6H<sub>2</sub>O; Baker Reagent Gd.) was added to the solution for measurement of the Cr<sup>3+</sup>/Cr<sup>2+</sup> redox reaction. For routine testing only, a 50 mM concentration of chromic chloride was used. The solution was stirred with the magnetic stirrer and by bubbling nitrogen for 20 to 30 minutes

after the salt addition. Dissolution of these quantities of chromic chloride occurred almost immediately; extensive stirring was used to ensure uniform concentration of reactants within the felt electrode structure and equilibrium with the bulk solution.

Cyclic voltammograms were again recorded over the +50 to -950 mV potential range at 10 mV/s starting at 0.0 V vs. SCE. The charging reaction ( $\text{Cr}^{3+}$  reduction) begins coincident with lead plating at about -525 mV vs. SCE and shows a peak at about -650 mV. Most electrodes showed a minimum in the cathodic current following the  $\text{Cr}^{3+}$  reduction peak and preceding the onset of hydrogen evolution. On the return sweep, the discharge reaction ( $\text{Cr}^{2+}$  oxidation) begins at about -650 mV vs. SCE and shows a major peak at about -550 mV; the trailing side of this oxidation peak generally exhibited a shoulder and smaller peaks trailing off towards 0.0 V. ....

#### E. Data Reduction Methods

In order to search for performance effects related to parameters such as catalyzation and type of felt substrate, it was necessary to extract and condense the information collected by cyclic voltammetry. This was done by tabulating selected anodic and cathodic current features and curve integrations to yield charge or coulombic capacity (current X time). These methods of selecting data points are described in detail below.

1. Current Data. The anodic and cathodic current data points that were typically selected from the voltammograms and tabulated for qualitative comparisons are illustrated in the representative voltammograms shown in Figures 3 and 4. The curves shown in Figure 3 are a composite of two separate voltammograms recorded on the same grid. The first curve

ORIGINAL PAGE IS  
OF POOR QUALITY

exhibits the electrochemical features displayed by a gold-activated carbon felt in hydrochloric acid before the addition of lead chloride. The only reaction observed is hydrogen evolution. The data point selected to represent the level of this reaction is the current measured at the potential sweep switching point, -950 mV vs. SCE. This is referenced as data point "1" in the figure, and has been symbolized as " $I_{C,H^+}$  on Au/C", the  $H^+$  reduction current on gold-on-carbon felt at -950 mV. This data point was found to be highly sensitive to the accuracy of iR compensation used and was thus somewhat less reproducible than other data points. The second curve in Figure 3 exhibits the electrochemical features displayed by a carbon felt electrode (similar features with or without gold) in hydrochloric acid after the addition of lead chloride. The cathodic reactions observed then were lead plating followed by hydrogen evolution and, on the return (anodic) sweep, lead deplating. The data point selected to represent the level of hydrogen evolution after the addition of lead chloride is referenced as point "2" in the figure, and has been symbolized as " $I_{C,H^+}$  on Pb/Au", the  $H^+$  reduction current at -950 mV vs. SCE. The level of the lead plating reaction is referenced as data point "5" in the figure, and has been symbolized as " $I_{C,Pb^{2+}}$ ", the Pb reduction current. The subsequent deplating reaction level is referenced as data point "6" and has been symbolized as " $I_{a,Pb}$ ", the Pb oxidation current.

The curve shown in Figure 4 illustrates the electrochemical feature displayed by a carbon felt electrode (with gold in this illustration) after the addition of both lead chloride (1 mM) and chromic chloride (50 mM) to the hydrochloric acid (1 N). The level of hydrogen evolution ( $H^+$  reductio

superimposed on  $\text{Cr}^{3+}$  reduction) at  $-950$  mV is referenced as data point "3". A data point collected to represent the cathodic minimum between the  $\text{Cr}^{3+}$  reduction peak and hydrogen evolution is identified as point "4" and has been symbolized as " $I_{\text{cH}^+}$  min."

The data point selected to represent the level of the negative electrode charging reaction is referenced as current peak "7" and has been symbolized as " $I_{\text{cCr}^{3+}}$ ", the  $\text{Cr}^{3+}$  reduction current. The data point selected to represent the level of the negative electrode discharge reaction is referenced as point "8" in the figure and has been symbolized as " $I_{\text{aCr}^{2+}}$ ", the  $\text{Cr}^{2+}$  oxidation current.

The data point numbers described above have been keyed to the columns of data shown in the Appendix Tables. The columns of data, representing different felt substrates and gold loadings or procedures, were then examined for trends.

2. Charge Data. The anodic and cathodic current data points described above are subject to some experimental error related to the accuracy of the iR compensation used and the degree to which the resistive elements are reproducible and amenable to compensation, e.g., ohmic potential drops (resistivity of the diffusion layer) versus liquid diffusion potential and surface film resistance. By comparison, the area defined by a curve (current X time) is less ambiguous. In addition, measurement of the charge permitted quantitative separation of various features of interest. For example, the amount of lead plated on the cathodic side can be determined (before the addition of chromic chloride) by measuring the area under the anodic part of the curve for lead oxidation, designated  $Q_{\text{aPb}}$ .

This value is relatively unambiguous compared to the cathodic charge, which is the sum of the lead plating charge,  $Q_{c,Pb^{2+}}$ , (both from within the felt and from bulk diffusion to the surfaces) and the  $H^+$  reduction charge,  $Q_{c,H^+}$ . The lead oxidation charge,  $Q_a,Pb$ , was assumed to be the same before and after the addition of chromic chloride. This assumption was made based on the appearance of the composite reactions for  $Pb^{2+}/Pb$  and  $Cr^{3+}/Cr^{2+}$  at the 10 mM  $Cr^{3+}$  concentration, investigated in the last program (16). Thus the lead oxidation charge,  $Q_a,Pb$ , (measured before the addition of chromic chloride) was subtracted from the total anodic charge measured for the combined reactions ( $Q_a,Pb + Q_a,Cr^{2+}$ ) after the addition of chromic chloride, to yield the  $Cr^{2+}$  oxidation charge,  $Q_a,Cr^{2+}$ . Since the catalytic surface changes through the anodic portion of the curve (i.e. lead deplates), the total chromium charge in some instances was separated into two segments, the major peak region before the end of lead deplating, referred to as " $Q_a,Cr^{2+}$  Peak", and the trailing region referred to as " $Q_a,Cr^{2+}$  Trailing". The trailing side of the lead oxidation peak was used as the dividing line. In addition, in order to provide a more complete analysis of the data in some instances, four cathodic area integrations of the same cyclic voltammograms were determined. These are described below:

- (1)  $Q_{c,Pb^{2+},H^+}$  - The cathodic charge in 1.0 mM  $Pb^{2+}$ , 1N HCl electrolyte.
- (2)  $Q_{c,H^+}$  - The cathodic charge due to hydrogen evolution in 1.0 mM  $Pb^{2+}$ , 1N HCl electrolyte.  $Q_{c,H^+}$  was obtained by subtracting  $Q_a,Pb$  from  $Q_{c,Pb^{2+},H^+}$ .
- (3)  $Q_{c,Cr^{3+}}$  - The total cathodic charge due to  $Cr^{3+}$  reduction in 1.0 mM  $Pb^{2+}$ , 50 mM  $Cr^{3+}$ , 1N HCl electrolyte.

(4)  $Q_{cd}Cr^{3+}$  - The cathodic charge due to  $Cr^{3+}$  reduction in excess of the anodic charge due to  $Cr^{2+}$  oxidation ( $Q_aCr^{2+}$ ), i.e.:

$$Q_{cd}Cr^{3+} = Q_cCr^{3+} - Q_aCr^{2+}.$$

This value probably represents an approximation of the reactant/product diffusion to and from the surface of the felt sample i.e.  $Cr^{3+}$  reduced at the surface may diffuse into the bulk of the solution and thus be unavailable for oxidation on the return sweep. Theoretical values for  $Cr^{3+}$  within the felt were also calculated ( $Q_tCr^{3+}$ ).

The various charge segments discussed here are illustrated in Figure 5. Curve segments were integrated by the paper weight-ratio method.

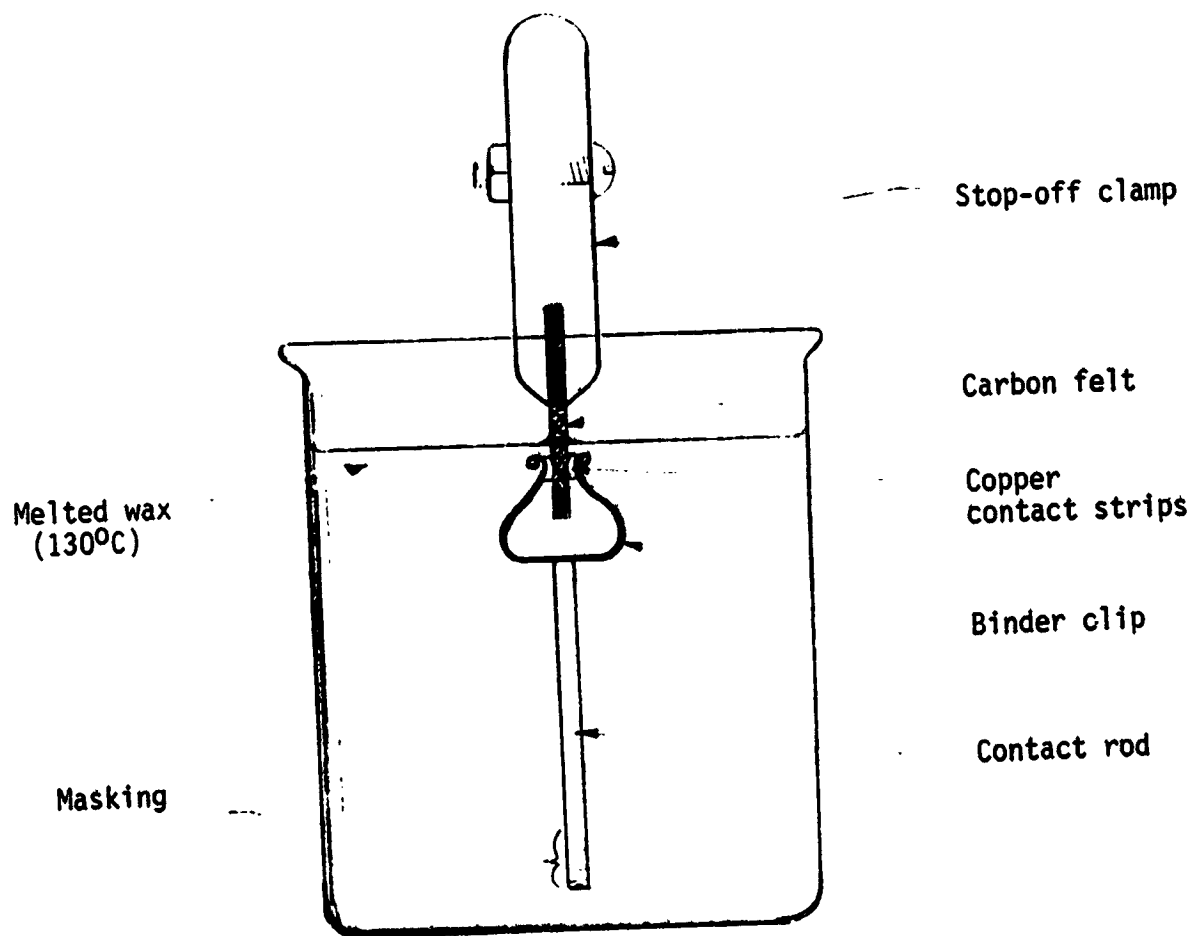


Figure 1. Waxed-clip Electrode Holder; Waxing Procedure

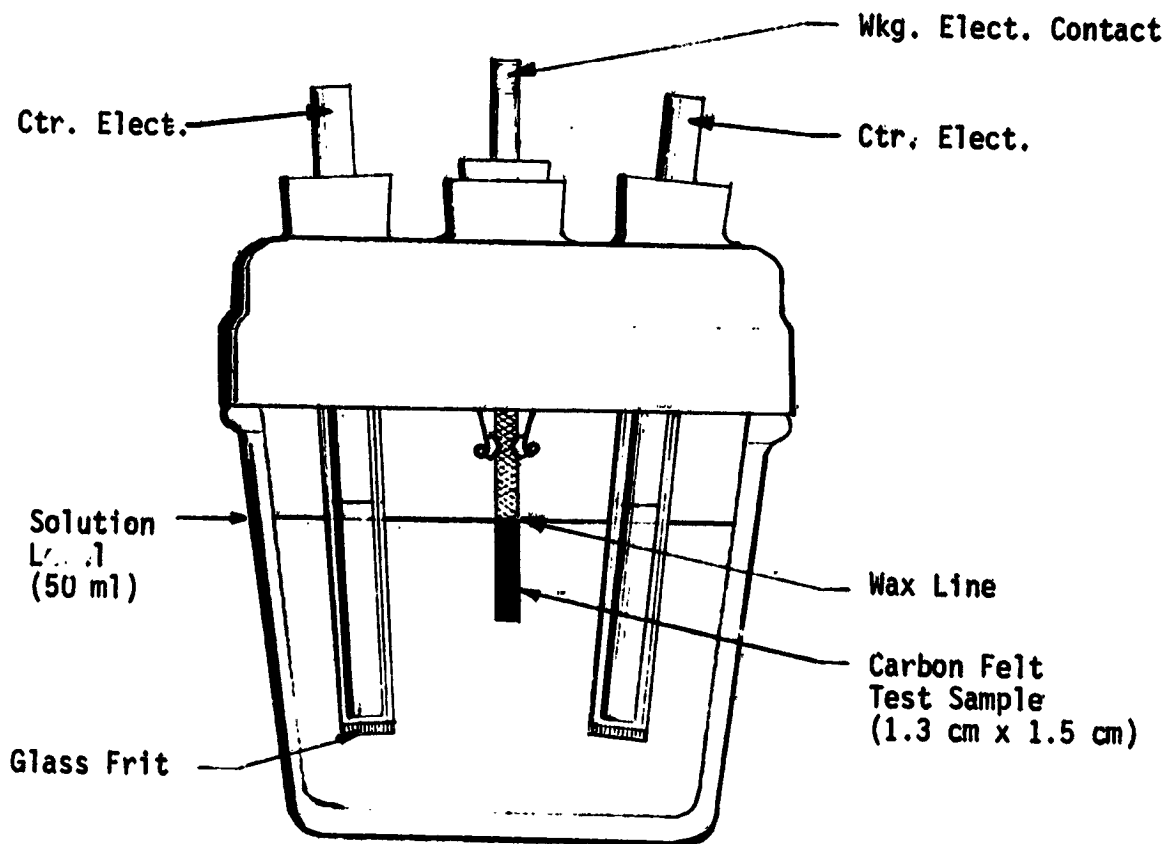
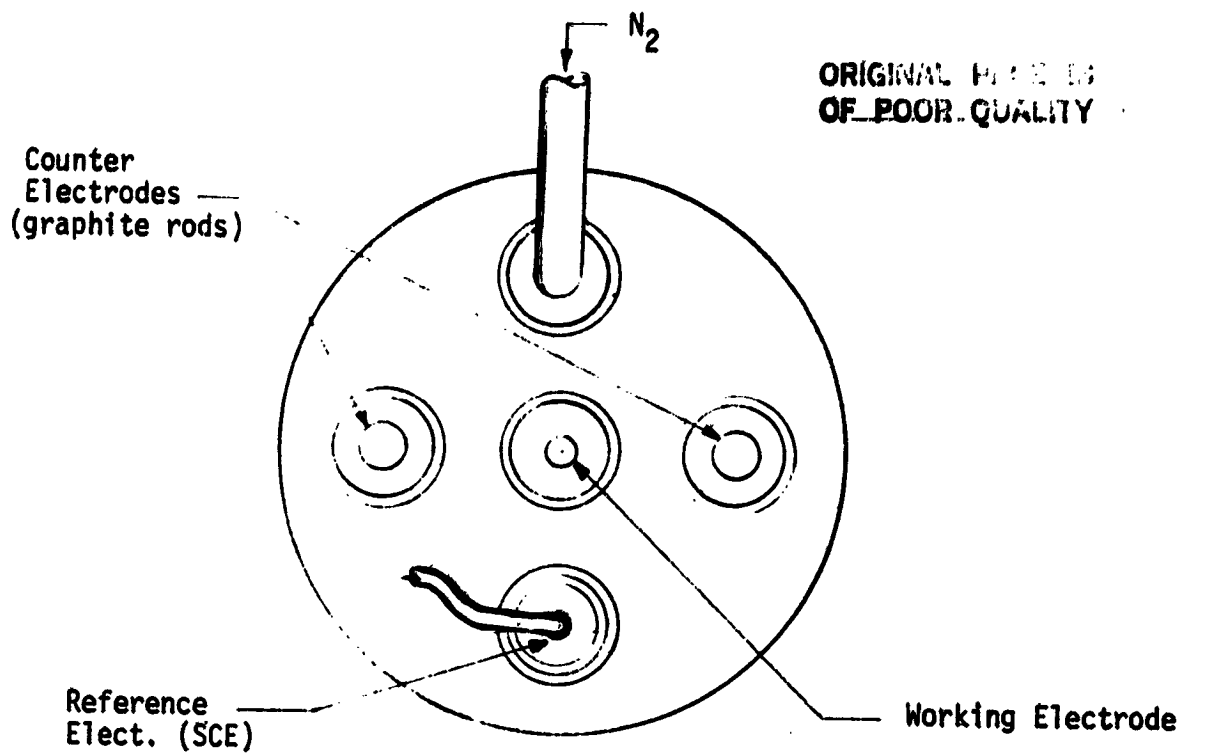


Figure 2. Cell Configuration with Waxed-Clip Holder

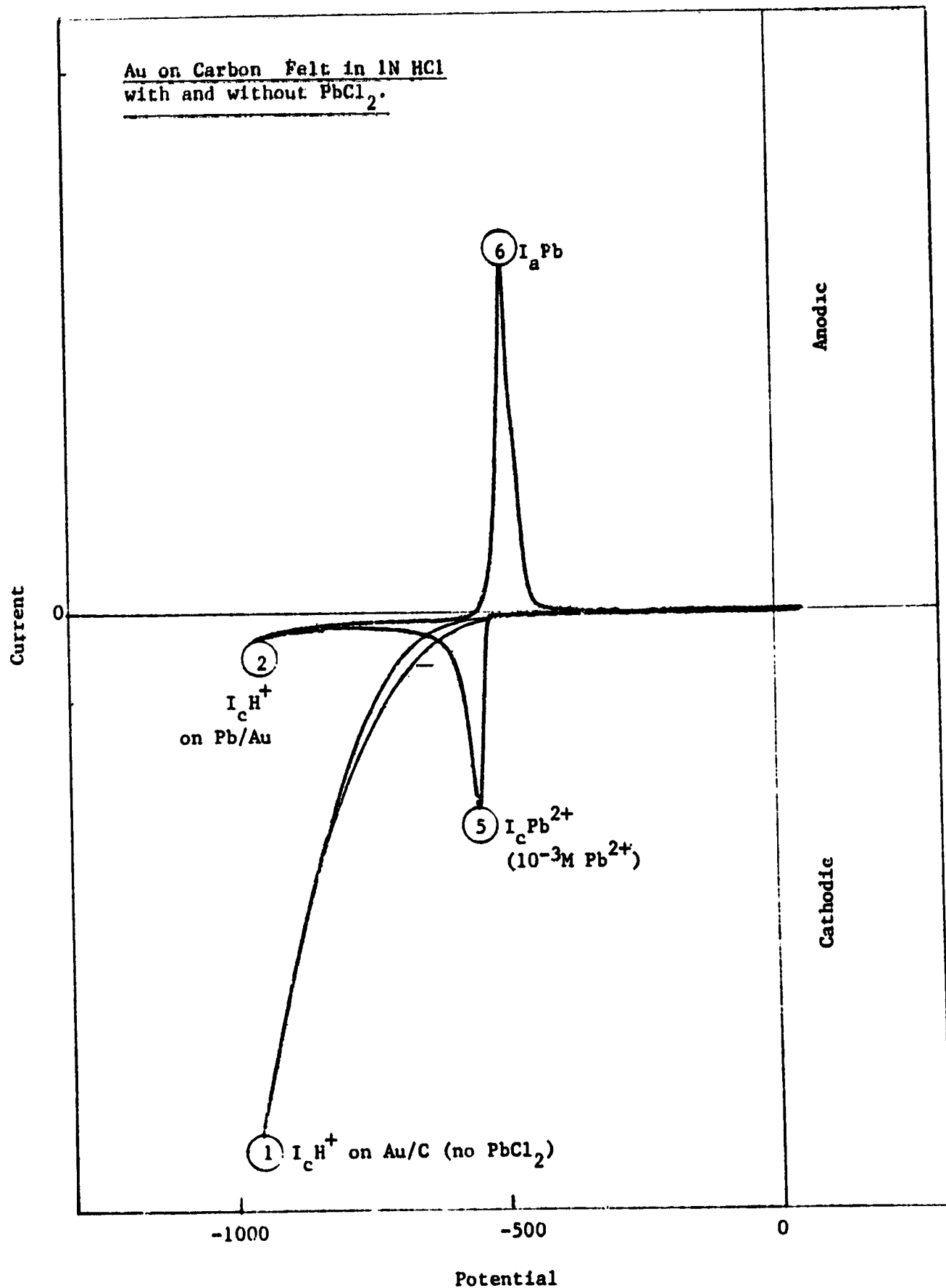


Figure 3. Representative Voltammogram Showing Pb<sup>2+</sup>/Pb Data Points Summarized in Tables.

Cr<sup>3+</sup>/Cr<sup>2+</sup> Redox Reaction in Pb/Au/Carbon Felt  
in 50mM Cr<sup>3+</sup> (1N HCl).

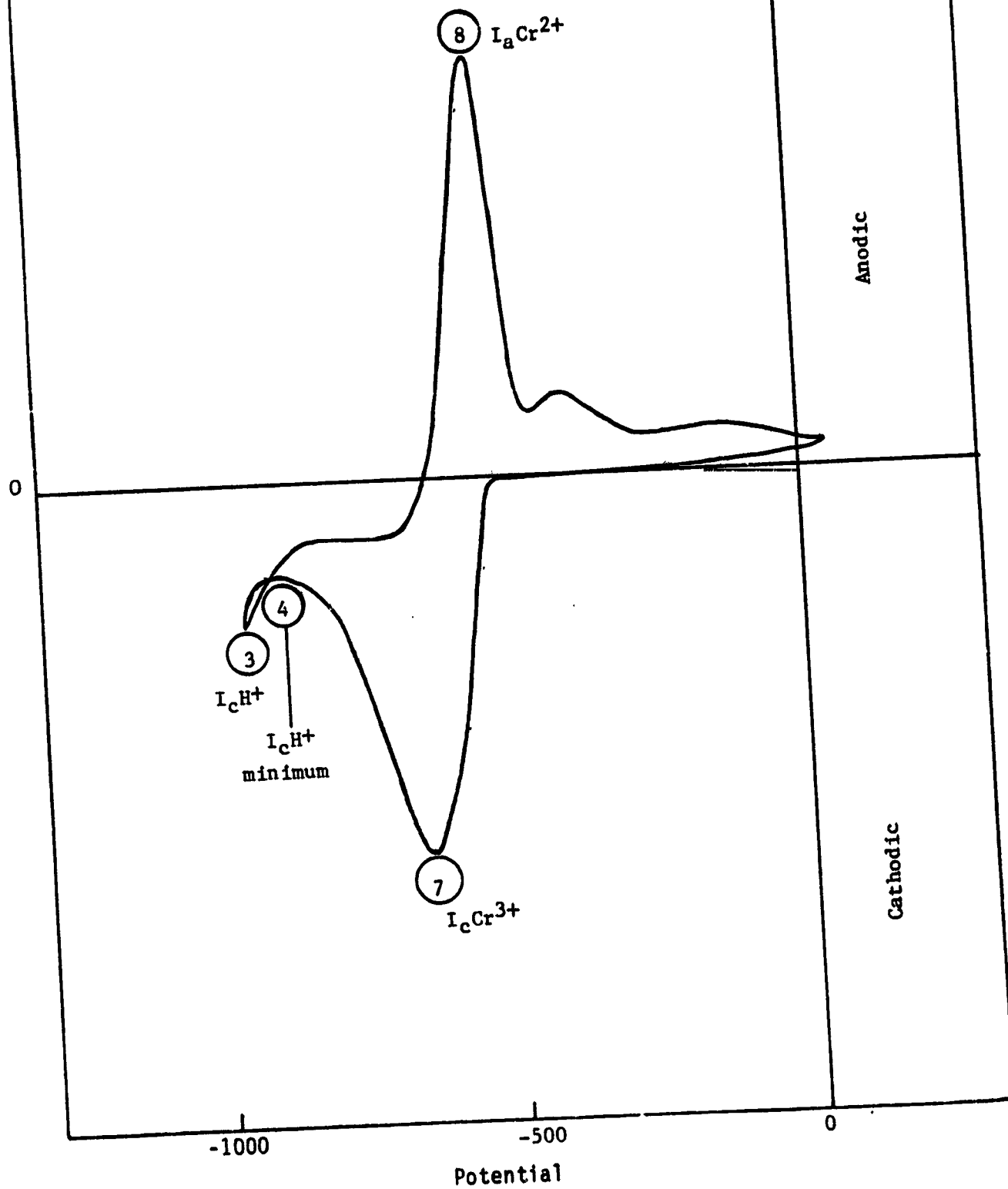


Figure 4. Representative Voltammogram Showing Cr<sup>3+</sup>/Cr<sup>2+</sup> Data Points Summarized in Tables.

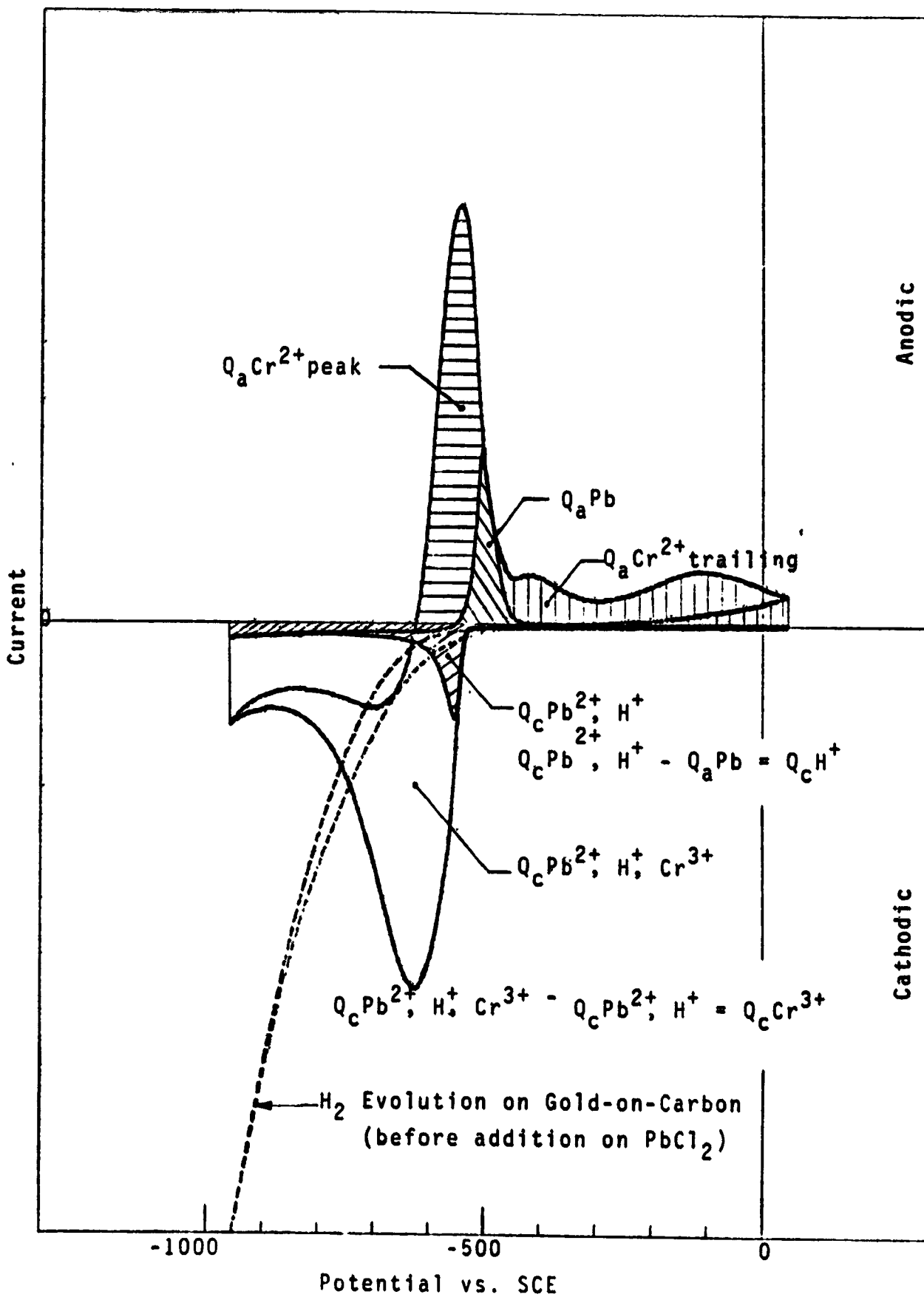


Figure 5. Definition of Anodic and Cathodic Charge Segments

### III. GOLD CATALYZATION METHODS

#### A. Double Immersion Process

In the previous program (16), carbon felts with widely varying physical properties and from several vendors were being investigated. Since control of the absolute quantity of gold deposited was a primary concern, a process was developed that tailored the gold solution volume approximately to the absorption capacity of the felt sample while holding the gold loading per square centimeter constant. This was referred to as the "Double Immersion" process (to distinguish it from earlier "dropwise" methods).

For this program, test samples 7 x 7 cm were cut from each temperature-run of felt. Each sample was cleaned according to procedures developed in the last program. The cleaning procedure consisted of vacuum filling the felt with .1N KOH, heating to 75 - 85°C for 30 minutes, rinsing to approximately neutral pH and drying at 100 - 110°C for 1 hour. (Some surface effects observed for this process are discussed in Section V-F-4.) Gold was deposited on the felt from an aqueous/methanol solution.

The use of alcohol as a co-solvent/wetting agent was first investigated on an earlier program (15). Initially, 50/50 isopropanol/water solutions were used. The current process, based on methanol, was developed in further experiments at NASA-LeRC (6-8,20), and has yielded excellent results in 1 kW, 11 kWh prototype system tests (6-8).

In an early attempt to prepare a relatively large selection of electrodes by the alcohol-assisted gold process, a large volume of appropriate solution was pre-mixed. Because of the processing time involved, a portion of the solution experienced several hours of standing in the container. Over this period of time (<8 hours), the initial yellow color of the gold

chloride solution was observed to fade significantly and small black fibrous strands and needles were observed throughout the solution, indicating precipitation of metallic gold. Since the premixed solution had not previously been stored for any length of time, the short-term instability of gold chloride in alcohol solution had not been observed. This potential problem of gold precipitation in the presence of alcohol was obviated by preparing and storing only the aqueous portion of the solution; the required quantity of methanol was then added to the exact volume of aqueous solution required immediately prior to use. The total volume of solution required for each type of felt was selected on the basis of the mean water absorption values measured; the gold concentration was adjusted in each case to give the desired gold loading. Tailoring of the solution volume and concentration in this way permitted complete wetting without excess solution for each felt type in spite of large variations in thickness, apparent density and liquid absorption capacity over the range of samples.

For this program, the standard gold loading was 12.5 micrograms/cm<sup>2</sup> of projected area. Half the quantity of aqueous gold solution needed for this loading was diluted with three parts absolute methanol to a volume sufficient to saturate the felt. The other half of the gold was applied in a second immersion cycle. The solution was transferred to a shallow polyethylene container of the approximate dimensions of the sample, 7 x 7 cm. The felt was then immersed in the solution and allowed to absorb the entire volume. Subsequently, it was dried for 2-3 hours at ambient temperature and then oven-dried at 100 - 110°C for an hour. This process was then repeated placing the felt into the aqueous/methanol gold chloride solution from the opposite face, to try to achieve uniform distribution of the gold.

Finally, each sample was baked at 265 - 275°C for 2 hours. This last step was considered to accomplish thermal reduction of the gold chloride deposit to metallic gold; the validity of this assumption is discussed in Sections V-A and B.

B. Standard NASA Process (NASA-1)

Electrodes delivered to NASA-LeRC on the last program (16) were reported to show performance characteristics in full cell tests that differ from the characteristics of electrodes prepared at NASA-LeRC. This was unexpected since the method used to prepare the electrodes (Double Immersion) was not intended to be a variation of any essential feature of the NASA-LeRC process, as understood at that time. A careful review of the details of the procedures in a NASA publication (8) at the beginning of this program, however, revealed several differences which, separately or in combination, could be significant; these are listed below:

Standard NASA Method

Double Immersion Method

- |  |  |
|--|--|
| 1. Pretreatment in 45% KOH for 2 hours 90°C.<br>(Both methods of pretreatment were used for electrodes delivered on last program, without apparent effect) | Pretreatment in 1N KOH for 30 minutes 80°C.      |
| 2. Felt is saturated with water and damp-dried before immersion in gold solution.  | Dry felt is immersed in gold solution.           |
| 3. Excess gold solution is used.   | No excess gold solution.                         |
| 4. Electrode soaked in gold solution in sealed plastic bag overnight before oven drying.   | Electrode air dried for 2-3 hours before drying. |

The most significant departures seemed to be in the third and fourth items listed above. In the NASA method the electrode is immersed in gold solution, removed and immersed in a second portion of gold solution, in

which it is allowed to stand in a sealed plastic bag overnight before oven drying. In the Double Immersion method, the electrode is immersed in gold solution for 1-2 minutes and then dried in air for 2-3 hours followed by oven drying; this process is repeated, immersing the electrode from the opposite face.

The next most significant departure would seem to be in the volume of gold solution used. In the Double Immersion method the quantity of solution used each time is approximately adequate to saturate the dry felt, and the total quantity of dissolved gold is deposited on the felt. In the NASA method there is a fair excess of gold solution (partially due to the use of a "damp-dry" felt) and no drying between immersions; thus the total quantity of gold deposited may be less accurately determined (the excess solutions show evidence of colloidal gold). In spite of this, the gold loading obtained in terms of particle size could be quite reproducible, and more importantly, the activity of the gold deposit could be higher; e.g., in the last program (16), the surface area of the gold deposit was found to be more significant than the actual gold loading.

#### C. Modified NASA Process (NASA-II)

In order to explore the possible effects of the "excess-volume" feature of the standard NASA process, a much larger excess of solution was used in some instances (this has been referred to as the "NASA-II" method in this report). In the standard NASA method, using 10 ml of solution for a 7 x 7 cm felt sample gave an excess volume of about 5 ml. For the NASA-II method, 20 ml of solution were used giving an excess volume of about 15 ml. The total potential gold loading in the NASA-II method, if all of the gold

were deposited on the felt, would still have been 12.5 micrograms/cm<sup>2</sup>, but the gold concentration in the solution was half that of the NASA-I method. This factor was explored further in a separate study presented in Section V-B.

The effects of the pre-catalyzation state of the carbon felt (dry, damp, residual pH and catalyzation temperature) are addressed in Section V-C. The test data obtained for these three catalyzation processes are covered in detail in Section V-A "Effects of Process Variations".

#### IV. CARBON FELT PROCESSING FACTORS

##### A. Sample Descriptions

For the characterization of carbon felts, Fiber Materials, Incorporated (FMI) processed strips from a single roll of rayon felt at six temperatures. The entire roll was first pyrolyzed ( $>500^{\circ}\text{C}$ ) and then cut into 8 - 9 inch wide strips for graphitization at the following six temperatures:  $1250^{\circ}$ ,  $1350^{\circ}$ ,  $1500^{\circ}$ ,  $1650^{\circ}$ ,  $1800^{\circ}$ , and  $2300^{\circ}\text{C}$  (referred to as Phase I, Lot 011882). The locations of the strips on the roll are shown in Figure 6.

Fiber Materials, Incorporated also prepared "scoured" samples for NASA-LeRC (Lot 021182) at the same six processing temperatures; scouring refers to solvent washing of the rayon felt precursor before pyrolysis to remove sizing. At the request of the contract monitor, these samples were included in the initial screening.

On the basis of early test results (see Figures 7 and 8), the unscoured felt sample processed at  $1650^{\circ}\text{C}$  appeared to give the optimum performance. This agreed with the results obtained in the previous program (16). On this basis, a second set of samples was ordered from FMI, processed at  $50^{\circ}$  intervals around  $1650^{\circ}\text{C}$  ( $1550^{\circ}$ ,  $1600^{\circ}$ ,  $1650^{\circ}$ ,  $1700^{\circ}$ ,  $1750^{\circ}\text{C}$ ; referred to as Phase II, Lot 051882), with the objective of more sharply defining the optimum processing temperature and/or establishing an acceptable range.

With the discovery of several discrepancies in the gold deposition processes between the standard NASA method (NASA-I) and the standard Giner, Inc. method (Double Immersion), the carbon felt characterization study was extended, overlapping the Catalyst Optimization Study (Section V). For this

reason, discussion of some of the data is deferred to the next section.

## B. Experimental Procedures

### 1. Physical Characteristics

Visual examination of the six Phase I rolls of felt indicated some thickness variation, particularly noticeable for the 1250°C felt. All materials were nominally 1/8 inch. The thickness of each felt roll was sampled in 10 places: 3 places across the width on each end, and 4 additional places down the length. The data points were taken by measuring across 2 x 2 inch metal plates placed on either side of the felt. The measurements for all six felts are presented in Table I. The 1250°C felt shows an average thickness of 70.7 mils (1.8 mm) compared to 143.5 mils (3.64 mm) for the 1650°C felt. The overall range is 54 - 150 mils. This variation in thickness presents some difficulties in making quantitative comparison of some properties.

Weight and thickness measurements of the scoured carbon felts are presented in Table II. These data and a value for carbon density of 2.0 g/cm<sup>2</sup> were used to calculate the theoretical quantities  $Q_{\text{Pb}^{2+}}$  and  $Q_{\text{Cr}^{3+}}$  which appear in some of the tabulated data. Similar data is presented in Table III for the Phase II felts; these samples were more uniform than the Phase I samples.

### 2. Gold Catalyzation

The Phase I unscoured carbon felts were catalyzed by all three of the procedures described in Section III, Double Immersion, NASA-I (standard procedure) and NASA-II (excess solution).

The Phase I scoured carbon felt samples were catalyzed by the Double Immersion method only.

The Phase II carbon felt samples were catalyzed by the NASA-I (standard) method only.

### 3. Testing

All samples were mounted in the "waxed-clip" holder as described in Section II-A and subjected to the standard cyclic voltammetry routines described in Section II-D. Representative voltammograms were shown in Figures 3 and 4.

#### C. Results

Comparative data were extracted from each of the voltammograms obtained by integrating portions of the curves to obtain the charge segments illustrated earlier in Figure 5.

For the Phase I felts catalyzed by the Double Immersion method, the charge segment data are presented in Table IV for unscoured samples and Tables V and VI for scoured samples (corresponding current data points are presented in Tables AI-I and AI-II in Appendix I). A number of the charge segment data points were plotted versus carbon felt processing temperature. These are: the hydrogen evolution charge  $Q_{\text{C}}\text{H}^+$  vs. T in Figure 9, lead deposited  $Q_{\text{a}}\text{Pb}$  vs. T in Figure 10, chromous ion oxidized  $Q_{\text{a}}\text{Cr}^{2+}$  vs. T in Figure 10a, and relative charging efficiency  $Q_{\text{a}}\text{Cr}^{2+}/Q_{\text{C}}\text{H}^+$  vs. T in Figure 11. It can be seen that the scoured felts exhibited more activity generally but showed lower charging efficiency, except for felts processed at 1800°C or higher. The unscoured felt processed at 1650°C appeared to represent a reasonable compromise in properties and the data obtained with unscoured felts were used as the basis for selecting the processing temperature range for Phase II felts. Reproducibility of the test data is discussed in Section V-D.

As discussed earlier, the set of Phase I unscoured felts were also catalyzed by the standard NASA method (NASA-I) and a modified NASA method (NASA-II). The charge segment data for both of these sets of samples are presented in Tables VII and VIII (corresponding current data points are presented in Table AI-III in Appendix I). The results obtained with the NASA-I method are compared to the results obtained with Double Immersion method and then with results obtained with the NASA-II method, in the following figures.

	NASA-I vs. Double Immersion	NASA-I vs. NASA-II
$Q_{C}H^{+}$ vs. T	Figure 12	Figure 16
$Q_{a}Pb$ vs. T	Figure 13	Figure 17
$Q_{a}Cr^{2+}$ vs. T	Figure 14	Figure 18
$Q_{a}Cr^{2+}/Q_{C}H^{+}$ vs. T.	Figure 15	Figure 19

The felts prepared by both the NASA-I and II methods showed higher activity in general than samples prepared by the Double Immersion method but some similar trends with felt processing temperature i.e. higher hydrogen evolution rates for the lower felt processing temperatures (1250° and 1350°C) and higher charging efficiencies in the mid-temperature range. The charging efficiency values for the graphite felt (2300°C) were exceptionally high in both cases, a feature not observed in any previous testing.

The Phase II samples, processed in a narrower temperature band around 1650°C, were catalyzed by the standard NASA method only. The charge segment data are presented in Tables IX and X (corresponding current data in Table AI-IV in Appendix I). The plots of charge segment data points versus carbon

felt processing temperature are as follows:  $Q_c H^+$  vs. T in Figure 20,  $Q_a Pb$  vs. T in Figure 21,  $Q_a Cr^{2+}$  vs. T in Figure 22 and  $Q_a Cr^{2+}/Q_c H^+$  vs. T in Figure 23. Although there is substantial variability in electrochemical performance over this processing temperature range and no clear optimum is apparent, it may be concluded that the entire range (1550 - 1750°C) yields carbon felt acceptable as a substrate for the negative electrode.

D. Conclusions and Recommendations

The expected negative electrode performance vs. carbon felt processing factors is as follows:

RECOMMENDED:

1650 - 1750°C; UNSCOURED

ACCEPTABLE:.....

1500 - 1800°C; UNSCOURED

QUESTIONABLE:

>1800°C; SCOURED

UNACCEPTABLE:

<1500°C; BOTH SCOURED AND UNSCOURED

HIGH ACTIVITY, LOW COST, BUT LOW CHARGING EFFICIENCY

>1800°C; UNSCOURED

LOW ACTIVITY, FRAGILE, EXPENSIVE

Inner End  
(Against Carbonizer Tube)

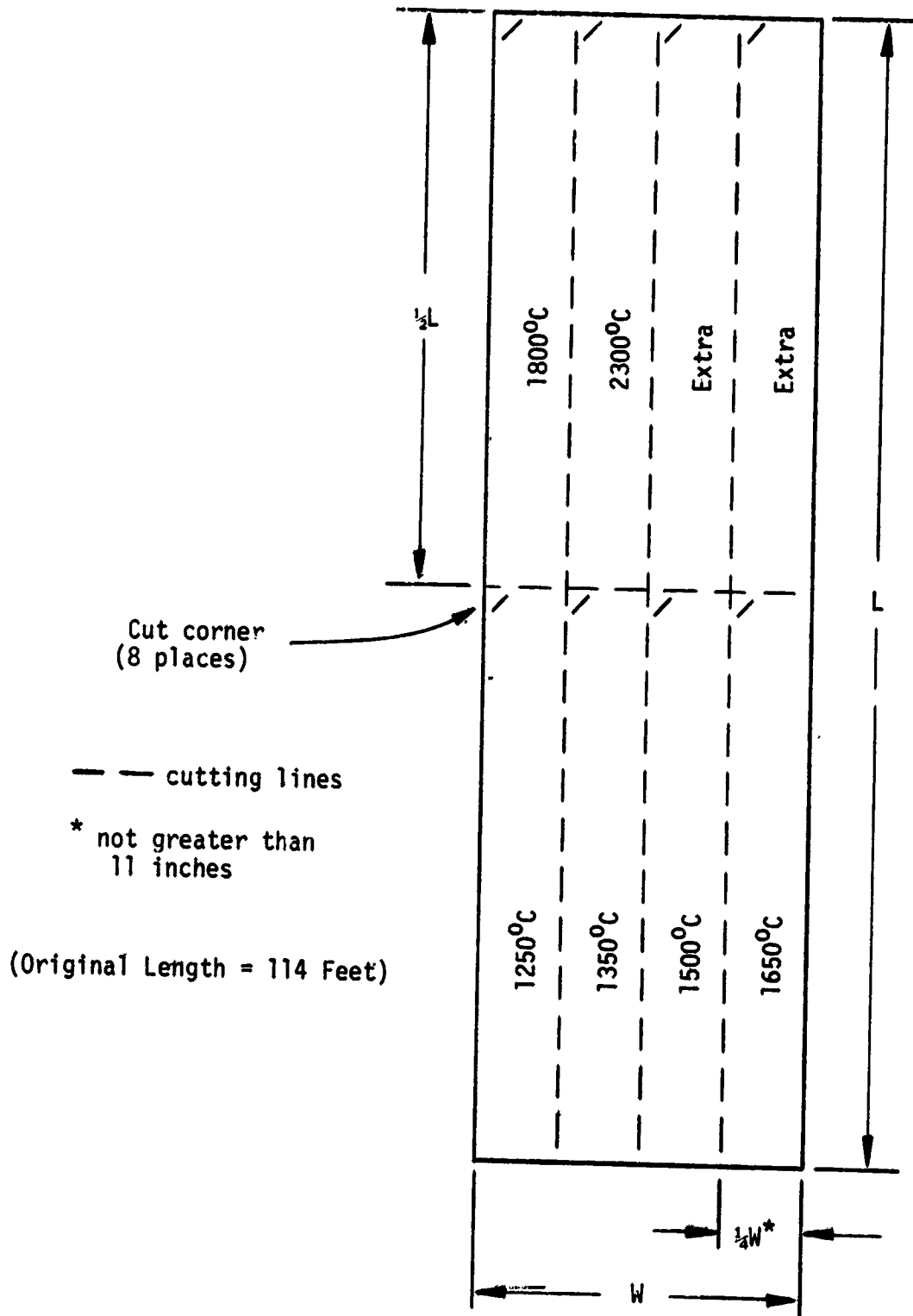


Figure 6. CUTTING PLAN FOR PHASE I CARBON FELT

Phase I Characterization Study  
 Data in Table IV.  
 Double Immersion Catalyzation Proc.

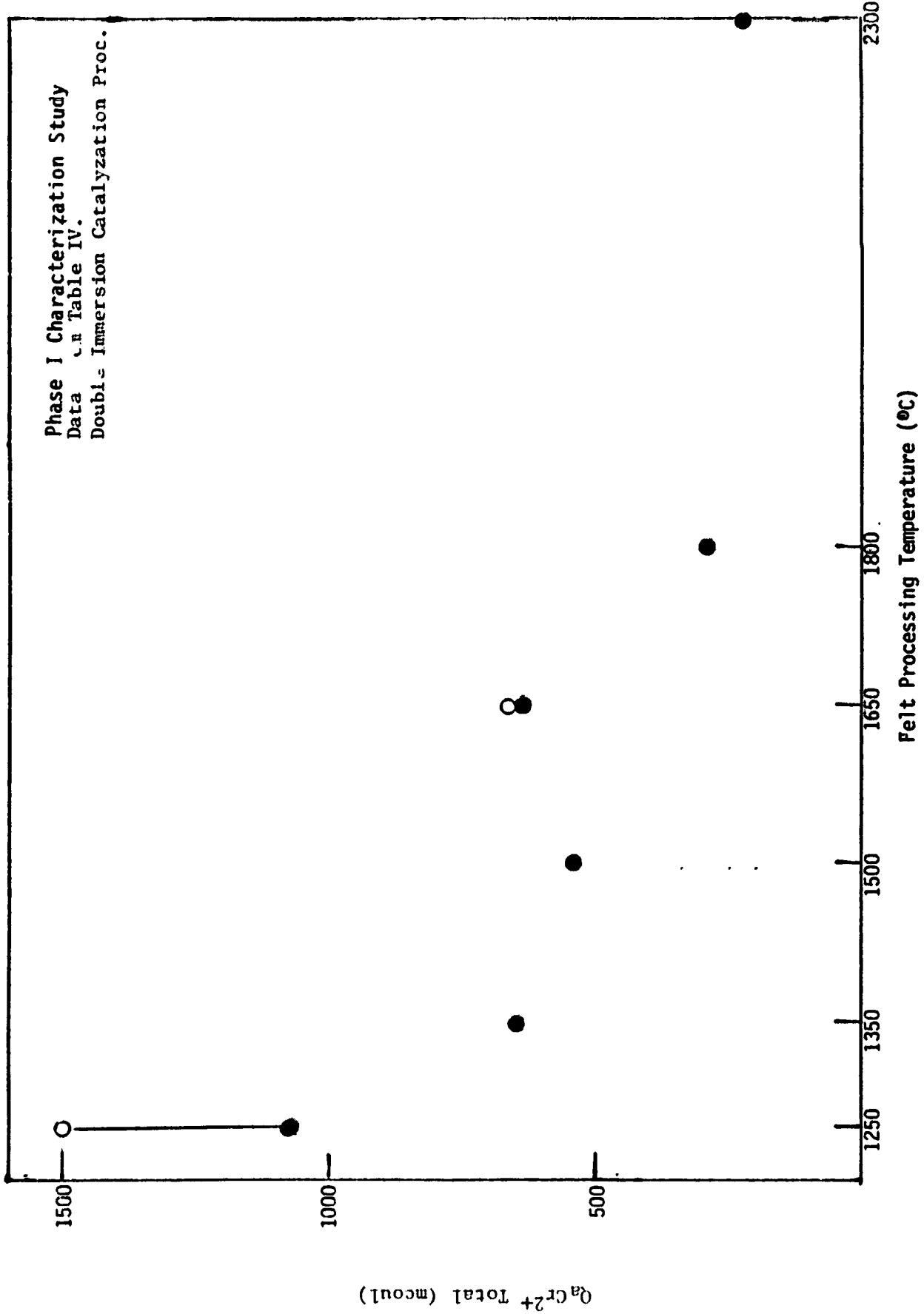


Figure 7. Total Anodic Chromium Charge versus Felt Processing Temperature

Phase I Characterization  
 Data from Table IV.  
 Double Immersion Catalyzation Proc.

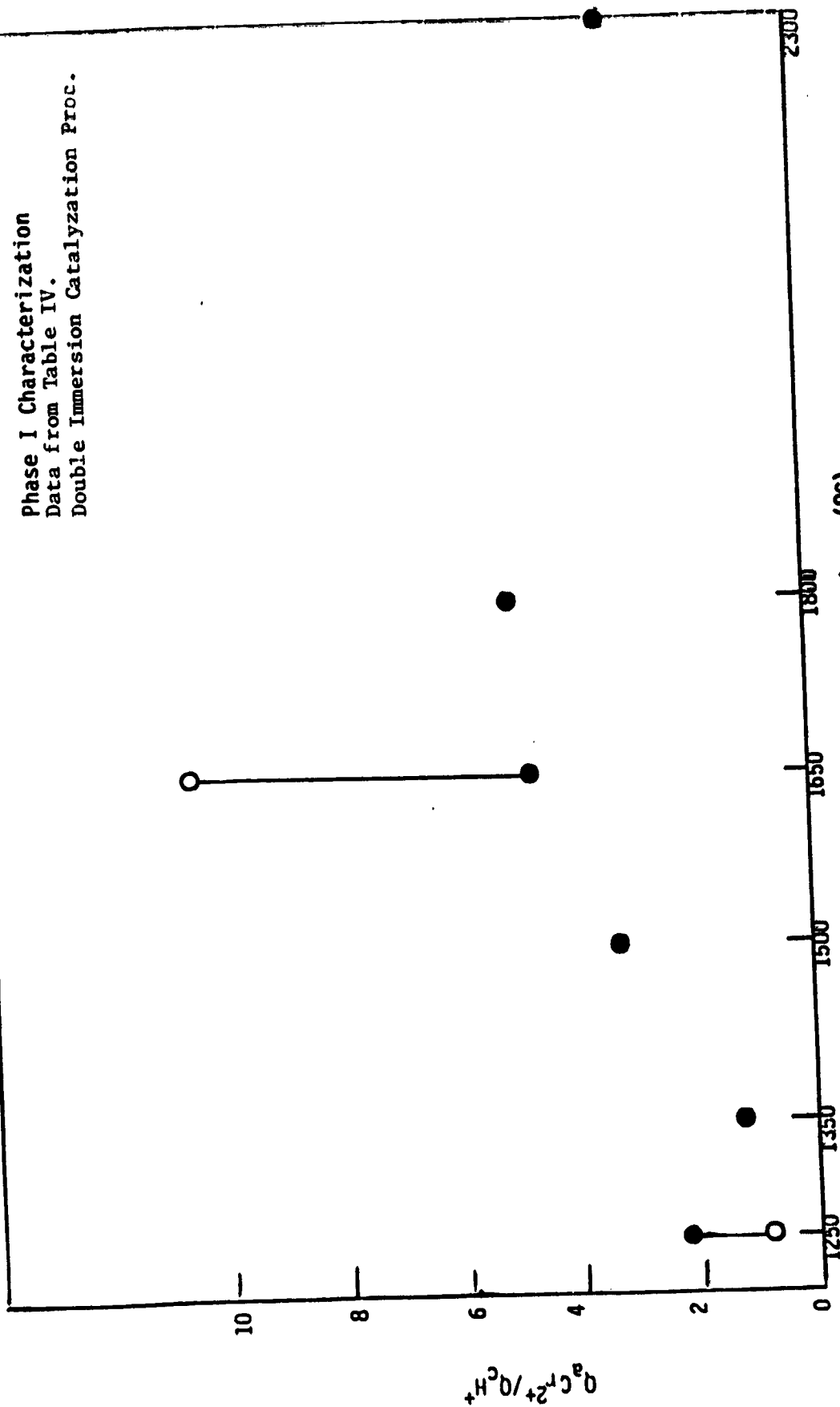


Figure 8. Ratio  $Q_a Cr^{2+} / Q_c H^+$  versus Felt Processing Temperature

TABLE I. PHASE I CHARACTERIZATION STUDY - UNSCURED FELTS

CARBON FELT THICKNESS MEASUREMENTS  
(FMI-C-1/8, Lot 011882, Unscoured)

<u>Felt Processing Temperature</u>	<u>Thickness by Location (mils)</u>						<u>Mean (mils)</u>	<u>Std. Dev.</u>
1250 <sup>o</sup> c	83					54	70.9	12.2
	80					55		
	82	73	71	85	71	55		
1350 <sup>o</sup> c	143					138	141.7	3.4
	139					144		
	141	135	145	143	145	144		
1500 <sup>o</sup> c	146					137	140.5	3.3
	143					141		
	142	141	143	136	140	136		
1650 <sup>o</sup> c	148					136	143.5	5.7
	150					143		
	150	148	137	146	136	141		
1800 <sup>o</sup> c	141					110	124.1	11.7
	139					114		
	135	123	109	126	128	116		
2300 <sup>o</sup> c	136					108	125.6	10.3
	136					113		
	134	128	120	130	134	117		

TABLE II. PHASE I CHARACTERIZATION STUDY - SCOURED FELTS

WEIGHT AND THICKNESS MEASUREMENTS OF 49 cm<sup>2</sup> SAMPLES  
 (FMI-C-1/8 Lot 021182, Scoured Carbon Felts)

<u>Felt Processing Temperature (°C)</u>	<u>Weight<sup>(1)</sup> (g)</u>	<u>Mean Weight (g)</u>	<u>Thickness<sup>(2)</sup> (mils)</u>	<u>Mean Thickness (mils)</u>	<u>Stand. Dev.</u>
1250	1.340 1.374	1.358	69, 63 70, 59	65	5.2
1350	1.266	1.266	61, 69, 60	63	4.9
1500	1.435 1.411	1.423	97, 103 137, 123	115	18.4
1650	1.448 1.413	1.431	125, 129 130, 121	126	4.1
1800	1.424 1.420	1.422	124, 123 143, 134	131	9.4
2300	1.281 1.208	1.244	136, 128 138, 131	133	4.6

(1) One measurement per sample.

(2) Multiple measurements per sample, one sample per line.

TABLE III. PHASE II CHARACTERIZATION STUDY

WEIGHT AND THICKNESS MEASUREMENTS OF 49 cm<sup>2</sup> SAMPLES  
(FMI-C-1/8 Lot 051882 Carbon Felt, Unscoured)

Felt Processing Temperature (°C)	Weight <sup>(1)</sup> (g)	Mean Weight (g)	Thickness <sup>(2)</sup> (mils)	Mean Thickness (mils)	Stand. Dev.
1550	1.33	1.36	130, 127, 134	130	3.5
	1.39				
1600	1.25	1.24	127, 129, 123	126	3.0
	1.24				
1650	1.30	1.28	117, 111, 127	118	8.1
	1.25				
1700	1.23	1.21	119, 119, 129	122	5.8
	1.19				
1750	1.36	1.30	126, 132, 144	134	9.2
	1.25				

(1) One measurement per sample.

(2) Multiple measurements on one 49 cm<sup>2</sup> sample.

TABLE IV. PHASE I CHARACTERIZATION STUDY (UNSCOURED FELTS)

Comparison of Quantities of Reactants Reduced or Oxidized to  
Quantities of Reactants Theoretically Available

All felts activated by Double Immersion Process -  $12.5\mu\text{g Au/cm}^2$ . Theoretical reactant quantities available based on calculated open volume of felt sample and solution concentration.

Felt Processing Temp. ( $^{\circ}\text{C}$ )	$Q_t\text{Pb}^{2+}$ Theor. (m coul)	$Q_a\text{Pb}$ Meas. (m coul)	$Q_c\text{H}^+$ Meas. (3) (m coul)	$Q_t\text{Cr}^{3+}$ Theor. (m coul)	$Q_c\text{Cr}^{3+}$ Meas. (4) (m coul)	$Q_a\text{Cr}^{2+}$ Meas. (m coul)	$Q_{cd}\text{Cr}^{3+}$ Calc. (5) (m coul)
1250	70	119	483	1740	1478	1073	405
1250 <sup>(1)</sup>	79	162	1898	1968	1990	1500	490
1350	130	105	520	3240	871	649	222
1500	121	108	164	3020	1031	538	493
1650	128	97	133	3190	1025	636	389
1650 <sup>(2)</sup>	128	112	63	3190	1261	666	595
1800	102	86	57	2540	619	289	330
2300	103	70	67	2570	580	217	363

1) Second Sample of 1250 $^{\circ}\text{C}$  felt

2) Values taken from  $\text{Fe}^{2+}$  Crossover test before addition of  $\text{Fe}^{2+}$

3)  $Q_c\text{H}^+ = Q_c\text{Pb}^{2+}, \text{H}^+ - Q_a\text{Pb}$  ( $Q_c\text{Pb}^{2+}$  is defined to be same as  $Q_a\text{Pb}$ )

4)  $Q_c\text{Cr}^{3+} = Q_c\text{Cr}^{3+}, \text{Pb}^{2+}, \text{H}^+ - *Q_c\text{Pb}^{2+}, \text{H}^+$ ; (\* meas. without  $\text{Cr}^{3+}$ )

5)  $Q_{cd}^{**}\text{Cr}^{3+} = Q_c\text{Cr}^{3+} - Q_a\text{Cr}^{2+}$ ; (\*\* charge attributable to diffusion)

TABLE V. PHASE I CHARACTERIZATION STUDY (SCOURED FELTS)

Comparison of Quantities of Reactants Reduced or Oxidized  
to Quantities of Reactants Theoretically Available

Theoretical reactant quantities available based on calculated open volume of felt sample and solution concentration.

Felt Processing Temp. (°C)	Q <sub>t</sub> Pb <sup>2+</sup> Theor. (mcoul)	Q <sub>a</sub> Pb Meas. (mcoul)	Q <sub>C</sub> H <sup>+</sup> Meas. (mcoul)	Q <sub>t</sub> Cr <sup>3+</sup> Theor. (mcoul)	Q <sub>C</sub> Cr <sup>3+</sup> Meas. (mcoul)	Q <sub>a</sub> Cr <sup>2+</sup> Meas. (mcoul)	Q <sub>Cd</sub> Cr <sup>3+</sup> Calc. (mcoul)
1250 <sup>(1)</sup>	57	178	669	1423	3297	1418	1879
1350 <sup>(1)</sup>	55	199	2685	1385	3002	1322	1680
1500 <sup>(1)</sup>	104	134	555	2610	2922	1013	1909
1650 <sup>(1)</sup>	115	115	234	2876	1271	888	383
1800 <sup>(1)</sup>	121	147	161	3020	5028	2829	2199
2300 <sup>(1)</sup>	123	129	226	3083	1770	1281	489

(1) FMI - C-1/8 Lot 021182, Scoured, Activated by Double Immersion

Process - 12.5µg/cm<sup>2</sup>.

TABLE VI. PHASE I CHARACTERIZATION STUDY (SCOURED FELTS)

Comparison of Peak and Trailing Cr<sup>2+</sup> Oxidation Charges

Felt Processing Temp. (°C)	Q <sub>a</sub> Cr <sup>2+</sup> (mCoul)	Q <sub>a</sub> Cr <sup>2+</sup> (peak) (mCoul)	Q <sub>a</sub> Cr <sup>2+</sup> (trailing) (mCoul)
1250 <sup>(1)</sup>	1,418	1,266	152
1350 <sup>(1)</sup>	1,322	1,062	260
1500 <sup>(1)</sup>	1,013	661	352
1650 <sup>(1)</sup>	888	348	540
1800 <sup>(1)</sup>	2,829	2,313	516
2300 <sup>(1)</sup>	1,281	699	582

(1) FMI-C-1/8 Lot 021182, Scoured, Activated by Double Immersion Process - 12.5µg/cm<sup>2</sup>.

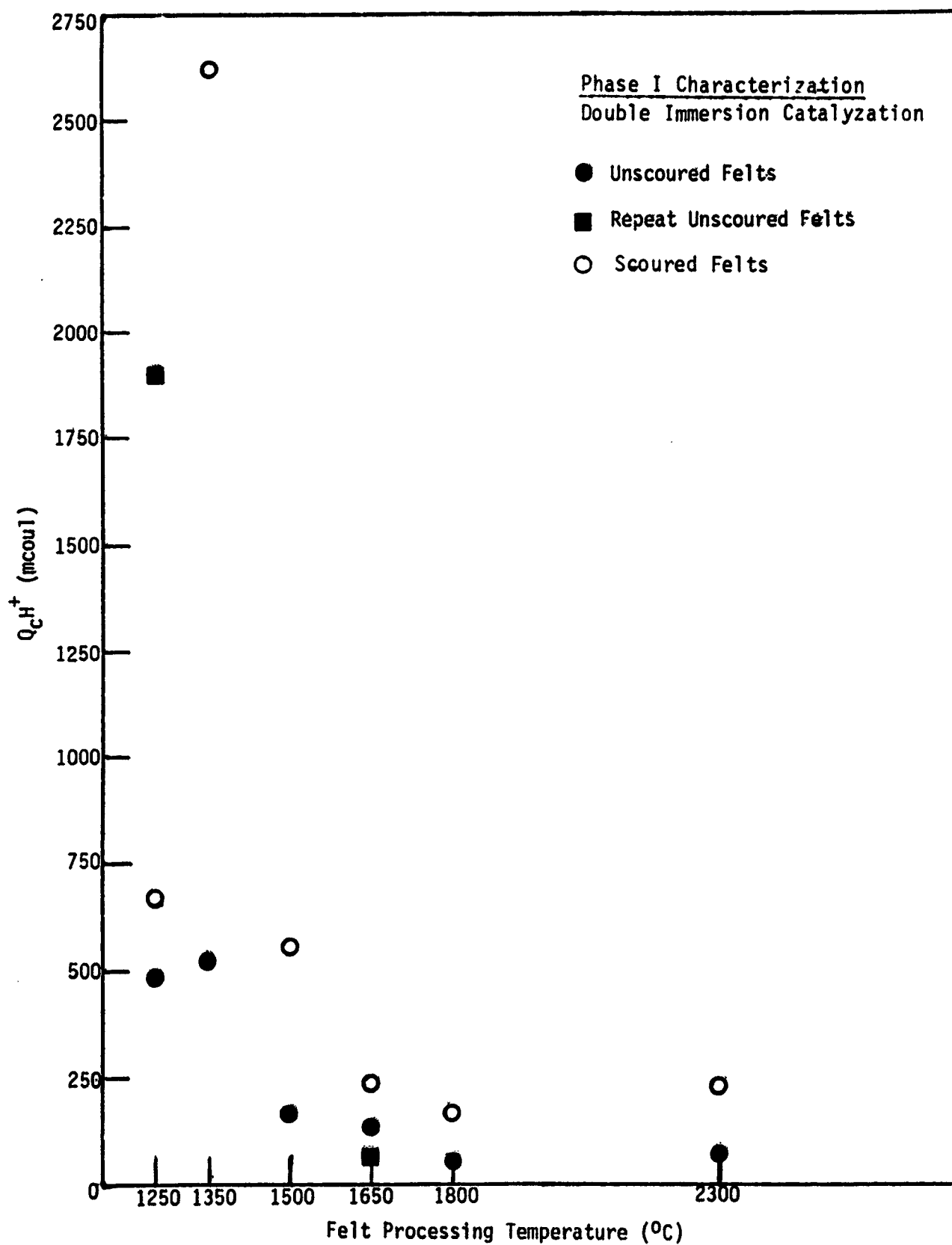


Figure 9. H<sup>+</sup> Reduction Charge (Q<sub>c</sub>H<sup>+</sup>) versus Felt Processing Temperature.

Figure 10. Lead Loading as Measured by the Anodic Lead Charge ( $Q_aPb$ ) versus Felt Processing Temperature.

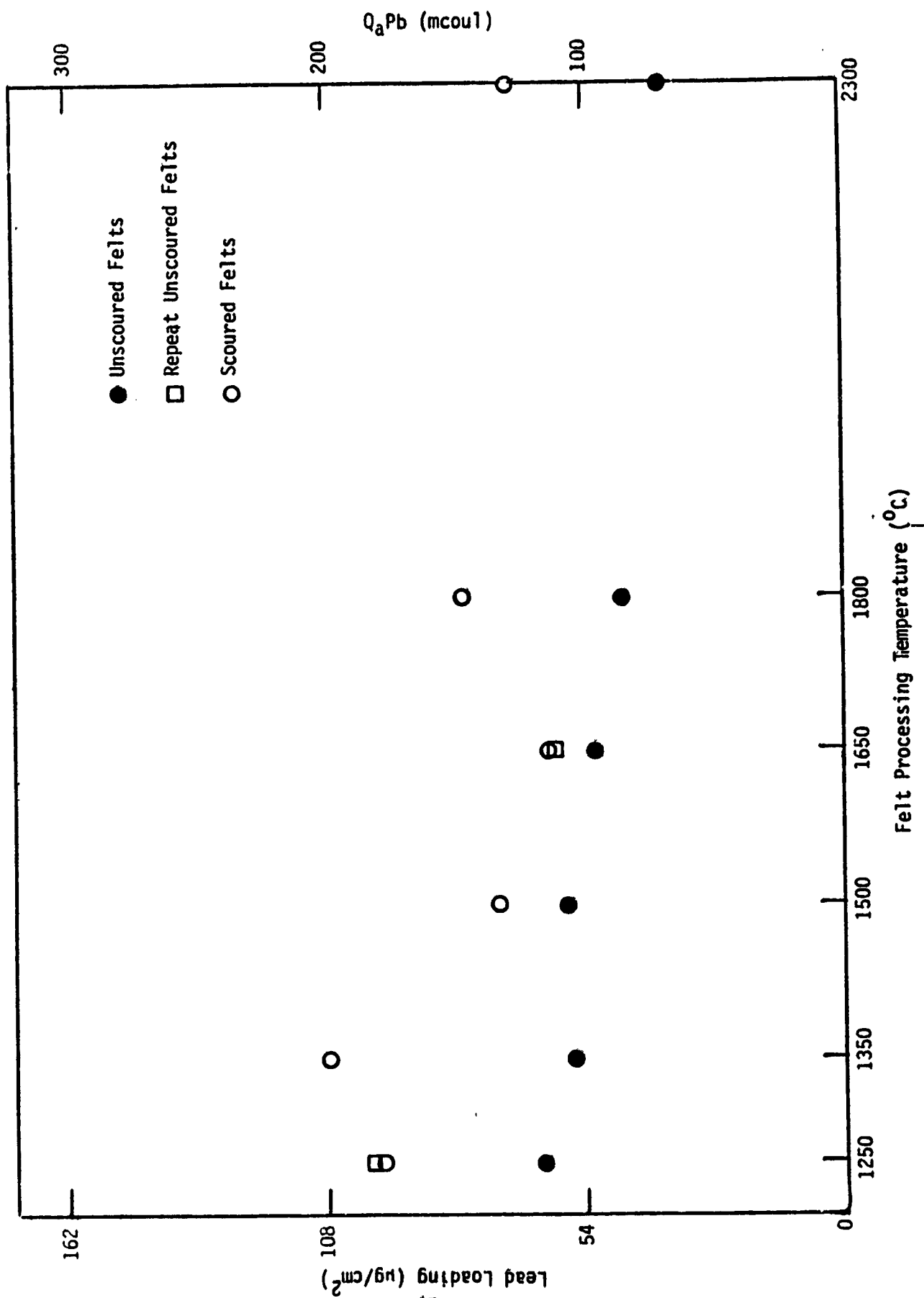
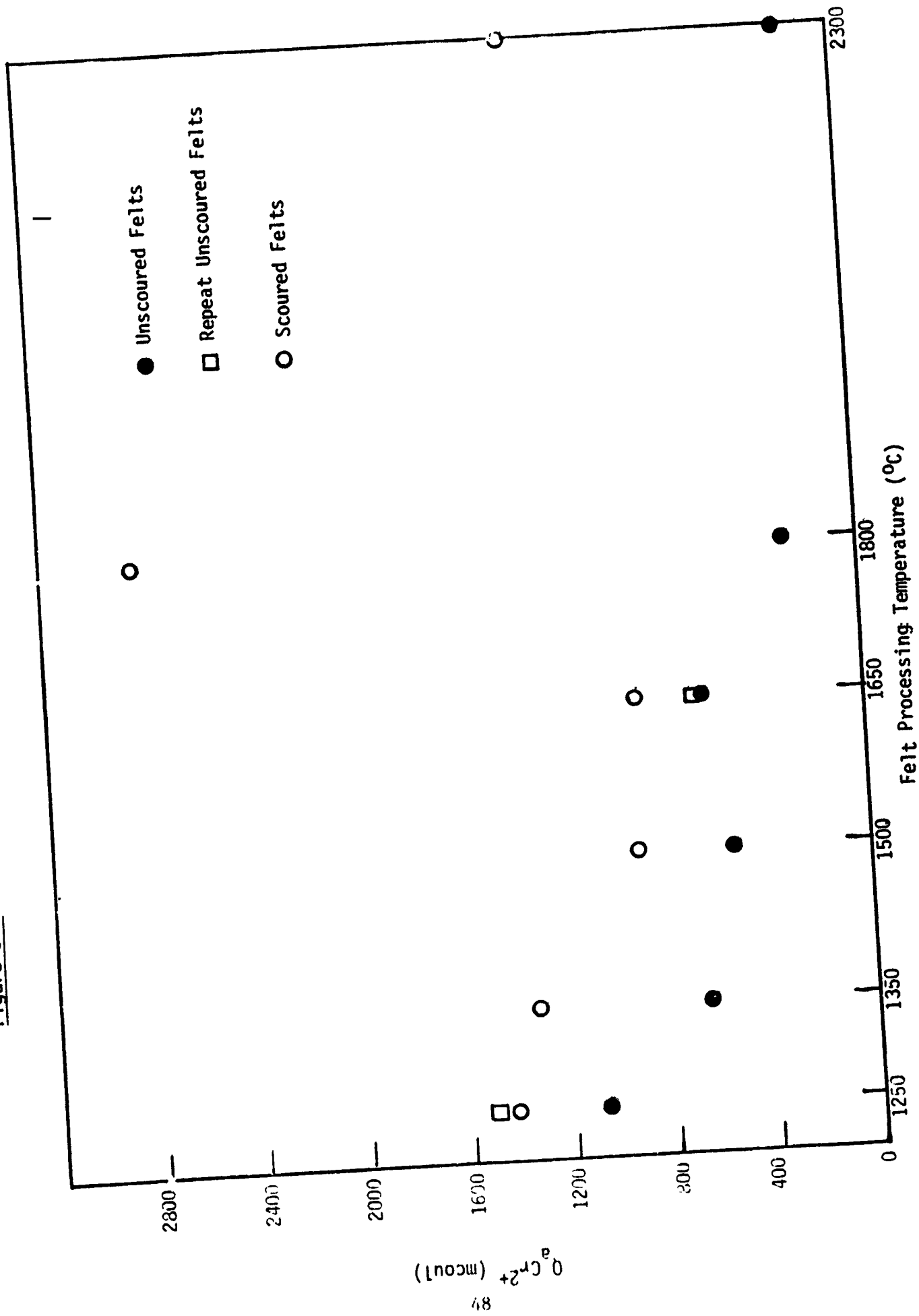


Figure 10a. Total Anodic Chromium Charge versus Felt Processing Temperature



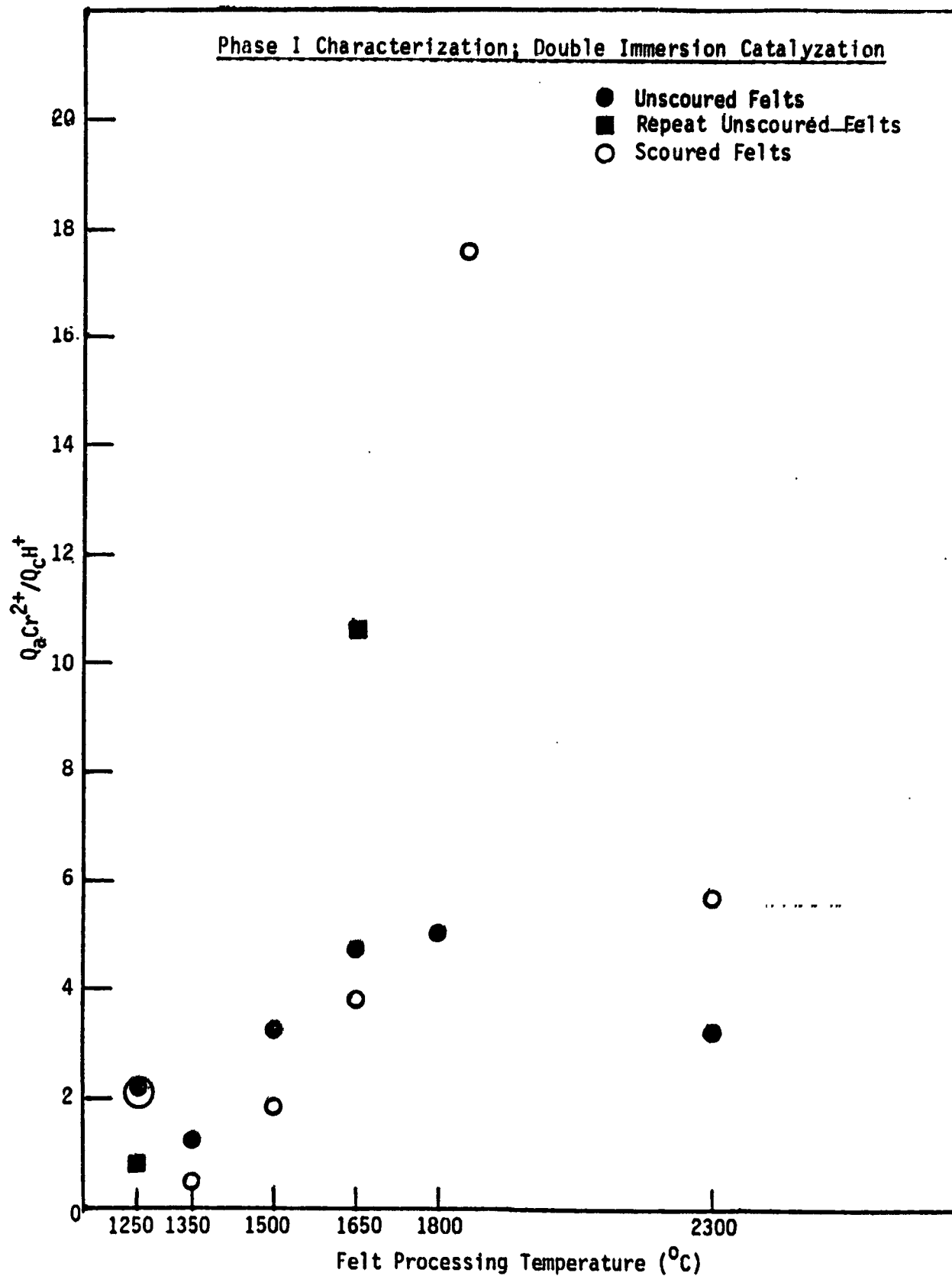


Figure 11. Ratio  $Q_{aCr^{2+}}/Q_{cH^+}$  versus Felt Processing Temperature.

TABLE VII. NASA-I VERSUS NASA-II CATALYZATION METHODS

Comparison of Quantities of Reactants Reduced or Oxidized to Quantities of Reactants Theoretically Available

Theoretical reactant quantities available based on calculated open volume of felt sample and solution concentration.

Felt Processing Temp. (°C)	$Q_t \text{Pb}^{2+}$ Theor. (mcoul)	$Q_a \text{Pb}$ Meas. (mcoul)	$Q_c \text{H}^+$ Meas. (mcoul)	$Q_t \text{Cr}^{3+}$ Theor. (mcoul)	$Q_c \text{Cr}^{3+}$ Meas. (mcoul)	$Q_a \text{Cr}^{2+}$ Meas. (mcoul)	$Q_{cd} \text{Cr}^{3+}$ Calc. (mcoul)
1250(1)	70	154	207	1740	2045	1149	896
1350	130	116	90	3240	1626	1187	439
1500	121	112	36	3020	2045	1275	770
1650	128	116	47	3190	1662	1109	553
1800	102	89	21	2540	914	346	568
2300	103	110	25	2570	1245	890	355
1250(2)	70	252	3129	1740	10892	2186	870 <sup>f</sup>
1350	130	197	472	3240	3462	1895	156 <sup>f</sup>
1500	121	177	302	3020	7438	2110	5328
1650	128	220	729	3190	5682	2284	3398
1800	102	265	548	2540	5905	2647	3258
2300	103	152	147	2570	2051	1391	660

(1) FMI-C-1/8 Lot 011882, Activated by NASA-I Method, 12.5µg/cm<sup>2</sup>.

(2) FMI-C-1/8 Lot 01182, Activated by NASA-II Method, 12.5µg/cm<sup>2</sup>.

TABLE VIII. NASA-I VERSUS NASA-II CATALYZATION METHODS

Comparison of Peak and Trailing Cr<sup>2+</sup> Oxidation Charges

Felt Processing Temp. (°C)	Q <sub>a</sub> Cr <sup>2+</sup> (mcou1)	Q <sub>a</sub> Cr <sup>2+</sup> (peak) (mcou1)	Q <sub>a</sub> Cr <sup>2+</sup> (trailing) (mcou1)
1250 <sup>(1)</sup>	1149	917	232
1350	1187	787	400
1500	1275	965	310
1650	1109	838	271
1800	346	217	129
2300	890	529	361
1250 <sup>(2)</sup>	2186	1082	1104
1350	1895	1372	523
1500	2110	1812	298
1650	2284	2013	271
1800	2647	2245	402
2300	1391	810	581

(1) FMI-C-1/8 Lot 011882, activated by NASA-I method, 12.5 μg Au/cm<sup>2</sup>

(2) FMI-C-1/8 Lot 011882, activated by NASA-II method, 12.5 μg Au/cm<sup>2</sup>

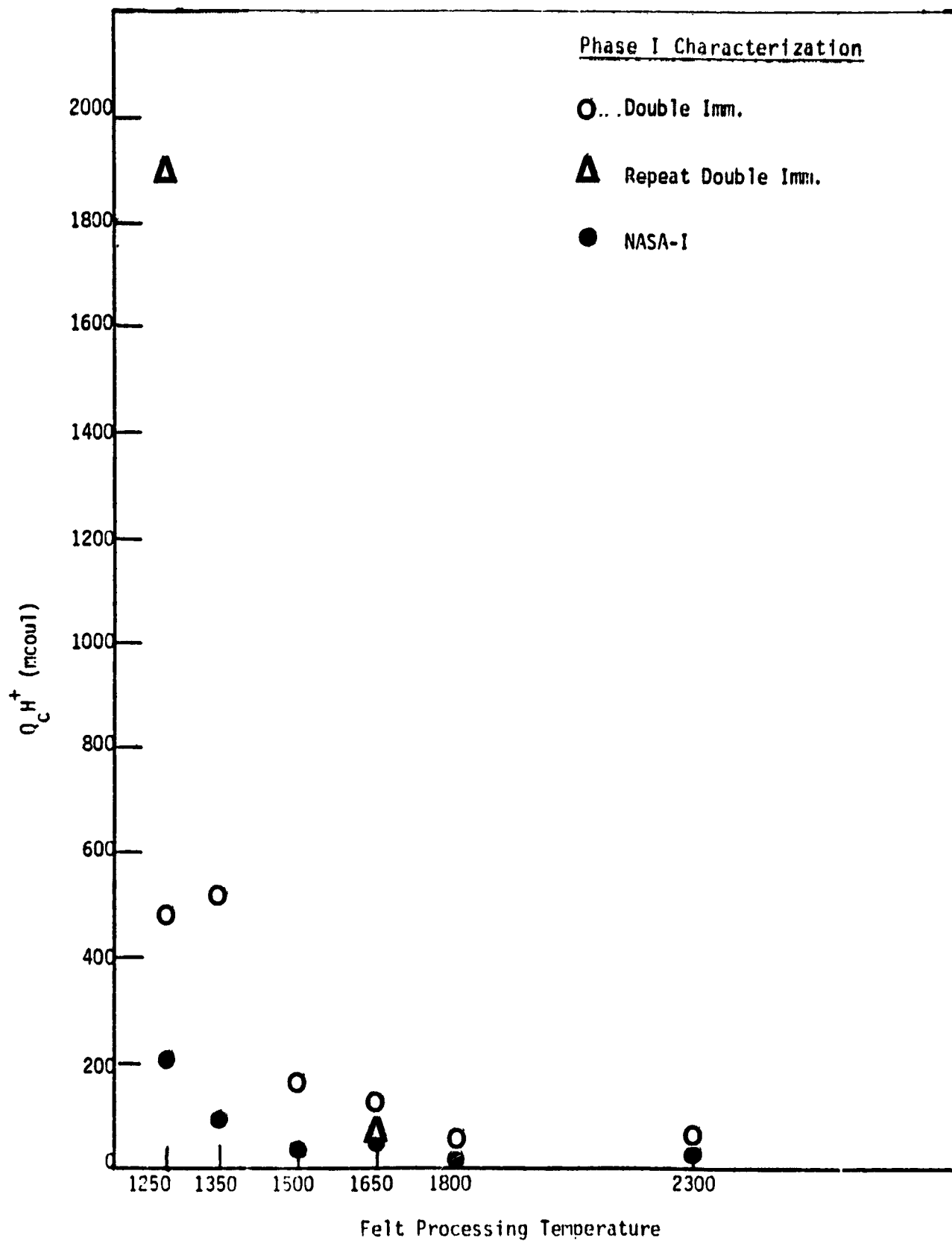


Figure 12. H<sup>+</sup> Reduction Charge (Q<sub>c</sub>H<sup>+</sup>) versus Felt Processing Temperature.

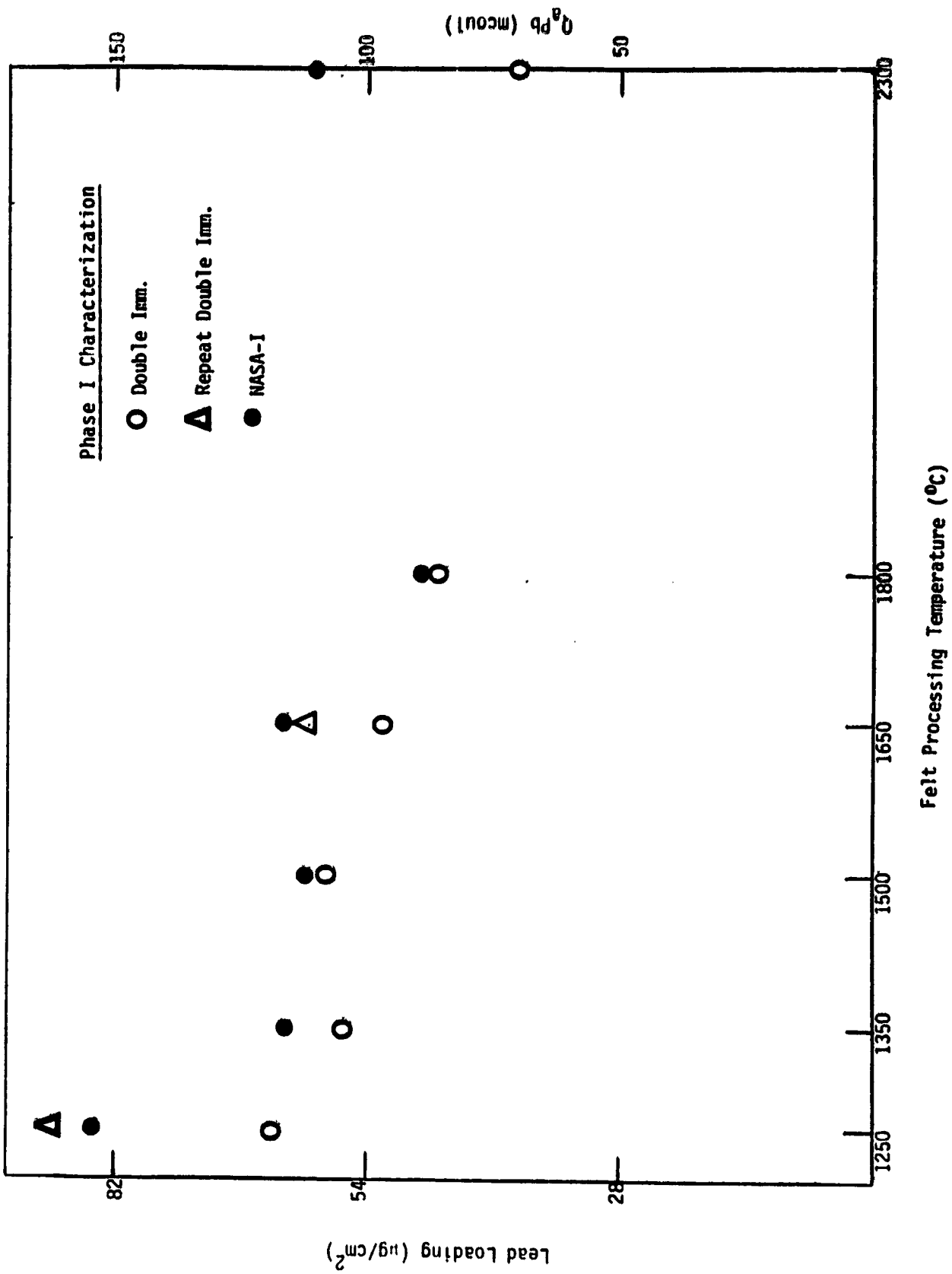


Figure 13. Lead Loading as Measured by the Anodic Lead Charge (Q<sub>a</sub>Pb) versus Felt Processing Temperature.

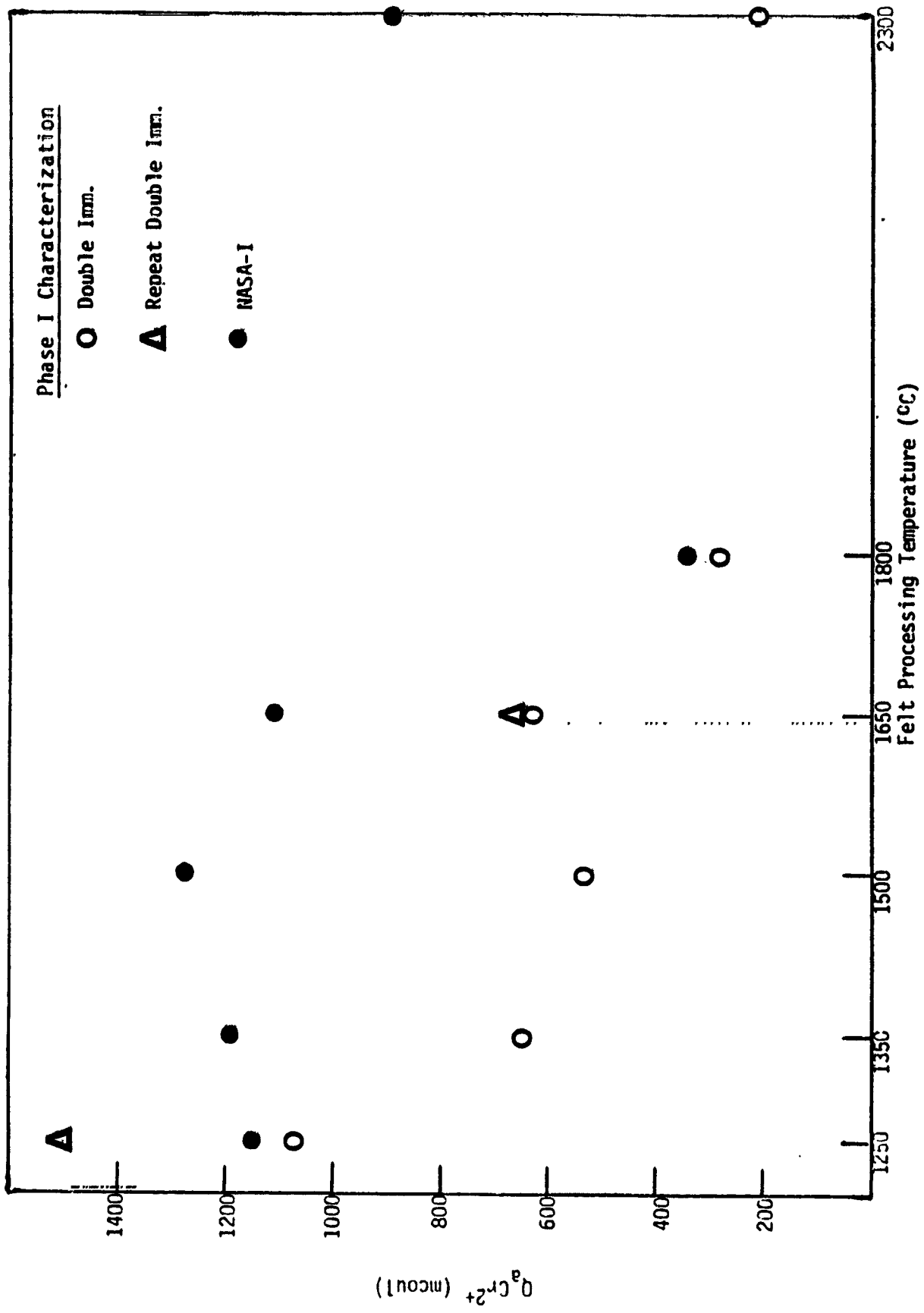


Figure 14. Total Anodic Chromium Charge versus Felt Processing Temperature.

Phase I Characterization

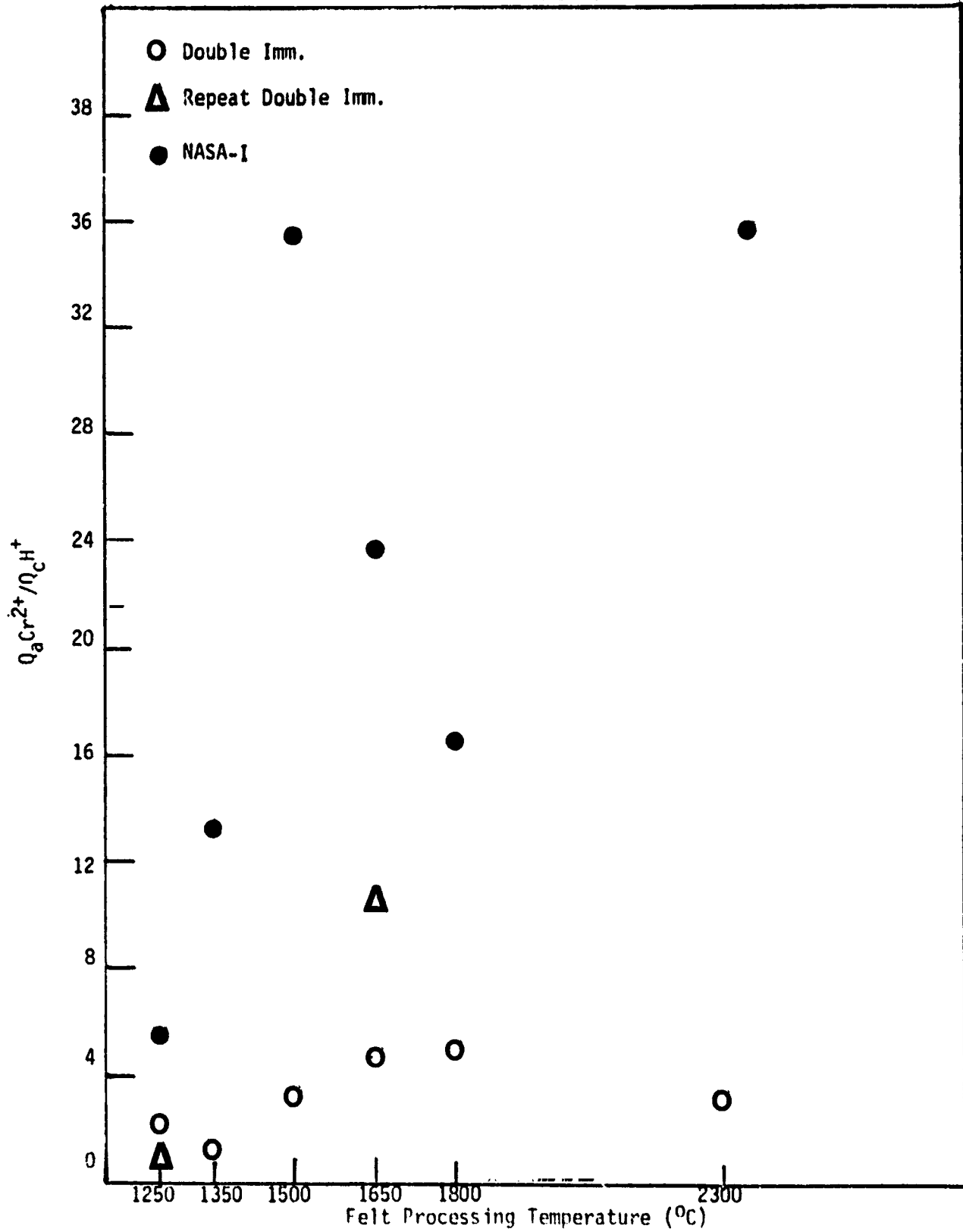


Figure 15. Ratio  $Q_dCr^{2+}/Q_cH^+$  versus Felt Processing Temperature.

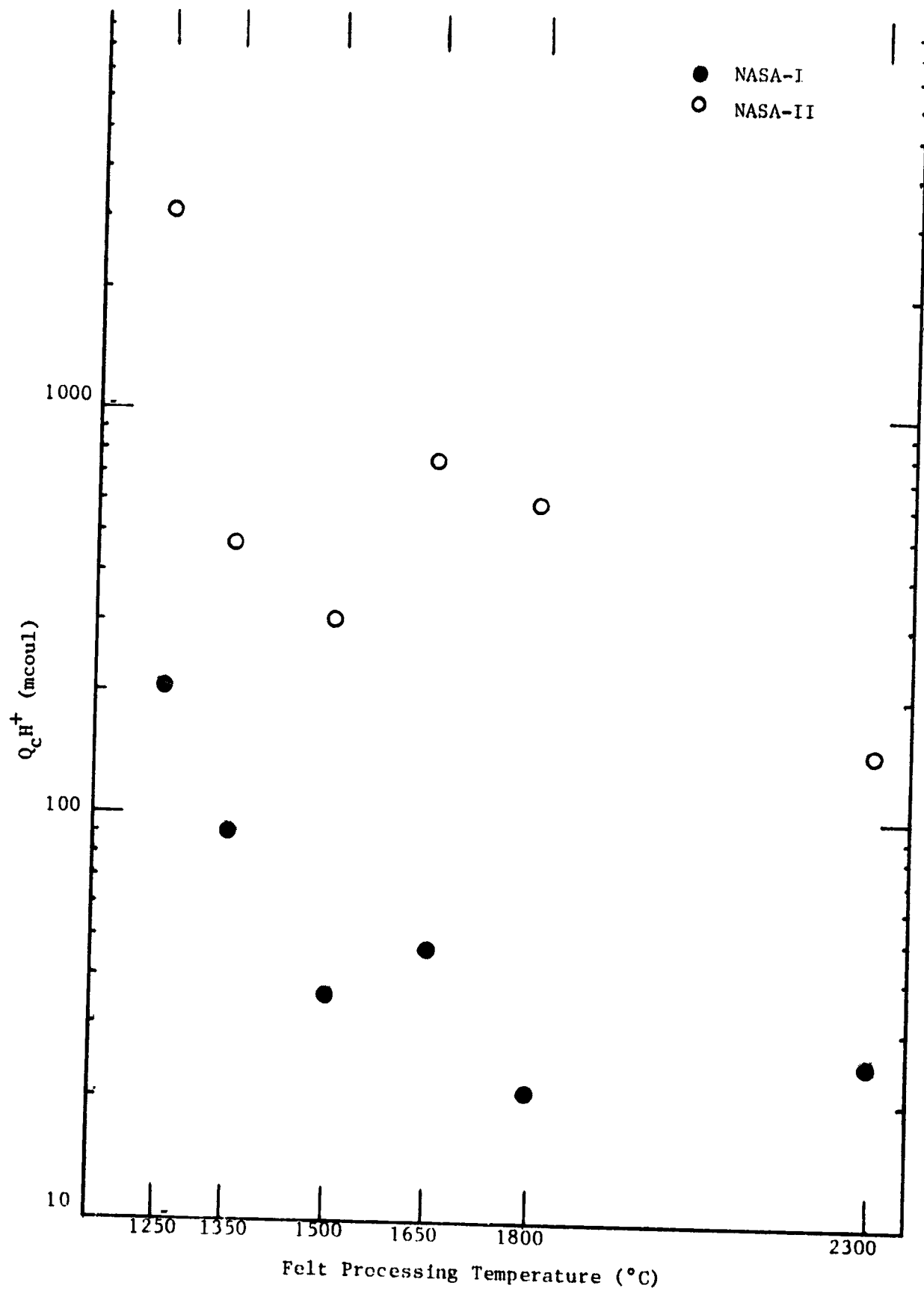
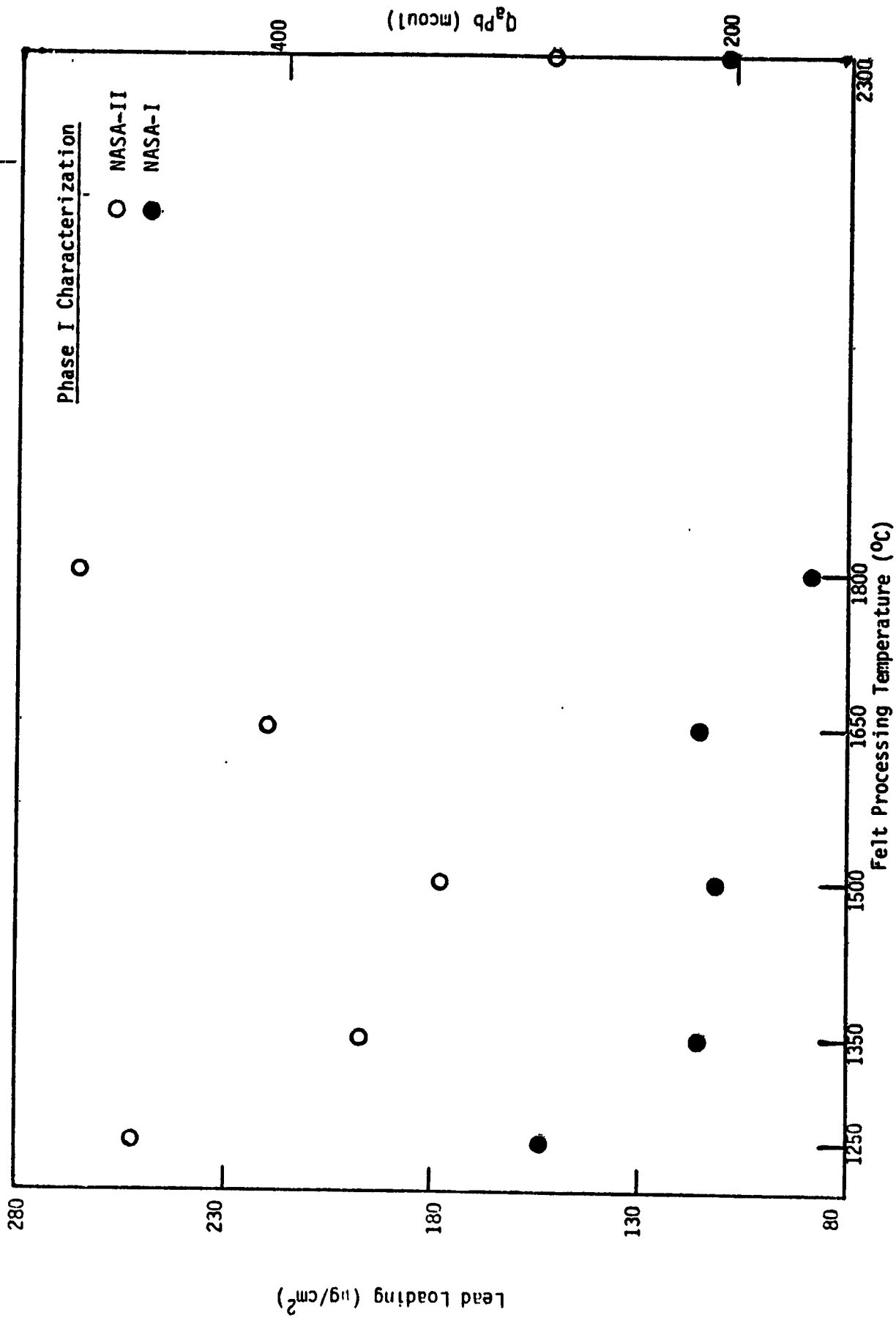
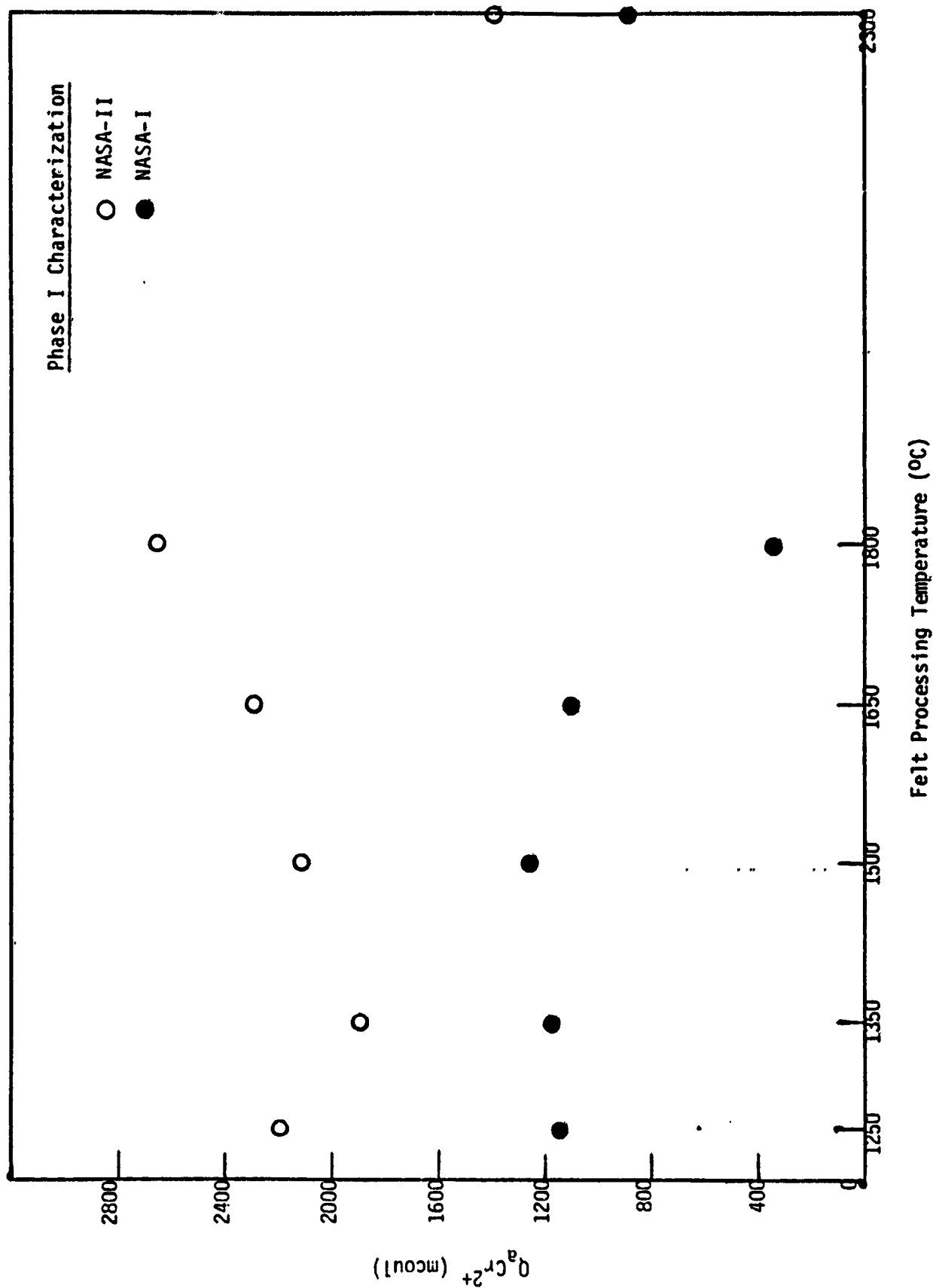


Figure 16.  $H^+$  Reduction Charge ( $Q_c H^+$ ) on Pb/Au versus Felt Processing Temperature.



**Figure 17.** Lead Loading as Measured by the Anodic Lead Charge (Q<sub>a</sub>Pb) versus Felt Processing Temperature.



**Figure 18.** Total Anodic Chromium Charge Versus Felt Processing Temperature.

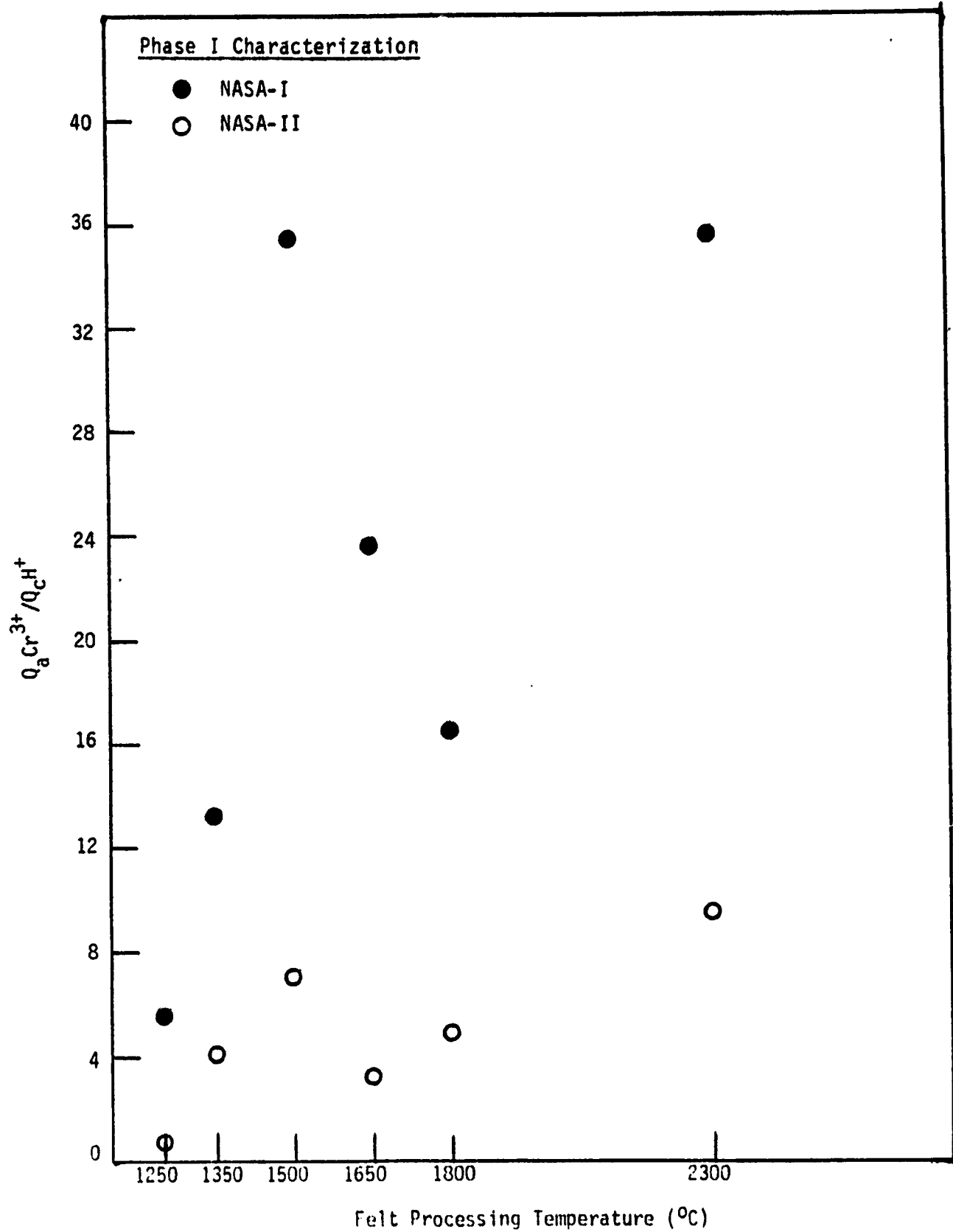


Figure 19. Ratio  $Q_aCr^{2+}/Q_cH^+$  versus Felt Processing Temperature.

TABLE IX. PHASE II CHARACTERIZATION STUDY

Comparison of Quantities of Reactants Reduced or Oxidized  
to Quantities of Reactants Theoretically Available

Theoretical reactant quantities available based on calculated open volume of felt sample and solution concentration.

Electrode Description (NASA-I Catalyzation)	Q <sub>t</sub> Pb <sup>2+</sup> Theor. (mcoul)	Q <sub>a</sub> Pb Meas. (mcoul)	Q <sub>c</sub> H <sup>+</sup> Meas. (mcoul)	Q <sub>t</sub> Cr <sup>3+</sup> Theor. (mcoul)	Q <sub>c</sub> Cr <sup>3+</sup> Meas. (mcoul)	Q <sub>a</sub> Cr <sup>2+</sup> Meas. (mcoul)	Q <sub>cd</sub> Cr <sup>3+</sup> Calc. (mcoul)
Felt Proc. Temp. 1550°C	119	116	9	2977	1571	1110	461
1600°C	116	148	26	2890	2296	1544	752
1650°C	108	86	16	2697	1549	1043	506
1700°C	112	93	8	2798	1208	746	482
1750°C	123	200	35	3078	2861	2032	829

TABLE X. PHASE II CHARACTERIZATION STUDY

Comparison of Peak and Trailing Cr<sup>2+</sup> Oxidation Charges

Electrode Description (NASA-I Catalyztion)	Q <sub>a</sub> Cr <sup>2+</sup> (mcoul)	Q <sub>a</sub> Cr <sup>2+</sup> (peak) (mcoul)	Q <sub>a</sub> Cr <sup>2+</sup> (trailing) (mcoul)	Q <sub>a</sub> Cr <sup>2+</sup> (peak) / Q <sub>a</sub> Cr <sup>2+</sup> (trailing)
Felt Proc. Temp.				
1550°C	1110	626	484	1.3
1600°C	1544	1110	434	2.6
1650°C	1043	811	232	3.5
1700°C	746	307	439	0.7
1750°C	2032	1464	568	2.6

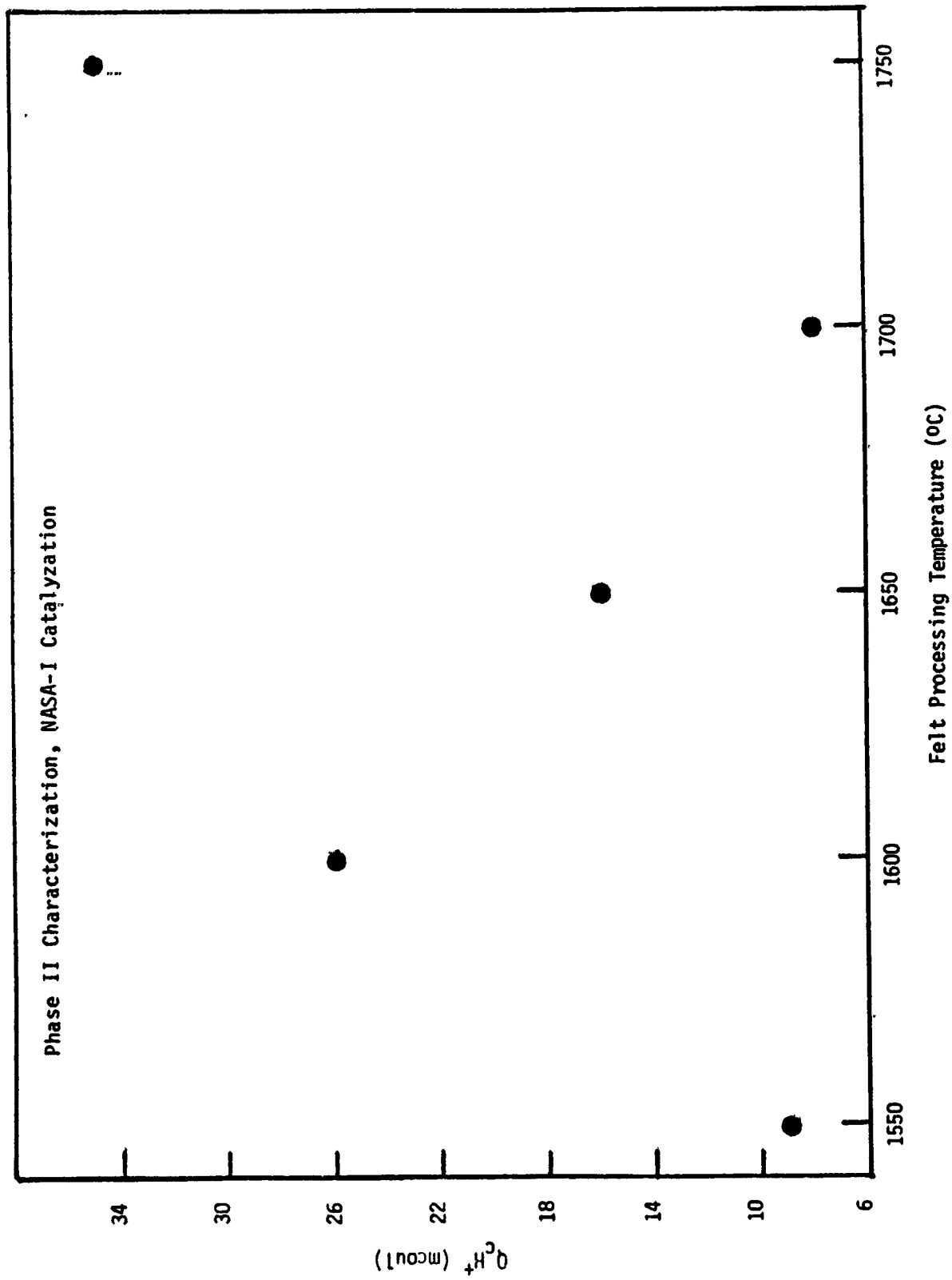


**Figure 20.**  $H^+$  Reduction Charge ( $Q_{cH^+}$ ) on Pb/Au versus Felt Processing Temperature.

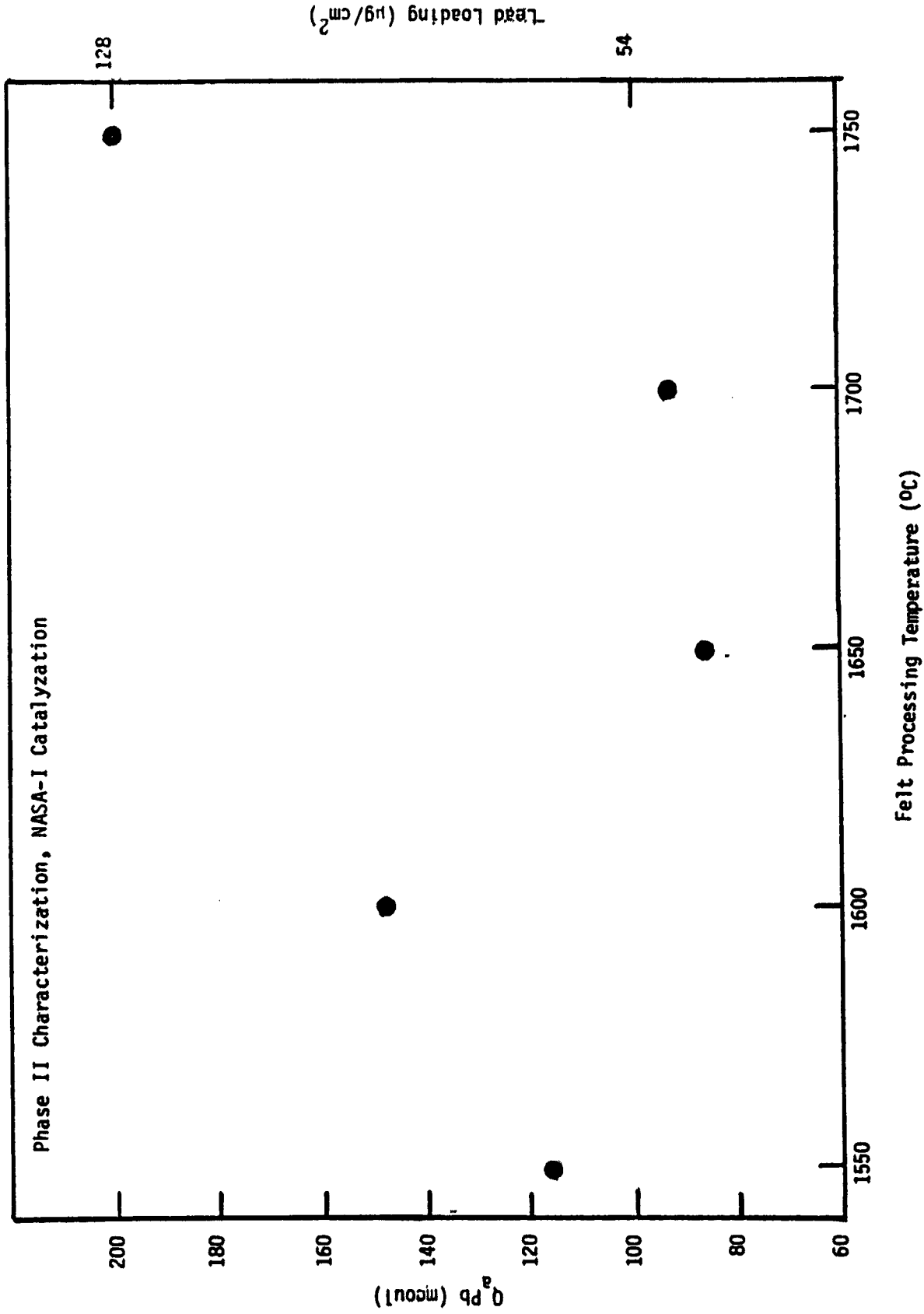


Figure 21. Lead Loading as Measured by the Anodic Lead Charge ( $Q_a \text{ Pb}$ ) versus Felt Processing Temperature.

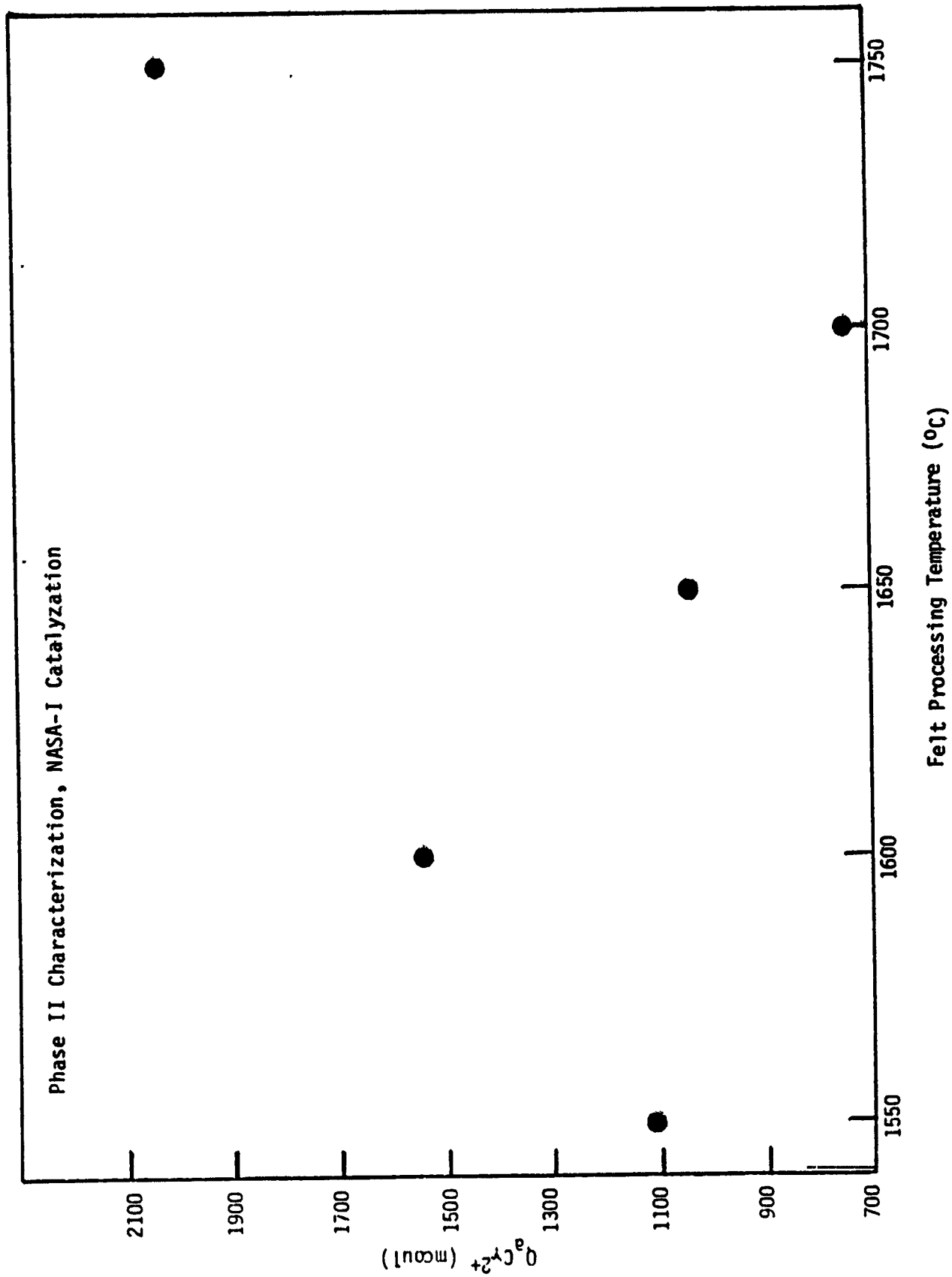


Figure 22. Total Anodic Chromium Charge versus Felt Processing Temperature.

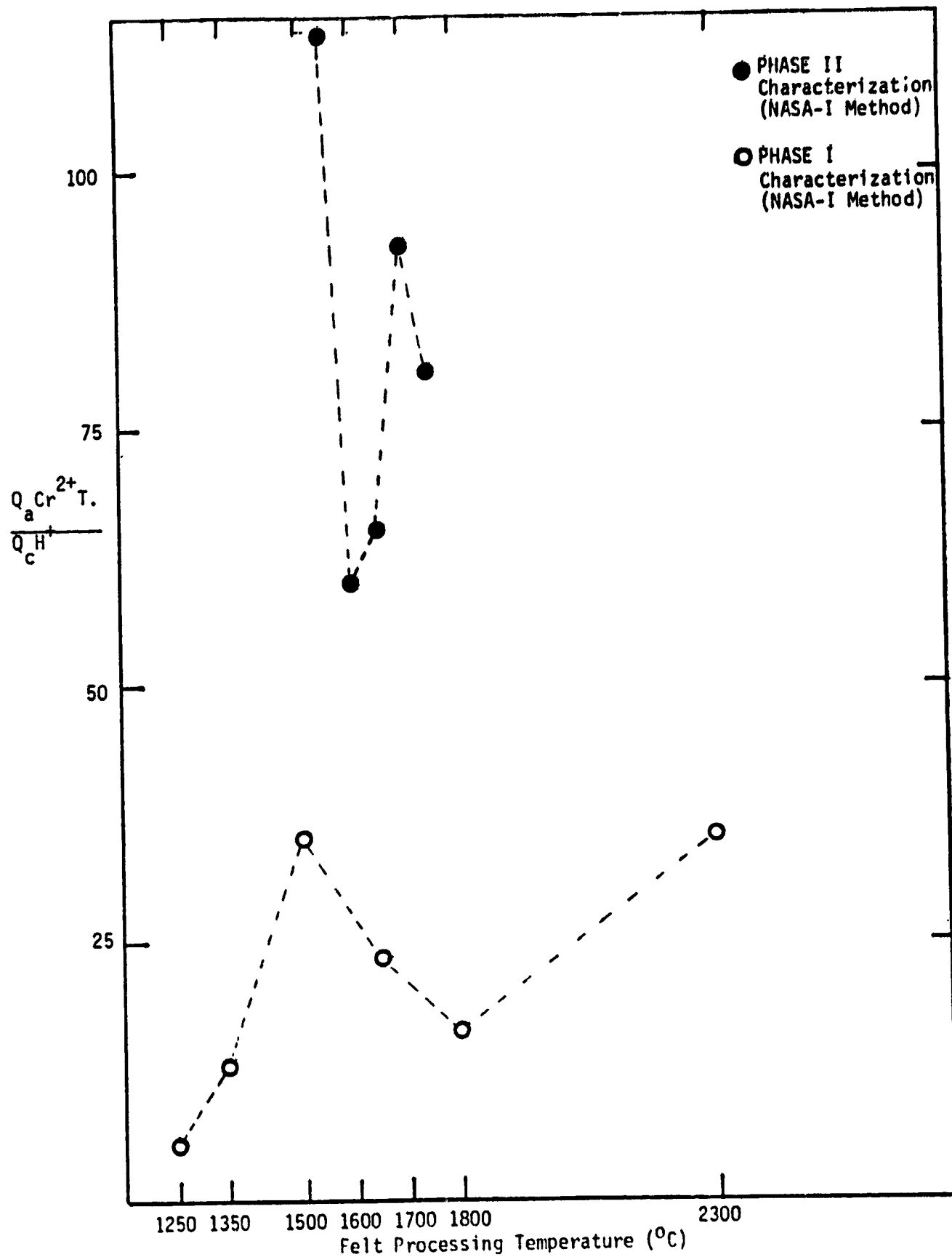


Figure 23. Negative Electrode Charging Efficiency versus Felt Processing Temperature; Phase I and Phase II Tests.

## V. OPTIMIZATION OF GOLD CATALYZATION

### A. Effects of Process Variations

As discussed in Section III, three variations of a basic methanolic/gold deposition process were used to catalyze carbon felt samples in the initial phase of this program. These were 1) the Double Immersion method, a set of procedures developed in the previous program for rigorous control of the total gold loading, 2) NASA-I, the standard method used at NASA-LeRC, and 3) NASA-II, a modification of the standard method in which the gold chloride concentration was reduced by half and the volume doubled.

The electrochemical performance of these electrodes and correlations to gold particle size are presented here. Some of the data has been presented under the heading of carbon felt processing factors (Section IV) since these two tasks were partially merged, as discussed there. All of the electrode samples were mounted in the waxed-clip holder and subjected to the cyclic voltammetry routines described in Section II. The cathodic and anodic charge segment data were extracted from the cyclic voltammograms in order to facilitate comparisons. The tabulated data were presented in Section IV, Tables IV, VII and VIII. Other graphical comparisons are discussed below.

#### 1. Comparison of NASA-I and Double Immersion Catalyzed Samples

##### a. Hydrogen Evolution Characteristics

The hydrogen evolution currents for NASA-I catalyzed felts at -950 mV vs. SCE on gold-on-carbon in HCl were similar in range to those observed for Double Immersion Catalyzed felts, (the complete sets of values are presented in column 1 of Table AI-I and Table AI-III, Appendix I), As has been noted in earlier reports, this parameter is probably only indicative of the presence or absence of gold. After the addition of  $\text{PbCl}_2$  (1 mM), the

hydrogen evolution currents in HCl are somewhat higher for Double Immersion electrodes than for NASA-I electrodes for all processing temperatures (column 2 of Tables AI-I and AI-III, Appendix I).

Figure 24 shows the total cathodic charge attributable to hydrogen evolution ( $Q_{\text{H}^+}$ ) versus felt processing temperature. By this measure the Double Immersion electrodes always exhibited more hydrogen evolution than the NASA-I electrodes, again suggesting the NASA-I electrodes are more favorable in this respect.

b. Pb<sup>2+</sup>/Pb Redox Characteristics

Lead loadings, as measured by anodic lead charge ( $Q_{\text{aPb}}$ ) are shown versus felt processing temperature in Figure 25. The loadings for NASA-I felts were always slightly higher than for Double Immersion felts (except for one 1250°C sample) but the values for both sets are generally close together.

The theoretical quantity of Pb<sup>2+</sup> available within the open volume of each felt ( $Q_{\text{tPb}^{2+}}$ ) was calculated for each sample for comparison to measured oxidation charge. These values are illustrated in Figure 26 as percent of theoretical ( $Q_{\text{aPb}}/Q_{\text{tPb}^{2+}}$ ) versus felt processing temperature. Both types of electrodes for 1250°C felt exhibited values greater than 100%. The other NASA-I felts had values generally less than 100% and in every case the values for NASA-I felts equalled or exceeded those for Double Immersion felts.

c. Cr<sup>3+</sup>/Cr<sup>2+</sup> Redox Characteristics

The Cr<sup>3+</sup>/Cr<sup>2+</sup> redox performance of the six Phase I felts catalyzed by both methods is illustrated in Figure 27 in terms of the total chromous ion oxidation charge. The NASA-I values exceed the Double

Immersion values and were almost invariant with processing temperature except at 1800°C. The patterns for the two sets of electrodes are clearly different.

The fraction of available chromic ion reduced ( $Q_{\text{Cr}^{3+}}/Q_{\text{Cr}^{3+}}$ ) is shown versus felt processing temperature in Figure 28. This fraction was always greater for NASA-I felts than Double Immersion felts, but followed a similar trend.

The fraction of available chromous ion oxidized is shown versus felt processing temperature in Figure 29. The NASA-I felts displayed higher values and there was less similarity between the sets of values.

Figure 30 shows the ratio of the "peak" anodic chromium charge to the "trailing" anodic chromium charge versus felt processing temperature. The NASA-I felts had the higher value of this ratio for every temperature.

The net efficiency of conversion, i.e., the fraction of chromous ion produced that is subsequently oxidized, is shown in Figure 31. There was more scatter in these sets of values, e.g., these efficiencies were greater for NASA-I felts for 1500°, 1650°C and 2300° but greater for Double Immersion felts for every other temperature.

#### d. $\text{H}^+$ , Pb and $\text{Cr}^{2+}$ Relationships

To illustrate the relationship to lead loading, the anodic chromium charge ( $Q_{\text{aCr}^{2+}}$ ) has been plotted versus lead loading (as  $Q_{\text{aPb}}$ ) in Figure 32. There appears to be a somewhat better correlation for the Double Immersion method, as found in previous testing (16), than for the NASA-I method. There is an overall correspondence between the two sets of values, however.

Figure 33 shows the ratio of anodic chromium charge to anodic lead

charge as a function of felt processing temperature. The maximum value for Double Immersion felts occurred at 1250°C. For this temperature the NASA-I felt has a lower ratio than the Double Immersion felt. For all other temperatures except 1800°C, however, the NASA-I felts exhibited much higher ratios with a maximum at 1500°C.

Figure 34 represents the ratio of anodic chromium charge to cathodic hydrogen charge versus felt processing temperature, which may be a relevant overall measure of relative charging efficiency. By this measure the NASA-I felts looked better than the Double Immersion felts at every temperature. There is a distinctive peak at 1500°C; this is matched by the value at 2300°C, which is an unusually high value for graphite felt.

## 2. Comparison of NASA-I and NASA-II Catalyzed Samples

### a. Hydrogen Evolution Characteristics

The hydrogen evolution current for NASA-II catalyzed felts (made with excess gold solution) at -950 mV vs. SCE on gold-on-carbon in HCl ranged from 580 mA for 1250°C felt to 960 mA for 1800°C felt. The NASA-II felts exhibited considerably higher hydrogen evolution than NASA-I felts for all process temperatures except 1250°C (the complete set of values is presented in Table AI-III, Appendix I).

Figure 35 shows the hydrogen evolution current for each felt at -950 mV in HCl after the addition of  $\text{PbCl}_2$  (1 mM). The currents in HCl were somewhat greater for NASA-II felts for all temperatures.

Figure 36 shows the total cathodic charge attributable to hydrogen evolution ( $Q_{\text{cH}^+}$ ) on Pb/Au versus felt processing temperature. The NASA-II electrodes followed the same pattern as NASA-I electrodes but showed considerably more hydrogen evolution. With extended cycling the rate of

hydrogen evolution decreased in both cases. For NASA-II electrodes the rate started at even higher values but decreased quite rapidly.

b. Pb<sup>2+</sup>/Pb Redox Characteristics

Lead loadings, as measured by anodic lead charge ( $Q_a\text{Pb}$ ) are shown versus felt processing temperature in Figure 37. The loadings for NASA-II felts were considerably greater than for NASA-I felts for every temperature. There was not a smooth trend in loading with processing temperature for NASA-II felts, nor was the pattern similar for NASA-I and NASA-II.

The theoretical quantity of  $\text{Pb}^{2+}$  available within the open volume of each felt ( $Q_t\text{Pb}^{2+}$ ) was calculated for each sample for comparison to measured oxidation charge. These values are illustrated in Figure 38 as percent of theoretical ( $Q_a\text{Pb}/Q_t\text{Pb}^{2+}$ ) versus felt processing temperature. All the NASA-II values exceeded 100% and were greater than the NASA-I values.

c. Cr<sup>3+</sup>/Cr<sup>2+</sup> Redox Characteristics

The total chromous ion oxidation charge is shown versus felt processing temperature in Figure 39. Similar plots for chromium reduction charge are given in Figure 40. The NASA-II chromium charges always exceeded the NASA-I chromium charges. The greatest chromous ion oxidation charge was shown by NASA-II 1800°C felt. The greatest chromic ion reduction charge was shown by NASA-II 1250°C.

The fraction of available chromic ion reduced is shown versus felt processing temperature in Figure 41. This fraction was greater for NASA-II felts for every processing temperature.

The fraction of available chromous ion oxidized is shown versus felt processing temperature in Figure 42. Again the NASA-II felts displayed the

higher values.

The net efficiency of conversion, i.e., the fraction of chromous ion produced that is subsequently oxidized, is shown in Figure 43. These efficiencies were greater for NASA-I felts for all temperatures except 1800°C.

Figure 44 shows the ratio of the "peak" anodic chromium charge to the "trailing" anodic chromium charge versus felt processing temperature. The NASA-I felts had the higher ratio at 1250° and 2300°C, while the NASA-II felts had the higher ratio at all other temperatures. The NASA-II values increased with increasing processing temperature until reaching a maximum at 1650° and thereafter declined.

#### d. $H^+$ , Pb and $Cr^{2+}$ Relationships

To illustrate the relationship to lead loading, the anodic chromium charge ( $Q_a Cr^{2+}$ ) has been plotted versus lead loading (as  $Q_a Pb$ ) in Figure 45. The values for both sets of electrodes show a fairly consistent increase in  $Cr^{3+}/Cr^{2+}$  redox activity with increasing lead loading, as found in previous testing.

Figure 46 shows the ratio of anodic chromium charge to anodic lead charge as a function of felt processing temperature. The values for both sets are similar, except at 1800°C.

Figure 47 represents the ratio of anodic chromium charge to cathodic hydrogen charge versus felt processing temperature, which may be a relevant overall measure of relative charging efficiency. By this measure the NASA-I felts looked better than the NASA-II felts at every temperature. The best performing electrodes were NASA-I 1500° and 2300°C.

### 3. Correlation with Gold Particle Size

The standard NASA catalyzation process (NASA-I), and more particularly the modified process (NASA-II), presented an opportunity to observe the solutions "in process" by way of the excess solution volume, in contrast to the Double Immersion method in which the solution was designed to be totally absorbed by the carbon felt sample. For NASA-II electrodes, it was immediately noticed that the excess gold chloride solution had a faint blue color. The appearance of the solution remained unchanged over several weeks of observation. For NASA-I electrodes, the excess gold chloride solution looked clear and colorless at first. After two hours, however, it changed to purple. The next day the solution was still purple and had become noticeably cloudy. These colors are most probably due to suspended gold particles, the formation of which is initiated by contact of gold chloride solution with the felt. Based on the blue color, observed in the NASA-II preparation, the particles should be very small, on the order of 1.0 nm diameter (nucleates). The purple color seen for NASA-I electrodes should indicate larger particles, on the order of 100 nm diameter (21). These observations also suggested that metallic gold is formed when the methanolic gold solution contacts the carbon felt. Previously it had been assumed that gold chloride was deposited, requiring thermal decomposition to gold.

In order to look at gold particle sizes in relation to catalyzation method and observed performance, a selection of the samples tested were submitted for examination by transmission electron microscopy (TEM). The resulting photographs showing representative views of gold particles on the carbon fiber surface in each case are presented in Appendix II. For purpose

of comparison, the length and width of each particle was measured and averaged to give a mean particle diameter ( $\bar{X}$ ) and the value of one standard deviation (s). These values are presented below for each catalyzation method together with selected charge segment data representative of electrochemical performance.

CATALYZATION METHOD, PERFORMANCE AND GOLD PARTICLE SIZE.  
(Mean Particle Sizes by TEM)

CATLYZ. METHOD	C-FELT TEMP. (°C)	Q <sub>a</sub> Pb (mC)	Q <sub>a</sub> Cr <sup>2+</sup> (mC)	Q <sub>C</sub> H <sup>+</sup> (mC)	QCr/QH	Au PARTICLE SIZE (nm) ( $\bar{X}$ ) (S)	
NASA-I	1800	89	346	21	16.5	31.2	34.7
NASA-I	2300	110	890	25	35.6	19.7	5.4
NASA-I	1500	112	1275	36	35.4	62.4	34.7
Dbl Imm	1800	86	289	57	5.1	37.8	10.6
Dbl Imm	1500	108	538	164	3.3	27.2	42.3
NASA-II	1500	177	2110	302	7.0	26.3	11.9
NASA-II	1800	265	2647	548	4.9	9.8	4.9

From this data there is some evidence that the NASA-II catalyzation procedure yielded smaller and more uniform gold particles which was reflected in higher electrochemical activity, including a higher level of hydrogen evolution; the latter resulted in low charging efficiency values, however. It can be seen that these electrodes had very high lead deposits which may be consistent with higher gold surface areas. These values

consistently exceeded the theoretical quantity of lead available, however, which may have resulted in some unplated gold leading to higher hydrogen evolution rates (such a condition would not be expected in a flow cell).

The NASA-I catalyzation procedure gave larger, less uniform particles resulting in lower electrochemical activity but higher charging efficiency values. The Double Immersion method yielded gold particle sizes within the same range as the NASA-I method. The electrochemical performance of electrodes catalyzed by this method, however, was quite different (low activity, low charging efficiency) suggesting the influence of factors in addition to gold particle size, or non-representative samplings.

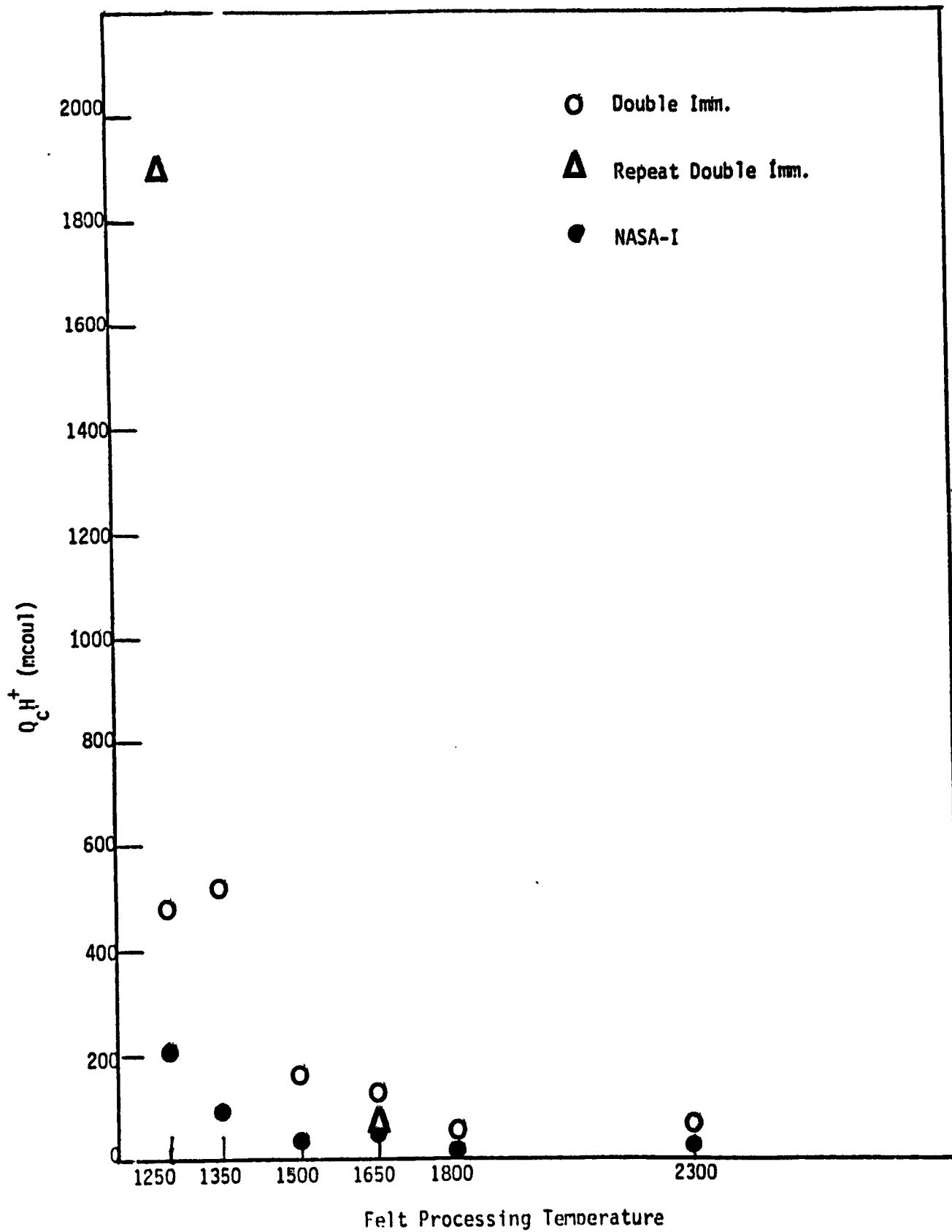


Figure 24.  $H^+$  Reduction Charge ( $Q_c H^+$ ) versus Felt Processing Temperature.

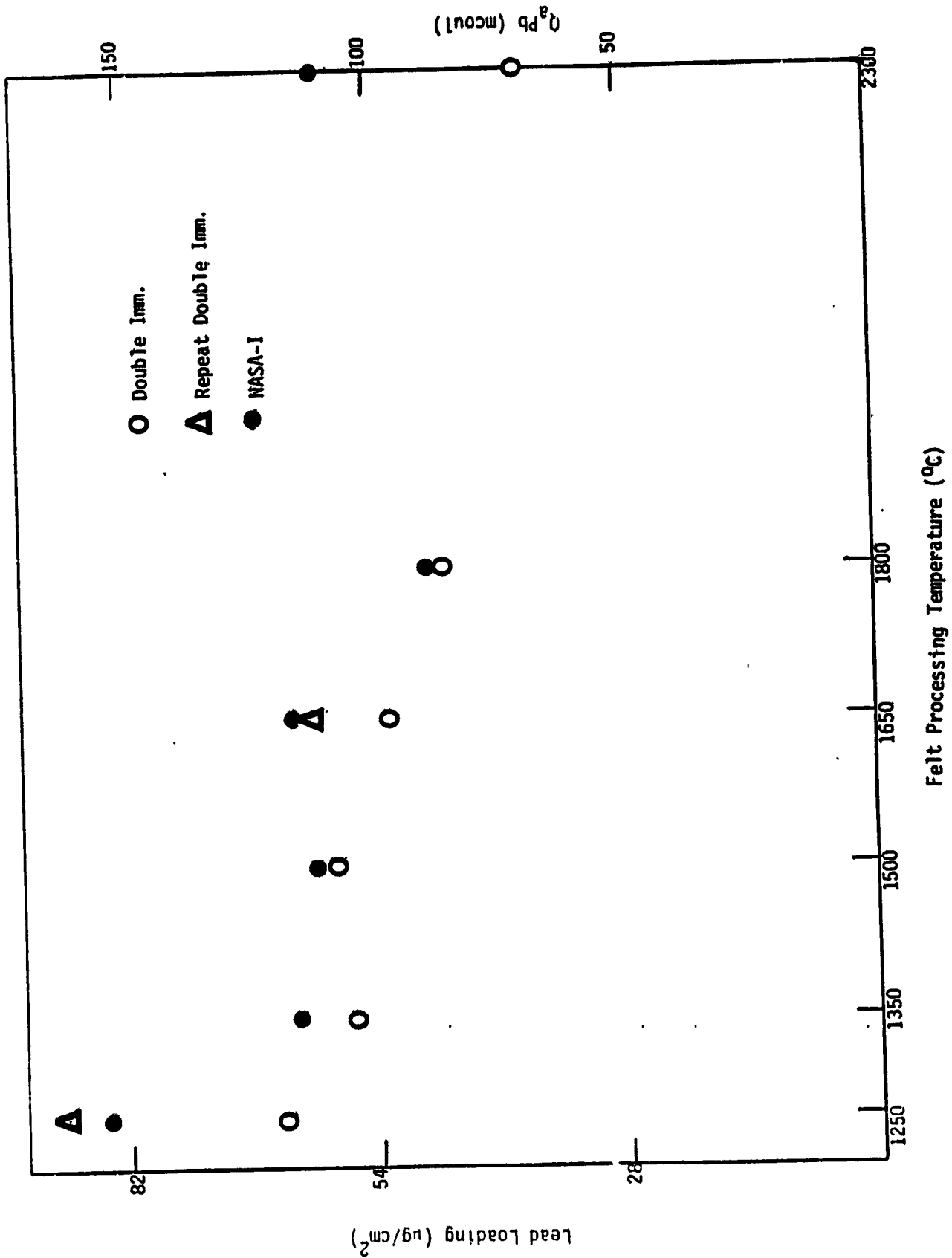


Figure 25. Lead Loading as Measured by the Anodic Lead Charge (QaPb) versus Felt Processing Temperature.

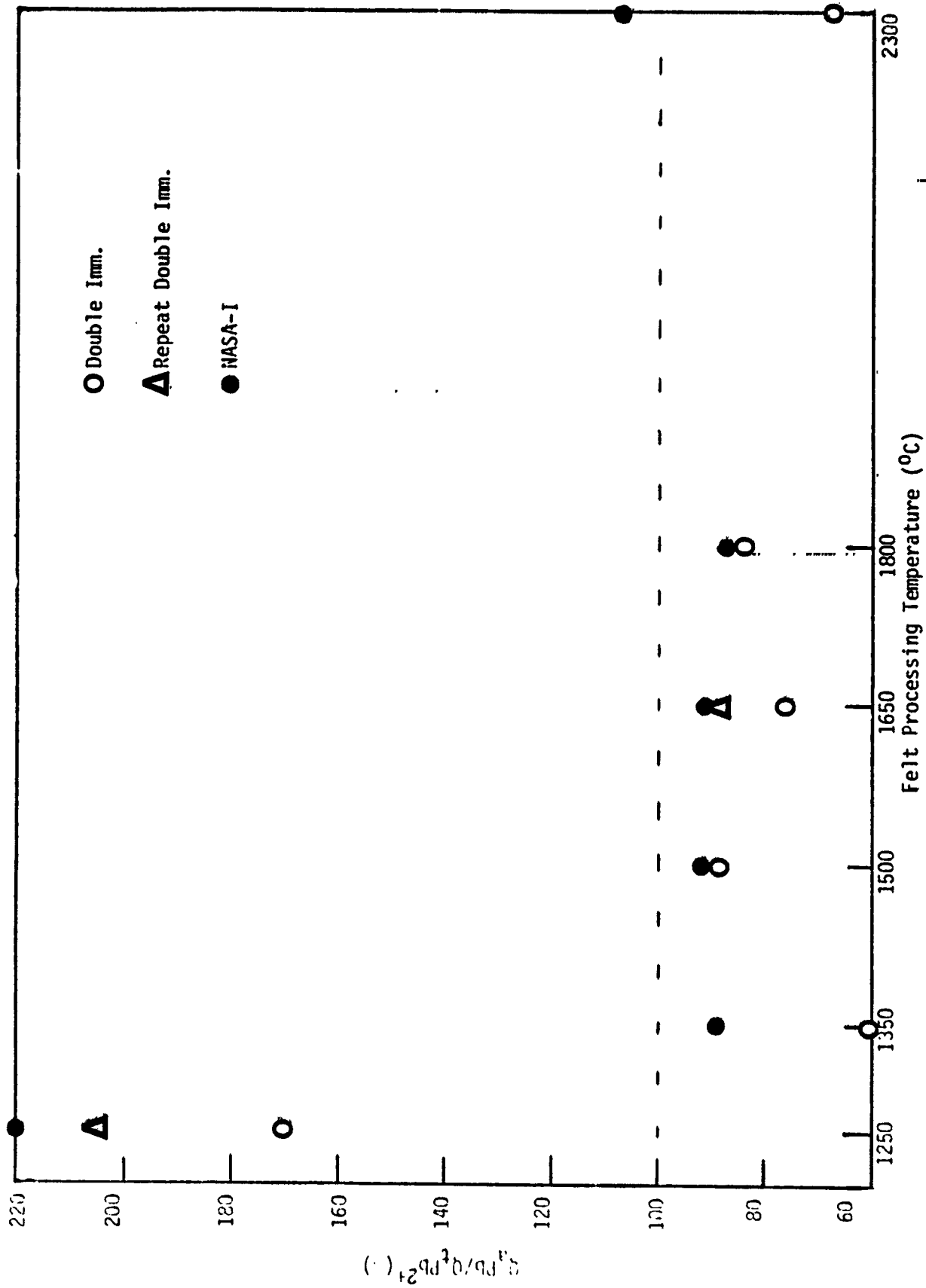


Figure 26. Percentage of Available Lead Deposited versus Felt Processing Temperature.

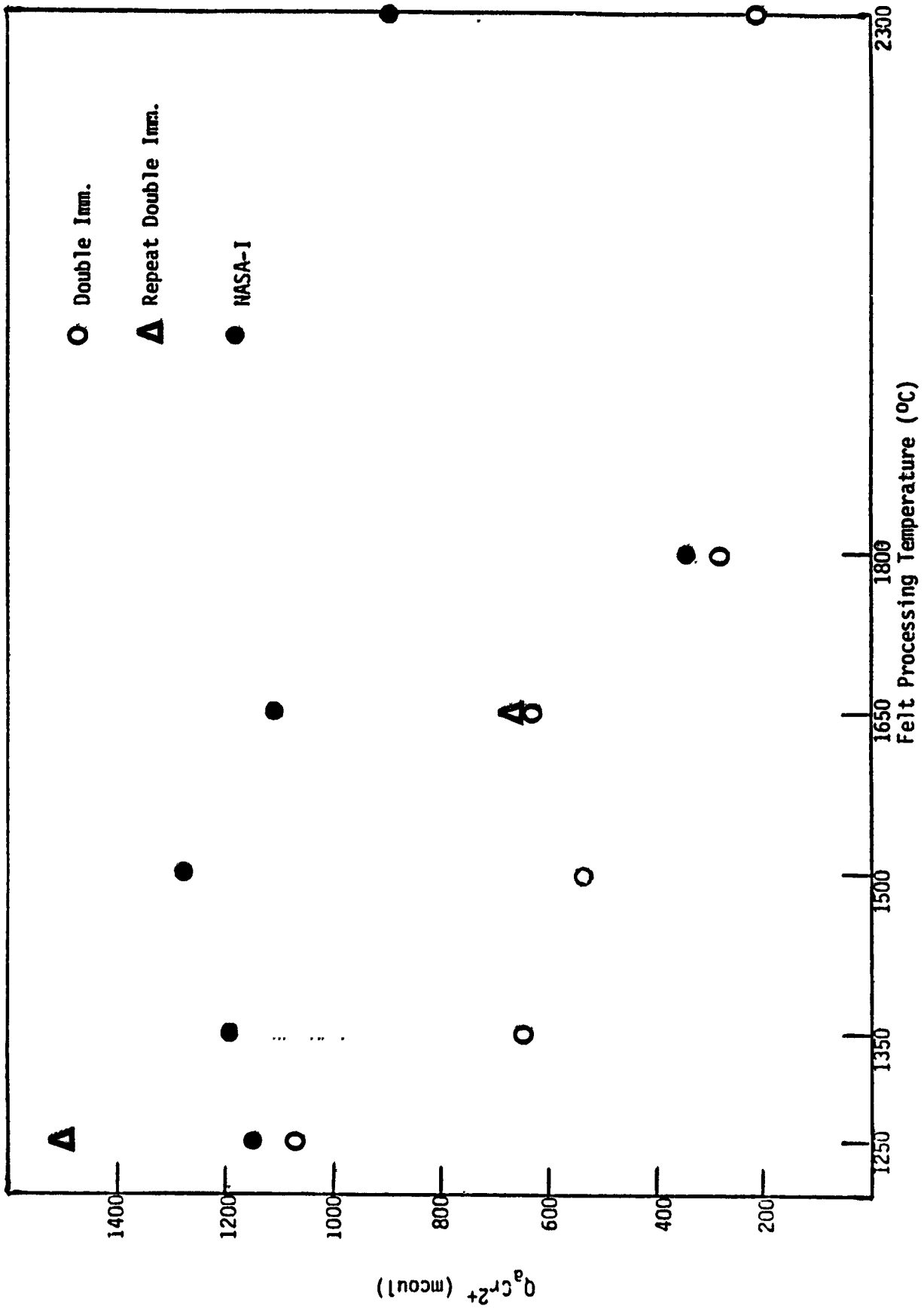


Figure 27. Total Anodic Chromium Charge versus Felt Processing Temperature.

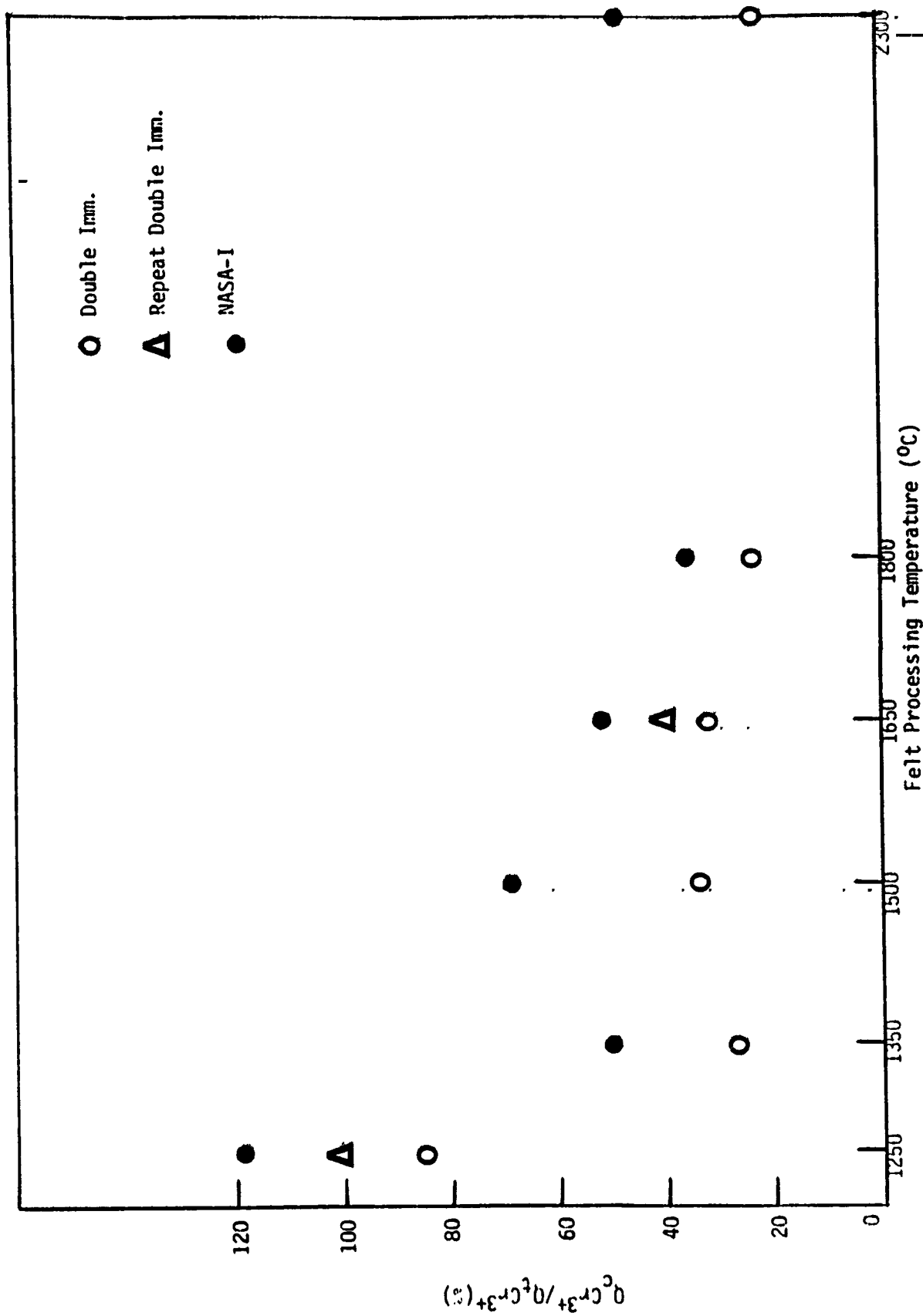


Figure 28. Fraction of Available Chromic Ion Reduced (%) versus Felt Processing Temperature.

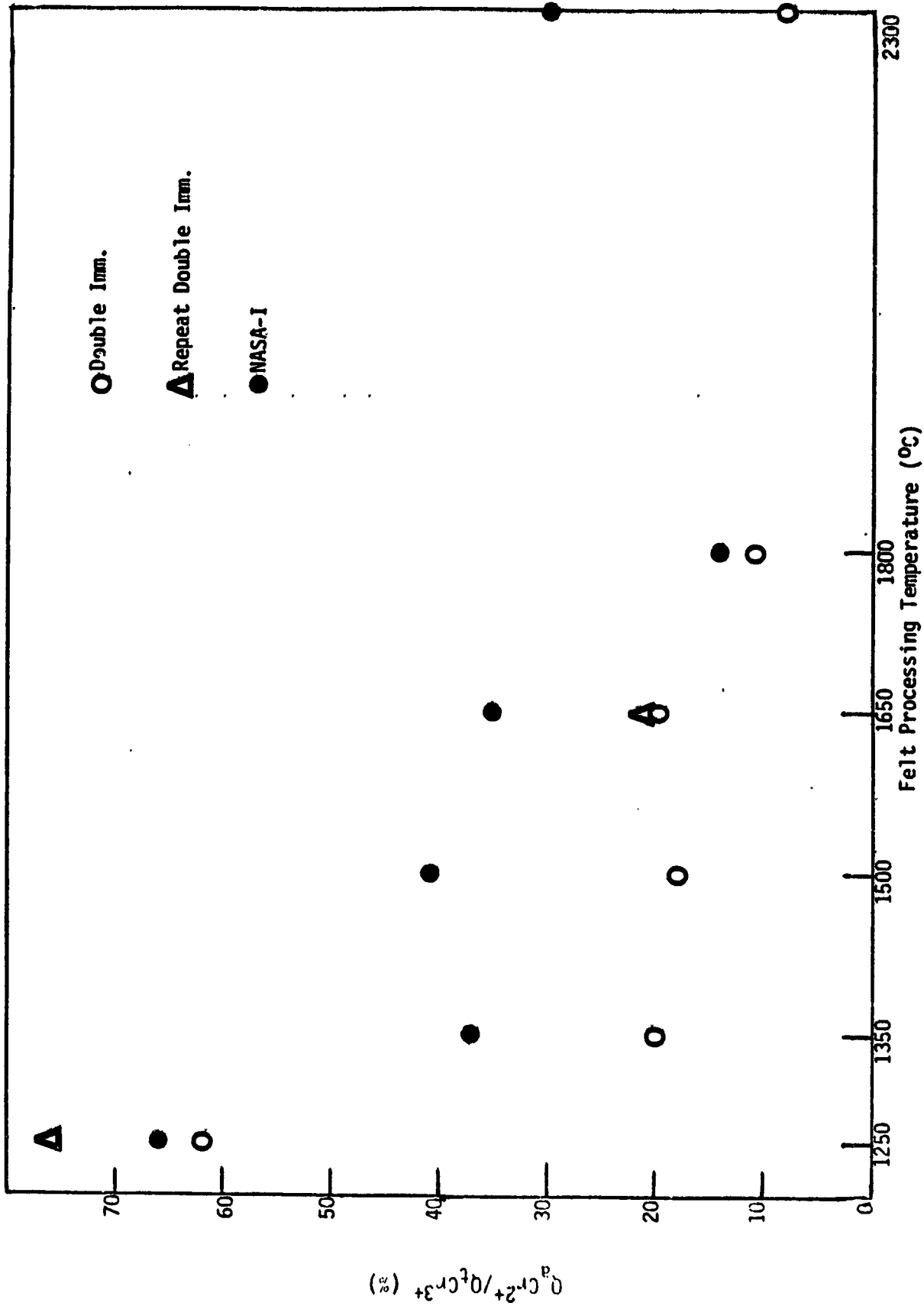


Figure 29. Quantity of  $Cr^{2+}$  Oxidized as a Fraction of Available  $Cr^{3+}$  (%) versus Felt Processing Temperature.

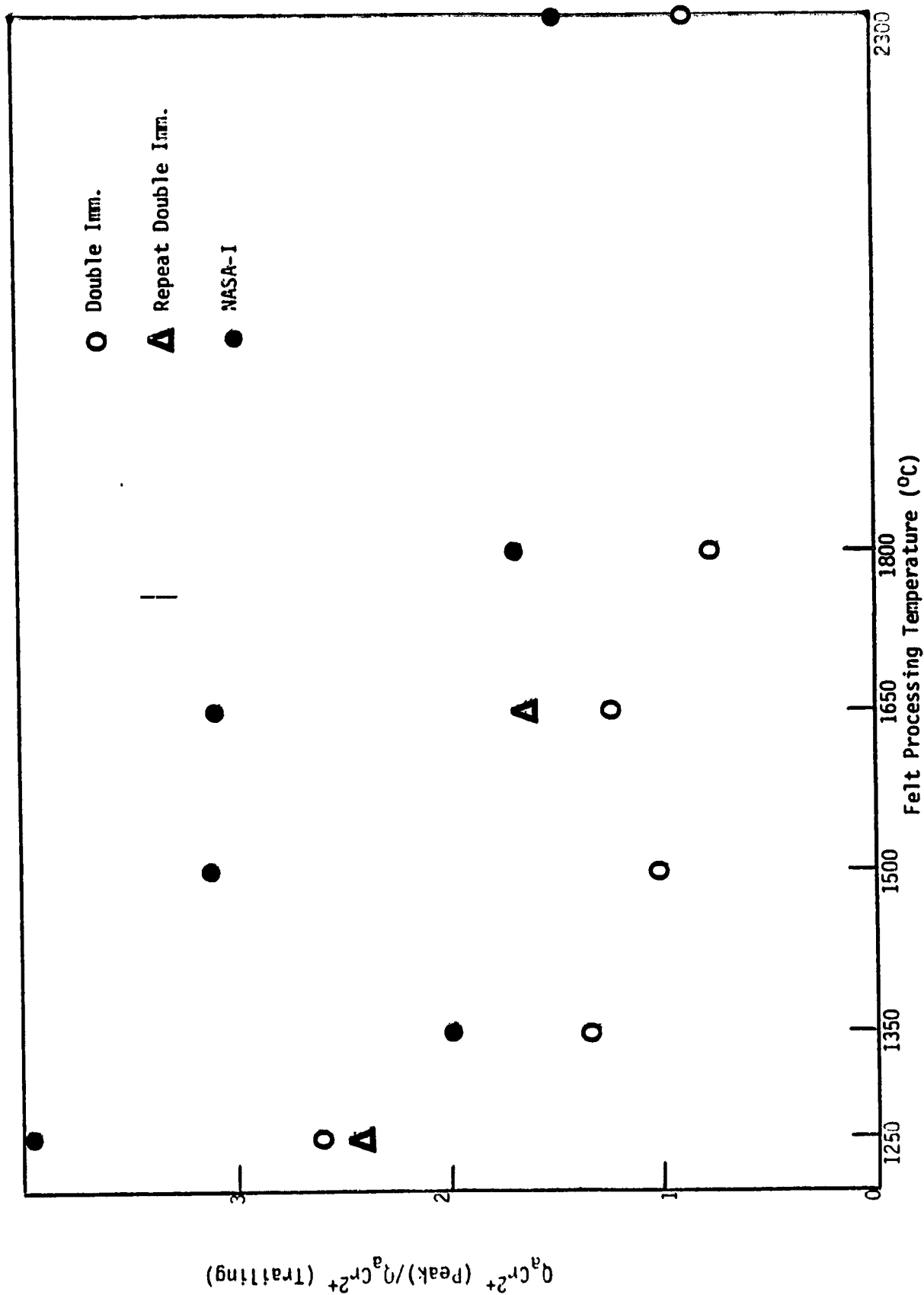


Figure 30. Ratio of Anodic Chromium Charge (Peak) to Anodic Chromium Charge (Trailing) versus Felt Processing Temperature.

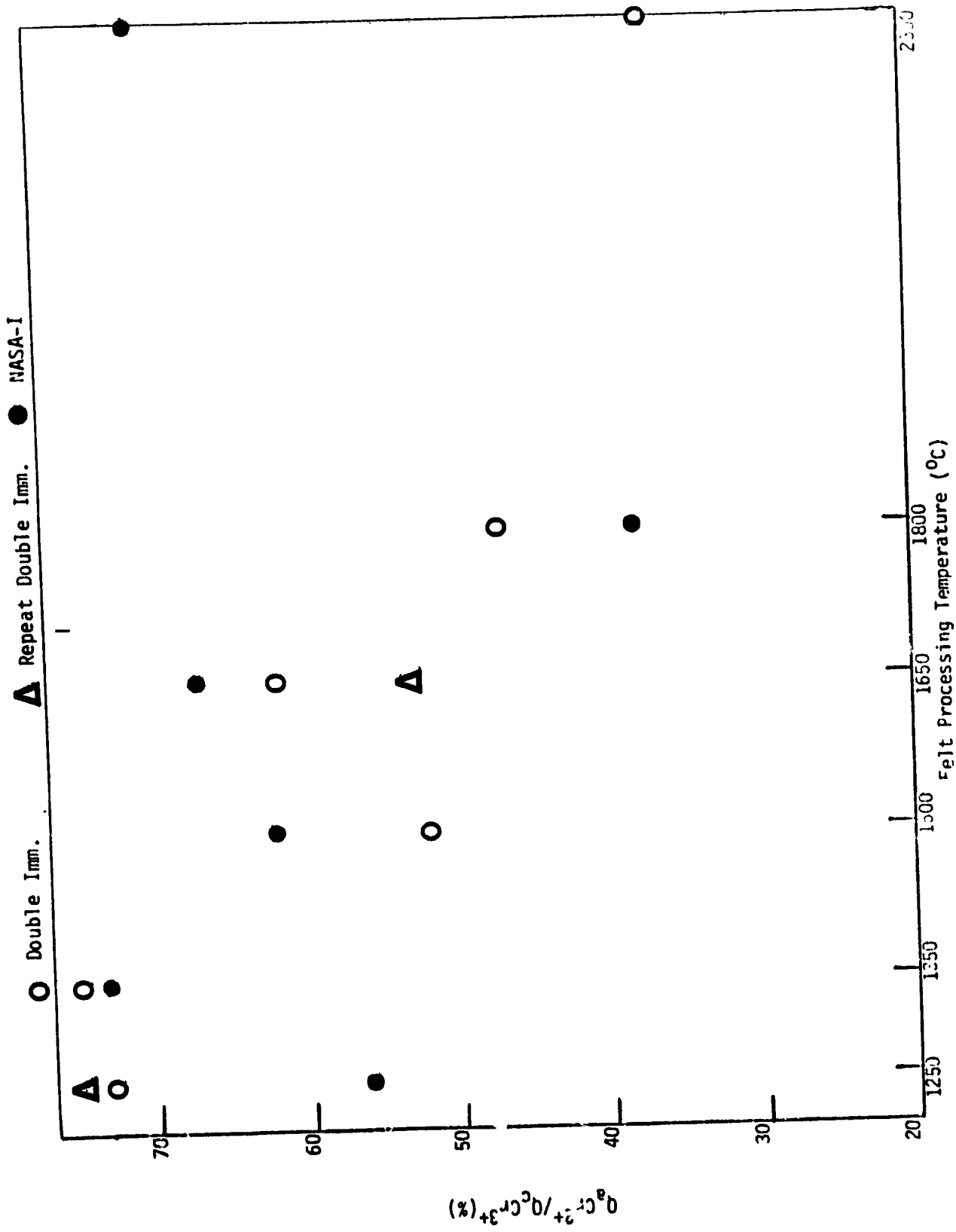


Figure 31.  $Q_{aCr^{2+}}/Q_{cCr^{3+}}$  versus Felt Processing Temperature.

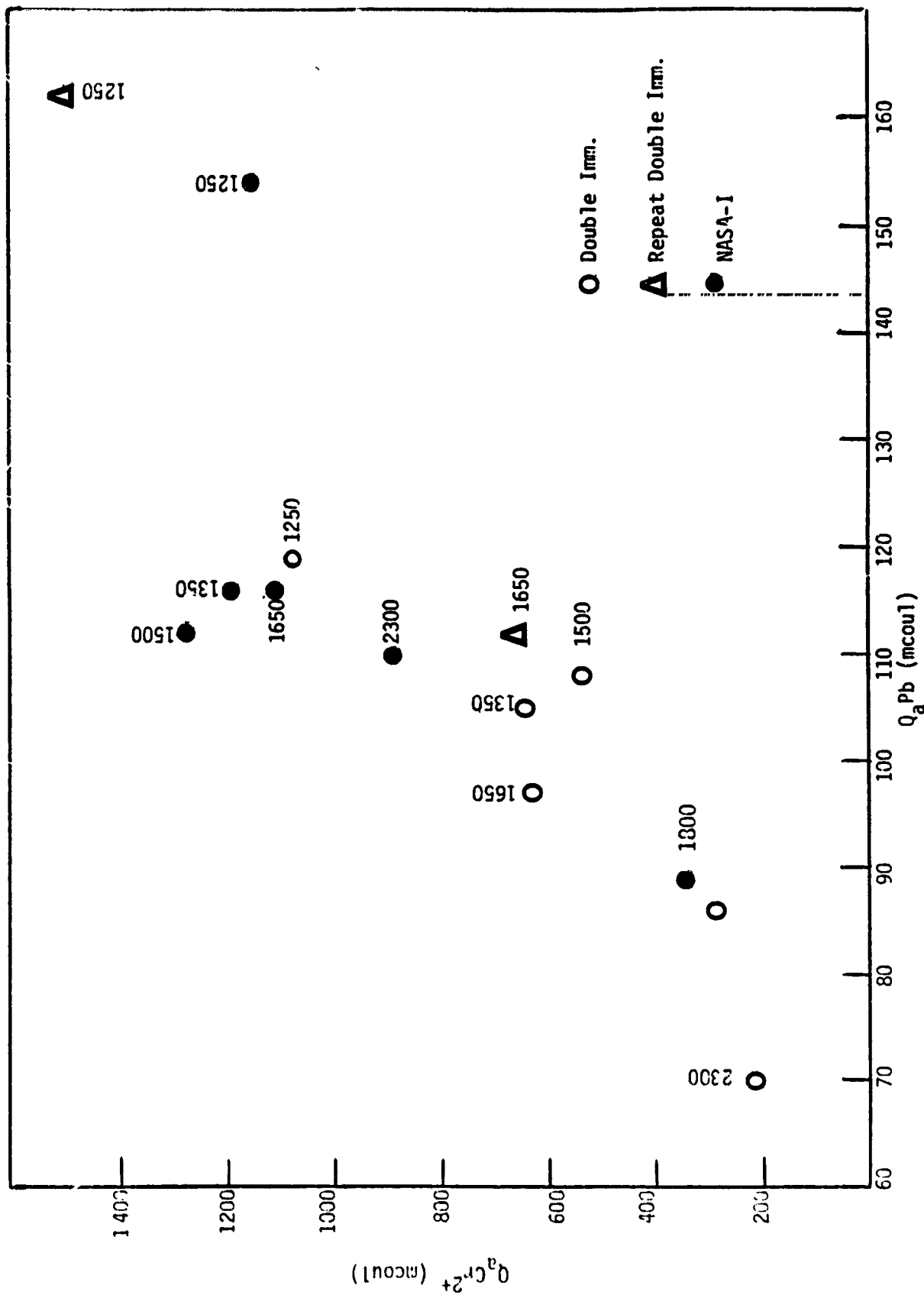


Figure 32. Total Anodic Chromium versus Anodic Lead Charge (100 mcoul is equivalent to  $54 \mu g Pb/cm^2$ ).

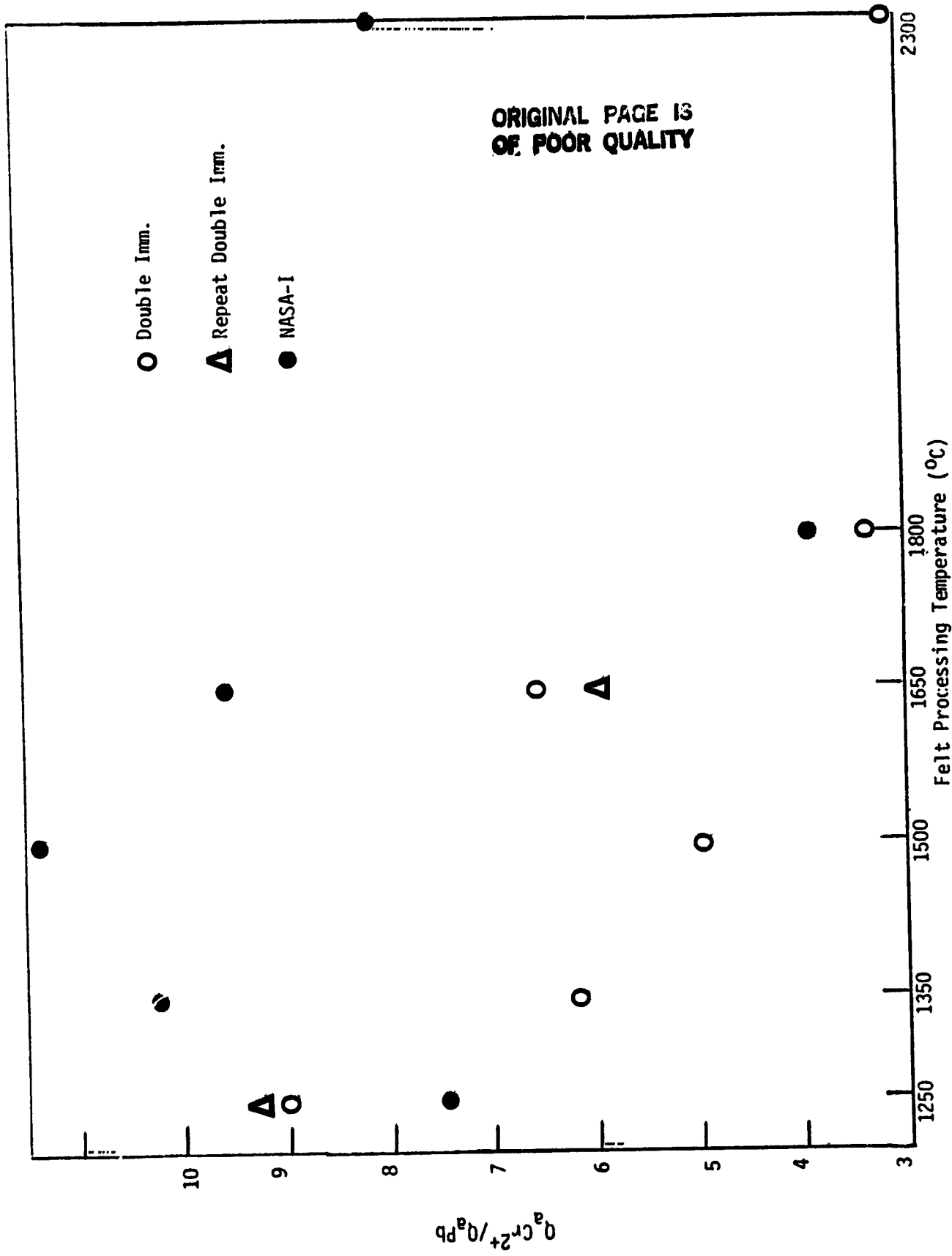


Figure 33. Ratio of Chromium Charge to Anodic Lead Charge Versus Felt Processing Temperature.

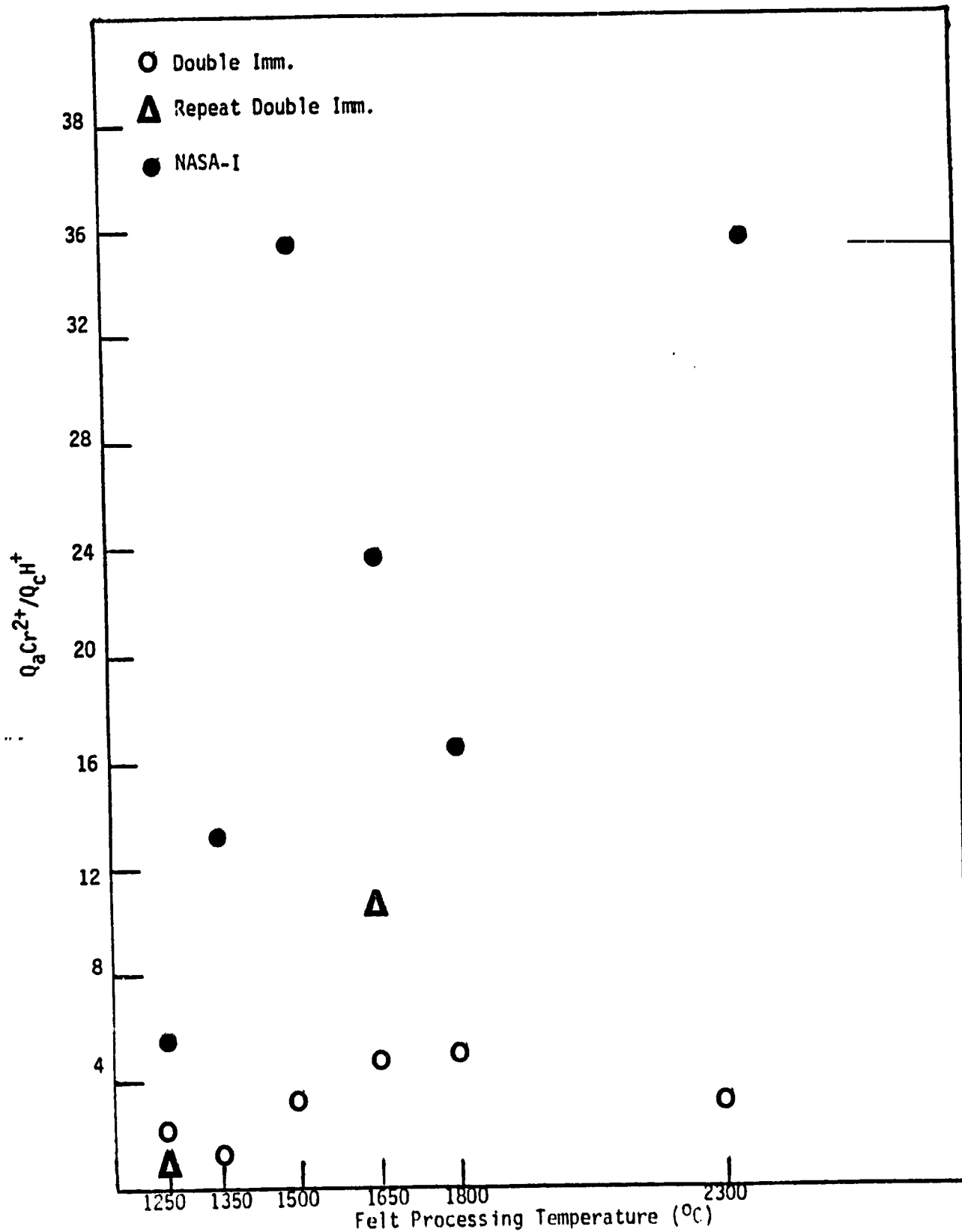
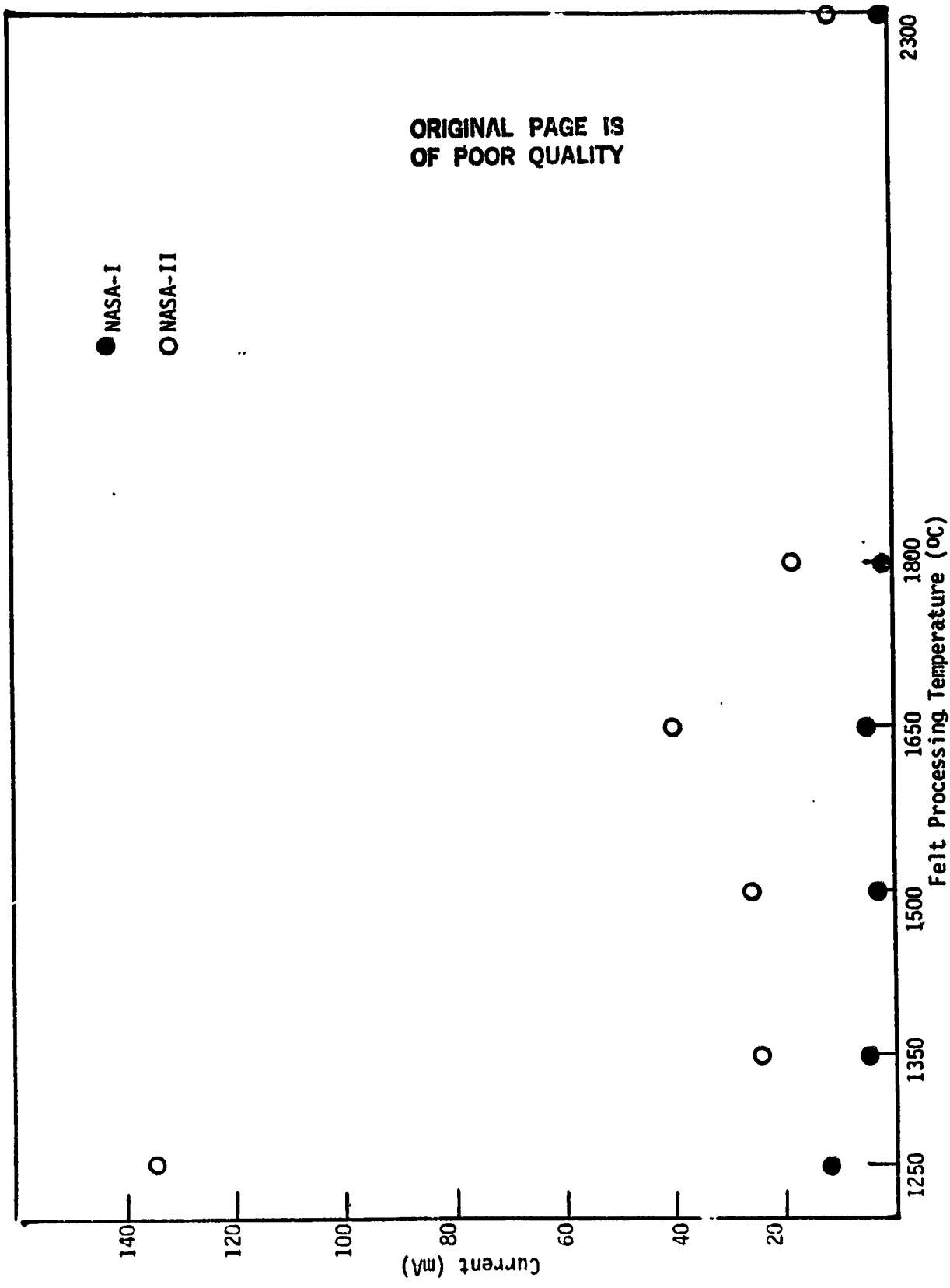


Figure 34. Ratio  $Q_aCr^{2+}/Q_cH^+$  versus Felt Processing Temperature.



Current (mA) versus Felt Processing Temperature (°C) at 0.50 ml on Ph/Au in HCl versus

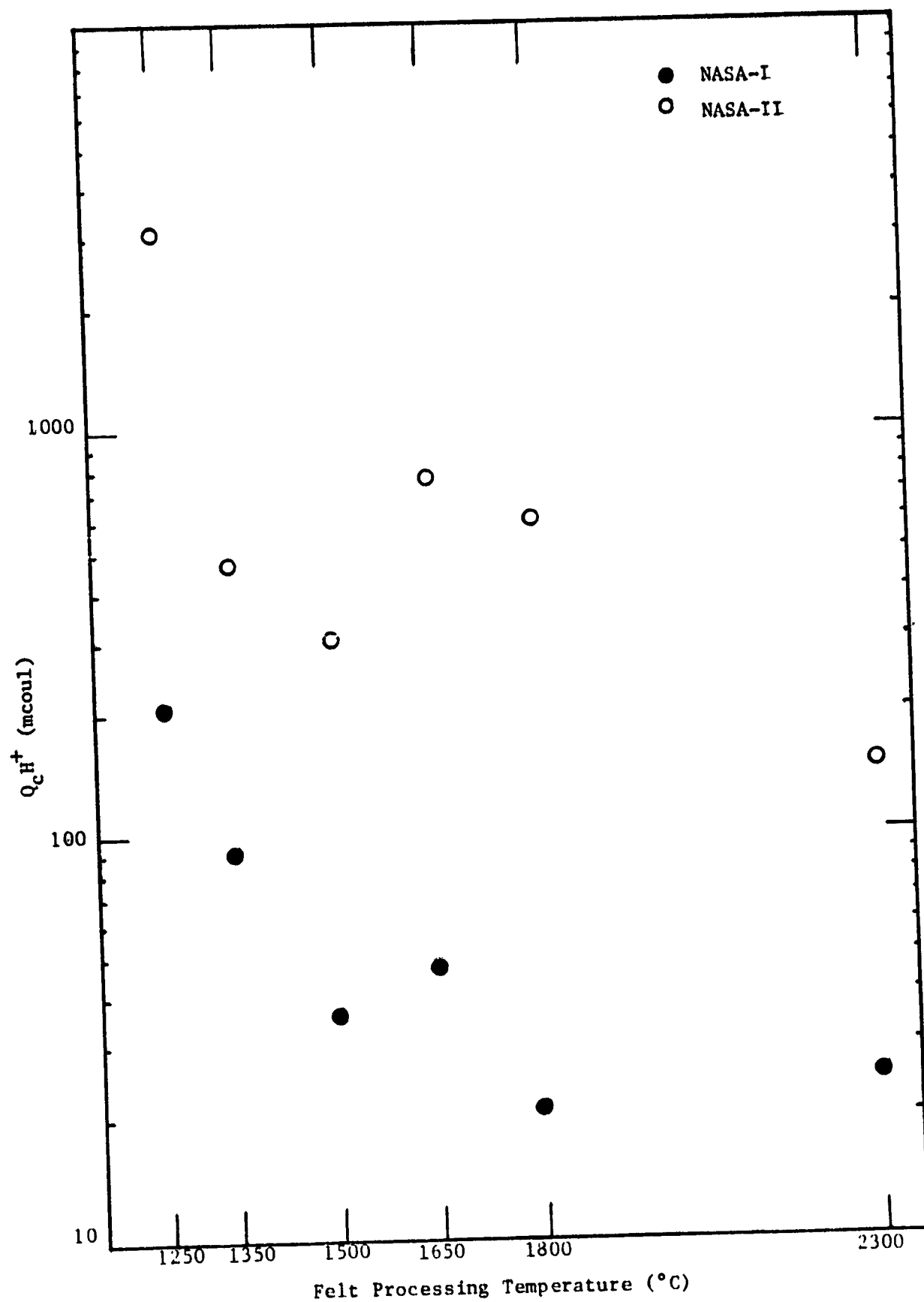


Figure 36.  $H^+$  Reduction Charge ( $Q_c H^+$ ) on Pb/Au versus Felt Processing Temperature.

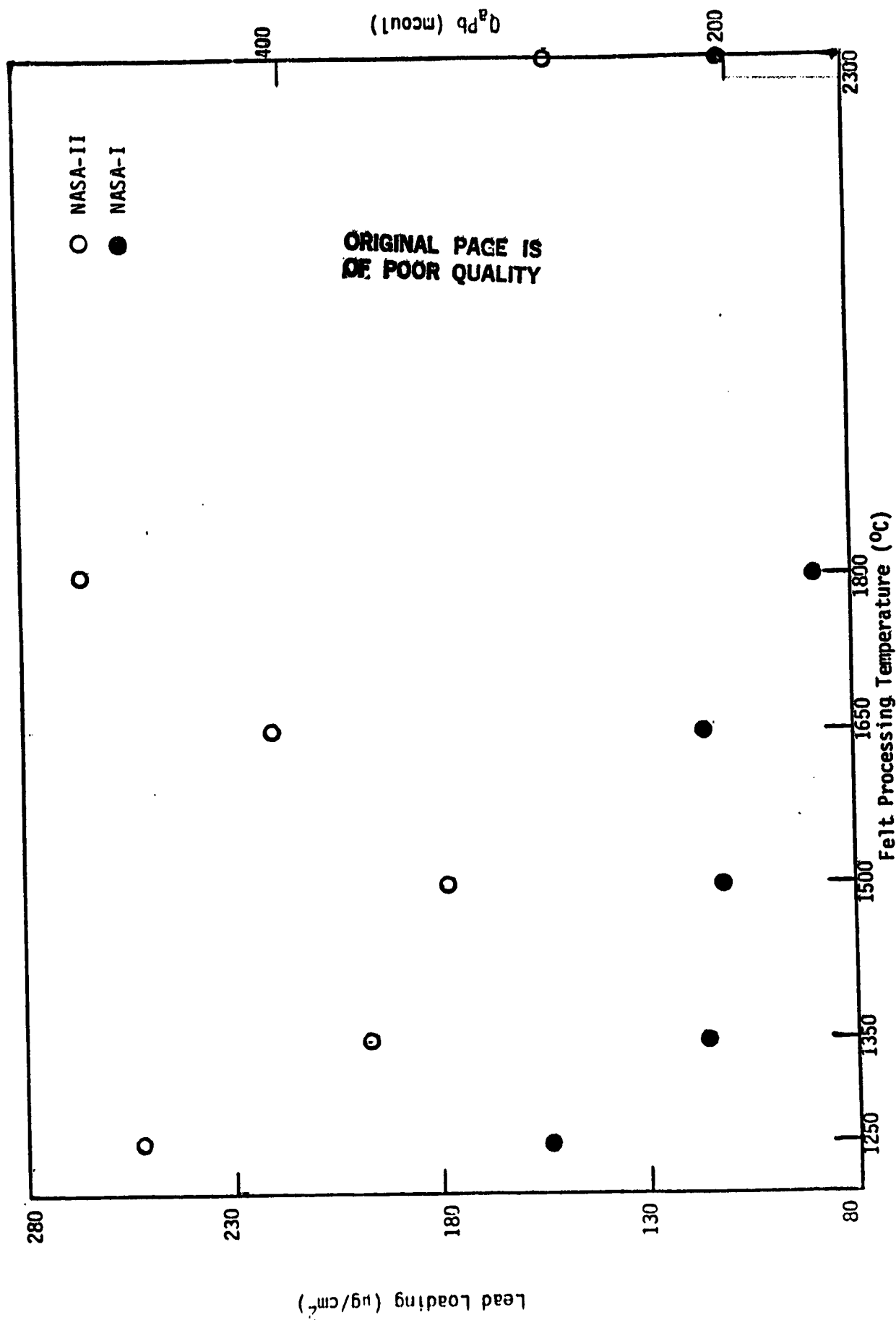


Figure 37. Lead Loading as Measured by the Amodic Lead Charge ( $Q_a\text{Pb}$ ) Versus Felt Processing Temperature.

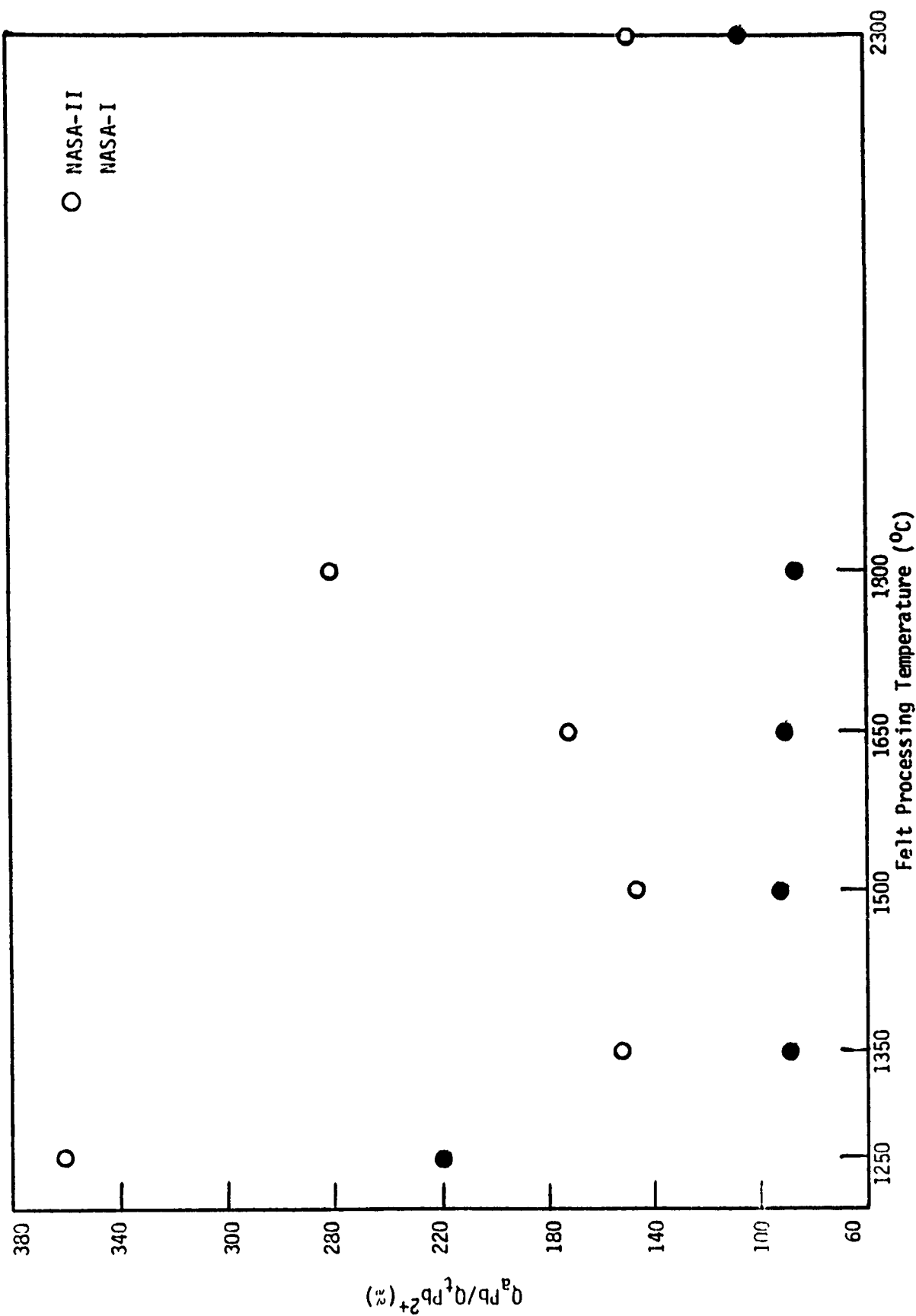


Figure 38. Percentage of Available Lead Deposited Versus Felt Processing Temperature.

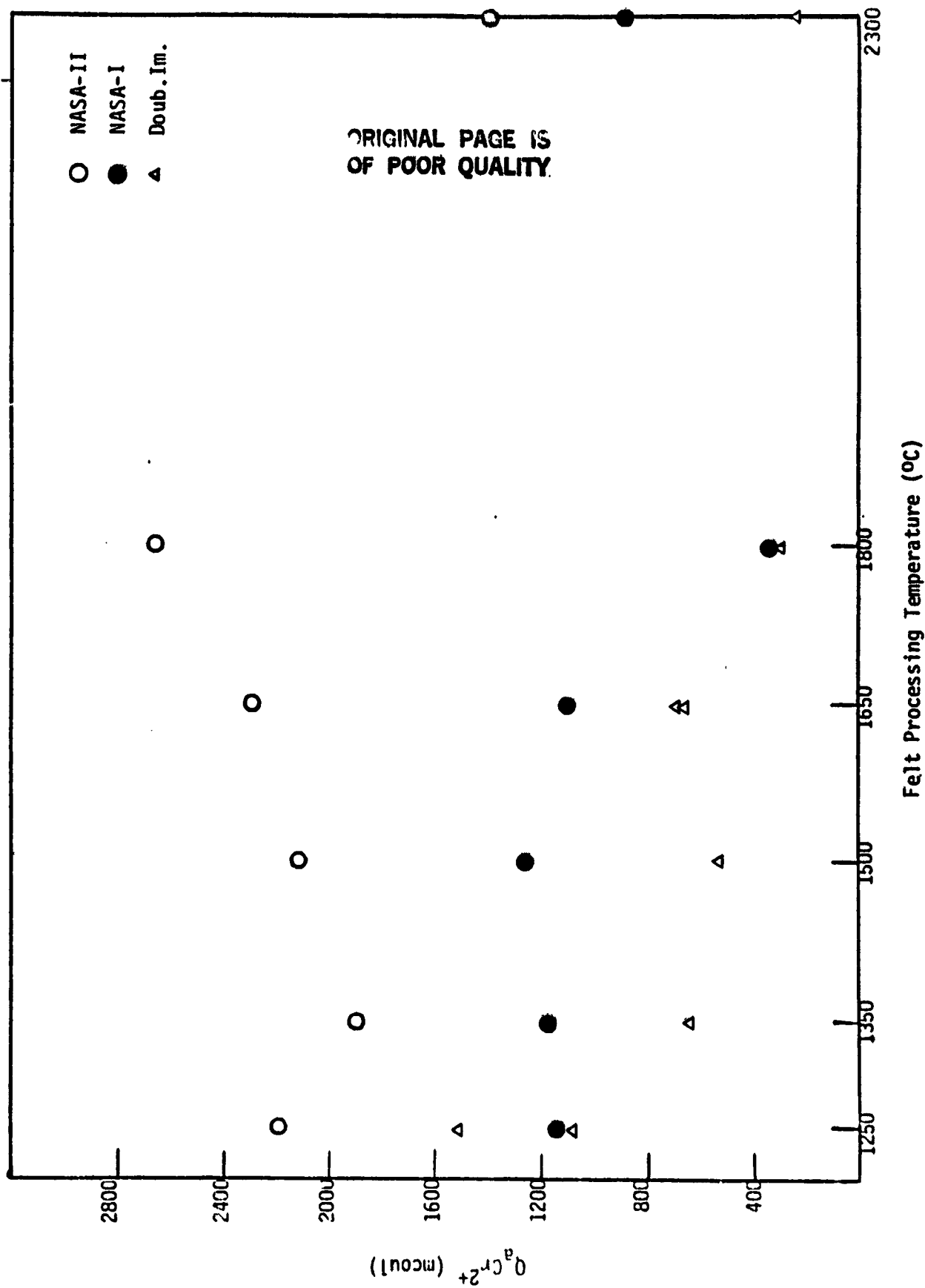


Figure 39. Total Anodic Chromium Charge Versus Felt Processing Temperature.

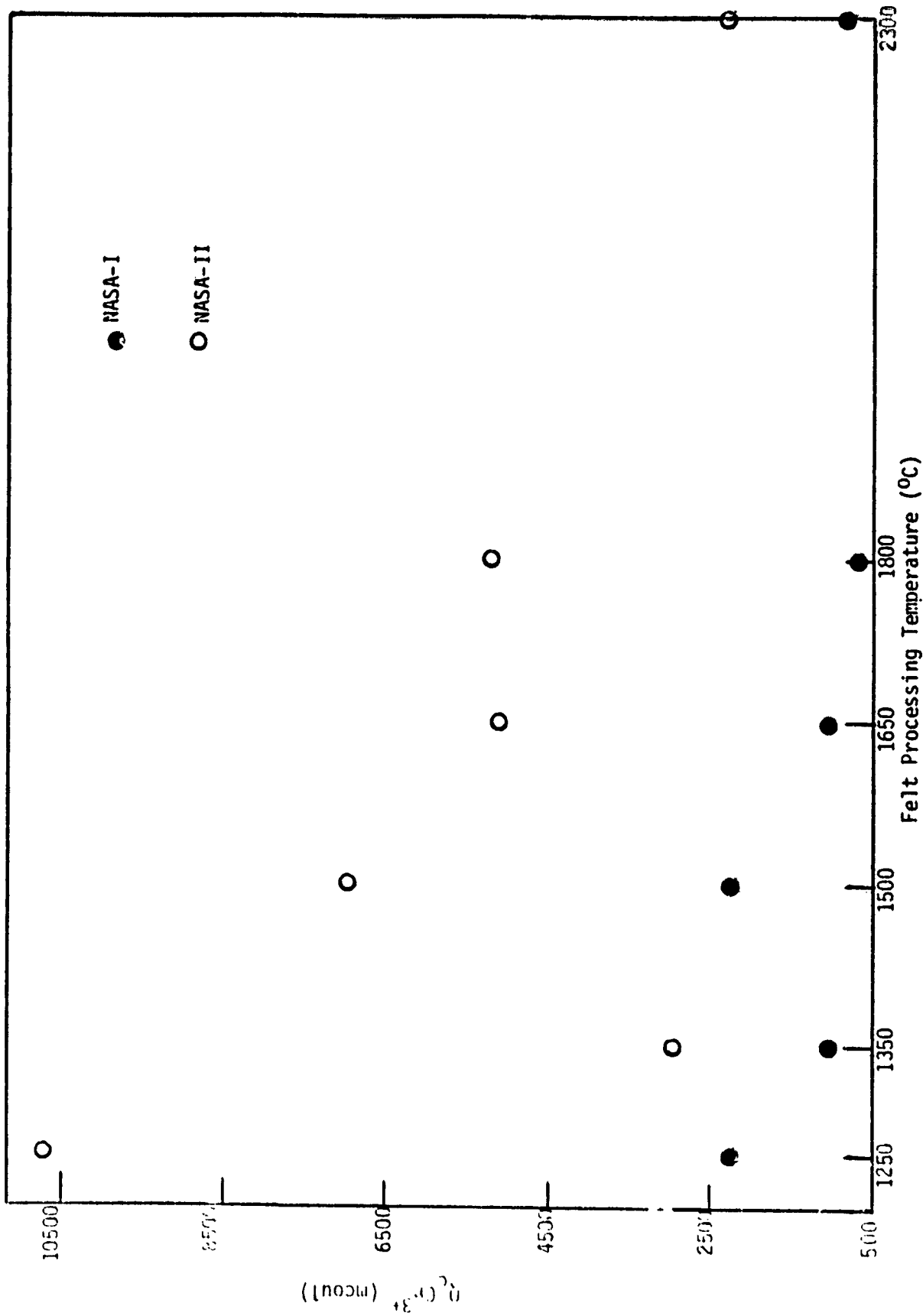


Figure 40. Cathodic Chromium Charge Versus Felt Processing Temperature.

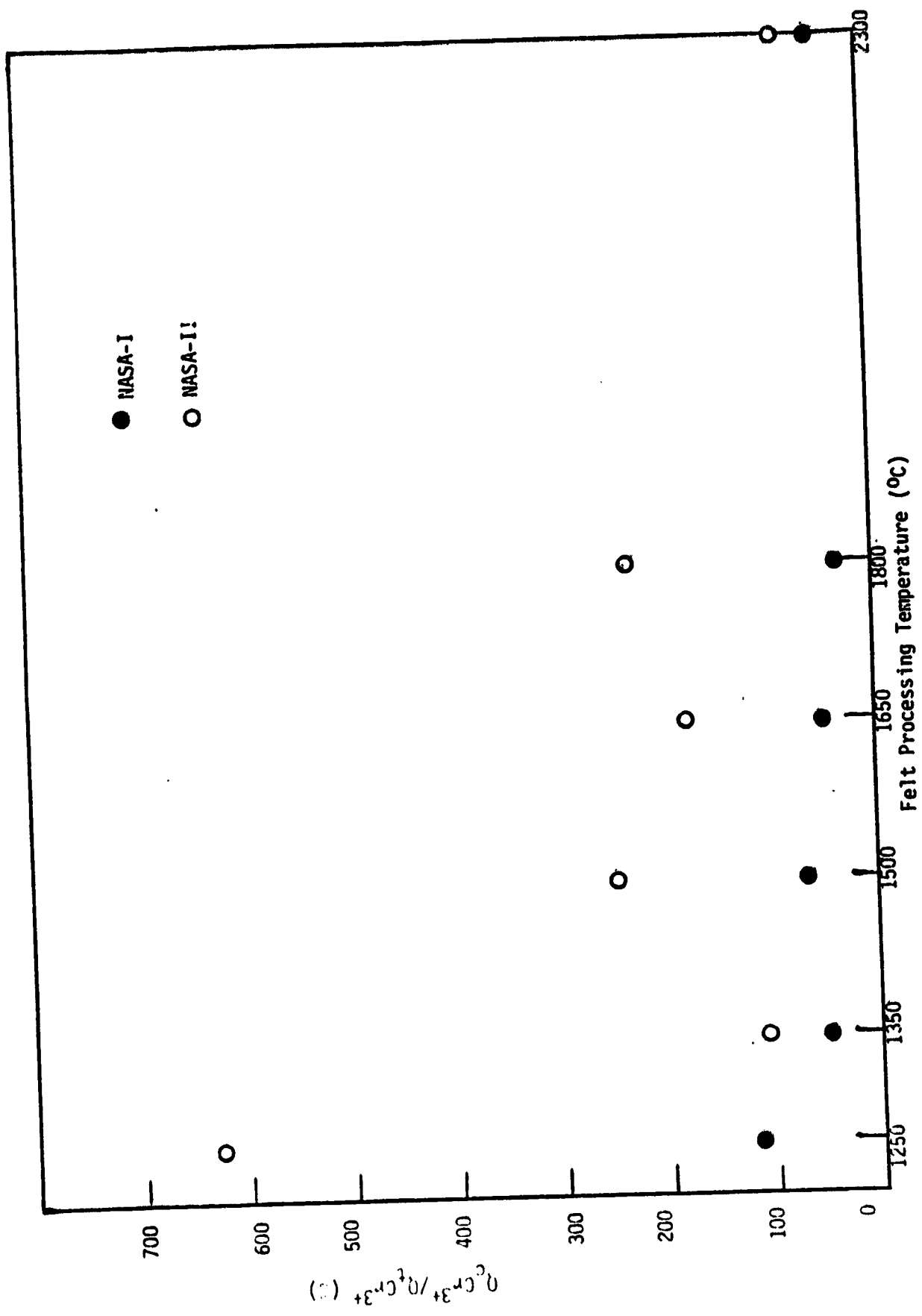


Figure 41. Fraction of Available Chromic Ion Reduced Versus Felt Processing Temperature.

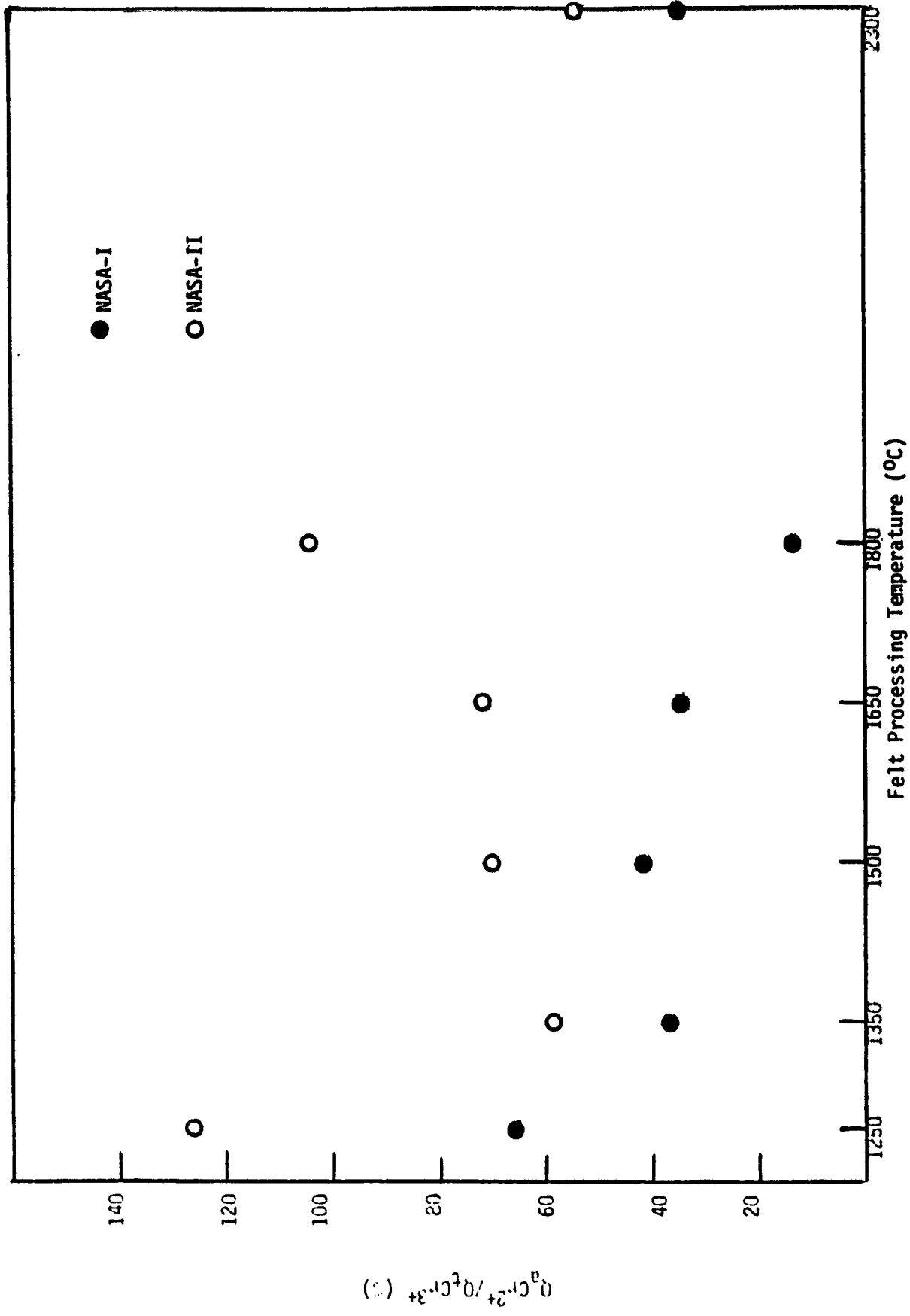


Figure 42. Quantity of Cr<sup>2+</sup> Oxidized as a Fraction of Available Cr<sup>3+</sup> (%) Versus Felt Processing Temperature.

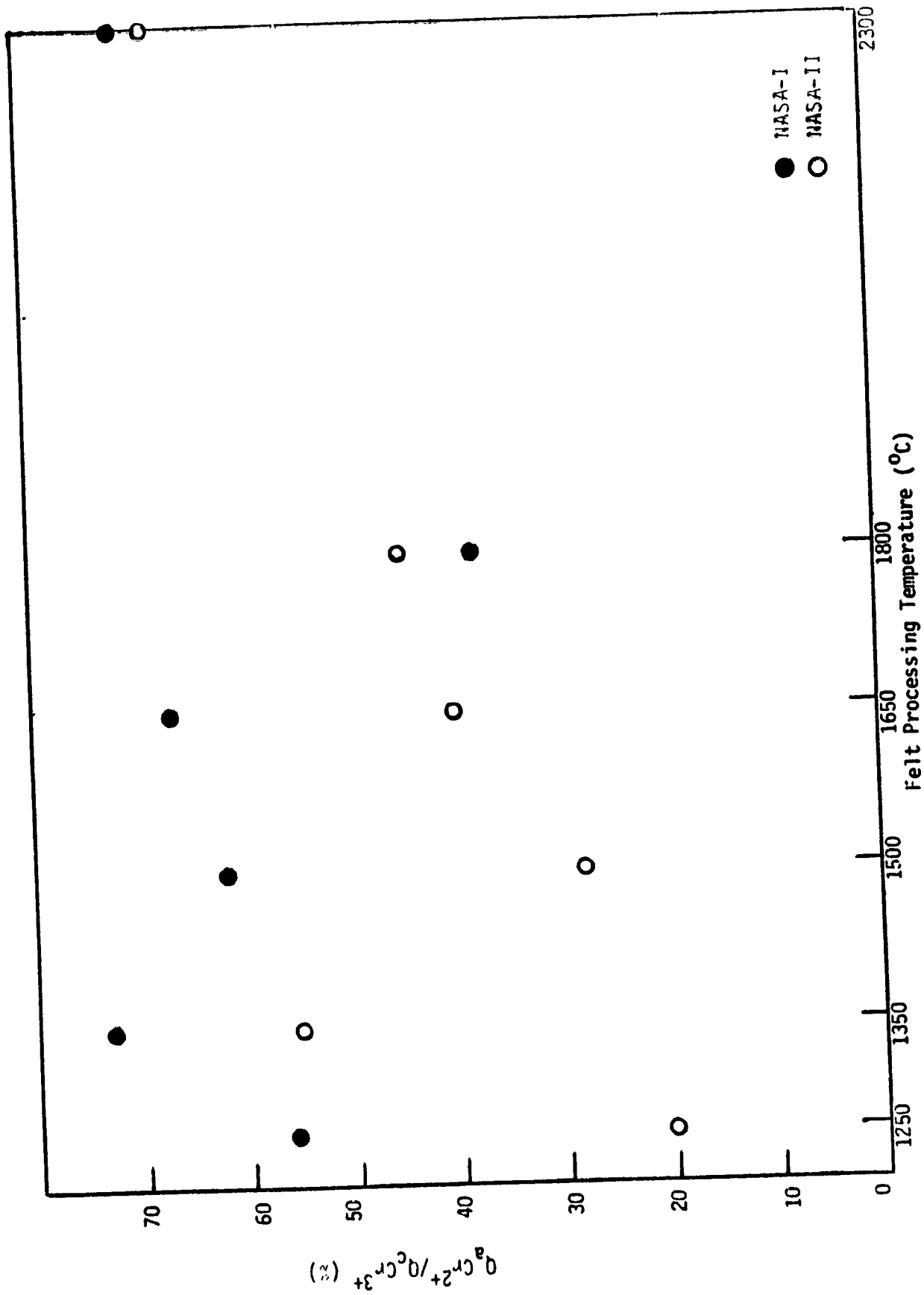


Figure 43.  $Q_{aCr2+}/Q_{cCr3+}$  (%) Versus Felt Processing Temperature.

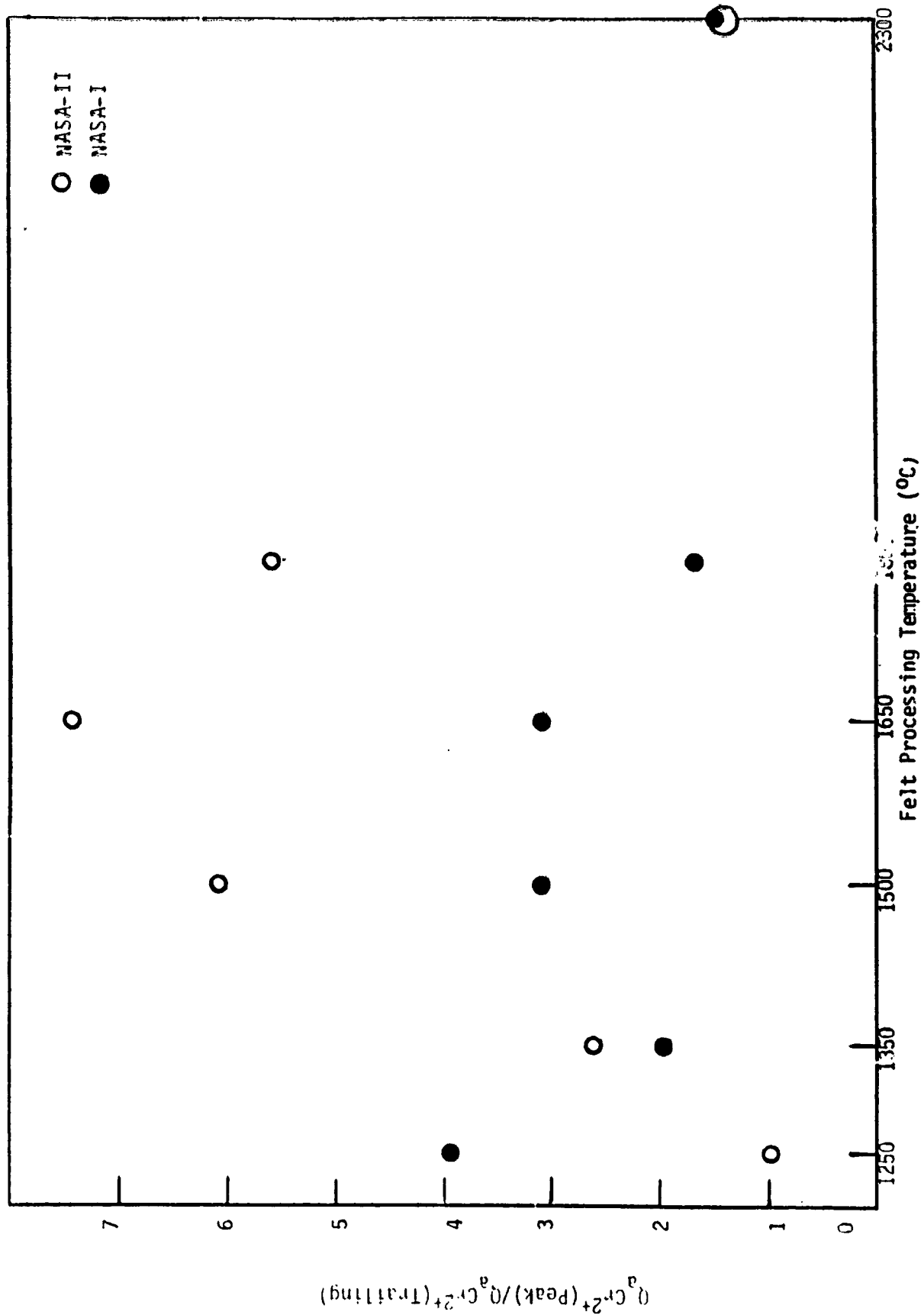


Figure 44. Ratio of Anodic Chromium Charge (Peak) to Anodic Chromium Charge (Trailing) Versus Felt Processing Temperature.



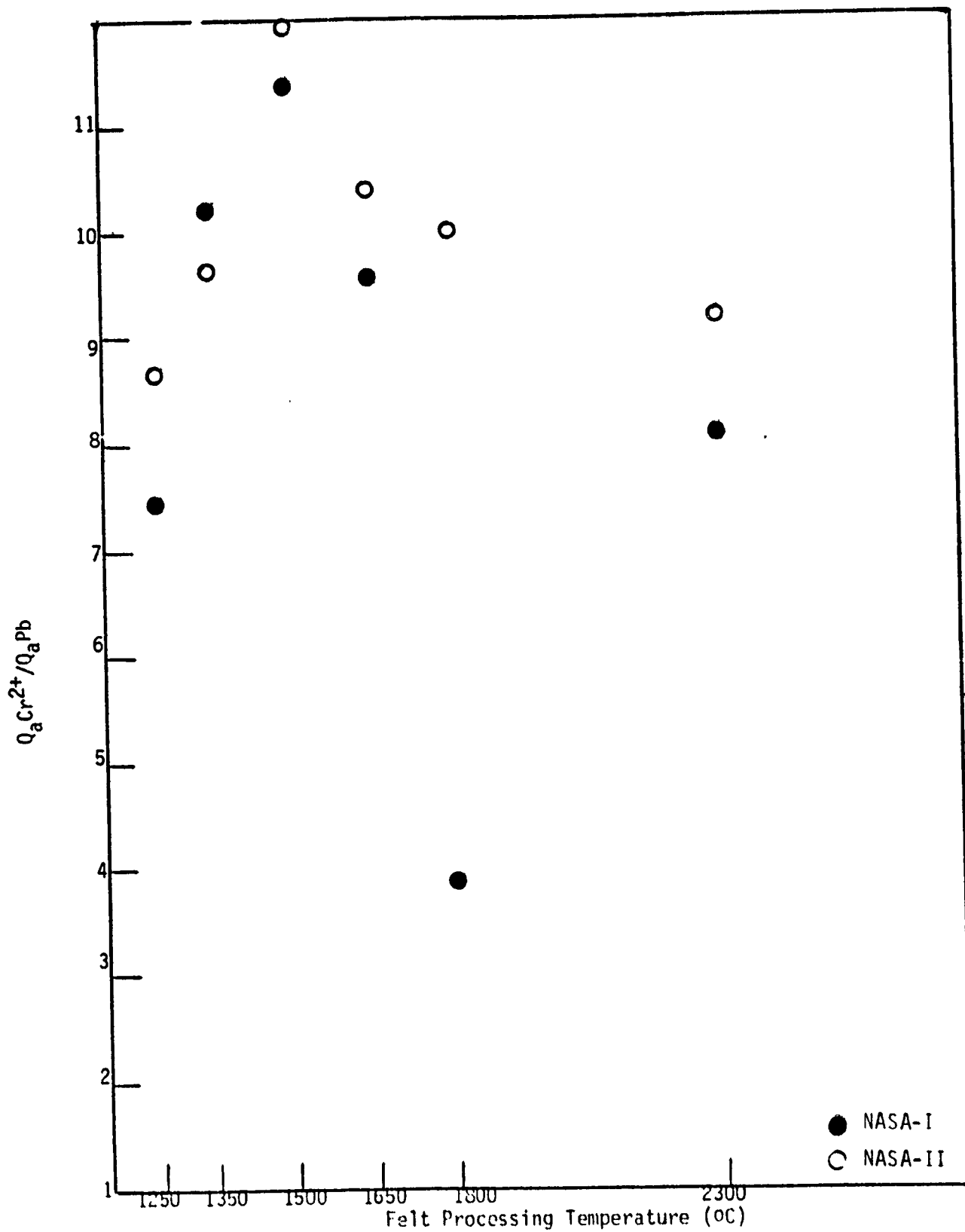


Figure 46. Ratio of Anodic Chromium Charge to Anodic Lead Charge Versus Felt Processing Temperature.

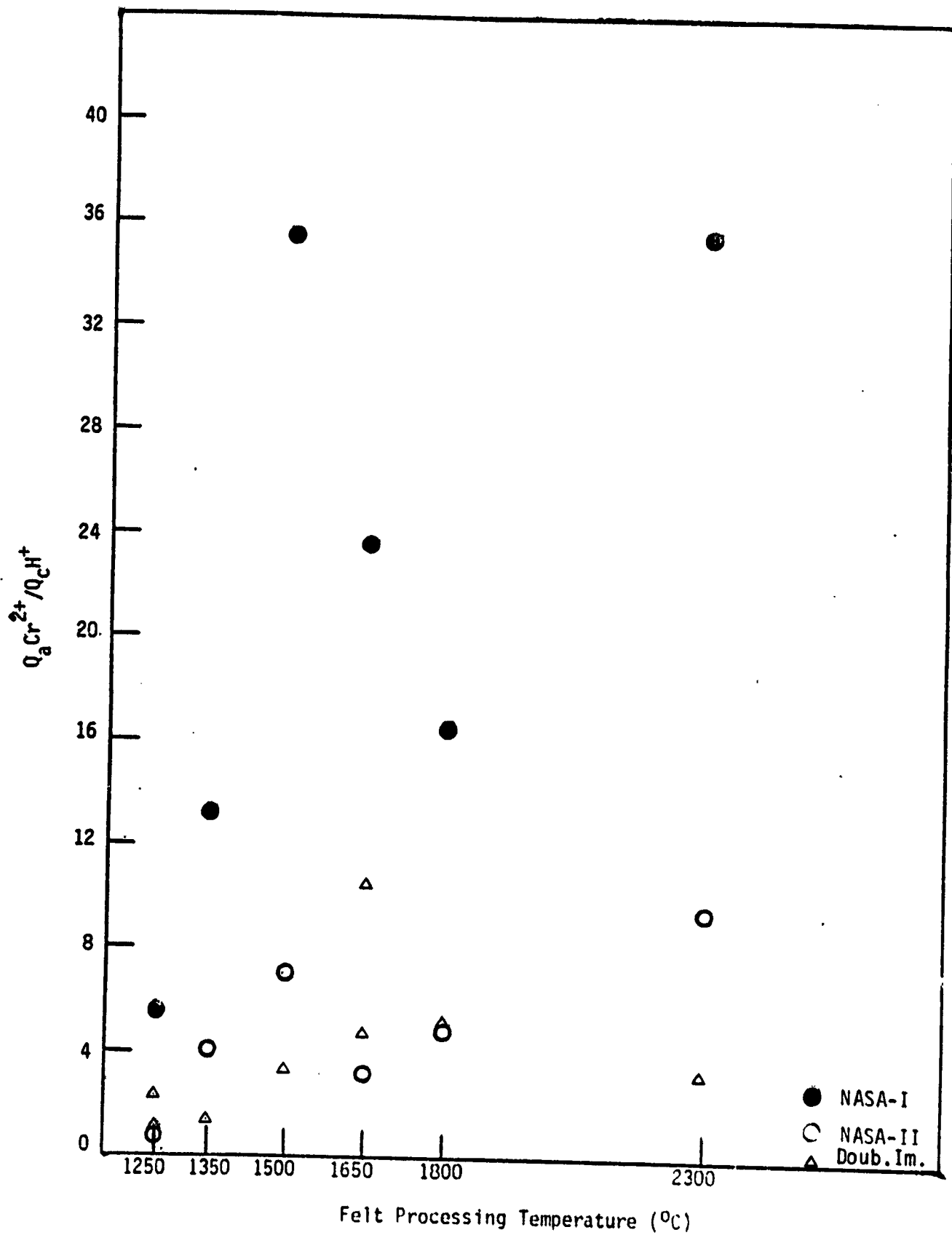


Figure 47. Ratio  $Q_aCr^{2+}/Q_cH^+$  Versus Felt Processing Temperature.

## B. Controlled Variations of Catalyzing Procedure

In the previous section, it was noted that variations in some of the steps in the catalyzation process resulted in clear differences in electrochemical performance and some variations in gold particle sizes. In order to explore this further, a set of carbon felt samples were catalyzed under carefully controlled conditions incorporating precise modifications. The modifications were directed primarily at the effects of gold solution concentration/volume, solution/felt contact conditions and time, and baking.

### 1. Procedure

Six 49 cm<sup>2</sup> samples were cut from Lot 011882 - 1650°C carbon felt for this study. Each sample was cleaned in 1N KOH for about 30 minutes at 90°C, rinsed thoroughly and dried at 110°C. All felts were exposed to the gold solution in the dry state (i.e., the damp-dried procedure was not used). All of the samples were subjected to the same initial immersion procedure, except for double solution volume in one case (DVP-16): five minutes in solution in air, with rotation of the sample after 2 minutes. After the initial 5 minute immersion, samples varied in the type of extended storage (open to the air or enclosed in a plastic bag) and the storage time (from zero to 16 hours). At the end of the storage periods, all of the samples were oven-dried at 110°C for 2 hours; then five of the six samples were baked at 270°C for 2 hours, the sixth sample (EVA-180) was not baked. These parameters are summarized in the table below:

Sample I.D.	Solution Vol.(ml)	Type of Storage	Wet-Storage Time (hrs.)	Baking Temp(°C)
EVP-16	16	closed*	16.0	270
DVP-16	32	closed*	16.0	270
EVA-5B	16	open	0.0	270
EVA-30B	16	open	0.5	270
EVA-180B	16	open	3.0	270
EVA-180	16	open	3.0	---

\*enclosed in plastic bag

## 2. Results

The electron micrographs obtained for each of these samples are shown in Appendix III, Figures AIII-1 to 6 (magnification 90,000X; 1 mm = 11  $\mu$ m). The three "open-immersion" samples (EVA-5B, EVA-30B and EVA-180B) do not show significant distinguishing features; all three samples show similar particle sizes, although the shorter exposure-time samples appear to include smaller particles in addition. The "flash evaporation" of the solvents from sample EVA-5B apparently did not give rise to large particles as was anticipated. The sample that was not baked at 270°C (EVA-180) shows one large particle and other particles of "typical" size, and the gold particles apparently form without the aid of thermal decomposition at 270°C. These findings may suggest that deposition occurs by adsorption from a colloidal gold state, induced by contact with the carbon felt (as discussed in Section A above, excess solutions were observed to be violet or blue in color, indicative of colloidal gold).

The sample prepared with double volume (and half the gold concentration) and stored in a plastic bag for 16 hours (DVP-16), exhibits a

particle size range similar to the open-exposure samples discussed above. The comparison sample, using no excess solution (EVP-16), shows an extraordinary range of particle sizes, from 10-400 nm, making an evaluation difficult.

In general, it is difficult to clearly identify a processing effect on particle size for the parameters examined. In view of the observations that gold particles are formed before the 270°C baking step and appear after only a brief immersion in solution followed by rapid oven drying, the initial moments of the catalyzation process could be a very significant phase in the preparation of an electrode.

Cyclic voltammograms were recorded, in the usual manner for all six of these samples. For comparison, selected data values were extracted from the voltammograms; charge segment data is presented in Table XI (corresponding current data points in Table AIII-I, Appendix III). Some of these values, representative of electrochemical performance, together with gold particle sizes (average diameter,  $\bar{x}$ , based on mean of length and width measurements, and one standard deviation,  $s$ ) are presented below. There is no obvious correlation between performance and gold particle size. The two samples prepared by variations of the NASA process, EVP-16 and DVP-16, exhibited  $\text{Cr}^{2+}$  redox activity in the range between NASA-I and NASA-II preparations. The DVP-16 sample prepared with excess volume showed an exceptionally low hydrogen evolution rate resulting in very high charging efficiency. The unbaked sample, EVA-180, showed the highest  $\text{Cr}^{2+}$  redox activity and was reproducible. These samples also show the highest lead loading. These factors would seem to indicate a high gold surface area but this was not confirmed by electron microscopy. In a similar inversion, the sample exhi-

biting the smallest particle sizes, EVA-5B, gave the lowest Cr<sup>2+</sup> redox activity.

Sample I.D.	Vol. (ml)	Exposure Condition	Time (hr)	Q <sub>a</sub> Pb (mC)	Q <sub>a</sub> Cr <sup>2+</sup> (mC)	Q <sub>C</sub> H <sup>+</sup> (mC)	QCr/OH	Size of Au Part. (nm) X̄ s	
EVP-16	16	Closed	16.0	136	1709	51	33.5	102	88
DVP-16	32	Closed	16.0	129	1458	7	208.0	27	25
EVA-5B	16	Open	0.0	123	1154	20	57.7	18	11
EVA-30B	16	Open	0.5	149	1838	171	10.7	18	19
EVA-180B	16	Open	3.0	147	1969	23	85.6	28	20
(REPEAT)	"	"	"	174	1993	143	13.9		
EVA-180*	16	Open	3.0	272	2361	327	7.2	89	109
(REPEAT)	"	"	"	270	2443	313	7.8		

\*sample not baked at 270°C

TABLE XI

Comparison of Quantities of Reactants Reduced or Oxidized to Quantities of

Catalyzation Parameter Variation:

Reactants Theoretically Available

Sample I.D.	*Q <sub>t</sub> Pb <sup>2+</sup> Theor. (mcoul)	Q <sub>a</sub> Pb Meas. (mcoul)	Q <sub>c</sub> H <sup>+</sup> Meas. (mcoul)	*Q <sub>t</sub> Cr <sup>3+</sup> Theor. (mcoul)	Q <sub>c</sub> Cr <sup>3+</sup> Meas. (mcoul)	Q <sub>a</sub> Cr <sup>2+</sup> Meas. (mcoul)	Q <sub>cd</sub> Cr <sup>3+</sup> Calc. (mcoul)	$\frac{Q_a Cr^{2+}}{Q_c H^+}$
EVP-16	128	136	51	3190	2167	1709	458	33.5
DVP-16	128	129	7	3190	1960	1458	502	208.0
EVA-5B	128	123	20	3190	1547	1154	393	57.7
EVA-30B	128	149	171	3190	2421	1838	583	10.7
EVA-180B	128	147	23	3190	2633	1969	664	85.6
EVA-180B(R) <sup>+</sup>	128	174	143	3190	2353	1993	360	13.9
EVA-180	128	272	327	3190	3001	2361	640	7.2
EVA-180(R) <sup>+</sup>	128	270	313	3190	3123	2443	680	7.8

\*Theoretical reactant quantities available based on calculated open volume of felt sample and solution concentration.

+ (R) = Rerun with another electrode from sample.

### C. Effects of Pre-Catalyzation State and Catalyzation Temperature

In the course of catalyzing electrodes over a period of many months, other process variables that could affect the gold deposit were noted. Some of these are related to the precatalyzation state of the carbon felt such as its moisture content, damp or dry and its residual pH. Other factors are the wetting agent used (methanol or acetone), and the temperature of the catalyzing process. The work done to determine the effects of these factors is discussed in this section.

#### 1. Effects of Damp or Dry Felt and Wetting Agent

In earlier work on this program, after the pretreatment process in KOH the felt was normally oven dried. The objective at that time was to control the total amount of gold deposited (to study gold loading effects) by using a quantity of gold solution equal to the absorption capacity of the felt sample (i.e. no excess solution). The absorption capacity of the felt was determined by weighing the water-saturated felt at the end of the pretreatment process and again after drying. At NASA-LeRC, the customary practice was to towel-dry the felt samples to a "damp" state after the pretreatment process and then proceed directly to catalyzation. In the damp state the carbon felt absorbs less gold solution giving rise to the "excess" solution noted in Section III. In the study of controlled variations in Section B above, all of the samples were prepared from dry felts (i.e. oven-dried after pretreatment). Examination of that data does not indicate a significant effect that could be attributed solely to the use of dry felts. In fact, sample preparation EVA-180B, which most closely resembled the Double Immersion process (a dry felt method), is quite different in electrochemical performance from electrodes prepared by the

Double Immersion process.

This same factor was investigated in a separate study in which the use of acetone rather than methanol was also examined. Four variations were studied using 1650°C felts. These are:

- 1) Methanol/dry
- 2) Methanol/damp (NASA-I)
- 3) Acetone/dry
- 4) Acetone/damp

a. Experimental Procedures

Four samples of 1650° felts (Lot 051882) were activated by following the standard NASA procedure (NASA-I) with certain modifications. The modification for the sample designated "methanol dry" was to apply the gold chloride solution to a thoroughly dried felt. For the sample designated "methanol damp", the standard procedures were used without modification. The modification for the sample designated "acetone damp" was to substitute acetone for methanol. The modifications for the sample designated "acetone dry" were to substitute acetone for methanol and to apply the gold chloride solution to a thoroughly dried felt.

"Dry" felts were thoroughly oven dried. The term "damp" was interpreted to mean internally moist but without visible external moisture. Damp felts were obtained by placing the wet felts between layers of absorbent towels (Shur-Wipe 125 Medium Duty, 2 Ply Wipers) and gently applying pressure with a hand roller. In all cases, 10 ml of solution containing 12.5 micrograms Au/cm<sup>2</sup> was applied to 49 cm<sup>2</sup> of felt, 5 ml to each side.

b. Results

The cathodic and anodic charge segment data extracted from the voltammograms are given in Table XII (corresponding current-data points from the voltammograms are given in Table AIV-I in Appendix IV).

The hydrogen evolution current ( $I_{\text{C}}\text{H}^+$ ) on Au/C in HCl at -950 mV (SCE) ranged from 160 mA for the methanol-damp electrode to 610 mA for the acetone-dry electrode.

From Table XII it is seen that the total cathodic charge attributable to hydrogen evolution ( $Q_{\text{C}}\text{H}^+$ ) varied from 10 mC for the acetone-damp sample to 117 mC for the acetone-dry sample. There was no particular correlation between  $Q_{\text{C}}\text{H}^+$  values and  $I_{\text{C}}\text{H}^+$  values. This is not unexpected based on previous results.

Lead loadings, as measured by anodic lead charge ( $Q_{\text{a}}\text{Pb}$ ) are shown for each optimization felt in Table XII. The values were within the range previously determined for standard NASA-I felts.

The  $\text{Cr}^{3+}/\text{Cr}^{2+}$  redox performance of the four samples is given in Table XII in terms of the total chromous ion oxidation charge. The  $Q_{\text{a}}\text{Cr}^{2+}$  values were within the range of values shown by the standard NASA-I felts except for the high value of 1580 mC for the acetone-dry sample.

To illustrate the relationship to lead loading, the anodic chromium charge ( $Q_{\text{a}}\text{Cr}^{2+}$ ) has been plotted versus lead loading (as  $Q_{\text{a}}\text{Pb}$ ) in Figure 48. The data exhibit the typical direct relationship observed and appear to approach a somewhat better linear correlation than usual.

Values for the ratio of anodic chromium charge ( $Q_{\text{a}}\text{Cr}^{2+}$ ) to cathodic hydrogen charge ( $Q_{\text{C}}\text{H}^+$ ), which may be a relevant overall measure of relative charging efficiency, are presented below. The values of this ratio for the four optimization felts are within the range of values found previously for NASA-I felts with the highest value being shown by the acetone-damp sample.

	$\frac{O_2Cr^{2+}}{O_2H^+}$	$O_2Cr^{2+}$	$O_2H^+$
Methanol/Dry	24.9	1144	46
Methanol/Damp	20.2	890	44
Acetone/Dry	13.5	1580	117
Acetone/Damp	80	802	10

From an examination of the above data it is clear that this small sample of test data is not sufficient to clearly differentiate the factors tested. Both wetting agents have been used successfully at NASA-LeRC. It was also concluded that the damp/dry condition of the felt per se, prior to catalyzation, was not a significant factor. A related factor, the residual pH of the felt after pretreatment in KOH, was considered to have more potential influence on the subsequent catalyzation. This is discussed below.

## 2. Effects of the Residual pH of the Carbon Felt

On this program the carbon felts have always been pretreated in KOH according to procedures developed on the last program (16). The felts were always thoroughly rinsed after this pretreatment, but it was observed that water dripping from the rinsed felt could vary from pH 5 to 9. For this reason, this factor was examined over this pH range under more controlled conditions.

### a. Experimental Procedure

Nine samples from the 1700°C felt (lot 051482) were soaked in methanol, rinsed, damp-dried and then placed in 45% KOH at 90°C for 2 hours. The samples were subsequently rinsed to pH 6, soaked in distilled water

overnight (pH 6) and then drained and dried. Subsequently, three samples each were immersed in water with pH adjusted to 5, 7 and 9 (using KOH or HCl), vacuum deaerated and allowed to soak for one and a half hours. From these pH controlled rinses, the samples were damp-dried and then catalyzed according to the rest of the standard NASA procedure (8). An additional control point was introduced by holding the temperature of the aqueous gold chloride solution at 25°C after mixing with methanol prior to immersion of the felt.

Two electrodes at each pH value were subjected to the standard cyclic voltammetry routines described in Section II. In addition, after completion of the last voltammogram (1N HCl, 1mM PbCl<sub>2</sub>, 50 mM CrCl<sub>3</sub>) at 25°C, the temperature was raised to 45°C and then 65°C. The usual charge segment data were extracted from the voltammogram for comparisons.

#### b. Results

Charge segment data are plotted in Figures 49 and 50 versus test temperature. It can be seen that the electrochemical performance was not reproducible for any pH value sample tested. A plot of  $Q_{aCr^{2+}}$  versus  $Q_{aPb}$  shown in Figure 51 illustrates the direct relationship usually found between these values, however.

These samples were also submitted for examination by transmission electron microscopy (TEM). The photographs are shown in Appendix IV. For comparison, the average gold particle size was determined in each case; these values together with selected electrochemical performance data are presented below:

CATALYZ.	PRE-CAT.	$Q_a^{Pb}$	$Q_a^{Cr^{2+}}$	$Q_c^{H^+}$	$Q_{Cr/OH}$	Au PARTICLE SIZE (nm)	
TEMP (°C)	pH	(mC)	(mC)	(mC)	(mC)	( $\bar{X}$ )	(s)
A 25	5	178	1883	132	14.3	66.3	68.8
B 25	5	113	832	12.3	67.6	53.7	31.2
A 25	7	138	1023	126	8.1	56.4	29.8
B 25	7	213	2155	108	20.0	31.6	16.1
A 25	9	236	2281	920	2.5	67.9	93.3
B 25	9	121	545	80	6.8	57.3	92.5

The mean particle size ( $\bar{X}$ ) is fairly consistent in all cases, but the range of sizes for the pH 9 samples was much larger as reflected in the large standard deviation values (s).

Again, the data do not permit any clear selection of conditions but suggest rather that 1) a pH range of 5 to 9 is an acceptable precatalyzation condition for the carbon felt, and 2) still other factors are influencing the catalyzation or testing process.

### 3. Effects of Catalyzation Temperature

It was noted that the mixing of the aqueous gold chloride and methanol was an exothermic process raising the solution temperature by 5 - 10°C. This could be of significance since the solution was customarily mixed immediately before use (to avoid precipitation of gold) and the first few minutes of contact with carbon felt may be crucial, as discussed in Section V-B above. In order to explore the possible effects of catalyzation temperature on electrochemical performance and gold particle size formation, carbon felts were catalyzed at three different temperatures with the extremes beyond any normal ambient range, 0°, 25°, and 50°C.

a. Experimental Procedure

Samples of 1700°C (lot 051482) felt were catalyzed according to the standard NASA procedure (8) with the addition of two important control points. In order to control any potential effects of residual felt pH, as discussed above, KOH-treated felts were soaked in water of neutral pH immediately before the damp-drying step prior to catalyzation. The actual criterion was that one and one half hours of soaking should produce no discernible change in the pH of previously boiled unbuffered distilled water of pH 7.0. In addition, the aqueous gold chloride solution and reagent grade methanol were thermostated in a water bath before and after mixing. The temperature of the gold deposition solution was monitored closely and the solution applied to the damp-dried felt only when it was within one degree of the specified temperature, 0°, 25° or 50°C. The felts were then held at the catalyzation temperature ( $\pm 5^\circ\text{C}$ ) for 16 hours.

Catalyzed felts were mounted and waxed as usual and tested by cyclic voltammetry, as described in Section II, first in a solution of 1mM  $\text{PbCl}_2$  in 1 N HCl at 25°C. Chromium chloride was then added (50 mM) and a second voltammogram was recorded at 25°C. These samples were also submitted for examination by transmission electron microscopy (TEM).

## b. Results

The TEM photographs are shown in Appendix IV, Figures AIV-6 to 8. Charge segment data were extracted from the voltammograms and are presented below together with mean gold particle sizes (X) in each case.

CTLYZ. TEMP. (°C)	PRE- CAT. pH	$Q_a$ Pb (mC)	$Q_a$ Cr <sup>2+</sup> (mC)	$Q_c$ H <sup>+</sup> (mC)	QCr/OH	Au PARTICLE SIZE (nm) (X)	(s)
0	7	176	1650	87	19.0	24.4	18.1
25	7	213	2155	108	20.0	56.4	29.8
50	7	132	932	28	33.3	62.0	63.1

It can be seen that there was a progressive increase in gold particle size with increasing catalyzation temperature as anticipated. The range of particle sizes (standard deviation, s) also increased with increasing temperature. The charge segment data is quite scattered but the values for relative charging efficiency improved somewhat with increasing catalyzation temperature. This data suggests that, although catalyzation temperature affects gold particle size in an expected manner, here again there are other factors influencing electrochemical performance.

TABLE XII. Catalyzation Optimization Study

Comparison of Quantities of Reactants Reduced or Oxidized to Quantities of Reactants Theoretically Available

Theoretical reactant quantities available based on calculated open volume of felt sample and solution concentration.

Electrode Description	$Q_{tPb^{2+}}$ Theor. (mcoul)	$Q_{aPb}$ Meas. (mcoul)	$Q_{cH^+}$ Meas. (mcoul)	$Q_{tCr^{3+}}$ Theor. (mcoul)	$Q_{cCr^{3+}}$ Meas. (mcoul)	$Q_{aCr^{2+}}$ Meas. (mcoul)	$Q_{cdCr^{3+}}$ Calc. (mcoul)
Optimization	108	120	46	2697	1524	1144	380
Methanol Dry	108	110	44	2697	1297	890	407
Methanol Damp	108	142	117	2697	2031	1580	451
Acetone Dry	108	107	10	2657	1175	802	373

ORIGINAL PAGE IS  
OF POOR QUALITY

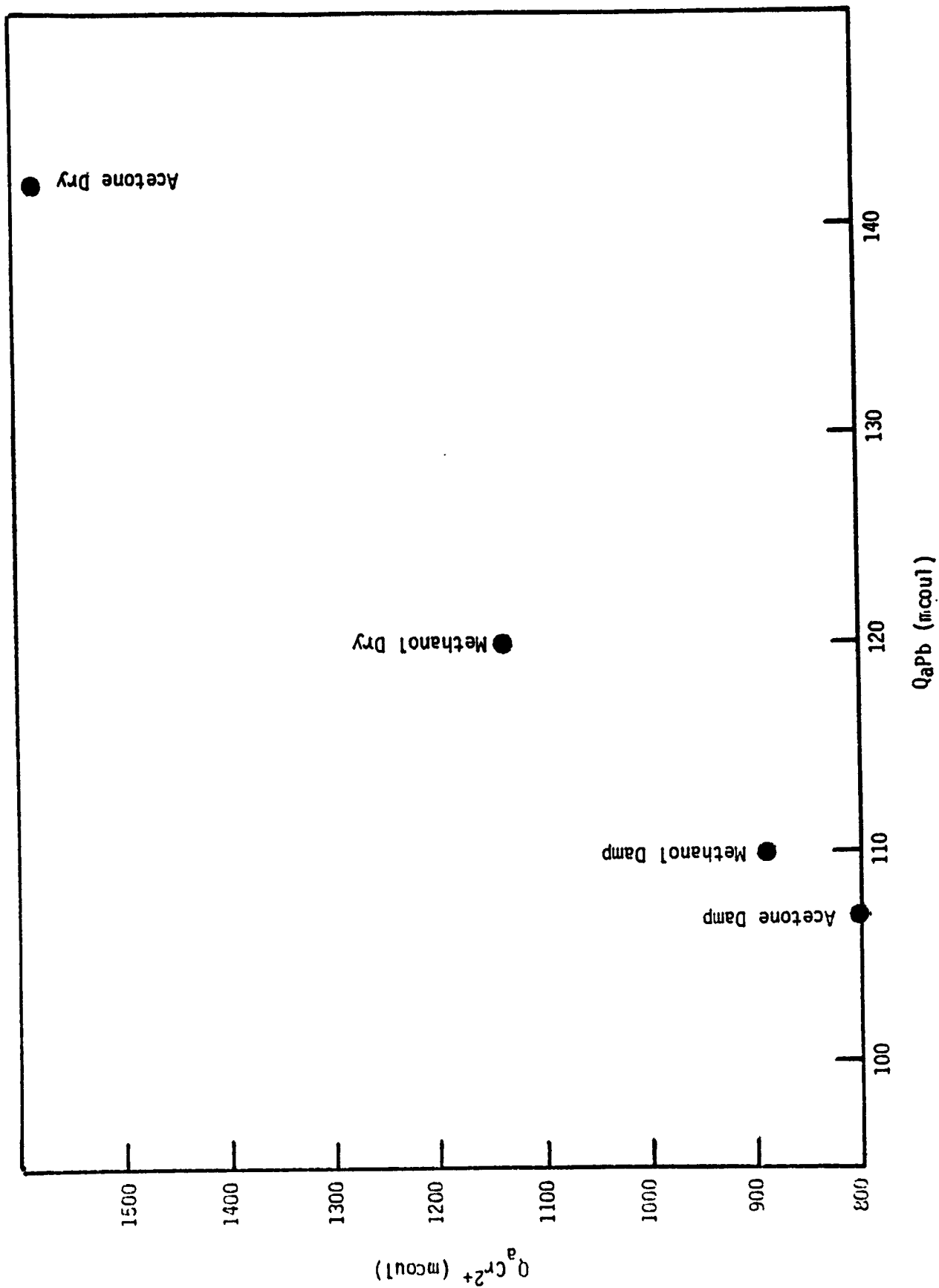


Figure 48. Total Anodic Chromium Charge Versus Anodic Lead Charge  
(Catalyzation Optimization Study)

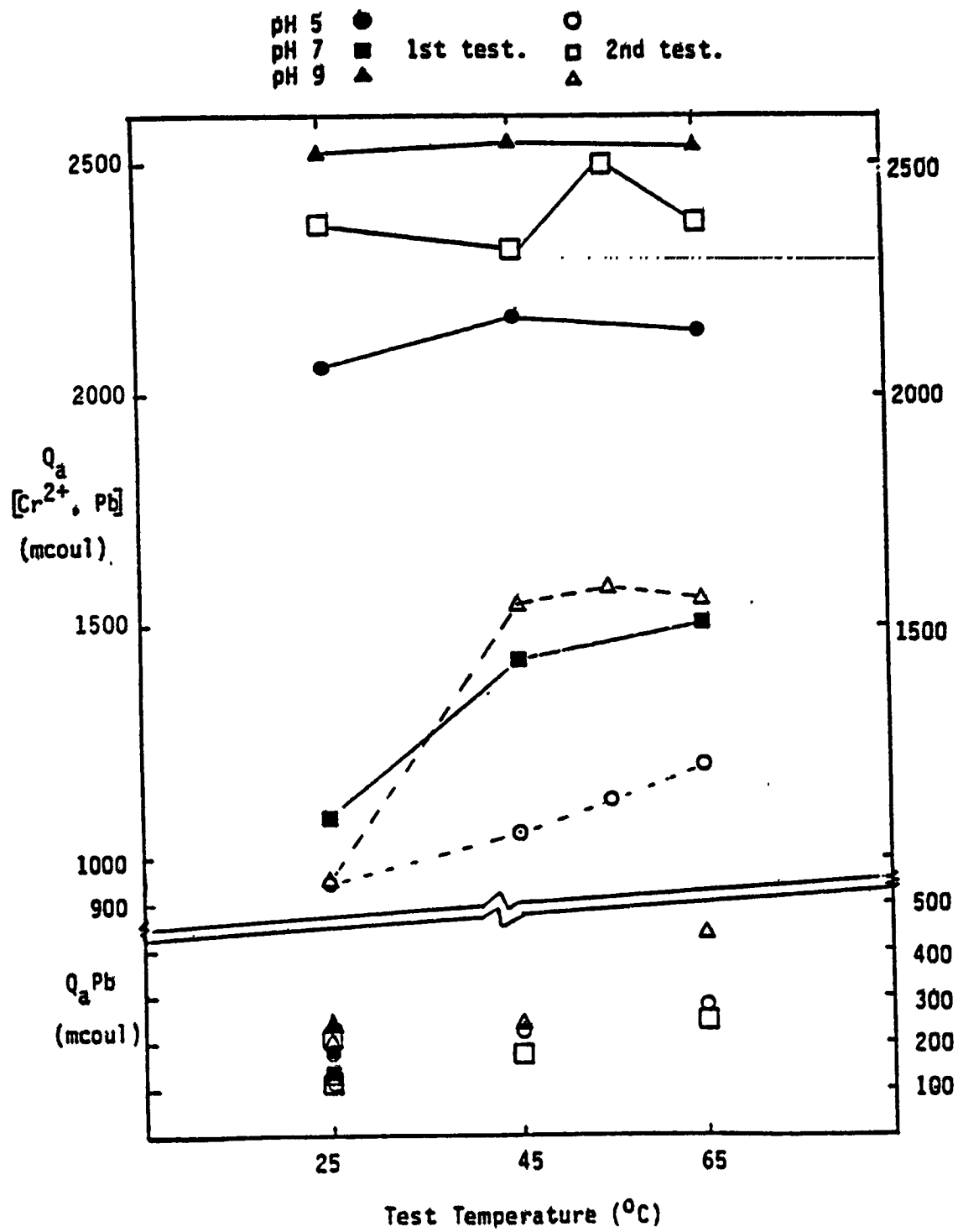


Figure 49. Anodic Charge versus Test Temperature and Precatalyzation Felt-pH.

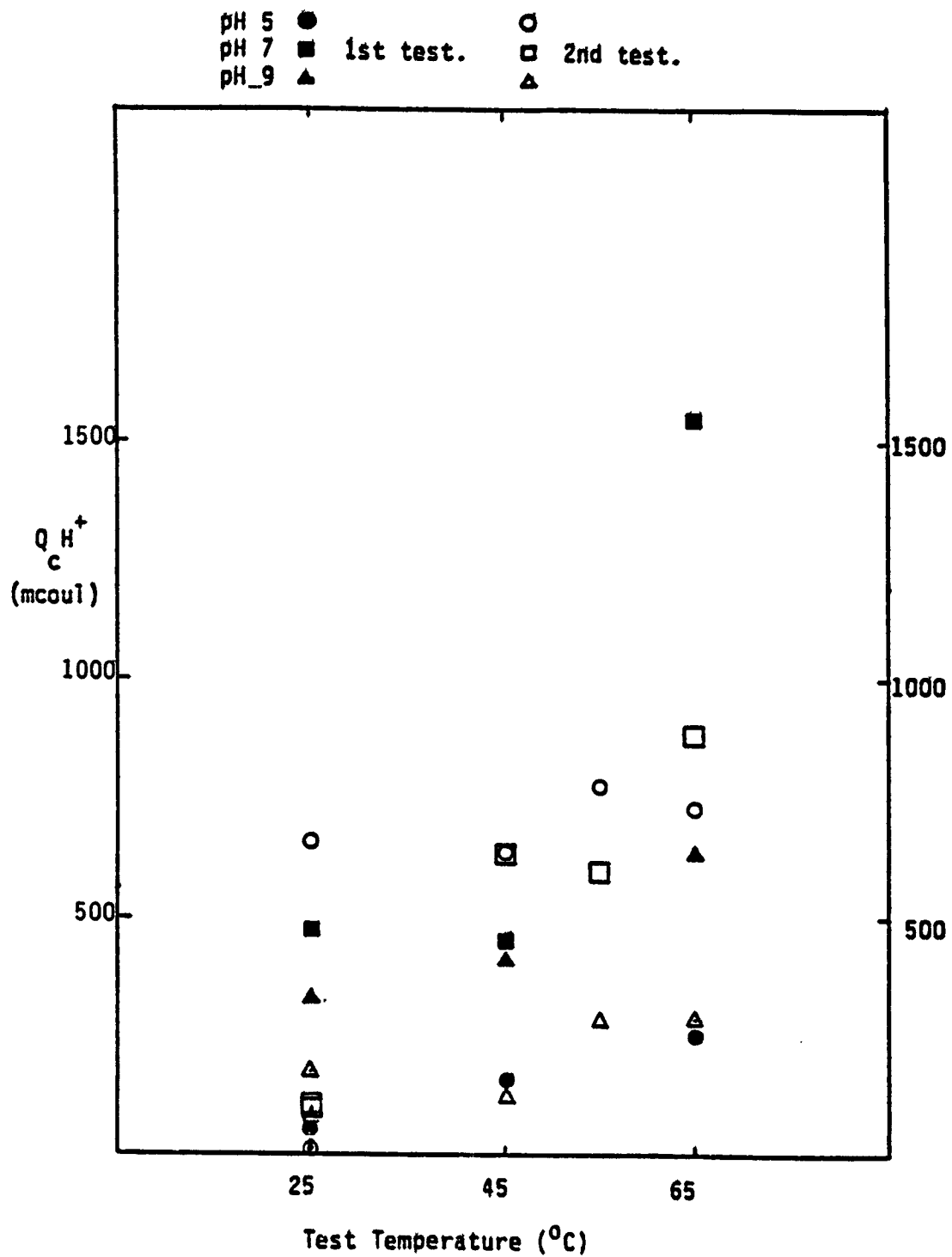


Figure 50. Relative Hydrogen Evolution Rate vs. Test Temperature and Precatalyzation Felt pH.

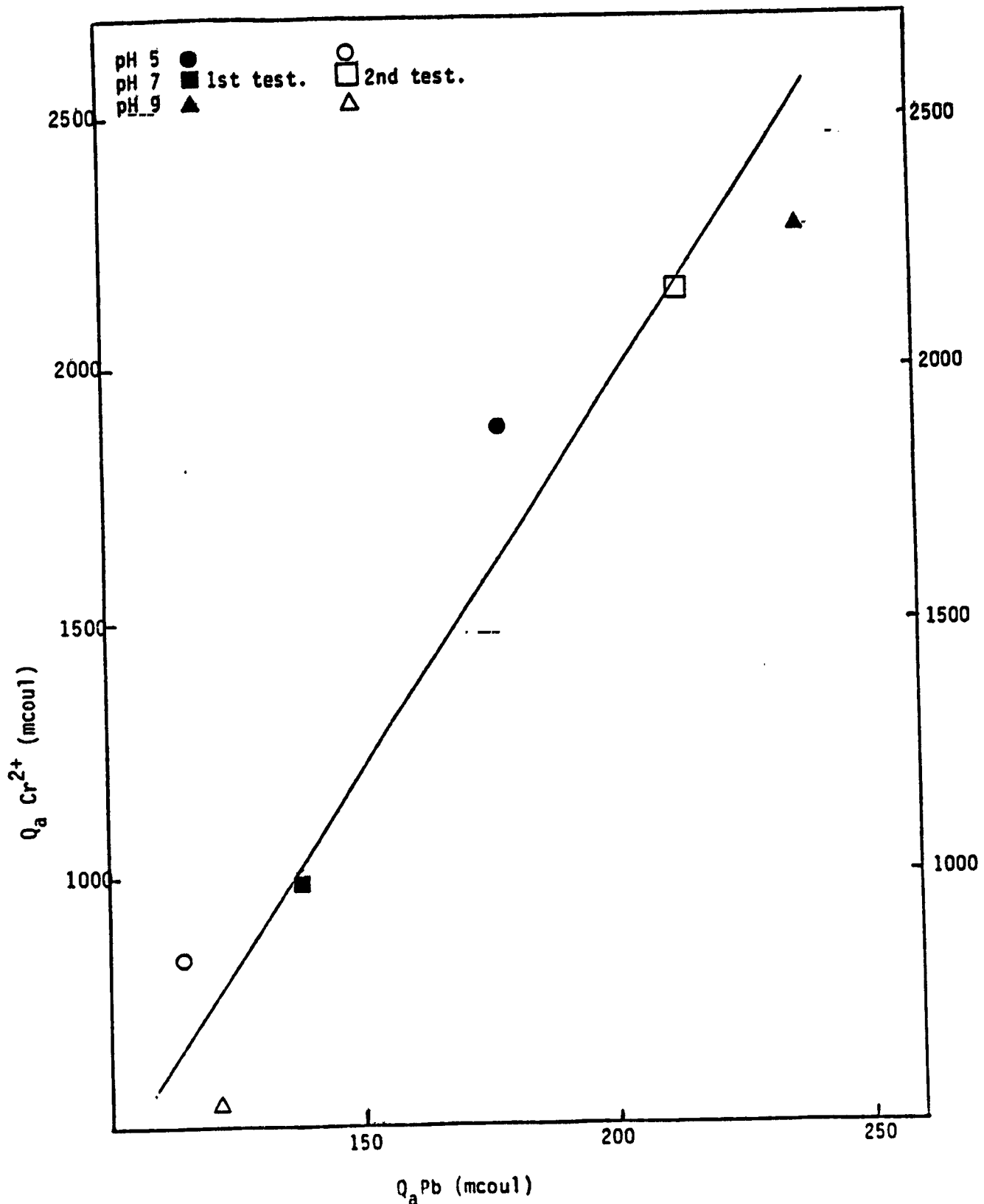


Figure 51.  $\text{Cr}^{2+}$  Oxidation Charge vs. Pb Loading (Pb Oxidation Charge) at  $25^{\circ}\text{C}$ .

#### D. Reproducibility of Electrochemical Performance

In the previous studies directed to defining the critical factors in the gold catalyzation process, discussed in Sections V A through C above, the electrochemical performance observed was frequently erratic suggesting that some influential factors were not being controlled. One such factor is the carbon felt substrate, which can exhibit variations in physical and chemical properties and has been found to influence performance, as discussed in Section IV. The KOH pretreatment process is directed to neutralizing some of the chemical properties of the felt, but it is obviously not completely effective and does not address variations in physical properties such as density, thickness and surface area. Thus the carbon felt remains as a potentially influential factor that is probably not completely controllable. Another factor is the cyclic voltammetry testing procedures used. This study was directed to the latter, assuming that the carbon felt substrate over a small area would be sufficiently uniform in properties. A concerted effort was made to control all other factors in the catalyzation and testing processes.

For this purpose, three felt samples (from a small section of one lot of felt) were catalyzed in three separate operations using the same catalyzation method (NASA-I). Each sample was then cut into three strips to provide a total of nine samples for electrochemical testing. In order to exercise greater control over the catalyzation process, each sample was pretreated in a measured quantity of potassium hydroxide and an individual quantity of aqueous gold solution was mixed with methanol (an exothermic process) immediately prior to use and thermostatted for a fixed period of time. The least controllable step in the process is damp-drying of the

felt. This procedure has not been found to be significant and was not intentionally modified, but the results were observed to be qualitatively different than in previous preparations.

#### 1. Experimental Procedures

Three 49 cm<sup>2</sup> samples were cut from carbon felt Lot 011882 - 1650°C. Each felt was placed in a separate beaker and covered with 200 ml of 1N KOH and a weight to keep it submerged. The beakers were evacuated three times in succession to remove air from the felt samples. The beakers were then removed from the vacuum dessicator and placed on hot plates. It took 20 minutes for the temperature of the KOH to reach 90°C. The temperature was maintained near 90°C for 30 minutes more. The felts were rinsed in tap water and then in distilled water. Subsequently the felts were submerged in distilled water and vacuum backfilled three times. Finally the samples were rinsed in distilled water again and submerged in deionized water for about 22 hours.

A 12.5 ml volume of aqueous gold chloride solution (245 micrograms/ml) was placed in a dry 50 ml volumetric. The volumetric was placed in a 24°C water bath and while stirring, reagent grade methanol was added to the mark. The time when methanol was added was noted for each sample. After the methanol/gold chloride solution was mixed, it was left in the water bath while a damp-dried felt was prepared. Two minutes of vigorous damp drying was used. The felts were observed to be qualitatively "drier" than in previous preparations. Immediately before use of the aqueous methanolic/gold chloride solution, a small quantity of methanol was added to bring the solution level back to the mark (the volume had slightly decreased due

to cooling).

Twelve minutes after the initial mixing with methanol, 5 ml of aqueous methanolic gold chloride solution was pipetted into a plastic tray. The damp-dry felt was placed in the tray and pressed for about 5 seconds with a glass beaker. The felt was stored in a Teflon pan while 5 ml more gold chloride solution was placed in the tray. The felt was flipped over, placed in the tray and physically manipulated as before. The felt was then transferred to a plastic bag. Two more felts were activated the same way. One hour and 25 minutes elapsed between the time the first felt was placed in a plastic bag and the third felt was placed in a plastic bag.

The felts were left in plastic bags overnight and then simultaneously air dried for five hours. The felts were heated for two hours in a preheated 110°C oven followed by two hours in a preheated 270°C oven.

## 2. Results

The voltammograms were obtained in identical fashion according to the procedures described in section II. The lead and chromium traces represent in each case the twenty-third iR-compensated cycle. Selected current data points from the voltammograms are presented in Table AV-I in Appendix V. The cathodic and anodic charge segment data extracted from the voltammograms are given in Table XIII. Table XIV shows comparisons of both peak and trailing  $\text{Cr}^{2+}$  charges and various charge ratios. An abbreviated table of values, together with some statistical data, is presented below.

PREP.	SAMPLE...	$Q_a\text{Pb}$ (mC)	$Q_a\text{Cr}^{2+}$ (mC)	$Q_c\text{H}_+$ (mC)	$Q_{\text{Cr}}/Q_{\text{H}}...$
1	A	181	2283	58	39
1	B	129	942	13	72
1	C	113	791	36	22
2	A	116	1380	49	28
2	B	107	970	29	33
2	C	191	1789	80	22
3	A	128	854	30	28
3	B	123	739	29	25
3	C	129	898	33	27
MEAN .		135	1183	40	33
STD. DEV.		30	531	20	16

a. Hydrogen Evolution Characteristics

As shown in Table AV-I, the hydrogen evolution current on Au/C HCl at -950mV (SCE) ranges from 220 mA for sample 3B to 550 mA for sample 1A. There is less variability within sample 3 than within samples 1 or 2.

b.  $\text{Pb}^{2+}/\text{Pb}$  Redox Characteristics

The lead loadings, as measured by anodic lead charge ( $Q_a\text{Pb}$ ), are shown in Table XIII. By this measure also, sample 3 appears uniform, while samples 1 and 2 do not. Seven of the nine values are fairly close together; samples 1A and 2C deviate the most.

c. Cr<sup>3+</sup>/Cr<sup>2+</sup> Redox Characteristics .....

The Cr<sup>3+</sup>/Cr<sup>2+</sup> redox performance of the three samples is presented in Table XIII in terms of total chromous oxidation charge (Q<sub>a</sub>Cr<sup>2+</sup>). Sample 3 is more uniform than samples 1 or 2. The mean values of Q<sub>a</sub>Cr<sup>2+</sup> (mC) and standard deviations for samples 1-3 are respectively: 1330 ± 821, 1380 ± 409, and 830 ± 82 mC.

The results from this study are shown in the context of a selection of previous test data in Figure 52. It can be seen that the data points nearly span the range and thus could mask any differences between catalyzation by the Double Immersion method through the NASA-II method. There is a definite grouping of points around a Q<sub>a</sub>Cr<sup>2+</sup> value of 900 mC; however, it is apparent that a large number of data points might be needed to obtain a statistically significant value.

Table XIV presents various charge ratios, which again show the greatest uniformity for sample 3. The charging efficiency values (ratio of chromous oxidation charge to hydrogen evolution charge), for example, for sample 3 show a mean value of 26.7 with a standard deviation of 1.5. Six of the nine values are fairly close together with a mean of 25.3 and a standard deviation of 2.8.

Presented in the context of the same previous test data in Figure 53, it can be seen that the charging efficiency values show a somewhat better grouping around the previous comparable data point (NASA-I, Phase I) than chromous oxidation charge values alone; nonetheless, there is still some very broad scatter that could skew the results.

TABLE XIII. Reproducibility Study: Summary of Quantities of Reactants Reduced or Oxidized and Quantities of Reactants Theoretically Available.

Electrode Description Sample	* $Q_t\text{Pb}^{2+}$ Theor. (mCoul)	$Q_a\text{Pb}$ Meas. (mCoul)	$Q_c\text{H}^+$ Meas. (mCoul)	* $Q_t\text{Cr}^{3+}$ Theor. (mCoul)	$Q_c\text{Cr}^{3+}$ Meas. (mCoul)	$Q_a\text{Cr}^{2+}$ Meas. (mCoul)	$Q_{cd}\text{Cr}^{3+}$ Calc. (mCoul)
1A	128	181	58	3190	3192	2283	909
1B	128	129	13	3190	1425	942	483
1C	128	113	36	3190	1101	791	310
2A	128	116	49	3190	1938	1380	558
2B	128	107	29	3190	1335	970	365
2C	128	191	80	3190	2303	1789	514
3A	128	128	30	3190	1202	854	348
3B	128	123	29	3190	1075	739	336
3C	128	129	33	3190	1169	898	271

\*Theoretical reactant quantities available based on calculated open volume of felt sample and solution concentration.



TABLE XIV

Reproducibility Study:--Summary of Charge Segments and Ratios.

<u>Electrode Sample</u>	<u>Q<sub>a</sub>Cr<sup>2+</sup>(peak) (m coul)</u>	<u>Q<sub>a</sub>Cr<sup>2+</sup>(trail) (m coul)</u>	<u><math>\frac{Q_{aCr^{2+}}(\text{peak})}{Q_{aCr^{2+}}(\text{trail})}</math></u>	<u>Q<sub>a</sub>Cr<sup>2+</sup>/Q<sub>a</sub>Pb</u>	<u>Q<sub>a</sub>Cr<sup>2+</sup>/Q<sub>C</sub>H<sup>+</sup></u>
1A	1638	645	2.5	12.6	39
1B	465	477	1.0	7.3	72
1C	265	526	0.5	7.0	22
2A	774	606	1.3	11.9	28
2B	441	529	0.8	9.1	33
2C	976	813	1.2	9.4	22
3A	269	594	0.4	6.7	28
3B	284	455	0.6	6.0	25
3C	323	575	0.6	7.0	27



### E. Study of Lead Distribution on Electrodes

The objective of this investigation was to prepare electrode samples for microscopic analysis of the active lead/gold catalyst structure. The size, shape and distribution of gold catalyst particles on carbon felt electrodes have been studied, principally by means of transmission electron microscopy, and reported here and under previous contracts (16). The catalyst actually present during the  $\text{Cr}^{2+}/\text{Cr}^{3+}$  redox reaction, however consists of metallic lead deposited from solution in addition to the aforementioned gold particles. The disposition of the lead component of the catalyst, while crucial to the performance of the negative electrode, has not been systematically studied. There are numerous possibilities: lead may exist, for example, as a thin plating on the gold crystallites, or even directly on the carbon fiber substrate; or as particles situated on, adjacent to, or far removed from the gold particles; or, of course, any combination of these. Furthermore, it cannot be anticipated that all lead/gold configurations would function as equally efficient electrocatalysts. Knowledge of the two-component catalyst structure could provide explanations for some of the performance variations observed. Thus, attempts were made to prepare suitable samples for microscopic examination. In addition to transmission electron microscopy, X-ray dot-mapping techniques were also tried to examine the lead versus gold distribution.

The intent was to plate lead on identical pairs of catalyzed carbon felt electrode samples under normal conditions and, after establishing some baseline performance characteristics, to preserve the lead/gold structure by quickly rinsing and drying the felts. One sample of each pair was retained for analysis; the second was returned to the half cell to determine whether

this treatment had caused changes in performance which might be indicative of degeneration of the catalyst.

### 1. Experimental Procedure

The samples chosen for this experiment had been prepared for the residual pH study discussed in Section V-D. These were processed from 1700°C felt (Lot 051482) which had been cleaned in 45% KOH at 90°C for 2 hours. Catalyzation was conducted according to the standard procedure described by NASA (8) with the addition of a soak in pH-adjusted water immediately prior to catalyzation, and adjustment of the aqueous gold chloride methanol solution to 25°C before use. One set of data was obtained for felts processed at each of pH 5, 7, and 9, respectively.

Electrodes were mounted, waxed, and tested at 25°C in 1mM PbCl<sub>2</sub> with 1N HCl in the manner described in Section II. An iR-compensated cyclic voltammogram was obtained as a measure of baseline performance.

As the potential next swept toward the region of hydrogen evolution, the cycling was stopped and potential held at -950 mV vs. SCE for five minutes, during which time the current was monitored. The potential was then monitored as the cell was switched to open circuit for an additional five minutes. The iR compensation was removed at this point, as application of a compensated potential tends to induce irreversible oscillation. By this routine, lead was plated onto the electrode which was then allowed to go to an open circuit potential. The potential was reapplied at -500 mV vs. SCE as it swept toward a more positive potential, allowing the lead to deplate (provided that it had remained stable at open circuit). The peak representing this lead dissolution, as well as the next complete cycle, were recorded without iR compensation.

Compensation was then added gradually and a steady state voltammogram was recorded. This was compared to the initial voltammogram and any changes in behavior were noted.

The potential was then held at  $-950$  mV for 5 minutes as before; however, when the cell was switched to open circuit, the electrode was immediately removed, rinsed successively in distilled water, 50 volume % methanol/water, and twice in anhydrous methanol, then dried under vacuum for one hour at ambient temperature.

The dry electrode was returned to the cell which was then subjected briefly to vacuum in order to draw the  $\text{PbCl}_2/\text{HCl}$  solution into the felt. Electrochemical characteristics of the lead/electrode interaction were studied as described previously by applying potential at  $-500$  mV and recording the initial lead dissolution peak and one additional plating/deplating cycle without iR compensation. A steady-state iR-compensated voltammogram was then recorded. Voltammograms obtained before and after drying of the electrode were then examined and compared. The lead plating/deplating peaks were integrated by the paper-weight ratio method to provide a quantitative basis for comparison.

A comparison electrode for each of those tested as above was prepared from an adjacent area of the same felt. The second electrode of each pair was tested as usual in  $1\text{mM}$   $\text{PbCl}_2$ , held for 5 minutes at  $-950$  mV, then removed, dried, and retained for microscopic analysis.

An additional sample, without gold, was prepared with the objective of retaining lead chloride in addition to any plated lead. This sample was plated at  $-950$  mV vs. SCE and then simply withdrawn from solution and dried without rinsing; it is referred to as the "lead chloride" sample.

## 2. Electrochemical Characterization

Initial steady-state voltammograms of lead oxidation/reduction were recorded for the six felts tested. An example is presented in Figures 54 and 55; the voltammogram obtained on the "control" felt is presented in the first figure, followed by the corresponding data on the sample intended for microanalysis. The voltammograms were generally typical in magnitude and form, of data obtained from similar electrodes in earlier testing. In particular, with the exception of the pH 5 felt, the voltammograms of electrode pairs match almost exactly, suggesting that the behavior of control felts would be representative of the condition of the felts held for analysis, which were treated in exactly the same manner. Although peaks obtained on the pH 5 control felt were large by comparison, the variation falls within limits of reproducibility previously observed on similar felts. For ease of comparison, the integrated peak areas for all comparable data on pH-controlled felts, discussed in Section V-C above, have been presented together with the results of this study in Table XV.

Control felts were then held at  $-950$  mV for five minutes, generating hydrogen gas to expel some of the lead solution from the felt. The electrode was then removed from potentiostatic control by switching to open circuit. These steps were intended both to simulate drying and removal of the electrode, and to eventually facilitate actual drying by providing a means to remove some of the liquid. We had hoped to obtain, by non-rigorous methods, an indication of how drying in a non-oxidizing atmosphere might affect the subsequent performance of the electrode.

The results were encouraging. While holding at  $-950$  mV the current remained nearly constant at  $-1.7$  to  $-1.4$  mA over five minutes, compared with

a current of about  $-1.7$  mA at  $-950$  mV for the same felt during cycling (Figure 54). Similar results were obtained on all three felts. On open circuit, the potential quickly rose to about  $-530$  mV in every case.

When the potential was reapplied at  $-500$  mV, the lead, which had apparently not been adversely affected, depleted as expected; an example is shown in Figure 56. Although the peak shapes are somewhat distorted due to the lack of  $iR$  compensation, the charges in Table XV are consistent and fairly reasonable. Allowing for the initial application of potential, about  $80$  mV more positive than the usual onset of Pb oxidation, the second set of peaks was unchanged from the first in each case. In addition, voltammograms obtained after the reintroduction of  $iR$  compensation were almost indistinguishable from those obtained before the interruption in cycling, e.g. Figure 57.

The results were different, however, when the felts were tested in the same way after drying and reimmersion. As shown in Figures 58-60, a pulse of cathodic current, rather than the anodic lead oxidation peak, was observed upon reapplication of potential. Both anodic and cathodic peaks were observed in the next cycle, but the peaks were reduced in size and the hydrogen reduction current exaggerated. The electrodes eventually regained most of their original performance characteristics (see Figure 61), with the exception of the pH 5 electrode, for which the peaks remained reduced in size.

Since the dried felts had been reimmersed in a solution containing  $PbCl_2$ , the cathodic pulse observed could result in plating of lead, obscuring the meaning of any subsequent lead oxidation observed. To eliminate this possibility, a third repetition of this electrode was

mounted, waxed, and subjected to exactly the same tests given the three control felts, except that the dried electrode was reimmersed in a 1N HCl solution without  $\text{PbCl}_2$ .

The results were in every way typical of those obtained previously, up to the point of reimmersion of the dried felt. Since no  $\text{PbCl}_2$  was added to the solution, the cathodic pulse observed upon application of controlled potential at -500 mV (Figure 62) may represent reduction of some other lead compound within the carbon felt structure. On the full sweep following reapplication of the potential, neither a cathodic nor an anodic peak typical of the  $\text{Pb}/\text{Pb}^{2+}$  redox reaction was exhibited at the level of recording sensitivity used. The hydrogen evolution rate is higher than before removal/drying, but in the complete absence of lead, gold on carbon felt would normally exhibit a hydrogen evolution level more than one order of magnitude higher; this strongly suggests the presence of a small amount of lead, which might have been detected by cyclic voltammetry at higher sensitivity.

### 3. Electron Microscopy Results

The samples were analyzed by transmission electron microscopy (TEM), scanning TEM (STEM), energy dispersive analysis by X-ray (EDAX) and X-ray dot mapping.

For the Pb-on-Au electrodes, prepared by the controlled removal and drying process described above, TEM photographs of the carbon fiber surfaces reveal discrete particles of gold as found in previous studies (16). The micrographs are presented in Appendix VI. The particles and surfaces do not differ in any way from no-Pb samples that would suggest lead particles or a coating. The same can be said of the STEM views of the fiber surfaces,

discussed below. The two samples prepared from felts at a precatalyzation pH of 5 and 7 were very similar, with the pH 7 sample showing somewhat finer particles. The "pH 9" sample showed very little evidence of gold on the carbon fibers examined. STEM photographs of the pH 7 sample are shown in Figure 63 at a magnification of 6400X, and in Figure 64 at a magnification of 25,000X. Gold particles appear as the larger bright spots in the photos. One of the particles, indicated in Figure 64, was identified as gold by EDAX as illustrated in Figure 65. The same figure shows that no lead was detectable by EDAX in the same area, nor anywhere on the fibers on any of these three samples. Figure 66 shows three particles on the surface of the "pH 5" sample at a magnification of 25,000X. Of the two particles that are closest together, the brighter one to the left (shown at 100,000X in Figure 67) was identified by EDAX as gold (Figure 68), again with no evidence of lead; the other particle is carbon. The third particle, upper right, was also identified as gold. An Au X-ray dot map of the same region at 25,000X does not clearly distinguish the gold particles (Figure 69); however, at 100,000X, as shown in Figure 70, the gold particle can be differentiated.

Examination of other fibers from these same samples by EDAX failed to show gold or lead. A STEM photograph of a carbon fiber from the "pH 5" sample shown at 3200X in Figure 71 gives little evidence of particles. A Pb X-ray dot map of the same area, shown at 3200X in Figure 72, also does not reveal any discrete particles or differentiated areas. Similar photographs are shown for the "pH 7" sample in Figures 73 and 74. These results seem to suggest a thin uniform layer of lead over the entire surface of the fibers, perhaps as a monolayer.

Analysis of the "lead chloride" sample also indicates that the lead is

present in a uniform layer, as shown in the STEM photograph in Figure 75 and the corresponding Pb X-ray dot map in Figure 76. In addition, there are differentiated areas in the X-ray dot map (Figure 77) that can be correlated with visible structures in the corresponding STEM photograph (Figure 78). These structures are most likely  $\text{PbCl}_2$  deposits, making the lead concentration high enough on this sample to be detected by EDAX (Figure 79).

#### 4. Observations of Carbon Fiber Surfaces

During the course of the Pb/Au analytical work described above it was noted that the carbon fiber surfaces showed a regular almost geometric pattern of very small particles or pits at magnifications greater than 25,000X such as shown in Figure 64 and 66. In order to explore the nature of these structures, two uncatalyzed samples were examined: ...1) a raw carbon felt, and 2) a carbon felt subjected to the standard pretreatment in KOH. Examination of these samples at 25,000X and 100,000X suggests that the pattern may be etch pits produced by the KOH pretreatment; see Figures 80 - 83.

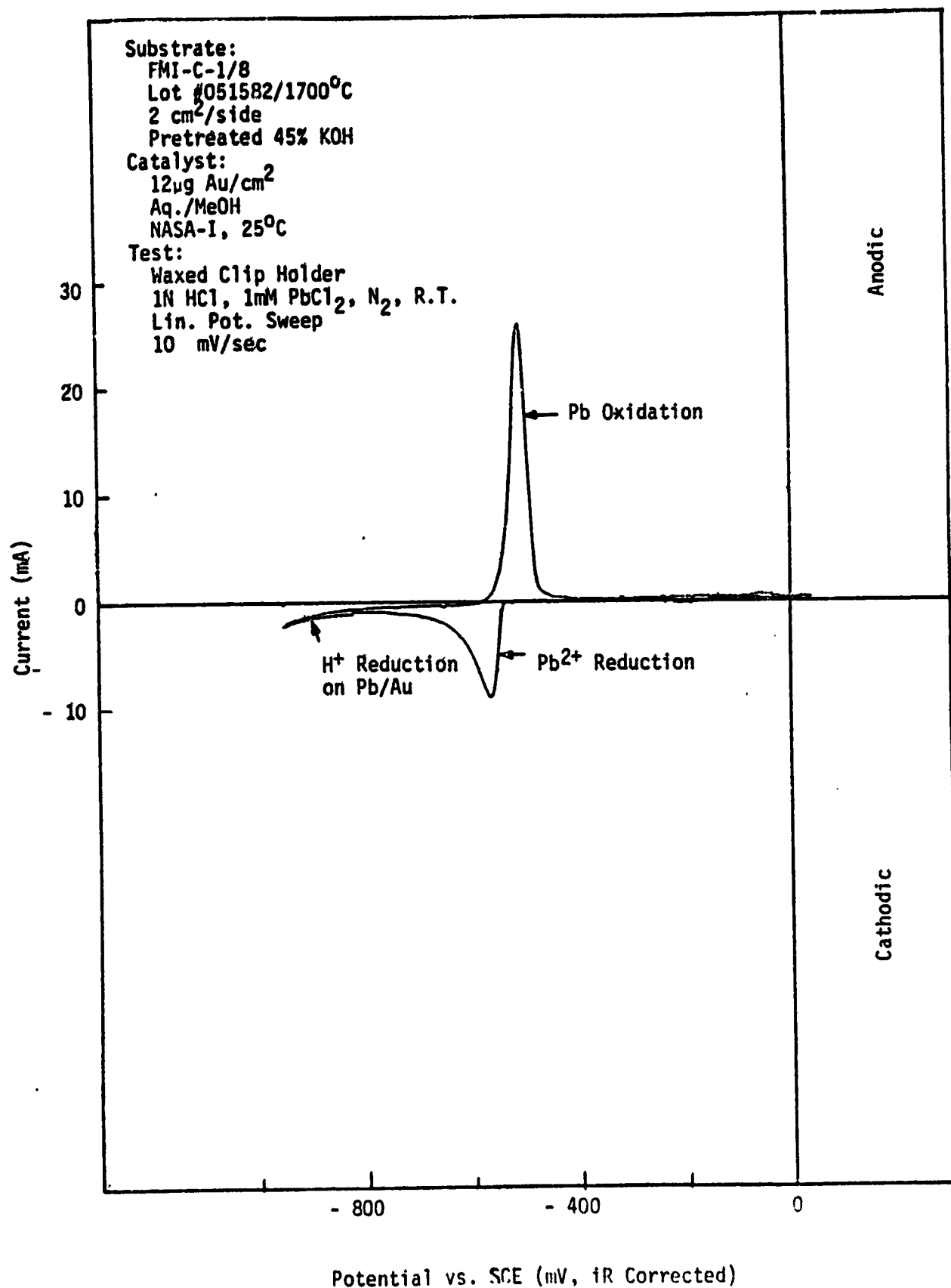


Figure 54. Steady-State Pb/Pb<sup>2+</sup> Voltammogram before Removal and Drying of Electrode (pH7 Felt; Control Sample).

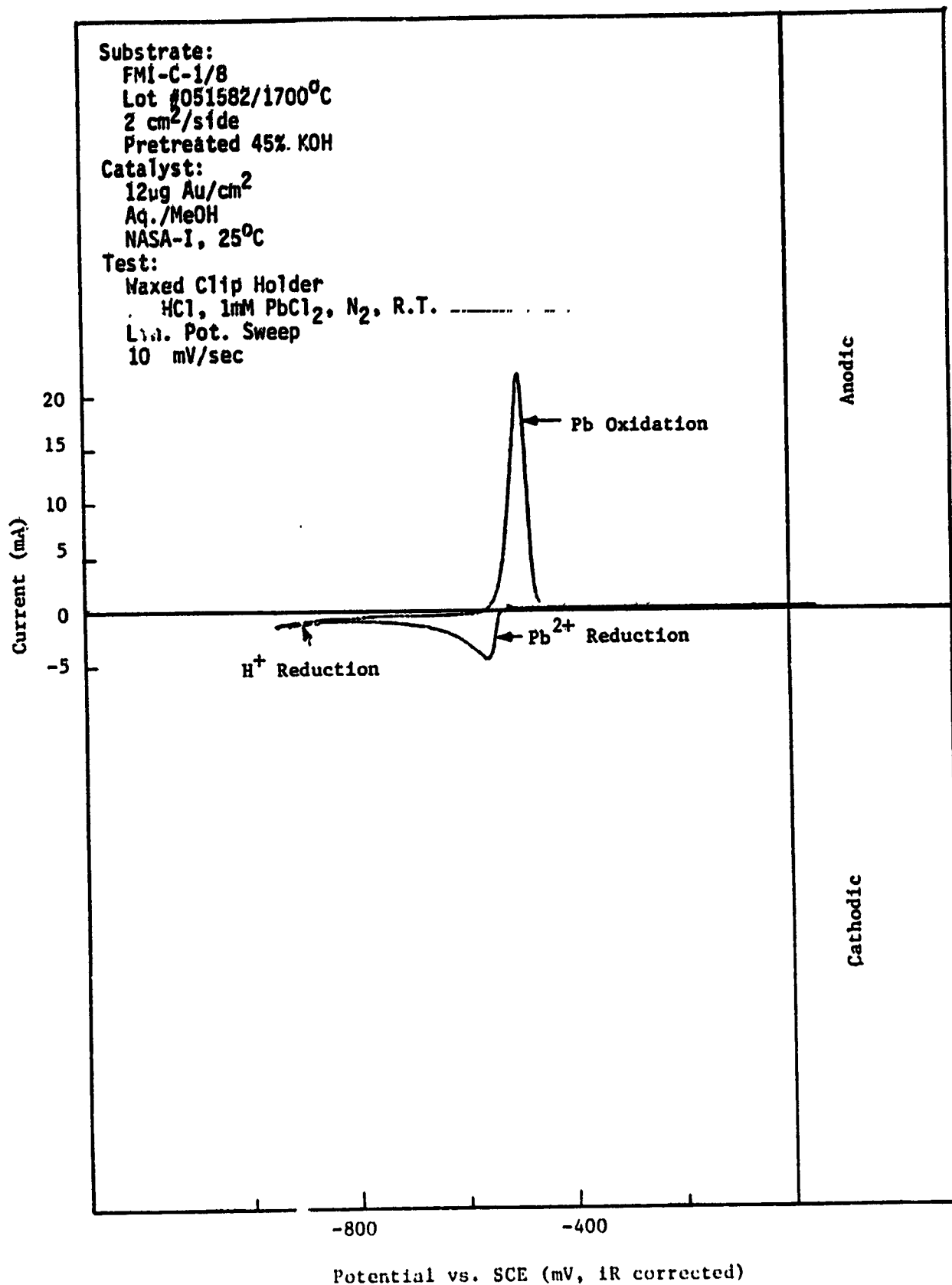


Figure 55. Steady-State Pb/Pb<sup>2+</sup> Voltammogram before Removal and Drying of Electrode (pH7 Felt; SEM Sample).

TABLE XV Charges Recorded for Pb Oxidation and Pb<sup>2+</sup> Reduction (Integrated Peak Areas).

	Charge (mCoul)					
	pH5 Felt		pH7 Felt		pH9 Felt	
	Anodic	Cathodic <sup>1</sup>	Anodic	Cathodic <sup>1</sup>	Anodic	Cathodic <sup>1</sup>
Previous Data A <sub>1</sub>	172		113		237	
A <sub>2</sub>	178		138		202	
B <sub>1</sub>	113	126	213	321	121	202
Electrodes for SEM	69	81	74	97	100	143
<u>Control Electrodes:</u>						
Initial Steady State	202	236	103	111	95	130
1st Peak After Hold <sup>(2)</sup>	348	---	115	---	136	---
Next Comp. Cycle <sup>(2)</sup>	357	293	138	126	160	220
Steady State After Hold	243	266	111	142	103	132
1st Comp. Cycle After Dry <sup>(2)</sup>			N.A.	N.A.	55	560
Steady State After Dry	48	194	134	126	108	96

1) Includes H<sup>+</sup> Reduction

2) No iR Compensation

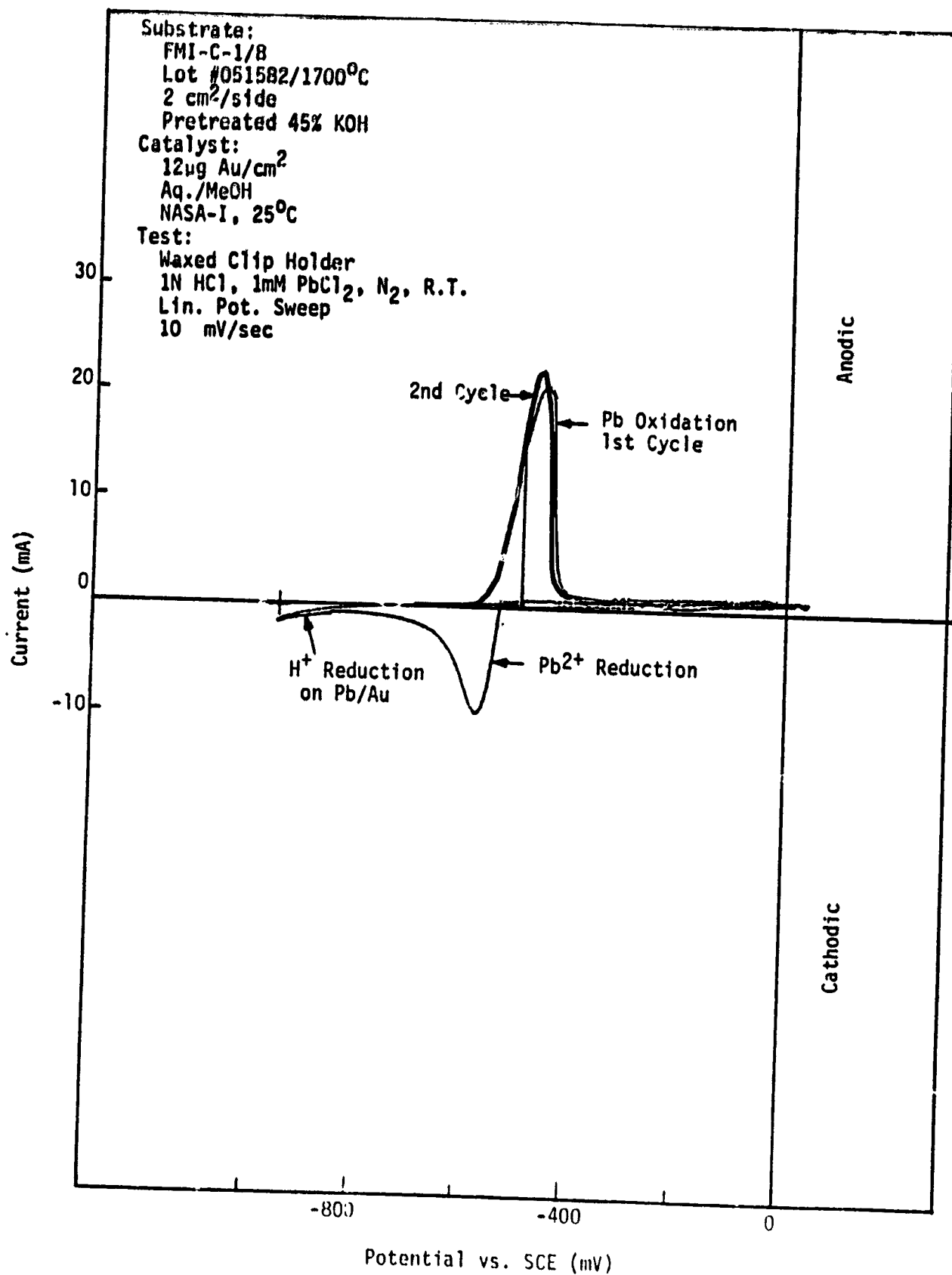


Figure 56. Pb/Pb<sup>2+</sup> Voltammograms after 5 minute hold  
 at -950 mV vs. SCE (pH7 Felt).

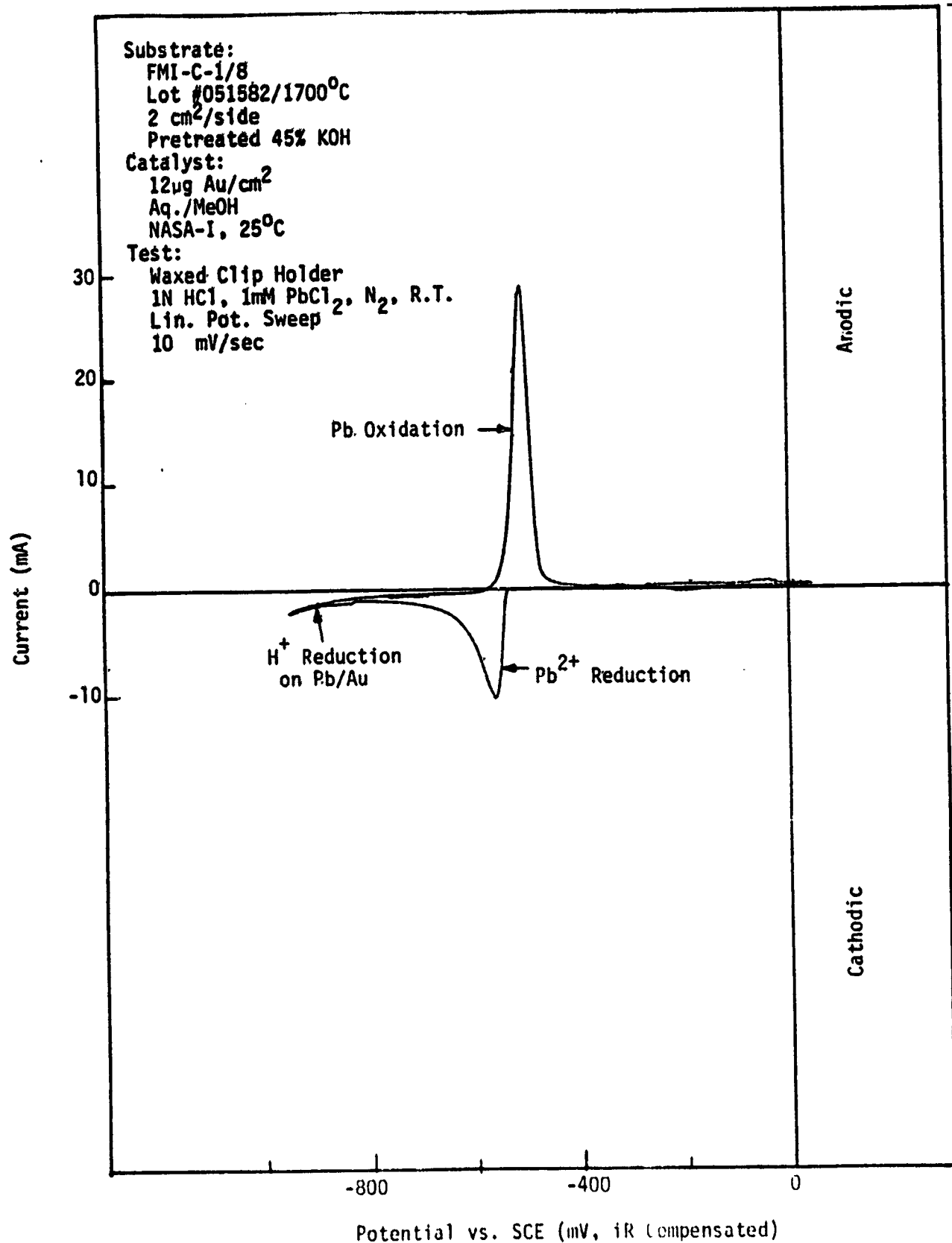


Figure 57. Steady-State Pb/Pb<sup>2+</sup> Voltammogram after 5 Minute Hold at -950 mV vs. SCE (pH 7 Felt).

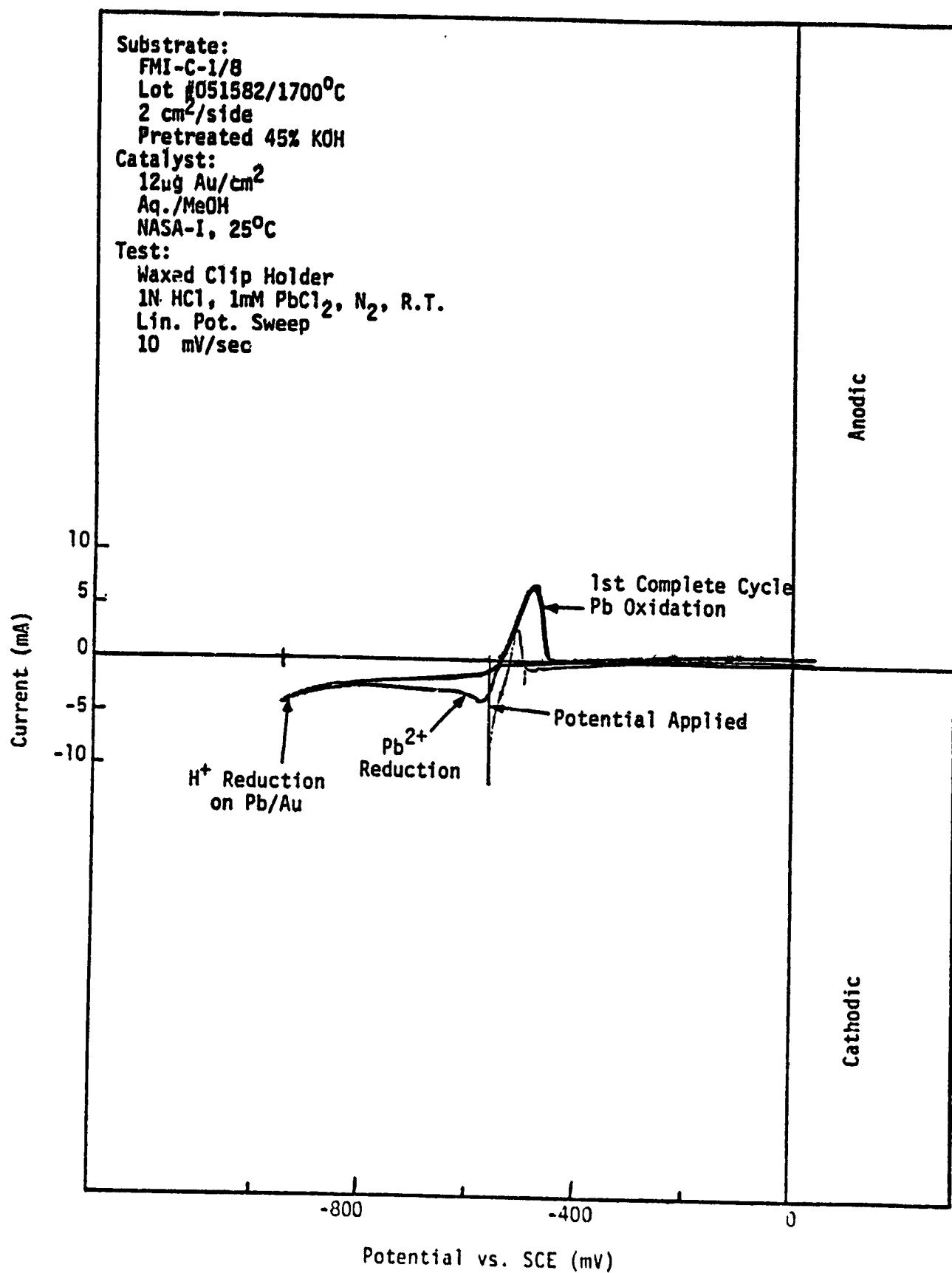


Figure 58. Pb/Pb<sup>2+</sup> Voltammograms Immediately After Reimmersion of Dried Electrode (pH5 Felt).

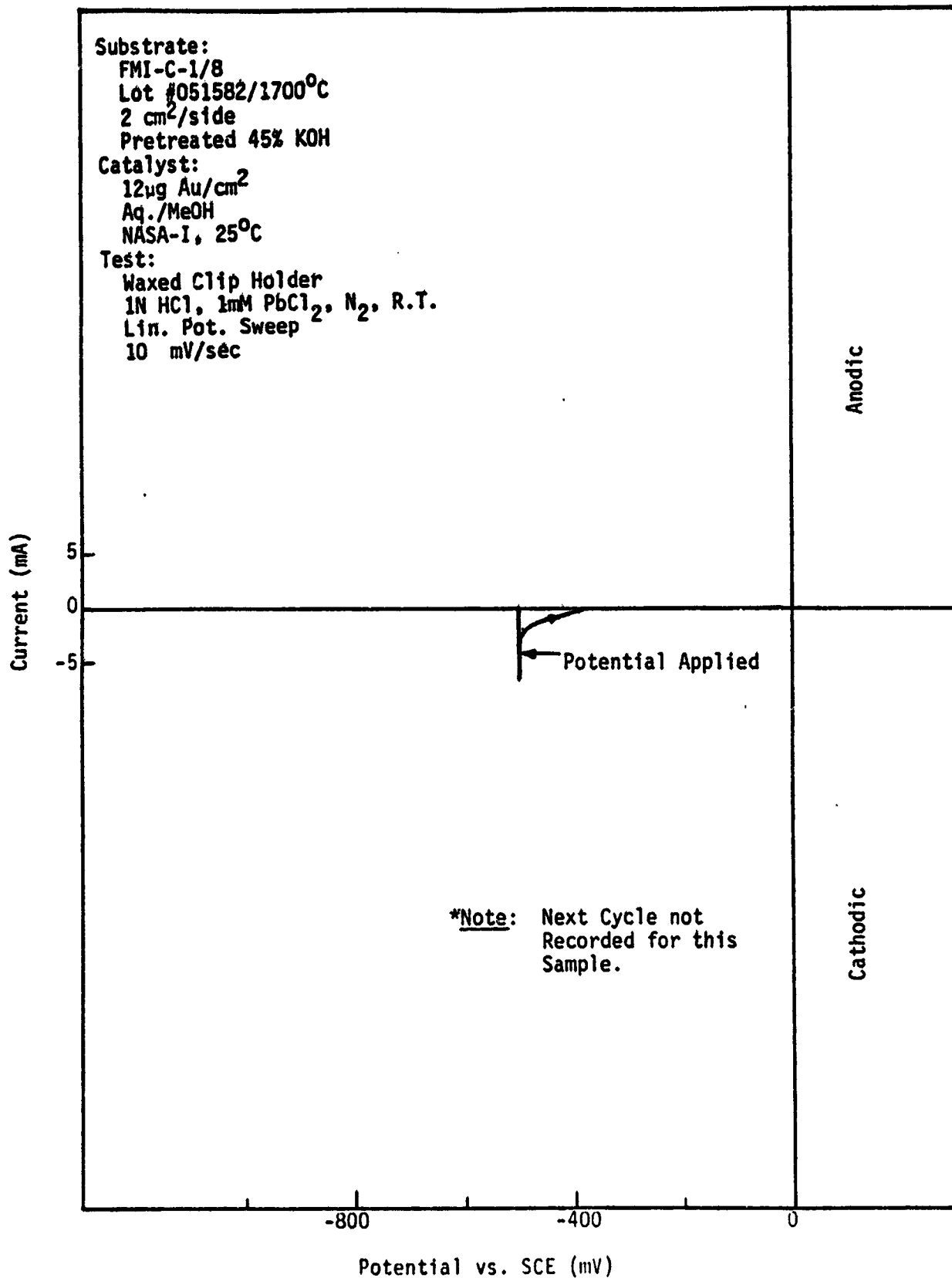


Figure 59. Pb/Pb<sup>2+</sup> Voltammogram\* Immediately after Reimmersion of Dried Electrode (pH7 Felt).

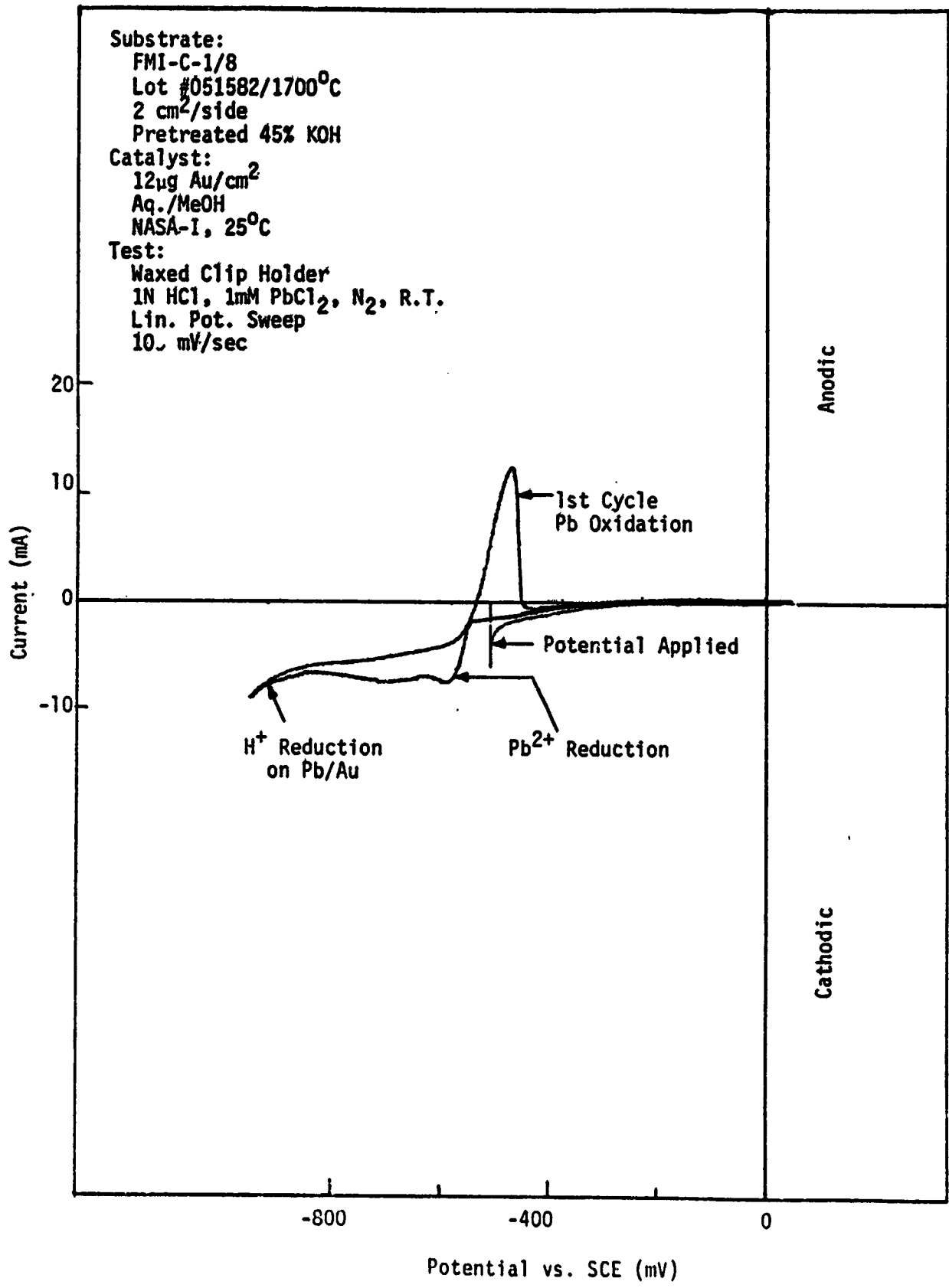


Figure 60. Pb/Pb<sup>2+</sup> Voltammograms Immediately after Reimmersion of Dried Electrode (pH9 Felt).

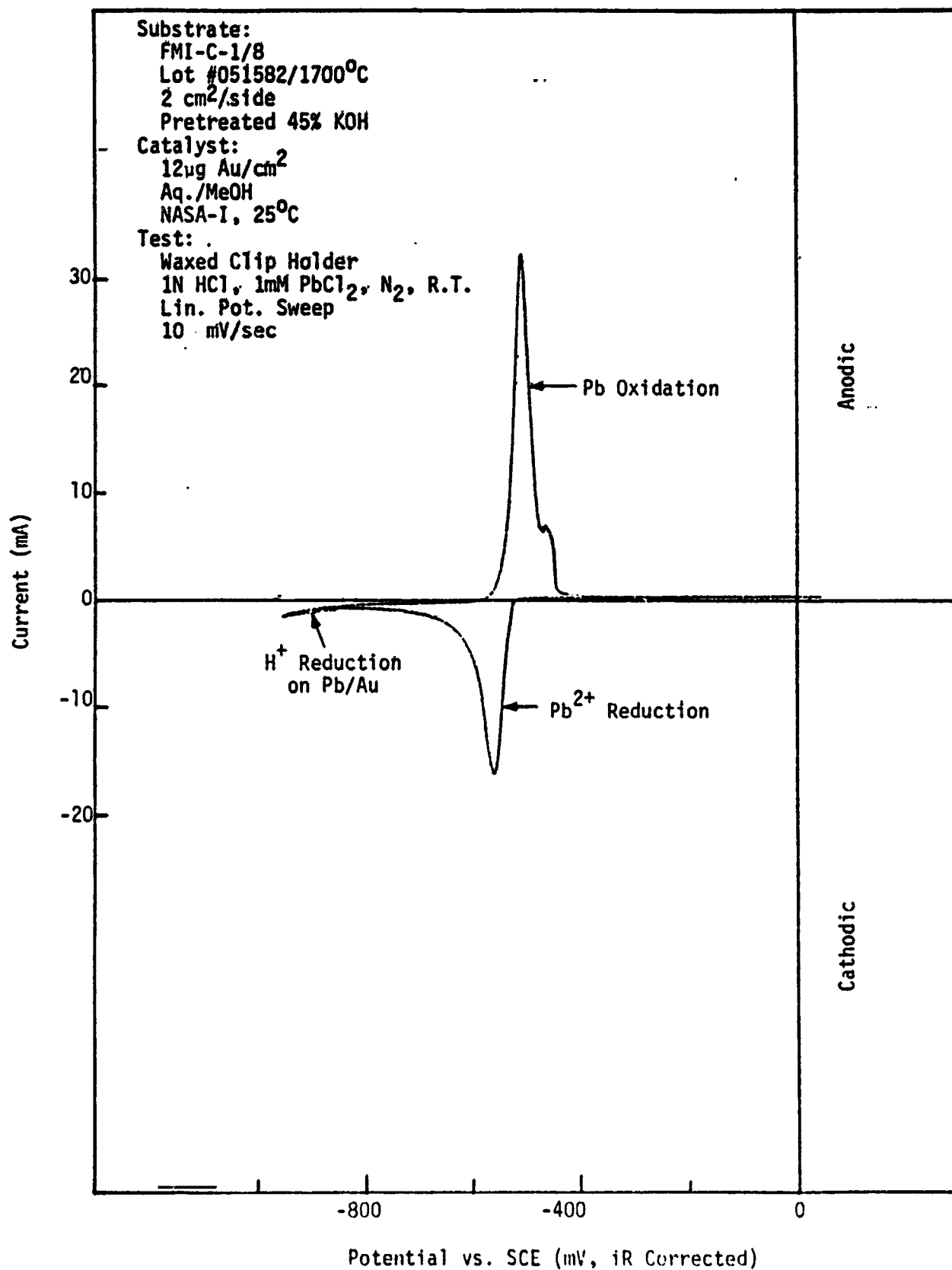


Figure 61. Steady-State Pb/Pb<sup>2+</sup> Voltammogram after Reimmersion of Dried Electrode (pH7 Felt).

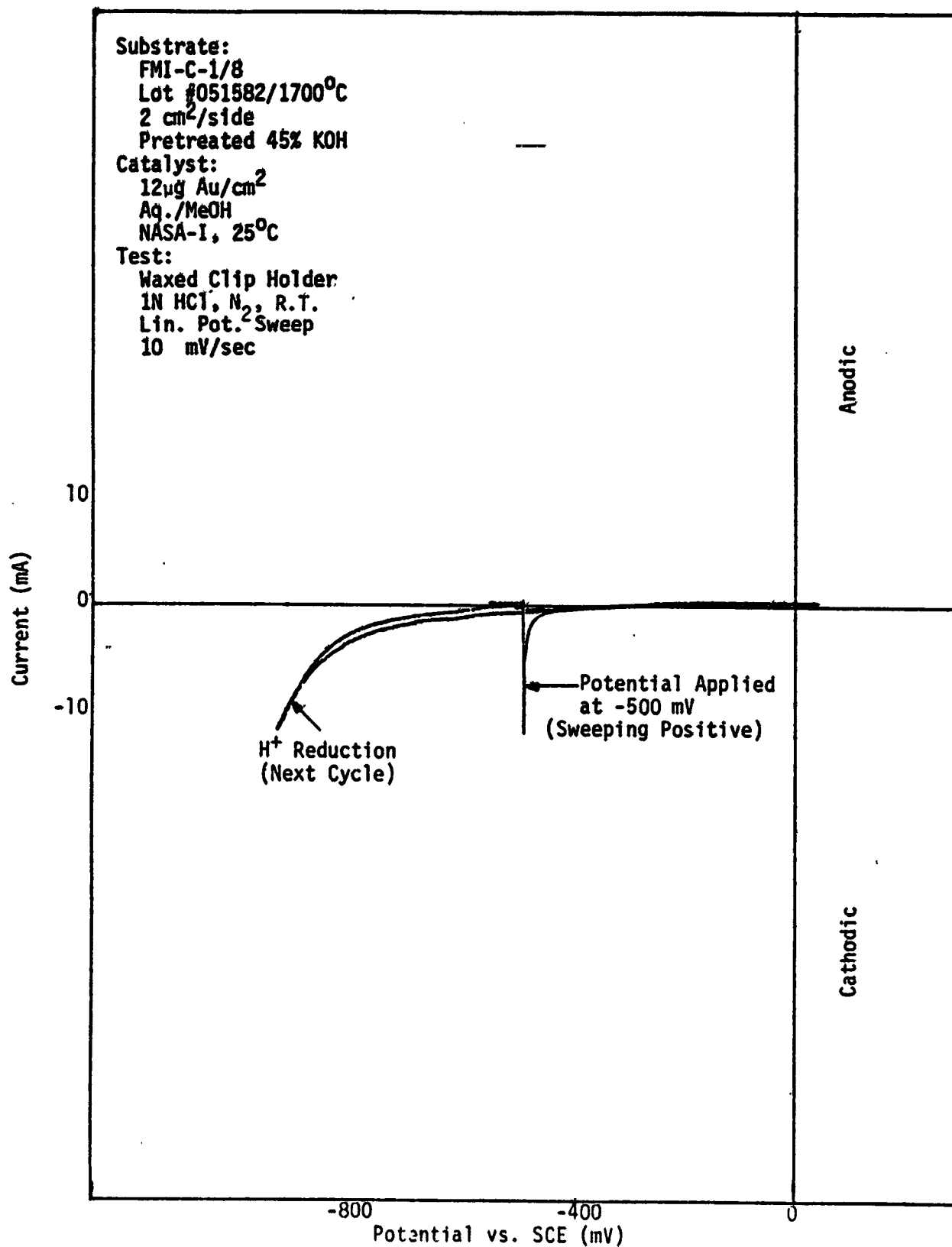


Figure 62. Voltammograms Recorded after Reimmersion of Dried Electrode in 1 N HCl with no PbCl<sub>2</sub>.

ORIGINAL PAGE IS  
OF POOR QUALITY

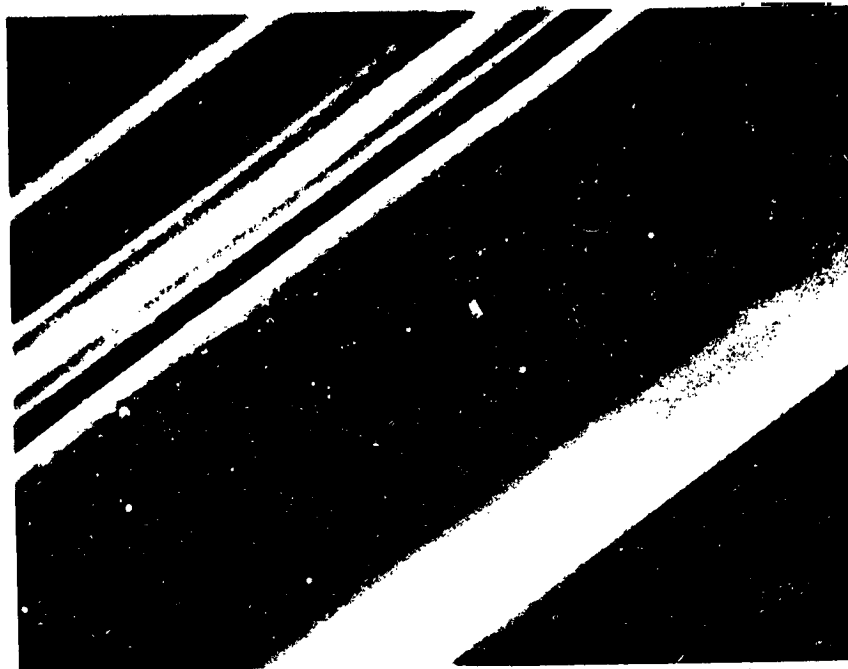


Figure 63. STEM Photograph of Carbon Fiber Surface ("pH 5" Pb/Au sample) showing Gold Particles. (bright spots); X6400.

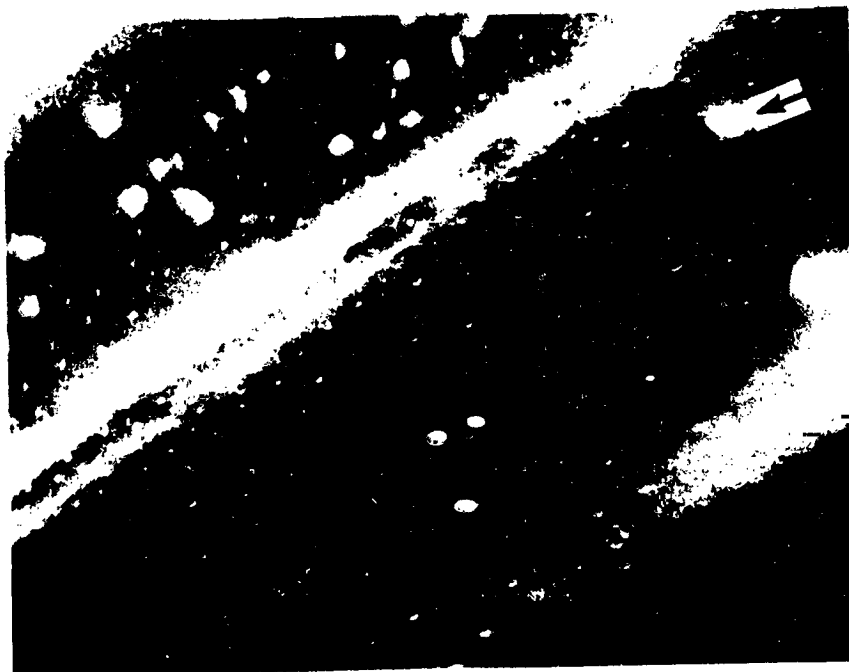


Figure-64. Same View as Figure 63 at 25,000X. The Particle Indicated Was Identified as Gold by EDAX (see Figure 65).

13-APR-83 16:02:06  
RATE: CPS TIME 100LSEC  
00-20KEV: 10EV/CH PRST: 100LSEC  
A: H-22-A B:  
FS= 378 MEM: A FS= 50

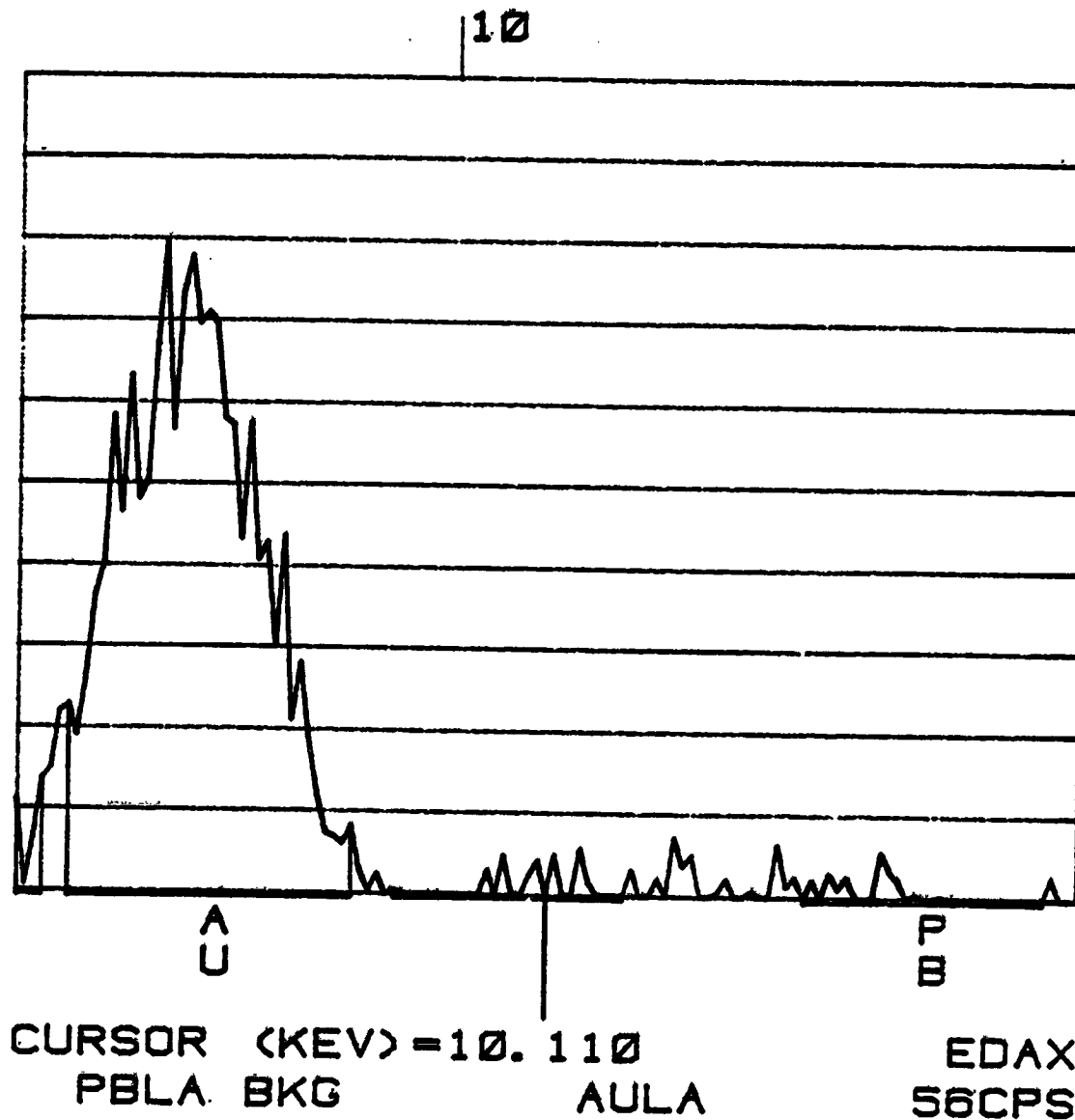


Figure 65. Energy Dispersive Analysis by X-ray of Particle shown in Figure 64.

ORIGINAL PAGE IS  
OF POOR QUALITY

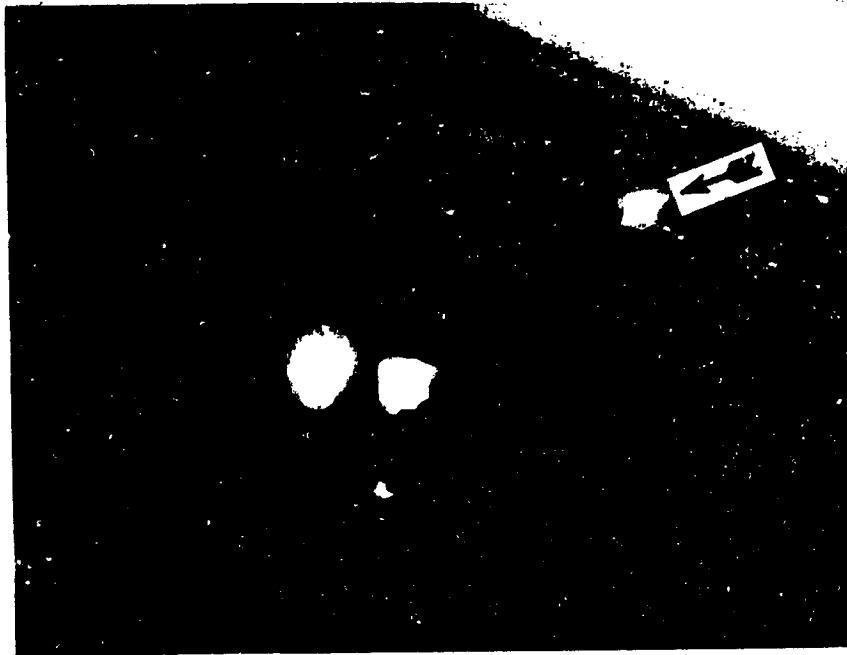


Figure 66. STEM Photograph of Carbon Fiber Surface ("pH 7" Pb/Au sample) showing Gold Particles (center particle is carbon); X25,000.

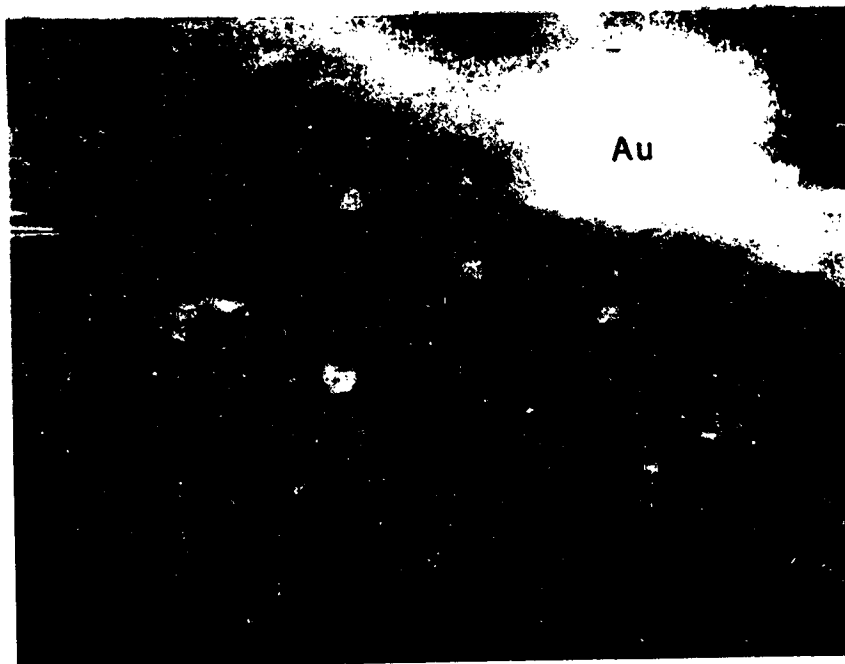


Figure 67. Same View as Figure 66 at 100,000X. The Large Bright Particle was Identified as Gold by EDAX (see Figure 68).

13-APR-83 12:48:53  
 RATE: CPS TIME 43LSEC  
 00-20KEV: 10EV/CH PRST: 100LSEC  
 A: G-7-C B:  
 FS= 792 MEM: A FS= 100

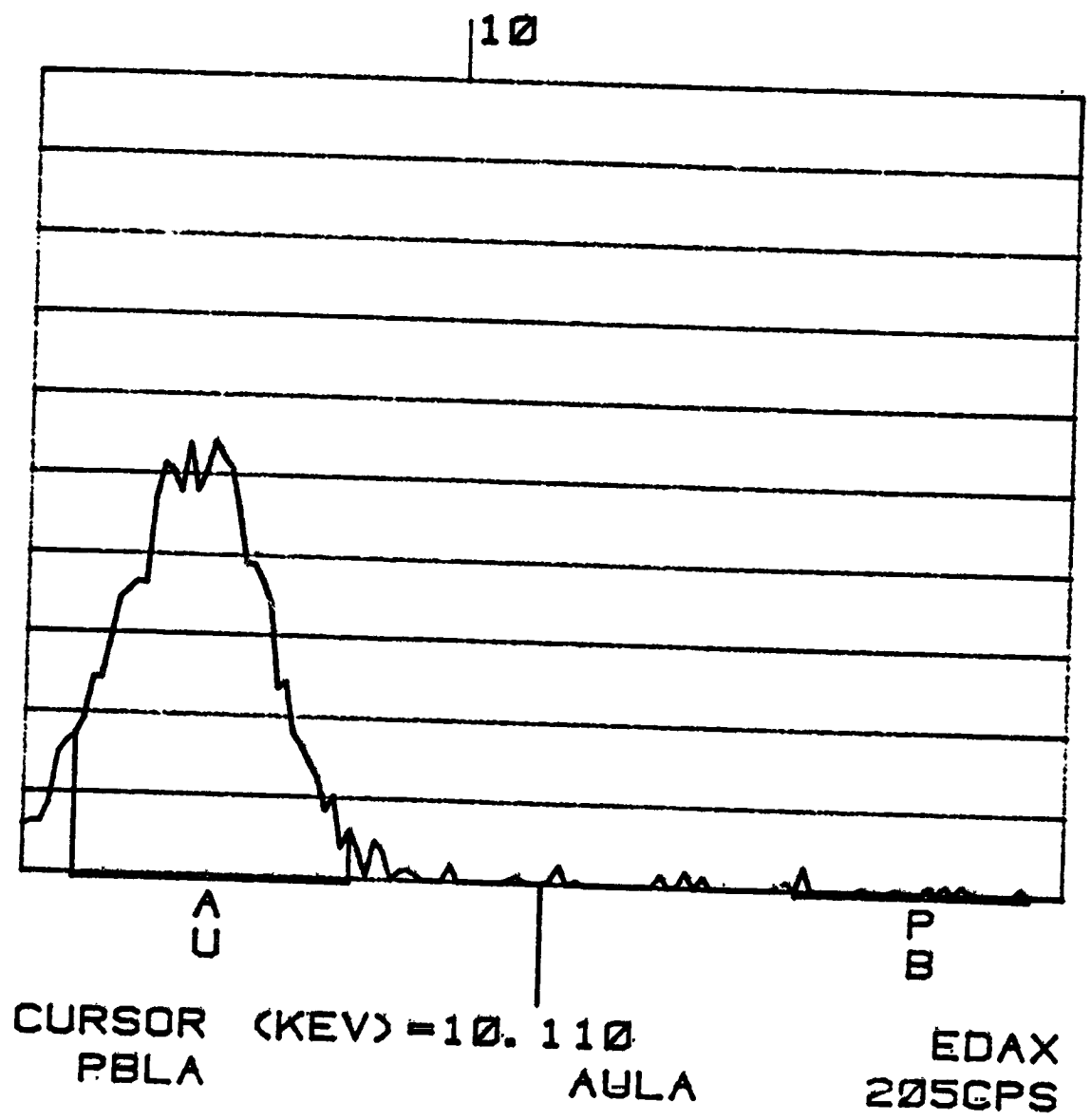


Figure 68. Energy Dispersive Analysis by X-ray  
 of Particle Shown in Figure 67.

ORIGINAL PAGE IS  
OF POOR QUALITY



Figure 69. Gold X-ray Dot Map at 25,000X Magnification of the Same Area shown in Figure 66.



Figure 70. Gold X-ray Dot Map at 100,000X Magnification of the same Approximate Area shown in Figure 67. Note differentiation over Gold Particle.

ORIGINAL PAGE IS  
OF POOR QUALITY



Figure 71. STEM Photograph of Carbon Fiber Surface  
("pH 5" Pb/Au Sample); 3200X.



Figure 72. Pb X-ray Dot Map of the Carbon Fiber  
Surface shown in Figure 71; 3200X.

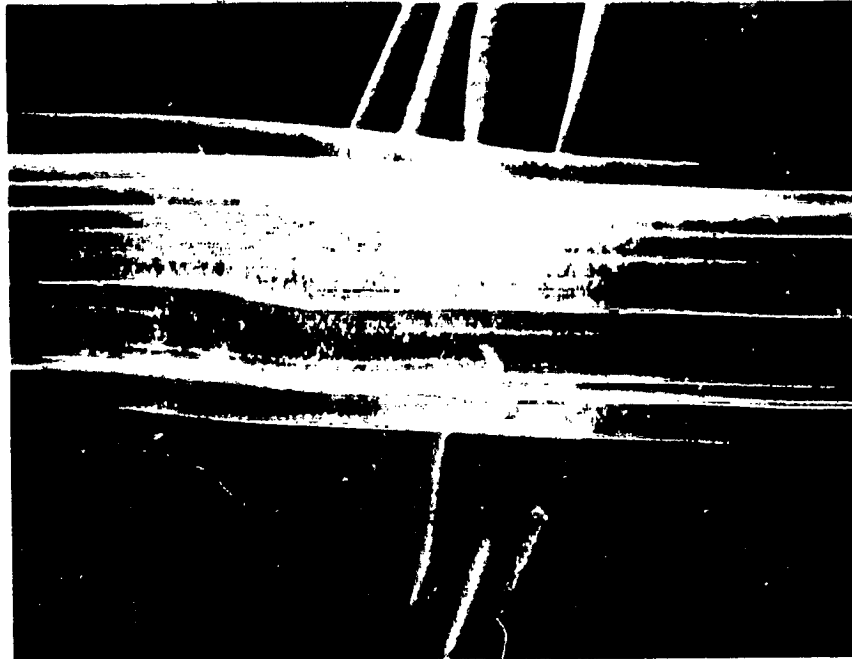


Figure 73. STEM Photograph of Carbon Fibers  
("pH 7" Pb/Au Sample); 3200X.



Figure 74. Pb X-ray Dot Map of the Carbon Fibers  
shown in Figure 73; 3200X.

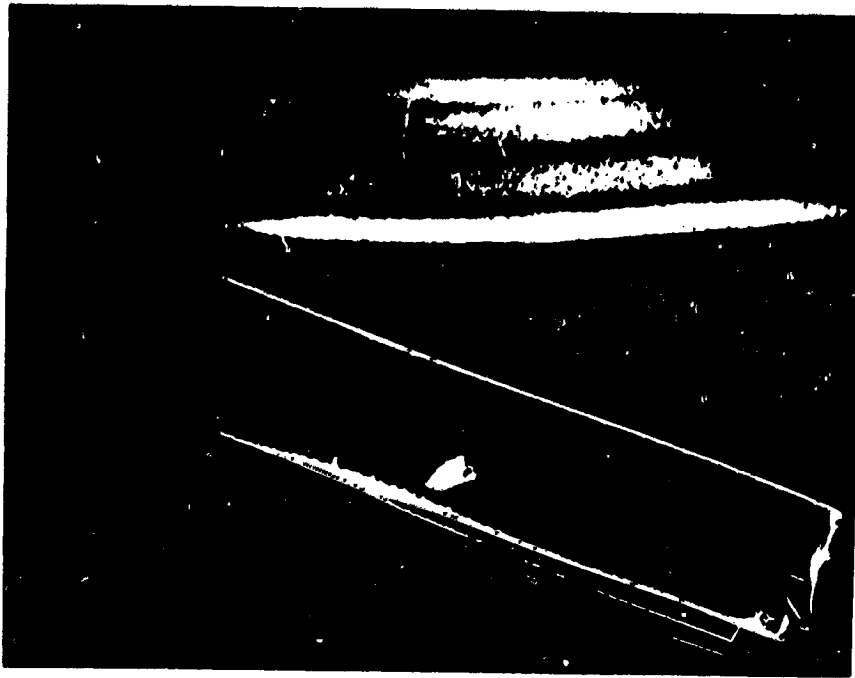


Figure 75. STEM Photograph of Carbon Fibers ("PbCl<sub>2</sub>" No-Gold Sample); 6400X.



Figure 76. Pb X-ray Dot Map Corresponding to Carbon Fibers in Figure 75; 6400X.

ORIGINAL PAGE IS  
OF POOR QUALITY

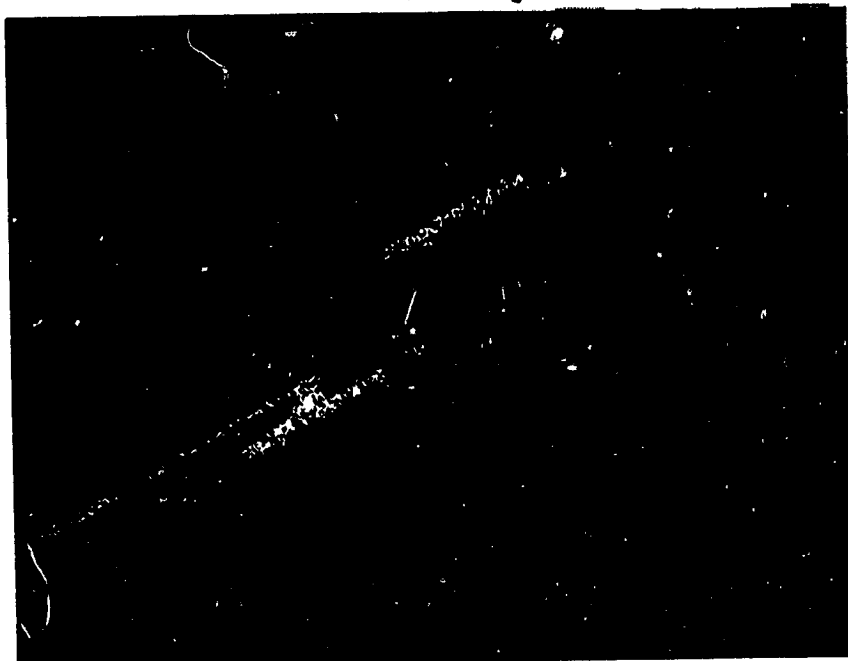


Figure 77. Pb X-ray Dot Map of Carbon Fiber  
("PbCl<sub>2</sub>" No-Gold Sample); 1600X.

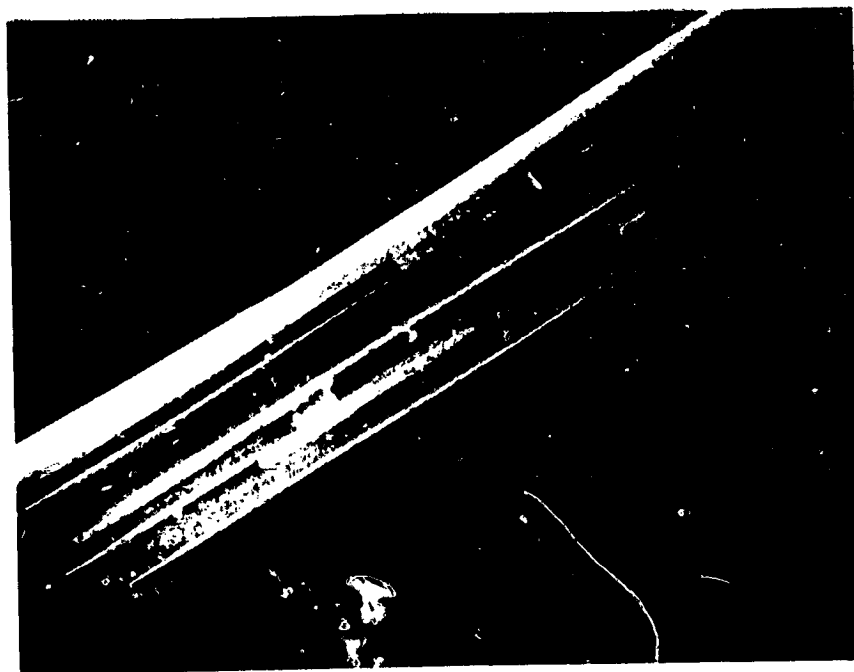


Figure 78. STEM Photograph of the Carbon Fiber  
shown in Figure 77. Note differentiation in Dot  
Map corresponding to Deposits of PbCl<sub>2</sub> in Flutes of  
Fiber (see EDAX Figure 79).

11-NOV-83 10:59:03  
 RATE: CPS TIME 3082LSEC  
 00-20KEV: 10EV/CH PRST: OFF  
 A: VJ0C B:  
 FS= 5018 MEM: A FS= 200

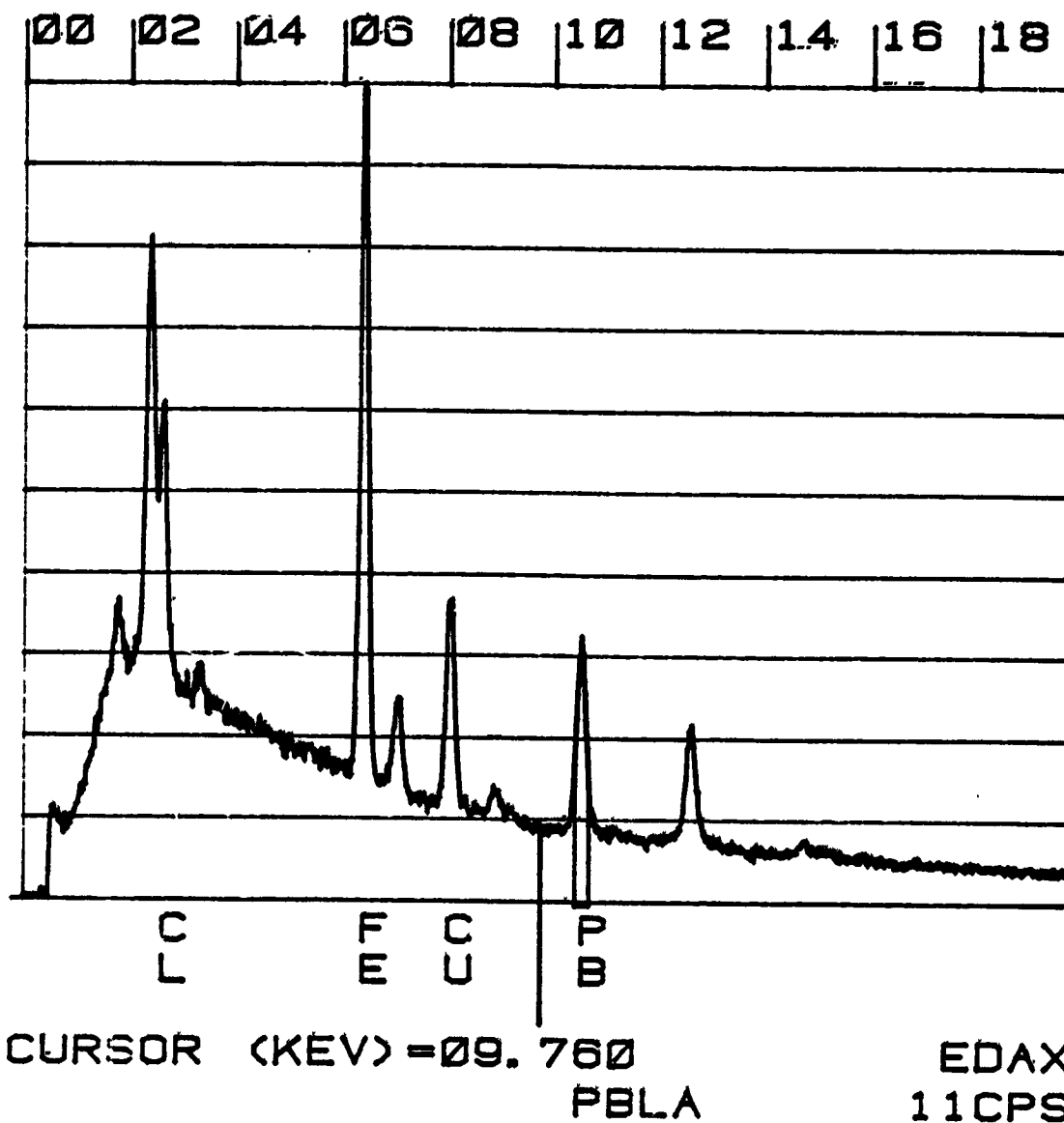


Figure 79. Energy Dispersive Analysis by X-ray  
 of  $PbCl_2$  Deposits on Carbon Fiber  
 shown in Figure 78.



Figure 80. Raw, Untreated and Uncatalyzed Carbon Fiber; STEM 25,000X.



Figure 81. Same Fiber Surface shown in Figure 80; STEM 100,000X.

ORIGINAL PAGE IS —  
OF POOR QUALITY



Figure 82. Uncatalyzed Carbon Fiber after Standard Pretreatment in Hot Potassium Hydroxide; STEM 25,000X (Note "etch pits"; reference Figure 64).

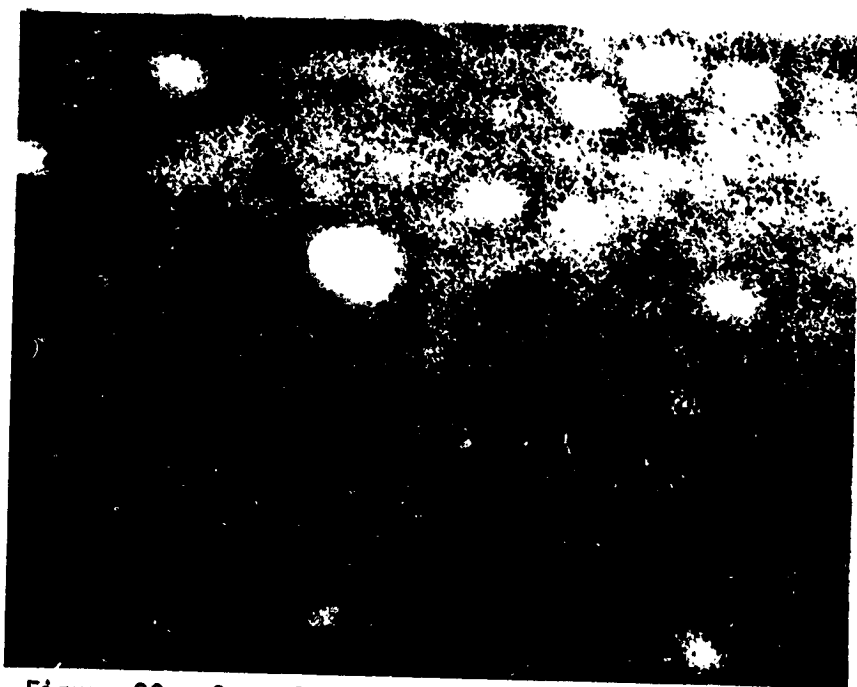


Figure 83. Same Carbon Fiber as shown in Figure 82; STEM 100,000X (reference Figure 67).

## F. Conclusions and Recommendations

At the completion of this study it was concluded that 1) there are factors influencing the gold catalyzation process that were not determined or sufficiently controlled for closely predictable results in terms of gold particle size or performance, 2) the cyclic voltammetry testing methods are only suitable for qualitative analysis and broad distinctions in performance; the results may be best interpreted on a statistical basis over many samples for the present state of refinement in cyclic voltammetry, electrode preparation and handling, and 3) the lead component of the catalyst system appears to be deposited as a thin uniform layer over the entire carbon surface, rather than concentrated on the gold or in discrete particles; additional analysis (e.g. by Auger spectroscopy) would be needed to confirm this, however.

The recommended catalyzation procedure is the standard procedure developed at NASA-LeRC (8). Some boundary conditions and additional controls have been defined as outlined below:

Loading: 10 - 15 micrograms gold/cm<sup>2</sup>

### Precatalyzation Treatment

10 - 40% KOH (depending on solution-to-felt volume ratio)

80 - 90° C for approx. 1 hour, rinse to pH 6 - 8

### Precatalyzation State

Damp dried after pH 7 soak

### Catalyzation

Solvent/Wetting Agent

Water/Methanol 1:3

-----  
**Solution**

Volume: about 50 - 100% in excess of felt saturation

Temperature: 20 - 30° C

Exposure: 1 - 16 hours, closed container

**Post-Catalyzation Treatment**

1 hour at 100° C and 1 hour at 250 - 270° C

## VI. EFFECTS OF REACTANT CROSS-MIXING

### A. Effects of Fe<sup>2+</sup> in the Negative Electrode Solution

#### 1. Experimental Procedure

The carbon felt processed at 1650°C was chosen for this study because it performed reasonably well in cyclic voltammetry and exhibited no unusual characteristics. Furthermore, its graphitization temperature is similar to that of felts studied extensively in the last program (Ref. 16; Lots 071379 and 122380).

The underlying characteristics of the catalyzed felt were first established by the usual cyclic voltammetry in 1N HCl, and 1N HCl with 1 mM Pb. Ferrous chloride was then added to the solution in increments and dissolved, followed in each case by cyclic voltammetric testing. The concentration of iron was changed from 50 mM, to 100 mM, to 250 mM and finally to 500 mM molar (in the actual redox battery, this amount of crossover would be achieved only by total intermixing of the two reactant solutions). The objective was to determine whether H<sub>2</sub> evolution and/or Pb plating/deplating would be affected by the presence of ferrous ion at various concentrations.

This procedure was repeated after the addition of chromium to the 1 mM Pb solution. A concentration of 50 mM rather than 0.5 M Cr<sup>3+</sup> was chosen so as not to obscure characteristic redox features, particularly the level of reduction current associated with the evolution of hydrogen. Note that the final iron concentration represents a ten-fold excess of the cross species.

In both tests, the half cell was cycled continuously over an extended period (several hours) after the final addition of iron. Voltammograms were

recorded periodically and compared to determine if the ferrous ion would produce any gradual or cumulative effects.

The same procedure was followed for the reactant crossover studies, with subsequent additions of  $\text{FeCl}_2 \cdot 4\text{H}_2\text{O}$  (also "Baker Analyzed" Reagent) to produce iron concentrations of 50, 100, 250, and 500 mM. Testing was conducted after each addition.

Both crossover studies were extended, at the 0.5 M iron level, by allowing cycling to continue, fully compensated for  $iR$ , for as long as practicable after the final iron addition; four hours in the case of iron in 1 mM Pb, somewhat over two hours for iron in 50 mM Cr with Pb. Voltammograms were taken at one-hour intervals for comparison.

## 2. Results

The effects of increasing  $\text{Fe}^{2+}$  in the negative electrode solution are shown first for a blank solution (i.e.  $\text{PbCl}_2$  in HCl but no  $\text{Cr}^{3+}$ ) in Figure 84. As the concentration was increased from 0.0 to 500 mM,  $\text{Pb}^{2+}/\text{Pb}$  redox reaction was shifted to increasingly more negative potentials. The Pb oxidation peak also assumed a different shape, with a shoulder on the trailing side becoming more pronounced with increasing  $\text{Fe}^{2+}$  concentration. Hydrogen evolution increased very slightly at the 500 mM  $\text{Fe}^{2+}$  level.

The cumulative effects on extended cycling at the 500 mM  $\text{Fe}^{2+}$  level are shown in figure 85 up to 4 hours or about 72 cycles. It can be seen that the  $\text{Pb}^{2+}/\text{Pb}$  redox reaction shifts back slightly in the positive direction with increasing cycling time, and  $\text{H}_2$  evolution decreases slightly.

The effects of increasing  $\text{Fe}^{2+}$  in the negative electrode solution are

shown in figure 86. As the concentration was increased from 0.0 to 500 mM, the  $\text{Cr}^{3+}/\text{Cr}^{2+}$  redox reaction was shifted to slightly more negative potentials and the total quantity of chromium reacted increased. In addition  $\text{H}_2$  evolution decreased with increasing  $\text{Fe}^{2+}$  concentration.

The cumulative effects on extended cycling at 500 mM  $\text{Fe}^{2+}$  level are shown in figure 87 up to 2 hours or about 36 cycles. It can be seen that there is little change in the  $\text{Cr}^{3+}/\text{Cr}^{2+}$  redox reaction over that time period and  $\text{H}_2$  evolution increased very slightly. (Note: the additional peaks in the 0.0 to -300 mV region appear to be impurities introduced into the solution with the  $\text{FeCl}_2$ .)

In general, there were a number of small changes in redox potentials and peak shapes and sizes, but no indications of a significant increase in the rate of  $\text{H}_2$  evolution attributable to the presence of  $\text{Fe}^{2+}$  in chromium solutions. There is, if anything, a slight beneficial effect, perhaps due to a shifting of the chromic ion equilibrium to favor the electrochemically active monochloropentaaquo species.

## B. Effects of $\text{Cr}^{3+}$ in the Positive Electrode Solution

### 1. Experimental Procedure

A 1650°C carbon felt was used for these crossover tests also. Since no special activation procedures are necessary for electrocatalysis of the  $\text{Fe}^{3+}/\text{Fe}^{2+}$  redox reaction, the felt was merely cleaned in KOH before use. Ferric chloride was used in preference to ferrous chloride to avoid any problems that might arise with air sensitivity, especially during extended cycling.

The lower end of the sweep was set at 0.0 V vs. SCE for the positive electrode region in order to overlap the upper end of the negative electrode region; the upper end of the sweep for the positive electrode region was set at 1.0 V vs. SCE to avoid the onset of oxidation reactions observed at higher potentials.

The cyclic voltammogram of  $\text{Fe}^{3+}$  in HCl is particularly simple. There was no evidence under our experimental conditions of any reaction other than the  $\text{Fe}^{3+}/\text{Fe}^{2+}$  redox reaction over the range of 0.0 V to 1.0 V vs. SCE. The effect of  $\text{Cr}^{3+}$  on the  $\text{Fe}^{3+}/\text{Fe}^{2+}$  reaction was tested both in a " $\text{Cr}^{3+}$  first" and a " $\text{Fe}^{3+}$  first" mode. In the former method successive quantities of  $\text{CrCl}_3 \cdot 6\text{H}_2\text{O}$  were added to HCl, and cyclic voltammograms in the potential region of the  $\text{Fe}^{3+}/\text{Fe}^{2+}$  reaction were obtained after each addition. The purpose was to check for any reactivity of impurities introduced with  $\text{CrCl}_3 \cdot 6\text{H}_2\text{O}$ . After the  $\text{Cr}^{3+}$  concentration had reached 0.5 M,  $\text{FeCl}_3 \cdot 6\text{H}_2\text{O}$  was added to make the solution 50 mM  $\text{Fe}^{3+}$ ; the cyclic voltammogram of  $\text{Fe}^{3+}/\text{Fe}^{2+}$  was then recorded. Extended cycling was conducted at this point to find any changes of reactivity with cycling time. The " $\text{Fe}^{3+}$  first" experiment was performed to determine the initial  $\text{Fe}^{3+}/\text{Fe}^{2+}$  redox characteristics without any possible interference from  $\text{Cr}^{3+}$ . The increments of  $\text{Cr}^{3+}$  added were identical to the " $\text{Cr}^{3+}$  first" experiment. Extended cycling was once again conducted after all additions of reagents were completed. The concentration of  $\text{Fe}^{3+}$  was held to 50 mM to stay within the limits of the test equipment and for greater sensitivity to the potential effects of  $\text{Cr}^{3+}$  on the  $\text{Fe}^{3+}/\text{Fe}^{2+}$  reaction.

The potential range for these experiments was 0 to 1.0 V (SCE), using a triangular waveform at a scan rate of 10 mV/s.

For the "Fe<sup>3+</sup> first" experiment the concentrations obtained by successive additions were, in the sequence tested:

- a. 1N HCl
- b. 50 mM Fe<sup>3+</sup>, 1N HCl
- c. 50 mM Fe<sup>3+</sup>, 50 mM Cr<sup>3+</sup>, 1N HCl
- d. 50 mM Fe<sup>3+</sup>, 100 mM Cr<sup>3+</sup>, 1N HCl
- e. 50 mM Fe<sup>3+</sup>, 250 mM Cr<sup>3+</sup>, 1N HCl
- f. 50 mM Fe<sup>3+</sup>, 500 mM Cr<sup>3+</sup>, 1N HCl.

The source of Fe<sup>3+</sup> was FeCl<sub>3</sub>.6H<sub>2</sub>O and the source of Cr<sup>3+</sup> was CrCl<sub>3</sub>.6H<sub>2</sub>O. Extended cycling was conducted for 231 minutes, equal to about 70 cycles (200 sec/cycle), with voltammograms recorded at times 0, 53, 139 and 227 minutes. The cell was sealed and allowed to sit quiescent overnight (14 hours) before resuming cycling for an additional 189 minutes. Voltammograms were recorded at times 0, 17, 83 and 189 minutes (57 cycles).

For the "Cr<sup>3+</sup> first" experiment the concentrations obtained by successive additions were, in the sequence tested:

- a. 50 mM Cr<sup>3+</sup>, 1N HCl
- b. 100 mM Cr<sup>3+</sup>, 1N HCl
- c. 250 mM Cr<sup>3+</sup>, 1N HCl
- d. 500 mM Cr<sup>3+</sup>, 1N HCl
- e. 500 mM Cr<sup>3+</sup>, 50 mM Fe<sup>3+</sup>, 1N HCl.

Extended cycling was conducted for 316 minutes, equal to about 95 cycles, with voltammograms recorded at times 0, 60, 102 and 316 minutes.

## 2. Results

### a) Reactivity on Carbon Felt in Positive Electrode Region in HCl Only.

Figure 88 shows the voltammogram for carbon felt in 1N HCl — in the positive electrode region (0.0 to 1.0 V vs. SCE), together with other voltammograms. It can be seen that there are no significant reactions apparent in this region in the absence of chromium and iron.

### b) Reactivity in Positive Electrode Region After Addition of CrCl<sub>3</sub>.

The effect of adding Cr<sup>3+</sup> in increasing amounts to the 1N HCl solution is shown in Figure 89, along with other voltammograms. Again, the voltammogram lies on the zero-current line from 0.0 to 1.0 V vs. SCE, the Cr<sup>3+</sup> concentrations from 50 mM to 500 mM; this indicates that no reactive impurities were introduced with the chromic chloride.

### c) Effects of Cr<sup>3+</sup> on the Fe<sup>3+</sup>/Fe<sup>2+</sup> Redox Reaction

In the "Fe<sup>3+</sup> First" experiment, a voltammogram for the Fe<sup>3+</sup>/Fe<sup>2+</sup> redox reaction was obtained in 50 mM FeCl<sub>3</sub>/1N HCl before adding any CrCl<sub>3</sub> to the solution; subsequently, CrCl<sub>3</sub> was added incrementally to record voltammograms at 50, 100, 250 and 500 mM Cr<sup>3+</sup>. These are shown together in Figure 88. The effect of added Cr<sup>3+</sup> is to increasingly depress the level of the Fe<sup>3+</sup>/Fe<sup>2+</sup> redox reaction.

With extended cycling at the 500 mM Cr<sup>3+</sup> level, shown in Figure 90, the voltammograms remained constant for 68 cycles. The system was then allowed to stand on open circuit under nitrogen overnight; on continued cycling the

next day there appeared to be a gradual slight shift towards the original higher  $\text{Fe}^{3+}/\text{Fe}^{2+}$  redox currents.

In the " $\text{Cr}^{3+}$  First" experiment,  $\text{CrCl}_3$  was added in increments up to a concentration of 500 mM before adding  $\text{FeCl}_3$ . As indicated in paragraph b above, no reactivity was observed before the addition of  $\text{FeCl}_3$ . After the addition of 50 mM  $\text{FeCl}_3$ , a voltammogram for the  $\text{Fe}^{3+}/\text{Fe}^{2+}$  reaction was obtained, as shown in Figure 89, which grew on extended cycling toward higher current peaks (95 cycles accumulated).

Compared to the results obtained for the negative electrode, it appears that there may be more interference from  $\text{Cr}^{3+}$  crossover to the positive electrode than from  $\text{Fe}^{2+}$  crossover to the negative electrode, perhaps by increasing the chloride complexation of the ferric ion. These general conclusions are supported by the encouraging results obtained in full cell testing with mixed reactants at NASA-LeRC (11).

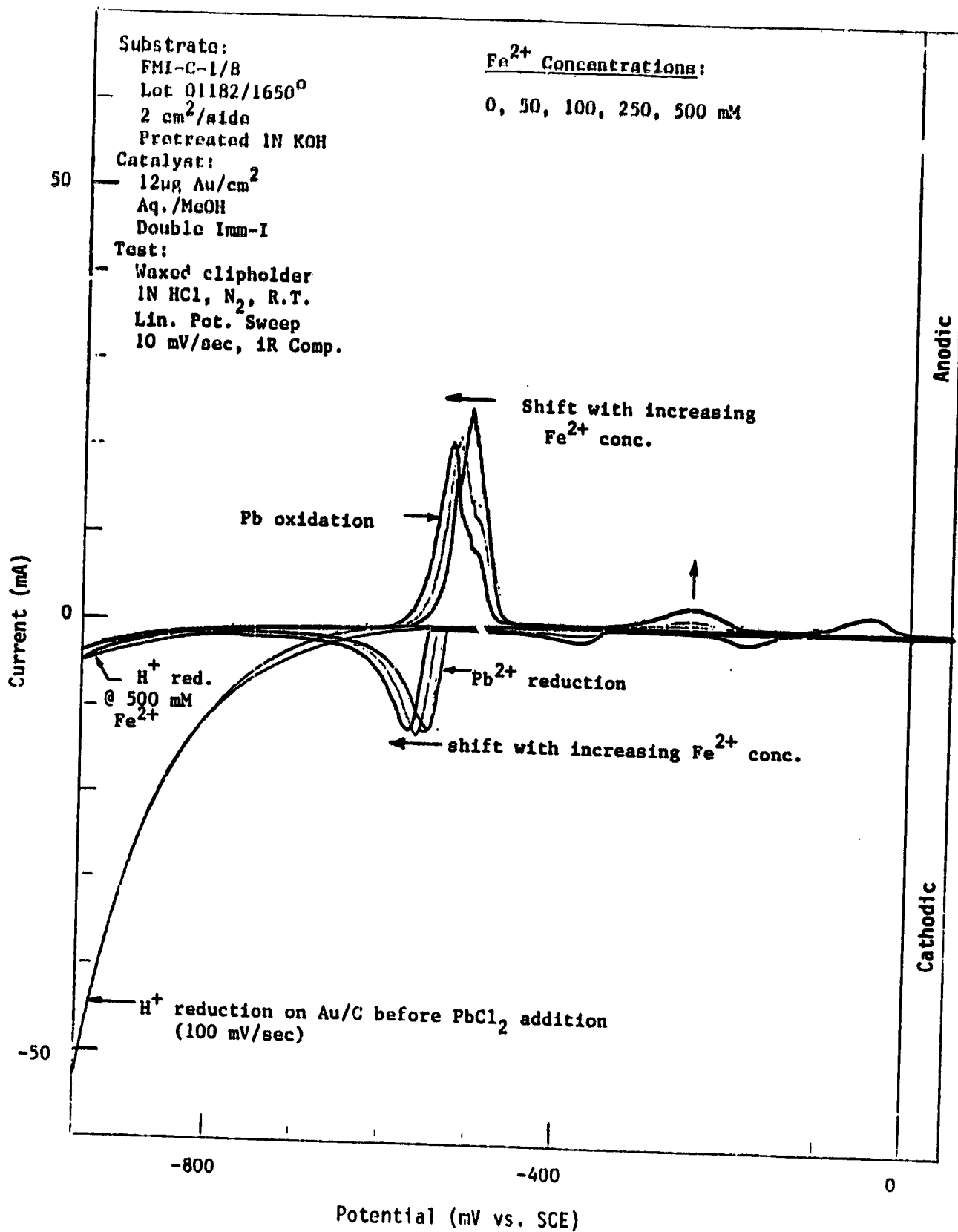


Figure 84. Crossover Effects: Increasing Fe<sup>2+</sup> in Negative Electrode Solution (HCl, Pb<sup>2+</sup>, No Cr<sup>3+</sup>).

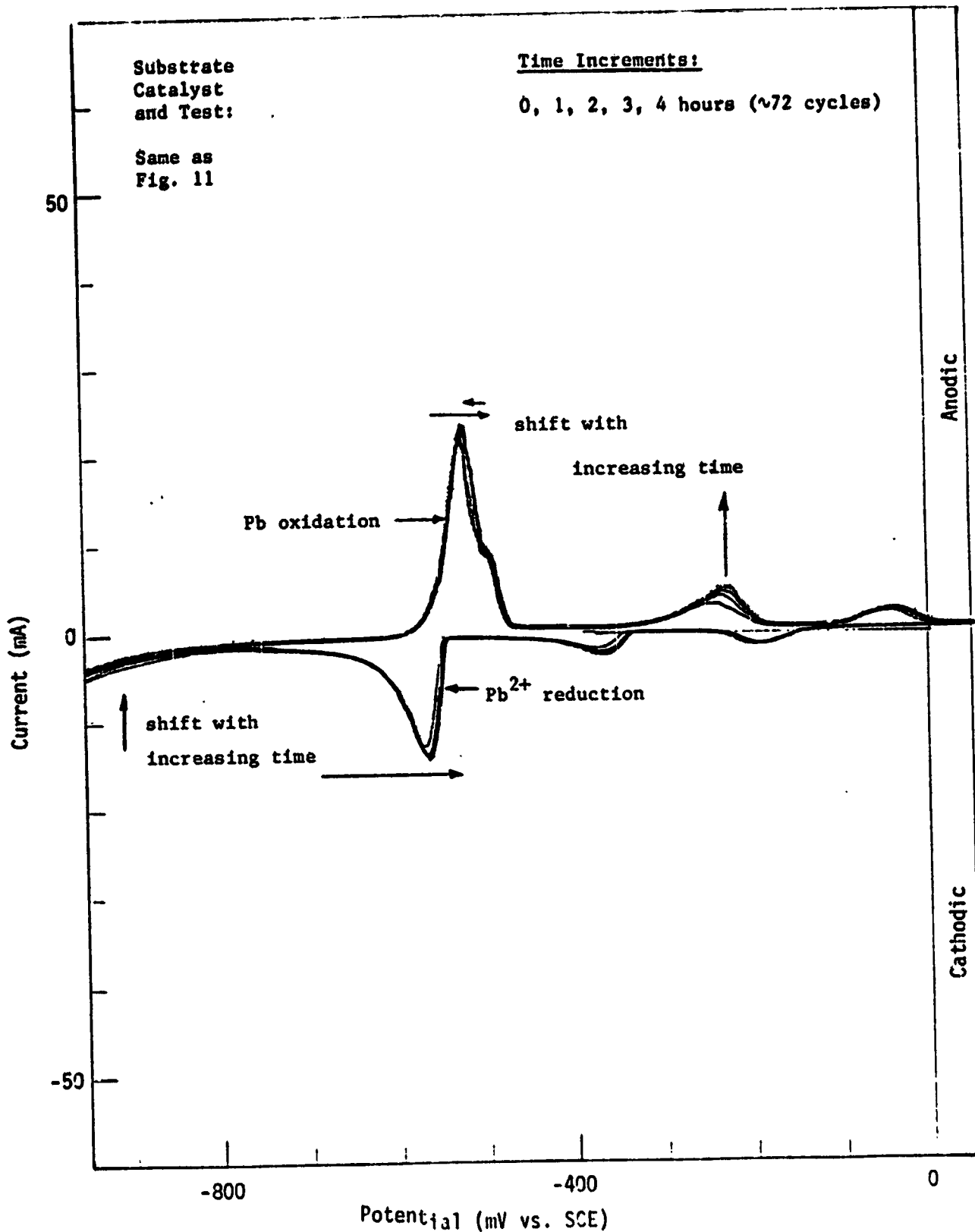


Figure 85. Crossover Effects: Extended Cycling with 500 mM Fe<sup>2+</sup> in Negative Electrode Solution (HCl, Pb<sup>2+</sup>, No Cr<sup>3+</sup>).

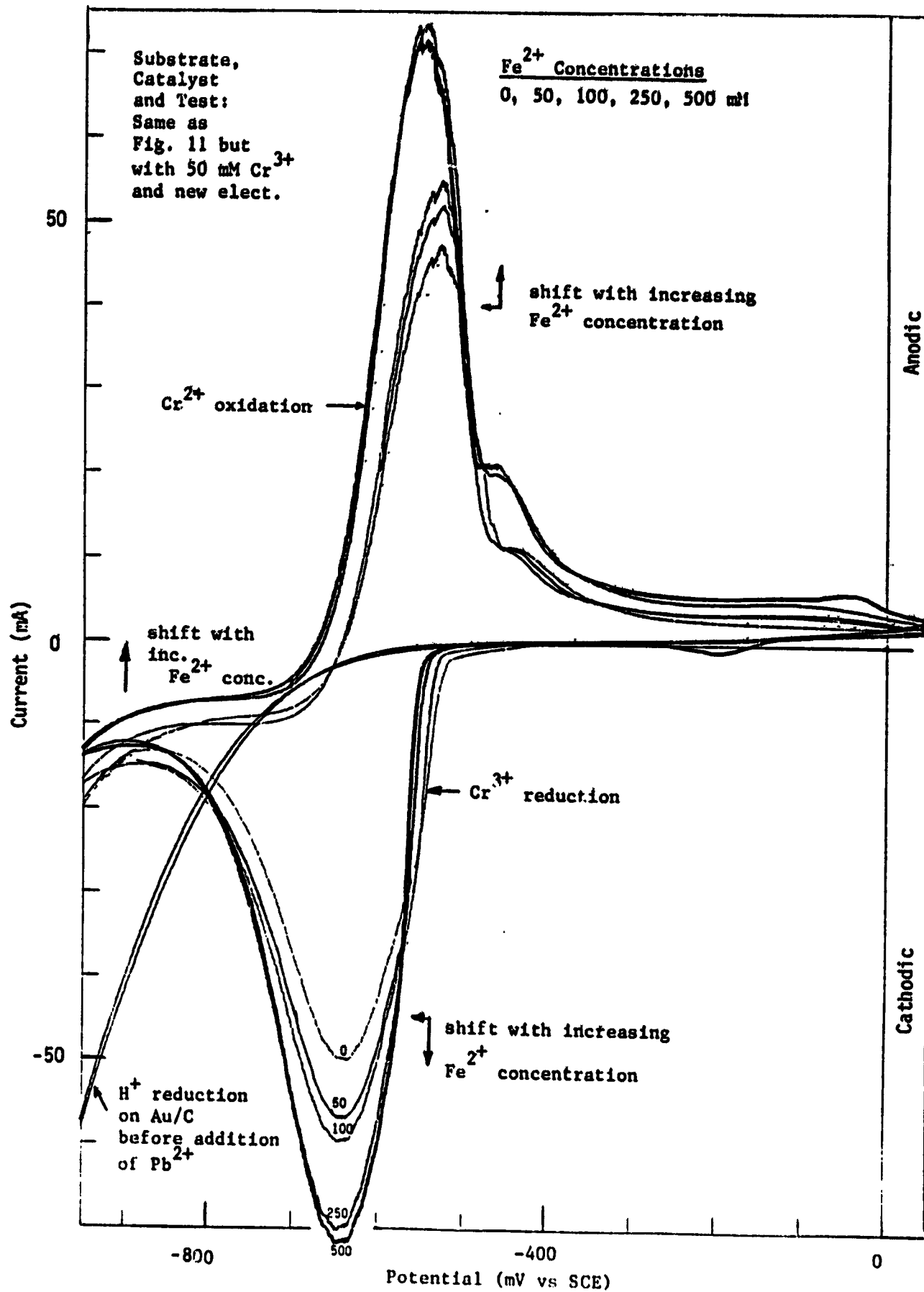


Figure 86. Crossover Effects: Increasing Fe<sup>2+</sup> in Negative Electrode Solution (HCl, Pb<sup>2+</sup>, 50 mM Cr<sup>3+</sup>).

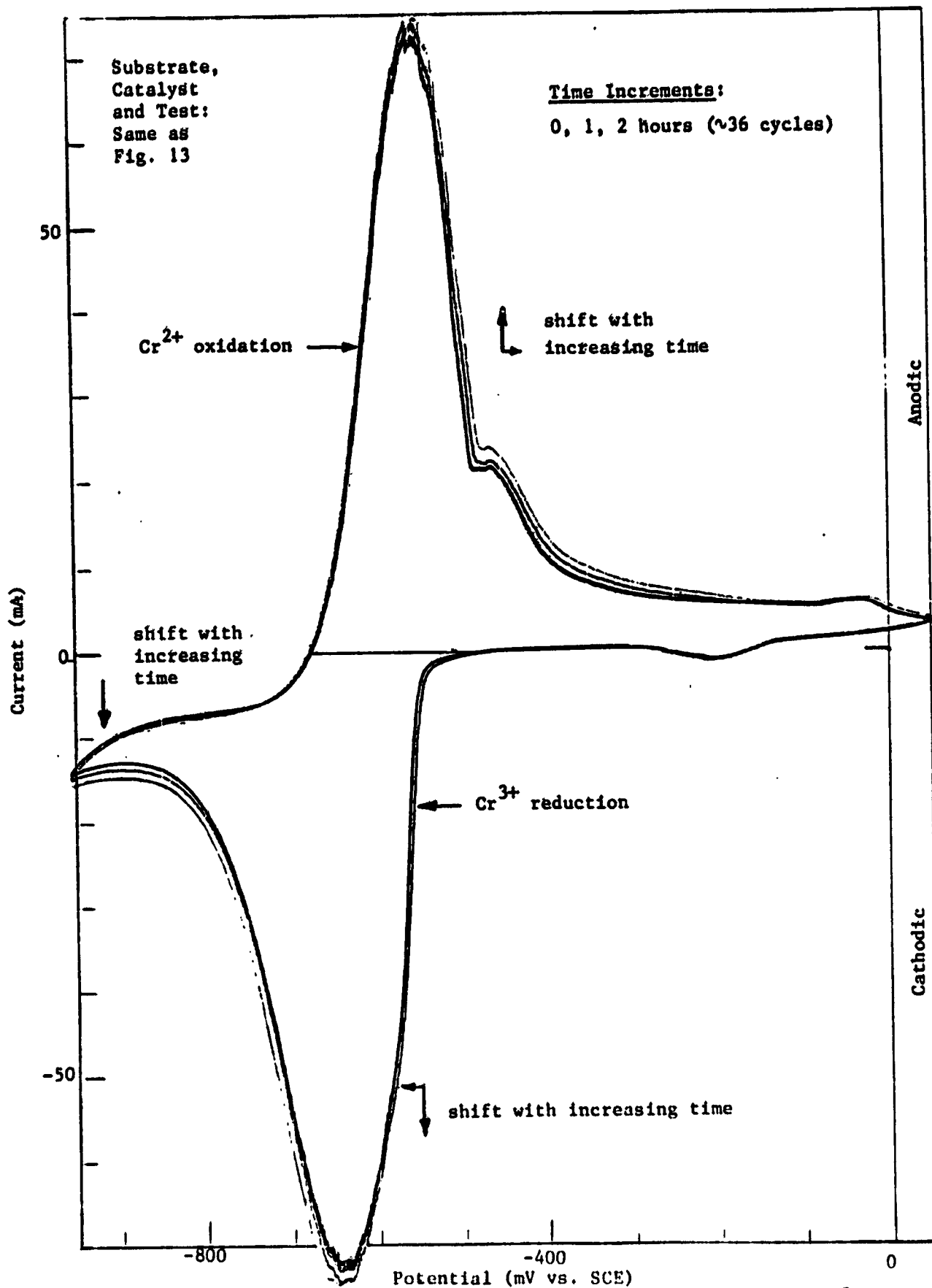


Figure 37. Crossover Effects: Extended Cycling with 500 mM Fe<sup>2+</sup> in Negative Electrode Solution (HCl, Pb<sup>2+</sup>, 50 mM Cr<sup>3+</sup>).

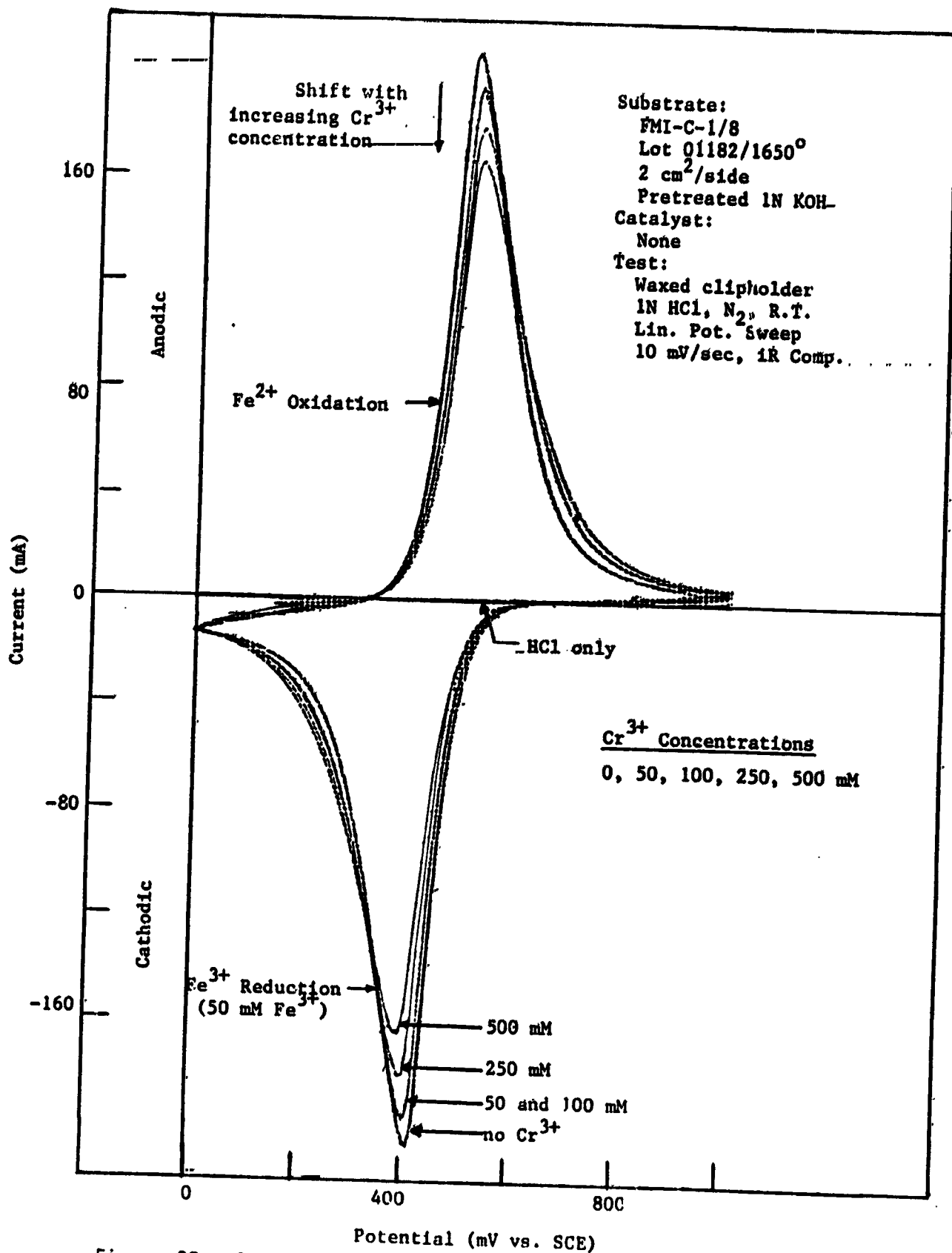


Figure 88. Crossover Effects: Effect of Added Cr<sup>3+</sup> in Positive Electrode Solution, "Fe<sup>3+</sup> First".

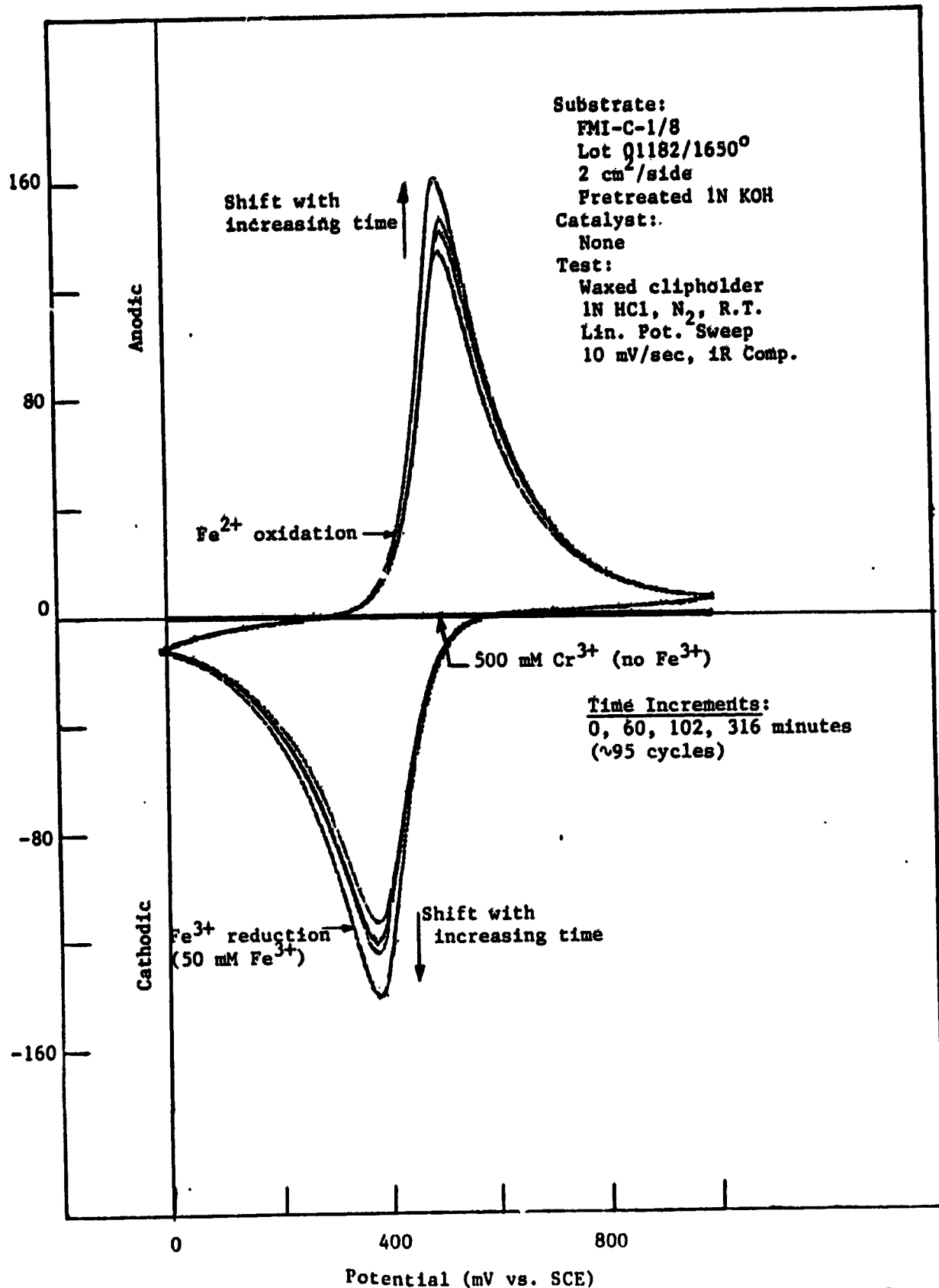


Figure 89. Crossover Effects: Extended Cycling with 500 mM Cr<sup>3+</sup> in Positive Electrode Solution, "Cr<sup>3+</sup> First".

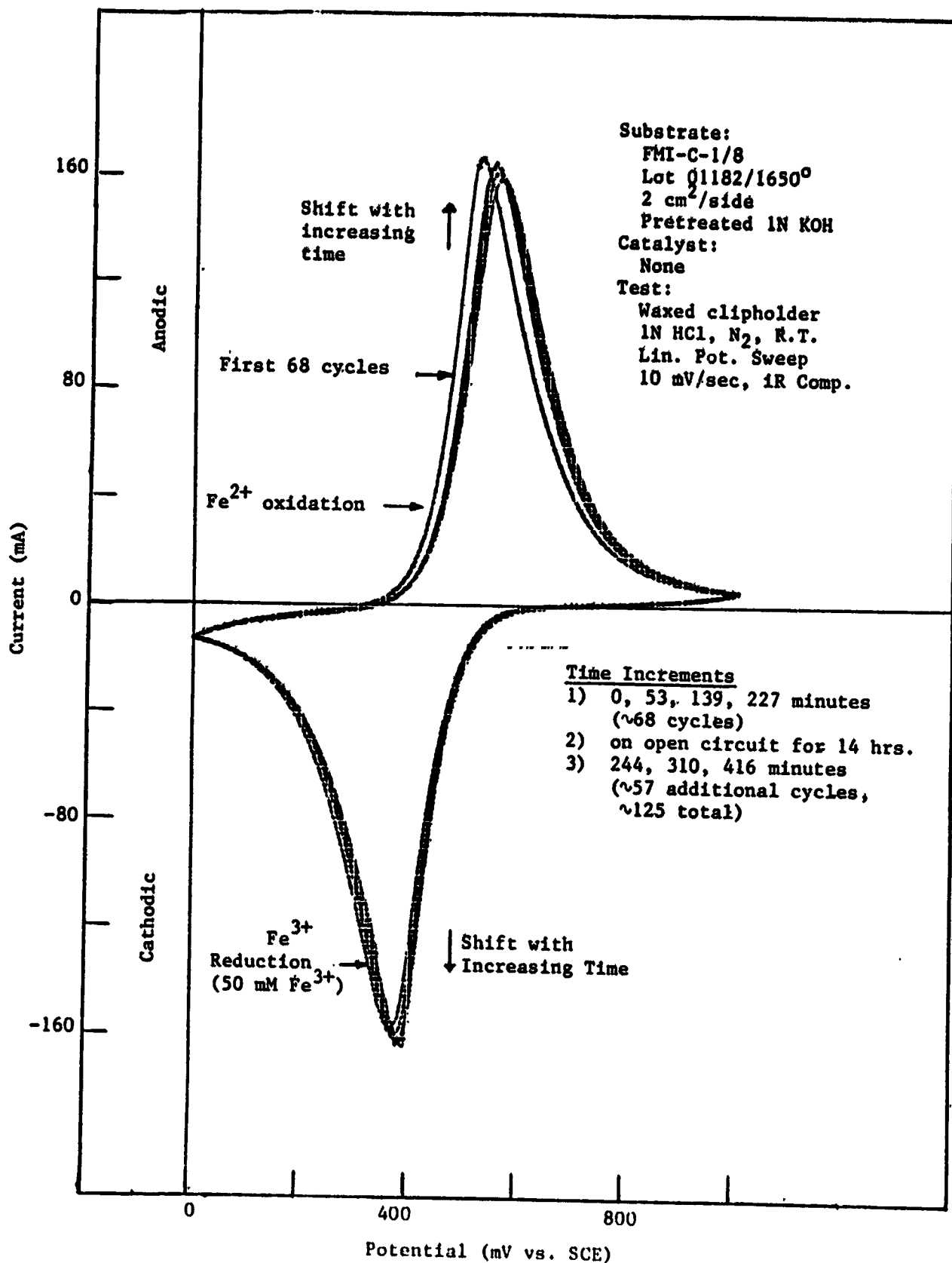


Figure 90. Crossover Effects: Extended Cycling with 500 mM Cr<sup>3+</sup> in Positive Electrode Solution, "Fe<sup>3+</sup> First".

## VII. EFFECTS OF ACIDITY LEVEL ON Fe/Cr REDOX REACTIONS

The purpose of varying the acidity was to determine by half-cell tests how much variation in electrochemical performance occurs with variation in acidity. The statement of work for this task called for equilibration of solutions for at least one month before conducting voltammetric tests. With the approval of the contract monitor, it was decided that it would only be necessary to equilibrate the  $\text{CrCl}_3$  solutions; the  $\text{FeCl}_3$  and  $\text{FeCl}_2$  solutions could be freshly made before testing. The rationale for this decision was that  $\text{CrCl}^{2+}$  is a kinetically inert complex while  $\text{FeCl}^{2+}$  and  $\text{FeCl}^+$  are rather labile. The half life of aquation of  $\text{CrCl}^{2+}$  to yield hexaquo-chromium (III) is reported to be approximately 700 hours (22). The half-life of aquation of  $\text{FeCl}^{2+}$  is approximately 0.3 sec and that of  $\text{FeCl}^+$  is probably even shorter (23).

### A. Acidity-Level Effects on the Positive Electrode Reactions

#### 1. Experimental

The only electrode material used in these tests was KOH-cleaned 1650°C carbon felt, which has been found to be suitable for battery operation in the previously studied acidity range of 1.0N to 2.0N HCl. The samples were mounted in the waxed-clip holder as described earlier. The ten solutions studied were as follows:

- (1) 50 mM  $\text{FeCl}_3$ , 0.1N HCl.
- (2) 50 mM  $\text{FeCl}_3$ , 0.5N HCl.
- (3) 50 mM  $\text{FeCl}_3$ , 1.0N HCl.
- (4) 50 mM  $\text{FeCl}_3$ , 2.0N HCl.
- (5) 50 mM  $\text{FeCl}_3$ , 4.0N HCl.
- (6) 50 mM  $\text{FeCl}_2$ , 0.1N HCl.

- (7) 50 mM FeCl<sub>2</sub>, 0.5N HCl.
- (8) 50 mM FeCl<sub>2</sub>, 1.0N HCl.
- (9) 50 mM FeCl<sub>2</sub>, 2.0N HCl.
- (10) 50 mM FeCl<sub>2</sub>, 4.0N HCl.

Cyclic voltammograms were run from 0.0 V to 1.0 V (SCE). Under these conditions Cl<sub>2</sub> evolution was avoided even in 4.0N HCl and the only experimentally observable Faradaic reactions were the oxidation of Fe<sup>2+</sup> and the reduction of Fe<sup>3+</sup>.

Chlorine evolution is only possible at somewhat higher potentials. The equilibrium potential on the standard hydrogen electrode scale is

$$E_0 = 1.359 + 0.0295 \log pCl - 0.029 \log [Cl]_2.$$

The standard potential of the Fe<sup>3+</sup>/Fe<sup>2+</sup> redox reaction is 770 mV (SHE), and the effect of chloride is to lower the electrode potential somewhat. Therefore under normal battery operating conditions Cl<sub>2</sub> evolution (at least as it is experimentally accessible in half-cell) is not expected. Under unusual conditions such as overcharge, Cl<sub>2</sub> evolution may play a role, but this was not investigated.

For reasons that were not determined, it was not possible to set the iR correction for these experiments in the usual manner. Typically, electronic iR compensation was increased until an oscillation point is reached. Then the iR compensation level was reduced very slightly. However, for these acidity-effect experiments an unusual level of iR compensation was necessary to reach the oscillation point. If the setting was then slightly reduced, oscillation still continued. It was necessary to greatly diminish the iR compensation to halt the oscillation. What was done in practice was to go through the process of setting the iR compensation twice.

## 2. Results

Cyclic voltammograms showing the effect of acidity on the  $\text{Fe}^{3+}/\text{Fe}^{2+}$  reaction are presented in Appendix VII (Figures VII-1 to VII-10). Table XVI gives peak separations and formal potentials as a function of HCl concentration, Table XVII lists anodic and cathodic charges as a function of HCl concentration.

Some of the results for  $\text{Fe}^{3+}$  electrolyte could be indicative of increasing reversibility of  $\text{Fe}^{3+}/\text{Fe}^{2+}$  redox reaction with increasing HCl concentration, because as the HCl concentration was changed from 0.1N to 4.0N the peak separation decreased continuously from 342 to 83 mV. The formal potentials,  $E_{\text{redox}}$ , decreased continuously from 509 mV (SCE) for 0.1N HCl to 417 mV (SCE) for 4.0N HCl. This probably reflects greater complexation by chloride of  $\text{Fe}^{3+}$  compared to  $\text{Fe}^{2+}$ . The  $Q_a\text{Fe}^{2+}$  value decreased continuously in the same HCl range from 4000 mC to 2785 mC, while  $Q_c\text{Fe}^{3+}$  decreased from 4490 mC to 2880 mC. The  $Q_c\text{Fe}^{3+}$  value was always greater than  $Q_a\text{Fe}^{2+}$ , as expected from previous work. The  $Q_a\text{Fe}^{2+}$  value exceeded  $Q_c\text{Fe}^{3+}$  (3190 mC, theoretical) by about 25% in one instance. This may reflect expansion of the felt in solution. The results for  $\text{Fe}^{2+}$  electrolyte are more difficult to interpret than those for  $\text{Fe}^{3+}$  electrolyte.

### B. Acidity-Level Effects on the Negative Electrode Reactions

For battery operation a high  $\text{Cr}^{3+}$  concentration (such as 1 M) is needed; for voltammetric testing a low  $\text{Cr}^{3+}$  concentration (such as 50 mM) is desirable. Equilibration of a 50 mM  $\text{Cr}^{3+}$  solution, however, might not yield the same percentage of chromium (III) hexaquo and chromium (III) chloro complexes as equilibration of 1 M  $\text{Cr}^{3+}$  solution. Therefore, both concentration levels at the five different acidities were prepared. The 1 M solu-

tions were to be diluted to 50 mM  $\text{CrCl}_3$  with acidified diluent at the time of testing. The time required for diluting and testing is short enough so that no significant change could occur in complex speciation. The ten following solutions, therefore, were prepared and set aside for equilibration:

- (1) 100 ml of 1M  $\text{CrCl}_3$ , 0.1N HCl
- (2) 100 ml of 1M  $\text{CrCl}_3$ , 0.5N HCl
- (3) 100 ml of 1M  $\text{CrCl}_3$ , 2.0N HCl
- (4) 100 ml of 1M  $\text{CrCl}_3$ , 2.0N HCl
- (5) 100 ml of 1M  $\text{CrCl}_3$ , 4.0N HCl
- (6) 1000 ml of 50 mM  $\text{CrCl}_3$ , 0.1N HCl
- (7) 1000 ml of 50 mM  $\text{CrCl}_3$ , 0.5N HCl
- (8) 1000 ml of 50 mM  $\text{CrCl}_3$ , 1.0N HCl
- (9) 1000 ml of 50 mM  $\text{CrCl}_3$ , 2.0N HCl
- (10) 1000 ml of 50 mM  $\text{CrCl}_3$ , 4.0N HCl.

After approximately six months of closed storage, the 1 M solutions were diluted to 50 mM and the colors compared to the original 50 mM solutions. The qualitative observations are summarized below:

<u>Acidity Level</u>	<u>Cr<sup>3+</sup> Concentration</u>	<u>Color</u>
4N	50 mM	Green-gray
	1M → 50 mM	Green
2N	50 mM	Violet-gray
	1M → 50 mM	Green-gray
1N	50 mM	Violet
	1M → 50 mM	Violet-green
0.5N	50 mM	Violet
	1M → 50 mM	Violet-green
0.1N	50 mM	Violet
	1M → 50 mM	Violet

The violet color is indicative of the conversion to the Cr(III) hexaquo complex. It was apparent that the diluted samples (50 mM Cr<sup>3+</sup>) experienced a greater degree of conversion to the Cr(III) hexaquo complex than the concentrated samples (1M Cr<sup>3+</sup>); for this reason the 50 mM samples were chosen for testing. There was also more conversion at the lower acidity levels; this was reflected in the electrochemical performance in these solutions as discussed below.

Cyclic voltammetry was performed in each solution, using a fresh electrode in each case (from a 1650°C felt, Double Immersion preparation) and 1mM PbCl<sub>2</sub>. The voltammograms are shown in Appendix VII (Figures AVII-11 to AVII-15). Performance dropped to a lower level at lower acid concentrations (and increasing Cr(III) hexaquo concentration). Below 4 N HCl, lead deposition dominates the cathodic wave. Anodic peak currents are as follows:

HCl	<u>4N</u>	<u>2N</u>	<u>1N</u>	<u>0.5N</u>	<u>0.1N</u>
I <sub>a</sub> (mA)	65	22	24	26	30

A qualitative conclusion is that higher concentrations of CrCl<sub>3</sub> and HCl will retard conversion to the Cr(III) hexaquo complex to some extent.

TABLE XVI

Peak Separation For Fe<sup>3+</sup>/Fe<sup>2+</sup> Redox Reaction  
As a Function of HCl Concentration

Solution Composition	$E_{pa} - E_{pc}$ (mV)	$E'_{redox}$ (SCE) (mV)
50 mM Fe <sup>3+</sup> , 0.1N HCl	342	509
50 mM Fe <sup>3+</sup> , 0.5N HCl	292	466
50 mM Fe <sup>3+</sup> , 1.0N HCl	229	450
50 mM Fe <sup>3+</sup> , 2.0N HCl	125	438
50 mM Fe <sup>3+</sup> , 4.0N HCl	83	417
50 mM Fe <sup>2+</sup> , 0.1N HCl	445	528
50 mM Fe <sup>2+</sup> , 0.5N HCl	291	458
50 mM Fe <sup>2+</sup> , 1.0N HCl	120	468
50 mM Fe <sup>2+</sup> , 2.0N HCl	87	452
50 mM Fe <sup>2+</sup> , 4.0N HCl	45	421

TABLE XVII

Fe<sup>3+</sup> Reduction and Fe<sup>2+</sup> Oxidation Charges  
As a Function of HCl Concentration

Solution Composition	Q <sub>a</sub> Fe <sup>2+</sup> (m coul)	Q <sub>c</sub> Fe <sup>3+</sup> (m coul)
50 mM Fe <sup>3+</sup> , 0.1N HCl	3999	4489
50 mM Fe <sup>3+</sup> , 0.5N HCl	3354	3586
50 mM Fe <sup>3+</sup> , 1.0N HCl	3290	3444
50 mM Fe <sup>3+</sup> , 2.0N HCl	2967	3109
50 mM Fe <sup>3+</sup> , 4.0N HCl	2786	2877
50 mM Fe <sup>2+</sup> , 0.1N HCl	2325	2045
50 mM Fe <sup>2+</sup> , 0.5N HCl	3483	2786
50 mM Fe <sup>2+</sup> , 1.0N HCl	4360	3857
50 mM Fe <sup>2+</sup> , 2.0N HCl	4889	4231
50 mM Fe <sup>2+</sup> , 4.0N HCl	4334	3560

Theoretical quantity of reactant, Q<sub>t</sub>, is equal to 3190 m coul

## VIII. TEMPERATURE DEPENDENCE

The objective of this task was to ascertain the effects of temperature (25° - 65°C) on the iron/chromium redox reactions over the reactant concentration range of 1.0, 1.5 and 2.0 M. The usual 50 mM concentration was included here for iron solutions as a reference point to earlier studies.

The typical cyclic voltammetry methods used in this program (Section II) were not entirely suitable for this study. There was the physical problem of the softening of the wax (used to define the electrode area and to isolate the contact region on the carbon felt) at higher temperatures, and generation of a film on the surface of the solution. There were also a number of instrumentation problems: at the higher reactant concentrations, the instrument limits were quickly exceeded necessitating a large reduction in sweep rate, and iR-compensation was more difficult.

In addition, one of the principal reasons for operating at elevated temperature is to shift the chromium complex equilibrium from the less active hexaquo species to the more active monochloropentaaquo species. Since the conversion to the hexaquo chromium species occurs slowly (22), the effects are not generally observed in short-term cyclic voltammetry with fresh solutions. Temperature effects, in general, have been addressed more directly and effectively in full cell testing at NASA-LeRC (1,10,11).

### A. Positive Electrode Studies.

#### 1. Experimental Procedures.

Samples of 1700°C felt (Lot 051482) were soaked in methanol, rinsed, and cleaned in 45% potassium hydroxide at 90°C for two hours. For the  $\text{Fe}^{3+}/\text{Fe}^{2+}$  reaction, no catalyzation is required.

Strips of felt were mounted and waxed as usual for testing by cyclic voltammetry in the half cell. The first of these tests was conducted in a solution of 0.050 M  $\text{FeCl}_3$  in 1.0 N HCl at 25°C. The  $\text{Fe}^{3+}/\text{Fe}^{2+}$  reaction was examined with a linear potential sweep over the range of 0 to +1.000 volt versus SCE. The sweep rate was 10 mV/sec for the 0.050 M iron solution.

Potential was first applied near +1.0 volt, before the onset of  $\text{Fe}^{3+}$  reduction. Compensation for iR was added after one cycle. A voltammogram was then recorded after allowing several cycles for equilibration. This procedure was repeated at 45°C, 55°C and 65°C, using the original felt electrode and 0.050 M iron solution. The series of tests at four temperatures was completed in a single day to obviate any effects of thermal cycling.

In order to accommodate the higher currents generated in concentrated iron solutions, it was necessary to reduce the sweep rate. This was accomplished through the use of a motor-driven slow-function generator with adjustable gear ratios. The actual sweep rate was determined by clocking the time required to produce a 1000 mV change in potential. A rate was further reduced to 0.88 mV/sec for the higher concentrations (1.5 M and 2.0 M). Since the function generator was equipped with a ramp function only, the direction of sweep had to be reversed manually at the extremes of the potential range. For this reason, and also to save time, the range was often intentionally reduced and the endpoints therefore do not correspond to 0 and +1.000 volt. This in no way affects the rate of sweep, however, and all reactions of interest occur in the range of +0.200 V to +0.800 V.

Otherwise, testing in concentrated iron solutions proceeded substantially as described above for the 50 mM iron solution, voltammograms

were obtained at each of the four temperatures in 1.0 M  $\text{FeCl}_3$  in 1.0 N HCl, 1.5 M  $\text{FeCl}_3$  in 1.0 N HCl, and 2.0 M  $\text{FeCl}_3$  in 1.0 N HCl. Because of the slow sweep rates, it was not possible to complete testing at all four temperatures within a single day. In such cases, the original felts and electrolytes were not retained. Newly waxed felts and fresh solutions were put in place at the start of each day.

## 2. Results

The voltammograms for the 50 mM  $\text{FeCl}_3$  are presented in Figures 91 through 94. The results are approximately as expected. The voltammograms for the higher concentrations are presented in Appendix VIII. With the slow sweep rates and high solute concentrations used in some of these experiments, an appreciable amount of ferric ion in the bulk solution could diffuse to the surface of the felt during the redox reaction. This had the effect of increasing the charge passed during  $\text{Fe}^{3+}$  reduction while decreasing the net oxidation charge. Thus the cathodic peak was generally several times larger than the anodic peak. Some of the ferrous ion generated may also have diffused out of the felt. Also note the unusually large separation between peak anodic and cathodic currents observed in 50 mM  $\text{FeCl}_3$  at 25°C (Figure 91). The reaction became more reversible as the temperature was raised. A similar phenomenon was not observed at higher iron concentrations.

When comparing voltammograms obtained at different concentrations of  $\text{FeCl}_3$ , it is necessary to take into account the fact that the amount of charge represented by the area under a peak is dependent upon the sweep rate as well as the scale. Each square centimeter in Figures 91 through 94 represents 0.200 Coulombs; in Figures AVIII-1 through AVIII-4 it is 2.78

Coulombs/cm<sup>2</sup>; in Figures AVIII-5 through AVIII-12 it is 5.68 Coulombs/cm<sup>2</sup>.

## B. Negative Electrode Studies.

### 1. Experimental Procedures.

Samples of 1700°C (lot 051582) carbon felt were catalyzed according to the standard NASA procedure (8) as modified below. Felts previously cleaned in 45 percent potassium hydroxide were rinsed thoroughly, soaked in distilled water for 16 hours, then soaked for one and one half hours in water of pH 7 immediately before the damp-drying step prior to catalyzation. In addition, the catalyst solution was warmed to 25°C before being applied to the damp-dried felt. The catalyzed felts were sealed in plastic bags and held at about 25°C for sixteen hours, then dried and baked.

Felts were then mounted and waxed as usual and tested by cyclic voltammetry in the half cell. The test solutions were 1.0N in HCl, 1 mM in PbCl<sub>2</sub>, and 1.0 M, 1.5M or 2.0 M in CrCl<sub>3</sub>. Steady state iR-compensated voltammograms were obtained at temperatures of 25, 45, 55, and 65°C at each concentration.

In order to accommodate the high currents at these concentrations, it was necessary to reduce the potential sweep rates in this study also, as discussed above. A rate of 0.885 mV/sec was initially chosen and used for the tests in 1.0 M CrCl<sub>3</sub>; the rate was thereafter increased to between 1.72 and 1.77 mV/sec. The exact sweep rate, calculated on the actual day of the experiment, is recorded on each voltammogram.

Due to the slow sweep rate, the number of experiments that could be completed in a single day was generally limited to two. In every case, fresh solutions were prepared and new electrode samples (cut from the same preparation) were waxed and mounted at the start of each day.

## 2. Results

The voltammograms obtained as above are presented in Appendix VIII Figures AVIII-13 through AVIII-24. When visually comparing peak areas, please note the following charge factors; in Figures AVIII-13 through 16, each square centimeter on the graph represents 5.65 coulombs; in Figures AVIII-17 and 18 the factor is 2.82 coul/cm<sup>2</sup>; in Figures AVIII-19 through 24 the factor is 2.86 coul/cm<sup>2</sup>.

As can be seen from the voltammograms, the results on the cathodic side were markedly different from those obtained in more dilute solutions of CrCl<sub>3</sub>. Voltammograms obtained in 1.0 M CrCl<sub>3</sub> all show a sharp spike in current at or near -670 mV vs. SCE, perhaps marking the onset of Pb<sup>2+</sup> reduction. The current declined thereafter, exhibiting a shallow minimum and increasing somewhat at more negative potentials where H<sup>+</sup> reduction becomes significant. Contrary to previous experience, a more normal rounded peak shape was exhibited only on the return sweep. With the exception of Figures AVIII-17 and 18, the remaining voltammograms show a long steady rise in cathodic current with increasingly negative potential. The cathodic current came to a sharp maximum near -850 mV vs. SCE in 1.5 M CrCl<sub>3</sub> and around -700 mV vs. SCE in the 2.0 M CrCl<sub>3</sub> solutions. After a brief but sudden drop following the maximum, the current decreased slightly and remained nearly constant toward more negative potential. On the return sweep, the current remained nearly constant for a time, then followed the initial rise in cathodic current back toward the anodic side. Similar behavior is observed in Figure AVIII-17 except that the sharp maximum in cathodic current is lacking. The voltammogram in Figure AVIII-18 is alone in showing a rounded cathodic peak more typical of previous data.

Except for a pronounced second peak in Figures AVIII-19 and 21, the anodic current behavior was unremarkable.

The rather large discrepancy in the magnitude of the anodic and cathodic charges can be explained by the comparatively long time allotted the oxidation and reduction reactions (about 20 minutes each, versus less than 3 minute in most previous data). During this time period, a significant amount of  $\text{Cr}^{3+}$  could diffuse into the felt and be reduced, contributing to the cathodic charge.

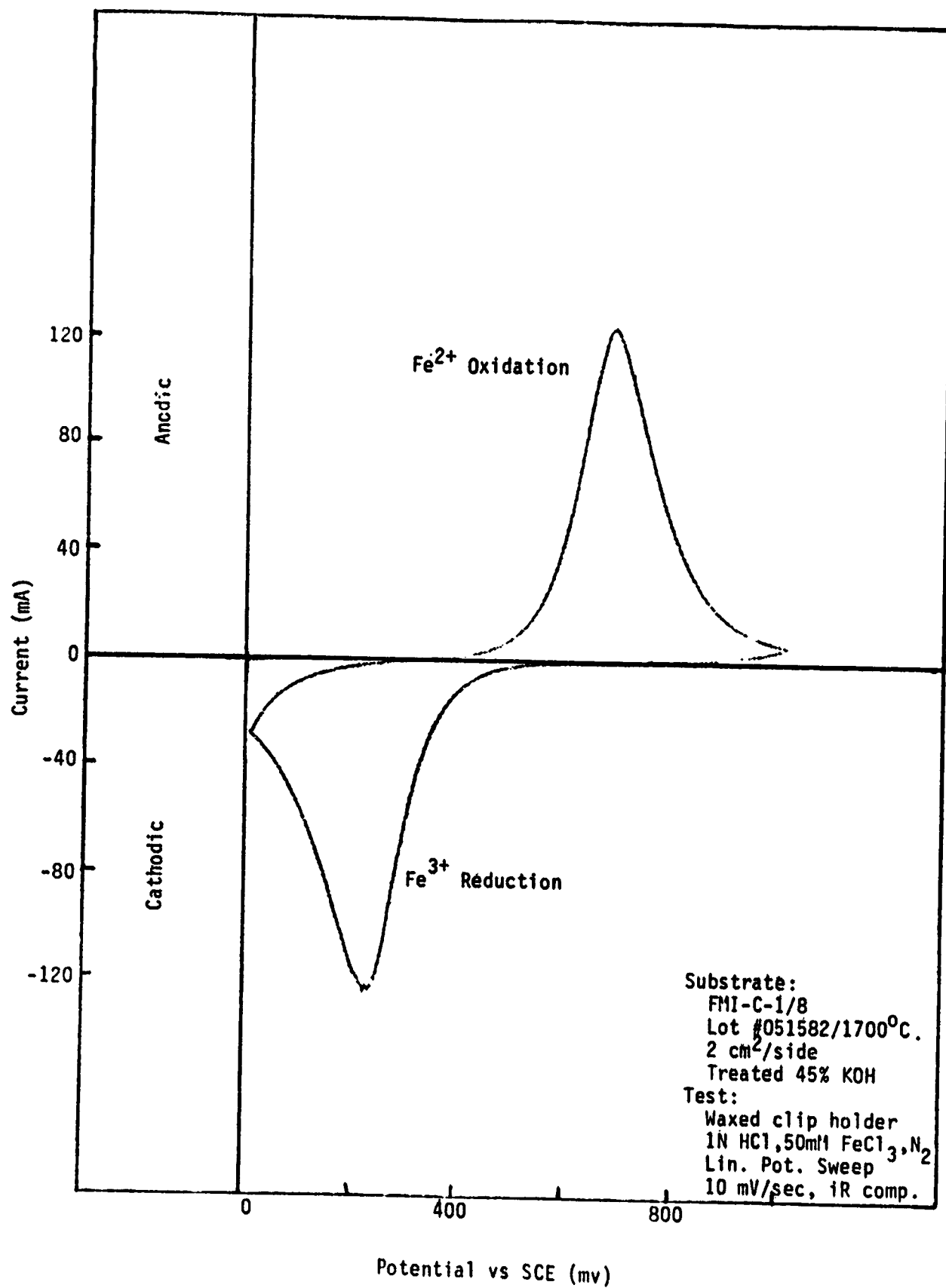


Figure 91. Fe<sup>3+</sup>/Fe<sup>2+</sup> Reaction at 25°C. in 0.050M FeCl<sub>3</sub>.

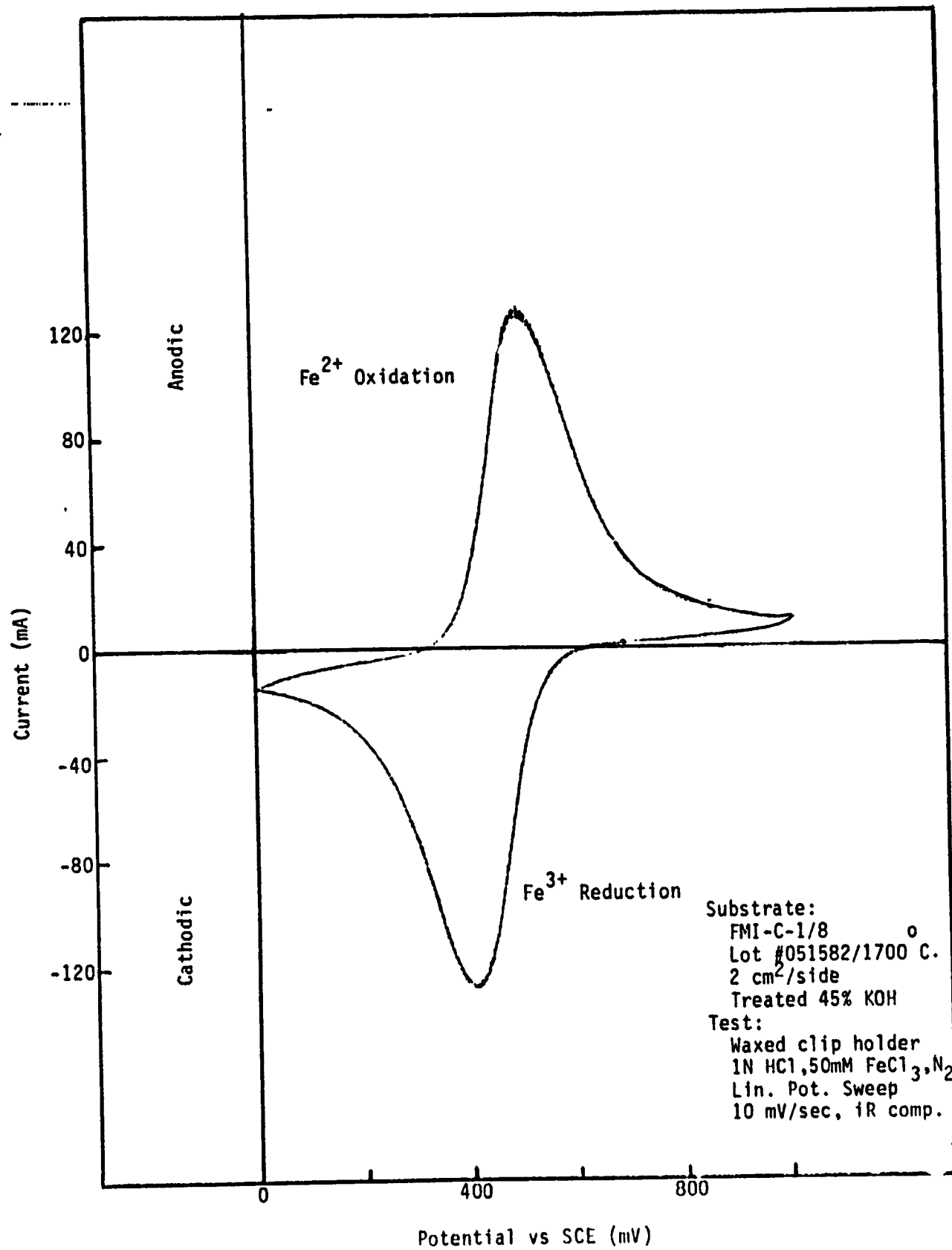


Figure 92. Fe<sup>3+</sup>/Fe<sup>2+</sup> Reaction at 45°C. in 0.050M FeCl<sub>3</sub>.

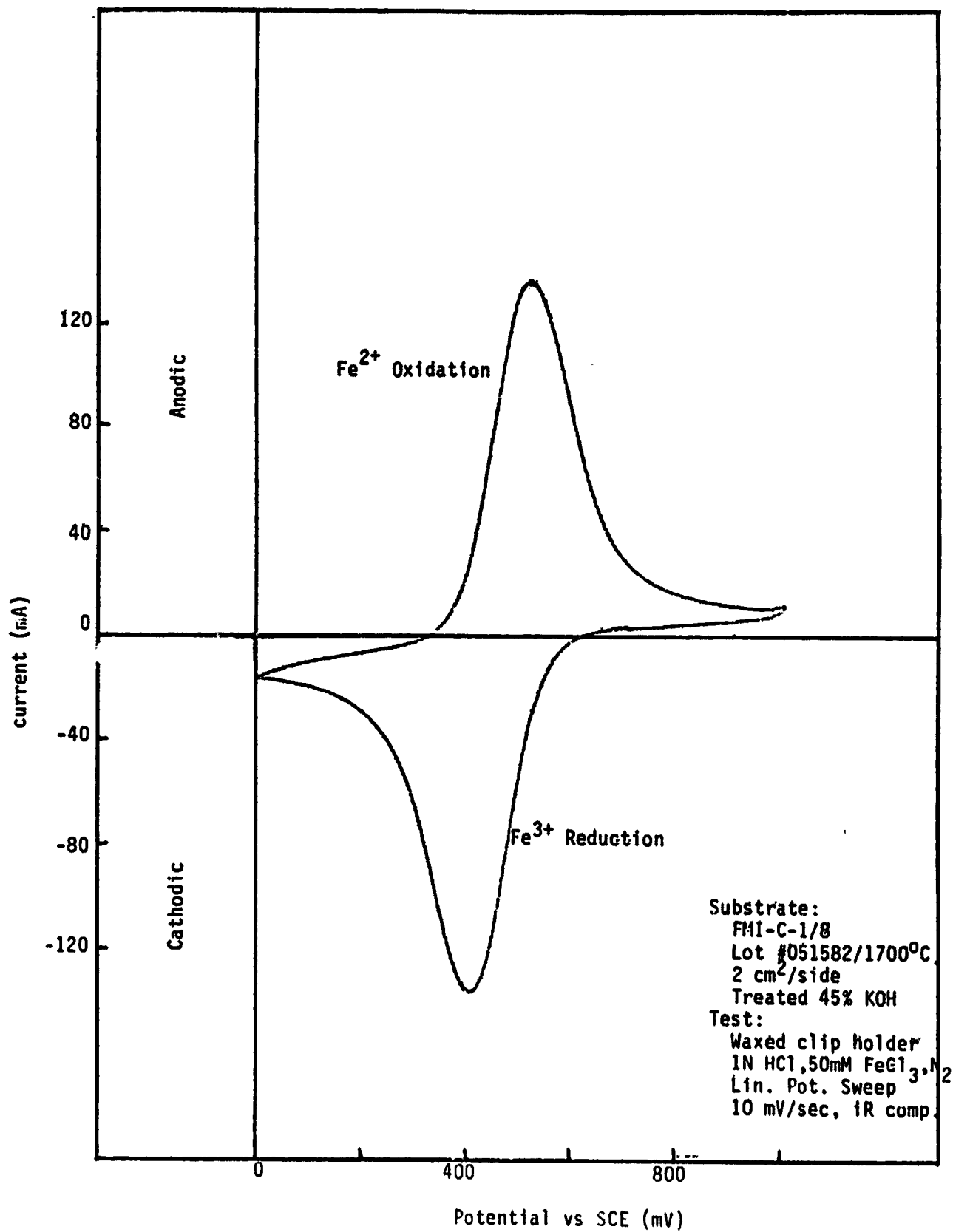


Figure 93. Fe<sup>3+</sup>/Fe<sup>2+</sup> Reaction at 55°C. in 0.050M FeCl<sub>3</sub>.

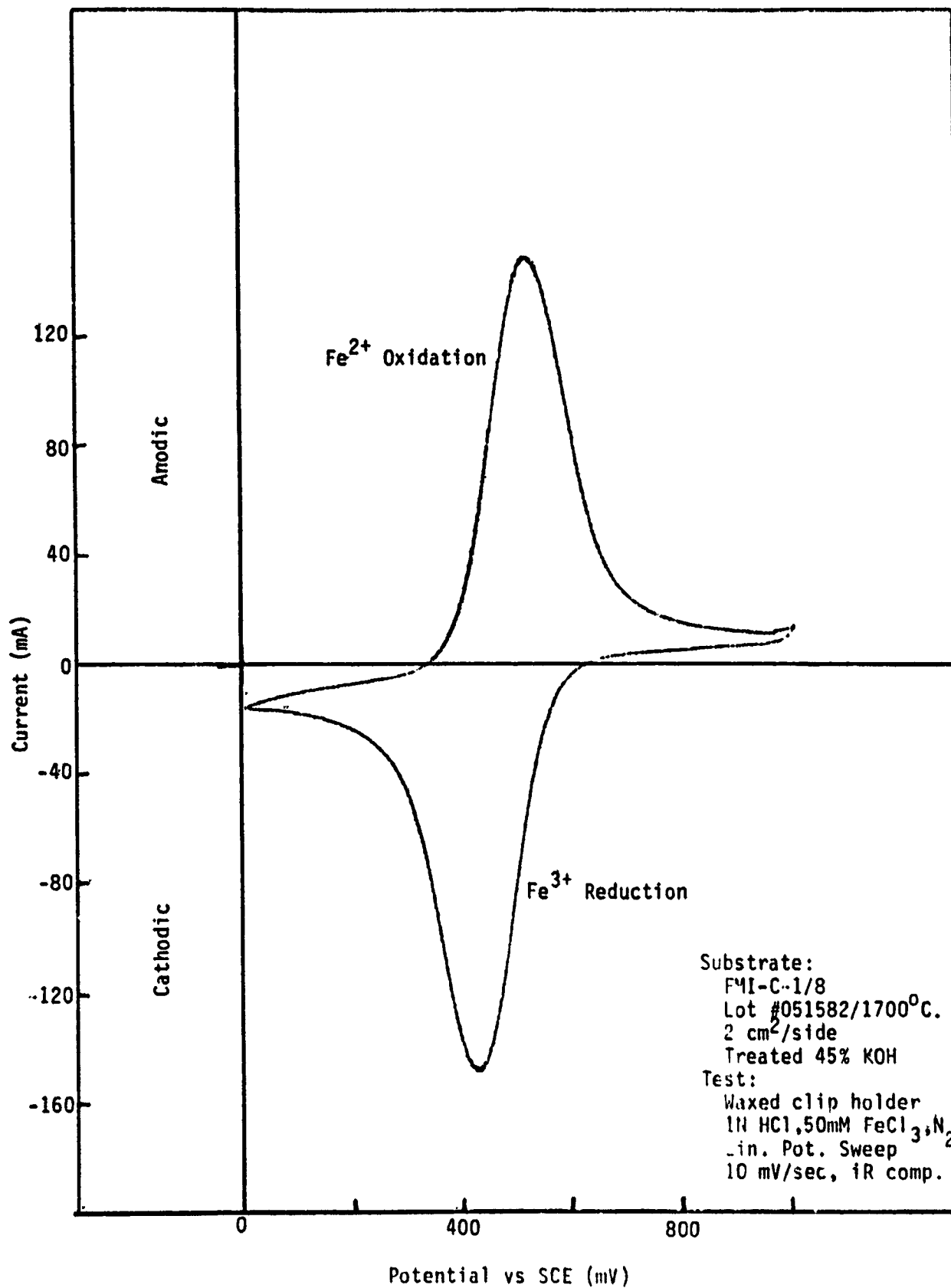


Figure 94.  $\text{Fe}^{3+}/\text{Fe}^{2+}$  Reaction at 65°C. in 0.050M  $\text{FeCl}_3$ .

## IX. PERFORMANCE IN SYSTEM HARDWARE

The final task in this program was testing of an optimized electrode in system hardware, a 1/3 square foot (300 cm<sup>2</sup>) flow cell. The carbon felt chosen was from the Phase II material processed at 1700°C (Lot 051482, Section I'). The samples were pretreated in 45% KOH and the negative electrode was catalyzed by the standard NASA procedure (8) with the added controls outlined in Section V-F. Specifically, the felt was rinsed to pH 7 before catalyzation and the catalyzation was done at 25°C. The membrane was an Ionics CDIL-AA5-LC.

A 14.5 cm<sup>2</sup> rebalance cell was used to measure hydrogen evolution. The iron electrode was the same KOH pretreated carbon felt as used in the redox cell. The negative electrode was a Giner, Inc., Type 2450 hydrogen/acid (Pt/C) electrode. In the first two trial runs, an Ionics CDIL-AA5-LC membrane was used; it was observed that there was iron crossover to the hydrogen electrode. At NASA-LeRC, using a similar rebalance cell configuration, it was also reported that platinum was migrating through the system resulting in aggravated hydrogen evolution at the chromium electrode on charge. For these reasons, for the 3rd and 4th runs Dupont Nafion membrane was used in the rebalance cell. With this membrane, no iron discoloration of the product water was ever observed, and the membrane remained clear.

The system was set up with 3 pumps, 2 flowmeters and 2 reservoirs of solution (one liter). The negative electrode solution was 0.9 M CrCl<sub>3</sub> and 10<sup>-4</sup> M PbCl<sub>2</sub> in 1 N HCl. The positive electrode solution was 1.1 M FeCl<sub>2</sub> in 1N HCl. The solution volume was 500 ml in each case (about 12 Ah). The solution was pumped through the cell at a rate of about 150 ml/minute on a full cycle. A third 2-channel bellows pump was used to pump the solutions

through the rebalance cell and a small OCV cell at about 30 ml/minute. All of the runs were done at ambient temperature.

For fast cycling, the pumps were turned off and the inlet ports to the redox flow cell were closed. The system was then set for automatic cycling at 3 amps on a 30 minute schedule. Charging in all cases was carried out at constant current until the cell voltage reached 1.3 V; the system then shifted automatically to voltage control. Discharge was carried out at constant current to a cell voltage cut-off of about 0.2 V.

A digital coulometer was used to record amp-hour capacities; the meter could also be switched to a higher sensitivity shunt across the rebalance cell to record hydrogen evolution rates.

The first full cycle for Run # 3 is shown in Figure 95. Appreciable hydrogen evolution was only observed in this first cycle; about 1.36 Ah was recorded with the rebalance cell. A polarization curve generally was recorded after about 50% discharge. The performance after 200 rapid cycles is shown in Figure 96. The cell was then discharged into reversal and subsequently charged and discharged to obtain a polarization curve. The three polarization curves are shown in Figure 97. Similar curves are shown for Run #4 in Figures 98 to 100. In all cases hydrogen evolution rates were almost undetectable.

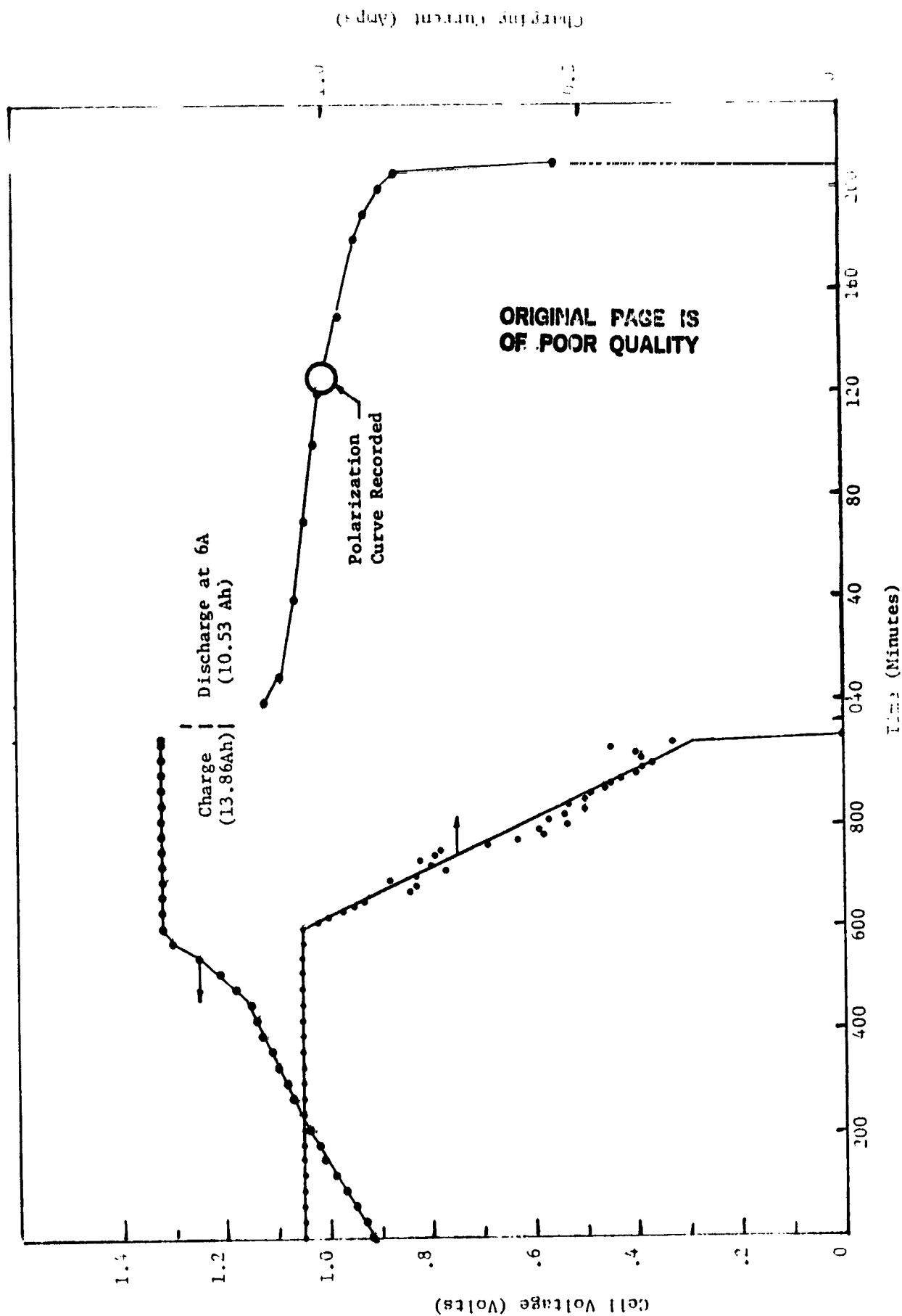


Figure 95. 1/3 Square Foot Redox Flow Cell Run #3; Initial Performance

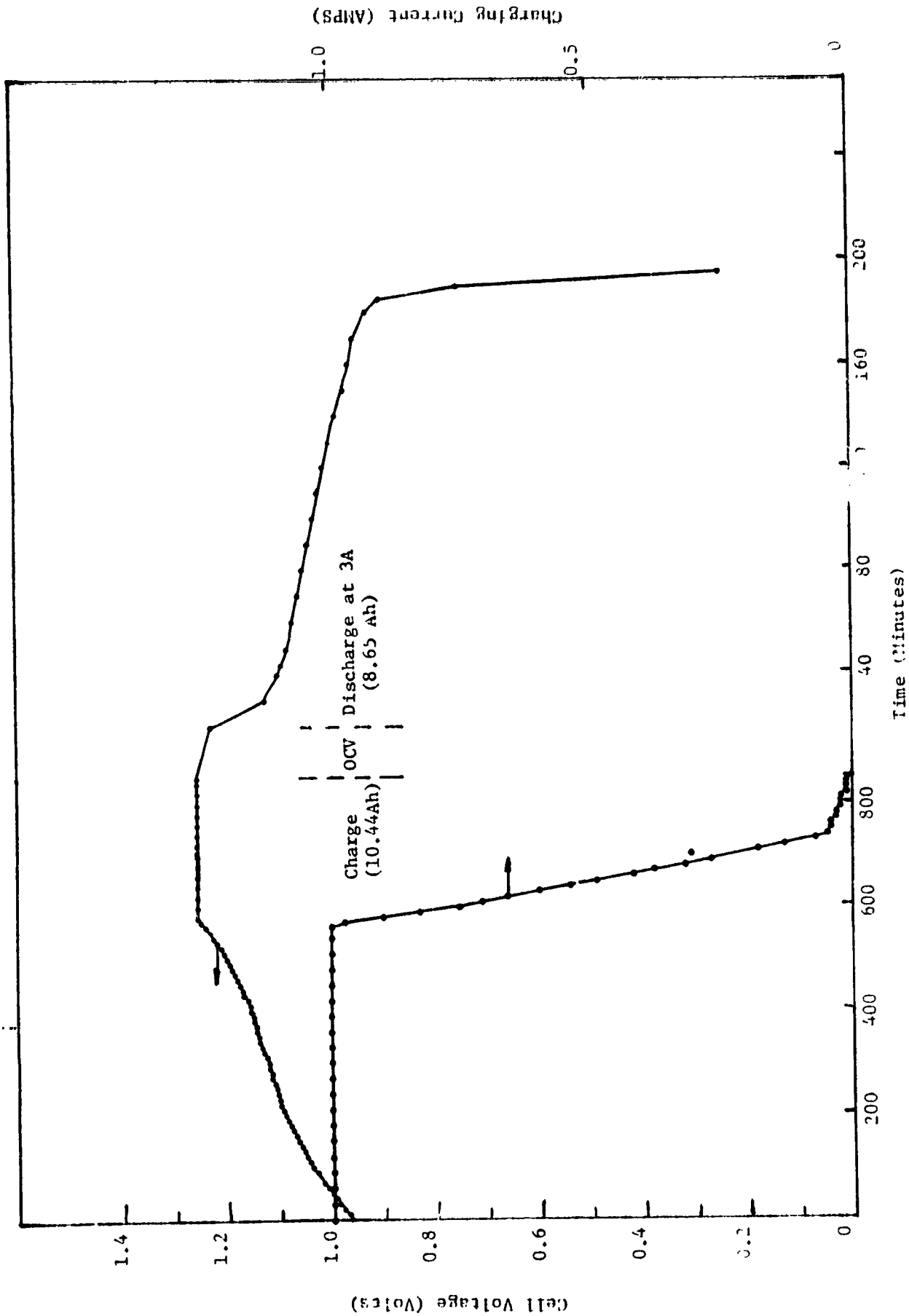


Figure 96. 1/3 Square Foot Redox Flow Cell Run #3; Performance After 200 Rapid Cycles

(Polarization Curves at 50% SOC.)  
 o 2nd Cycle, ● 201st cycle, + after cell reversal

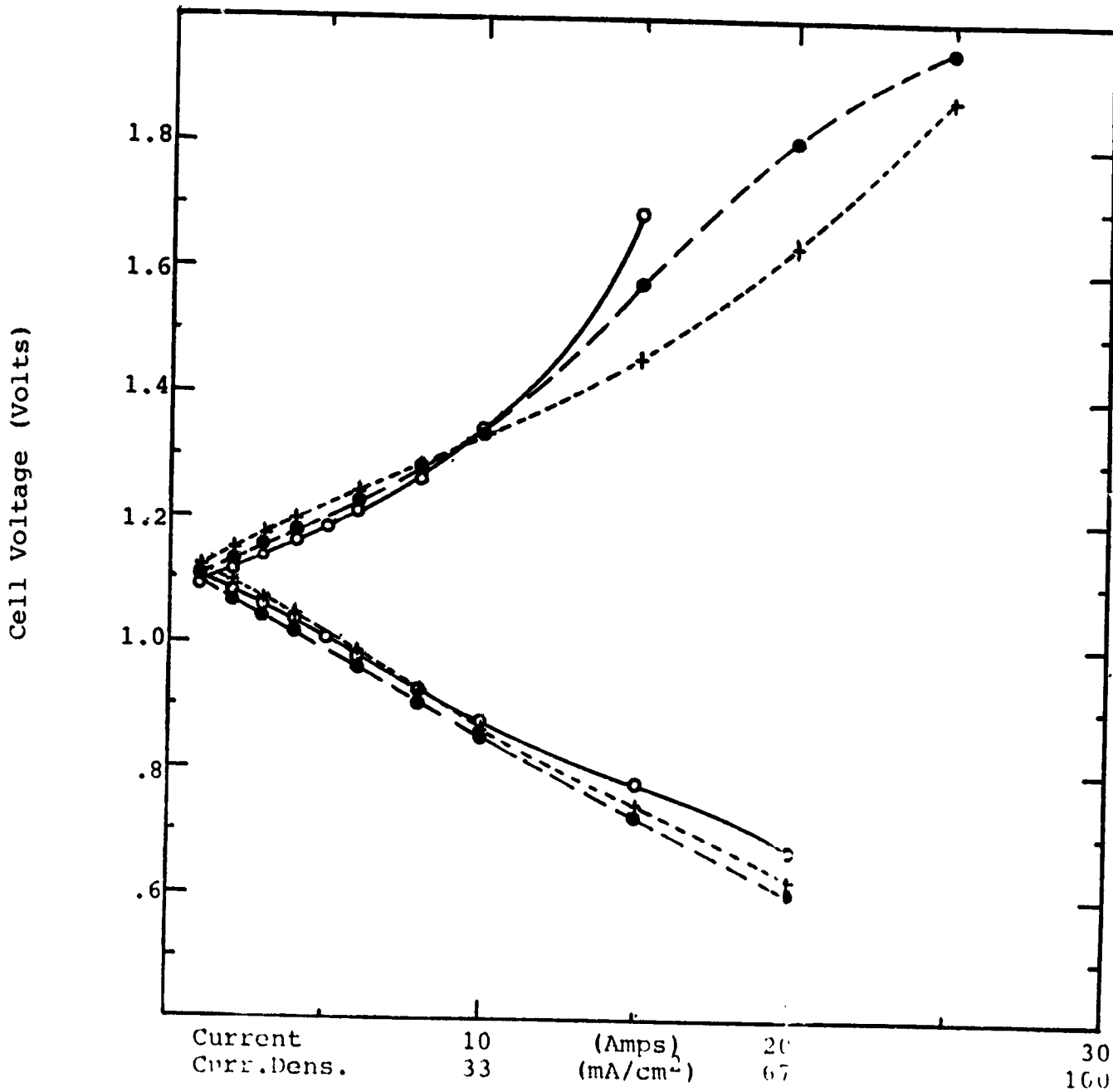


Figure 97. Fe/Cr Redox Flow Cell; 1/3 Sq. Ft.; Run 3

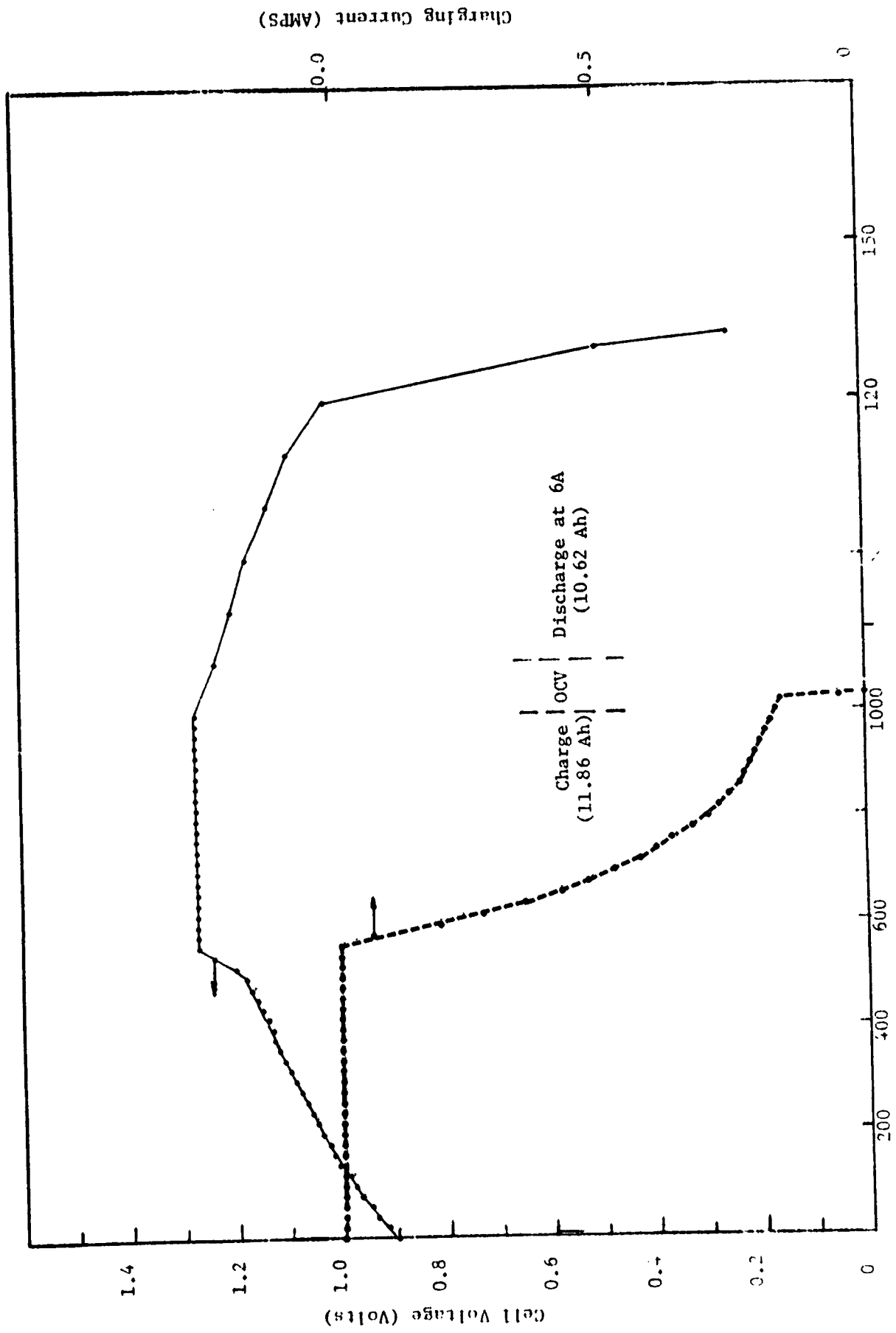


Figure 95. 1/3 Square Foot Redox Flow Cell Run #4; Initial performance.

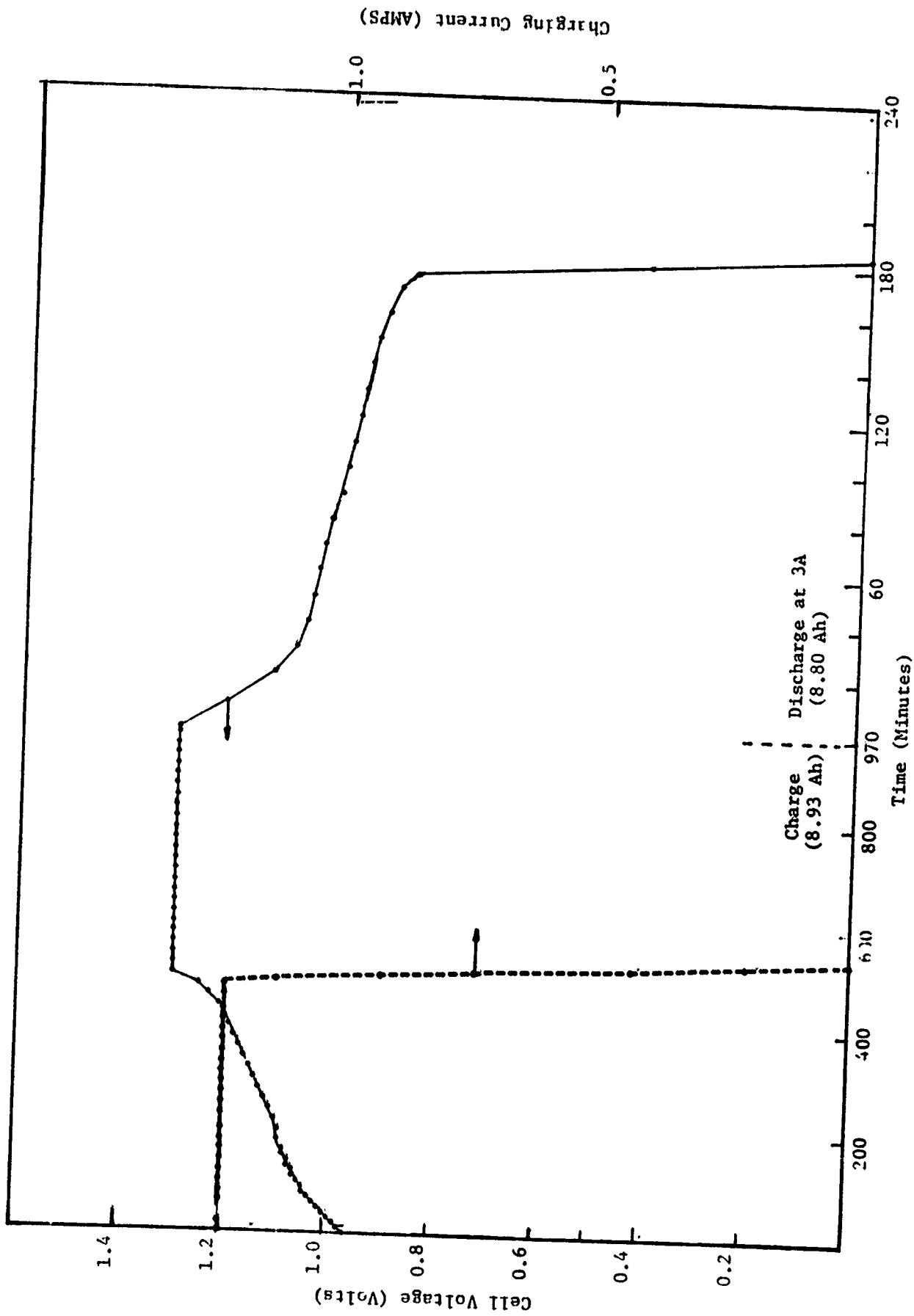


Figure 99. 1/3 Square Foot Redox Flow Cell Run #4; Performance after 123 Rapid Cycles.

(Polarization curves at 50% SOC)  
 o 2nd cycle, ● 223 cycle, + after cell reversal

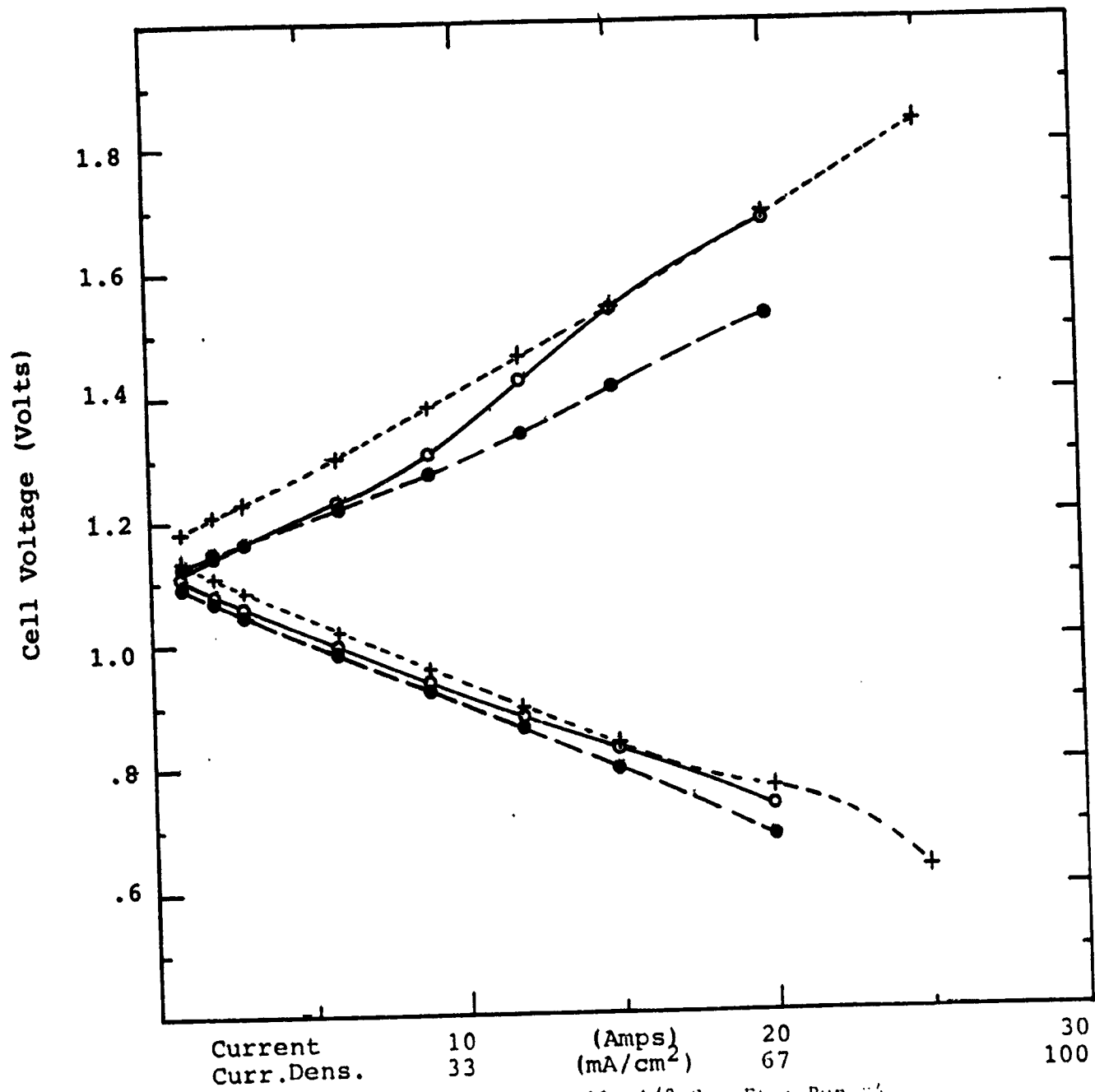


Figure 100. Fe/Cr Redox Flow Cell; 1/3 Sq. Ft.; Run #4

## X. REFERENCES

1. Gahn, R. F.; Johnson, J. A.; and Ling, J. S.: "Single Cell Testing of the NASA Fe/Cr Redox System at Elevated Temperatures". Presented at the Electrochemical Society Meeting (Detroit, Mich.), Oct. 17-22, 1982.
2. Hagedorn, N. H.; and Thaller, L. H.: "Design Flexibility of Redox Flow Systems". DOE/NASA/12726-16, NASA TM-82854, 1982.
3. Ling, J. S.; and Charleston, J.: "Advances in Membrane Technology for the NASA Redox Energy Storage System". DOE/NASA/12726-12, NASA TM-82701, 1980.
4. Thaller, L. H.: "Redox Flow Cell Energy Storage Systems," Dept. of Energy, Washington, D. C., DOE/NASA/1002-79/3, National Aeronautics and Space Admin., Washington, D. C., NASA TM-79143 (1979).
5. Thaller, L. H.: "Recent Advances in Redox Flow Cell Storage Systems," Dept. of Energy, Washington, D. C., DOE/NASA/1002-79-4, National Aeronautics and Space Admin., Washington, D. C., NASA TM-79186 (1979).
6. Reid, M. A.; and Thaller, L. H.: "Improvement and Scale-up of the NASA Redox Storage System," NASA Lewis Research Center; U. S. Dept. of Energy, DOE/NASA/12726-6, National Aeronautics and Space Admin., NASA TM-81632, 15th IECEC, Seattle, WA, (August, 1980).
7. Reid, M. A.; Gahn, R. F.; Ling, J. S.; and Charleston, J.: "Preparation and Characterization of Electrodes for the NASA Redox Storage System," NASA-Lewis Research Center; U. S. Dept. of Energy, DOE/NASA/12726-13; NASA TM-82724 (September, 1981).
8. Gahn, R. F.; Charleston, J.; Ling, J. S.; and Reid, M. A.: "Performance of Advanced Chromium Electrodes for the NASA Redox Energy Storage System," NASA-Lewis Research Center; U. S. Dept. of Energy, DOE/NASA/12726-15; NASA TM-82724 (November, 1981).
9. "NASA Redox Storage System Development Project", Calendar Year 1981; NASA-Lewis Research Center, DOE/NASA/12726-19, NASA TM-83087 (April, 1983).
10. "NASA Redox Storage System Development Project", Calendar Year 1982; NASA-Lewis Research Center, DOE/NASA/12726-23, NASA TM-83649 (October, 1983).
11. Gahn, R. F.; Hagedorn, N. H.; and Ling, J. S.: "Single Cell Performance Studies on the Fe/Cr Redox Energy Storage System Using Mixed Reactant Solutions at Elevated Temperature"; DOE/NASA/12726-21, NASA TM-83385; 18th IECEC, Orlando, Florida (August, 1983).

12. Hodgdon, R. B.; and Waite, W. A.: "Anion Permselective Membrane," DOE/NASA/0204-1, NASA CR-167872, Apr. 1982.
13. Giner, J.; Swette, L.; and Cahill, K.: "Screening of Redox Couples and Electrode Materials," Final Report, Giner, Inc., Waltham, MA; U. S. Energy Research and Development Admin. and NASA-Lewis Research Center Contract No. NAS3-19760, NASA CR-159738 (1980).
14. Giner, J.; and Cahill, K.: "Advanced Screening of Electrode Couples," Final Report, Giner, Inc., Waltham, MA; U. S. Dept. of Energy, DOE/NASA/0794-80/1; NASA-Lewis Research Center, NASA CR-159738 (1980).
15. Jalan, V.; Stark, H.; and Giner, J.: "Requirements for Optimization of Electrodes and Electrolyte for the Iron/Chromium Redox Flow Cell," Final Report, Giner, Inc., Waltham, MA; U. S. Dept. of Energy; DOE/NASA/0097 80/1, NASA-Lewis Research Center NASA CR-165218 (1981).
16. Jalan, V.; Morriveau, B.; Swette, L.: Optimization and Fabrication of Porous Carbon Electrodes for Iron/Chromium Redox Flow Cells. DOE/NASA/0198-1, NASA CR-167921, July 1982.
17. Jalan, V.; Cahill, K.; DeMuth, D.; and Giner, J.: "Electrocatalysts for the  $\text{Cr}^{3+}/\text{Cr}^{2+}$  Redox Couple," Extended Abstracts, 157th Spring Meeting of Electrochemical Society, St. Louis, Missouri, Vol. 80-1, Paper No. 351, pp. 874-6, (May 11-16, 1980).
18. Jalan, V.; and Stark, H.: "Gold-Lead Catalysts for  $\text{Cr}^{3+}/\text{Cr}^{2+}$  Redox Reactions," Extended Abstracts, Electrochemical Society Meeting, Hollywood, Florida, Vol. 80-2, Paper No. 150, pp.410-2, (October, 1980).
19. Giner, J.; and Cahill, K.: "Catalyst Surfaces for the Chromous/Chromic Redox Couple," U. S. Patent No. 4,192,910 (March 11, 1980) and No. 4,270,984, (June 2, 1981).
20. Jalan, V.; Reid, M.; and Charleston, J.: U. S. Patent filed, NASA Patent Application, Case No. 13653-1.
21. Frens, G.: "Controlled Nucleation for the Regulation of the Particle Size in Monodisperse Gold Suspensions," Nature Phys. Sci., 241, 20 (1973).
22. Angelici, R. J.: Synthesis and Techniques In Inorganic Chemistry, W. B. Saunders Co., (1969), page 61).
23. Basolo, F.; and Pearson, R. G.: Mechanisms of Inorganic Reactions, John Wiley and Sons, Inc. (1968), pages 152 and 198).

APPENDIX I. - CARBON FELT PROCESSING FACTORS (SUPPLEMENTAL DATA)

TABLE AI-I. PHASE I CHARACTERIZATION STUDY (UNSCOURED FELTS)

Summary of Electrochemical Features vs. Felt Processing Temperatures

Electrode Description	Fig. Ref.	1		2		3		4		5		6		7		8	
		$I_{cH^+}$ *Au/C (mA)	$I_{cH^+}$ Pb/Au (mA)	$I_{cH^+}$ Cr <sup>3+</sup> Pb/Au (mA)	$I_{cH^+}$ min. (mA)	$I_{cPb^{2+}}$ peak (mA)	$I_{aPb}$ peak (mA)	$I_c$ peak (mA)	$E_c$ (mV)	$I_c$ (mA)	$E_c$ (mV)	$I_2$ (mA)	$E_a$ (mV)				
FMI-C-1/8 Lot 011882	3	620	30.5	38.3	17.9	23.6	26.6	74.6	r635	85.8	-555						
	4	570	25.0	29.0	15.7	15.0	27.3	50.3	-660	51.5	-540						
	5	240	11.0	19.3	13.8	14.4	25.8	43.0	-660	44.8	-540						
	6	210	7.5	18.0	12.7	13.8	25.8	45.6	-650	47.8	-540						
	7	500	2.9	8.2	7.9	12.0	21.6	25.9	-645	27.1	-540						
	8	470	3.0	8.2	8.0	9.4	17.0	25.8	-695	19.0	-600						

2 cm<sup>2</sup>/side  
Pretreated 1N KOH

Catalyst:  
12 $\mu$ g Au/cm<sup>2</sup>  
Aq./MeOH  
Double Imm.-I

Test:  
Waxed clip holder  
1N HCl, N<sub>2</sub>, R.T.  
Lin. pot. sweep  
\*10 mV/sec, iR comp. +  
100 mV/sec. for  $I_{cH^+}$  Au/C

ORIGINAL PAGE IS  
OF POOR QUALITY

TABLE AI-II. PHASE I CHARACTERIZATION STUDY (SCoured FELTS)

Summary of Electrochemical Features vs. Felt Processing Temperatures

Electrode Description	Fig. Ref.	$I_{cH^+}$ at -950mV		$I_{cH^+Cr^{3+}}$ min. (mA)	$I_{cPb^{2+}}$ peak (mA)	$I_{aPb}$ peak (mA)	$I_{cCr^{3+}}$ Cath. Peak (mA)	$I_{aCr^{2+}}$ Anod. Peak (mA)
		Au/C (mA)	Pb/Au (mA)					
1250°	1	520	27	30	34	30	92	92
1350°	2	670	130	28	48	47	106	117
1500°	3	350	25	28	18	35	60	66
1650°	4	940	13	13	14	26	51	49
1800°	5	465	9	32	23	41	163	172
2300°	6	585	14	16	16	28	82	87

FMI-C-1/8 Lot 021182, Scoured

TABLE AI-III. NASA-I VERSUS NASA-II CATALYZATION METHODS  
 Summary of Electrochemical Features vs. Felt Processing Temperatures

Electrode Description	Fig. Ref.	1 I <sub>C</sub> <sup>H</sup> at -950 mV		2	3	4	5	6	7	8
		Au/C (mA)	Pb/Au (mA)	Pb <sup>3+</sup> /Au (mA)	I <sub>C</sub> <sup>H</sup> Cr <sup>3+</sup> (mA)	peak (mA)	min. (mA)	peak (mA)	I <sub>C</sub> (mA)	I <sub>a</sub> (mA)
FMI-C-1/B Lot 011882										
NASA-I										
1250 <sup>o</sup>	1	670	12	52	19	23	28	82	93	
1350 <sup>o</sup>	2	300	5	26	15	18	31	74	81	
1500 <sup>o</sup>	3	300	3	42	17	13	26	80	89	
1650 <sup>o</sup>	4	380	5	22	14	14	26	75	78	
1800 <sup>o</sup>	5	260	2	12	9	10	21	36	34	
2300 <sup>o</sup>	6	415	2	11	9	12	24	57	63	
FMI-C-1/B Lot 011882										
NASA-II										
1250 <sup>o</sup>	7	580	134	425	90	44	43	113	104	
1350 <sup>o</sup>	8	680	24	100	30	31	46	119	132	
1500 <sup>o</sup>	9	640	26	200	40	43	51	163	178	
1650 <sup>o</sup>	10	720	40	195	33	33	45	168	182	
1800 <sup>o</sup>	11	960	18	220	38	27	35	137	150	
2300 <sup>o</sup>	12	780	11	33	16	27	36	87	92	

ORIGINAL PAGE IS OF POOR QUALITY

TABLE AI-IV. PHASE II CHARACTERIZATION STUDY

Summary of Selected Current-Data Points

Electrode Description	Fig. Ref.	1		2		3		4		5		6		7		8		
		$I_{cH}^+$ (mA)	Au/C (mA)	Pb/Au (mA)	Pb/Au (mA)	$I_{cH}^+$ (mA)	Cr <sup>3+</sup> (mA)											
FMI-C-1/8 Lot 051882																		
Phase-II, Characterization																		
1550 <sup>o</sup>	10	530	3	20	14													
1600 <sup>o</sup>	11	640	2	40	20													
1650 <sup>o</sup>	12	40	2	16	12													
1700 <sup>o</sup>	13	160	2	13	11													
1750 <sup>o</sup>	14	620	3	30	20													

ORIGINAL PAGE IS  
OF POOR QUALITY

ORIGINAL PAGE IS  
OF POOR QUALITY

APPENDIX II. - EFFECTS OF PROCESS VARIATIONS ON GOLD CATALYZATION  
(SUPPLEMENTAL DATA)

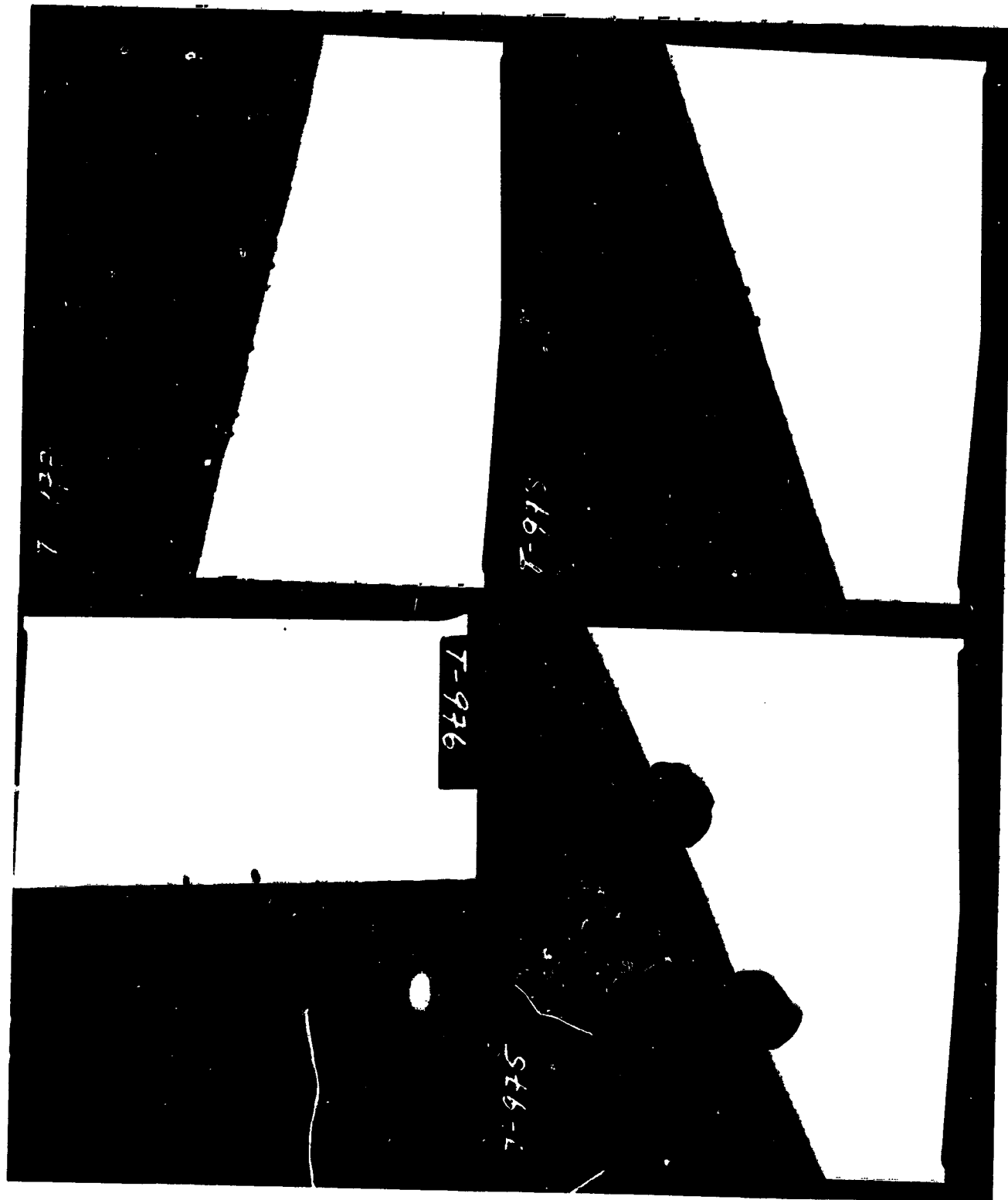


Figure AII-1 Transmission Electron Micrograph of 1500°C Felt Sample  
Catalyzed by Double Immersion Method, 12.5 $\mu$ g Au/cm<sup>2</sup>.  
(90,000 X magnification; 1 mm = 11 nm).

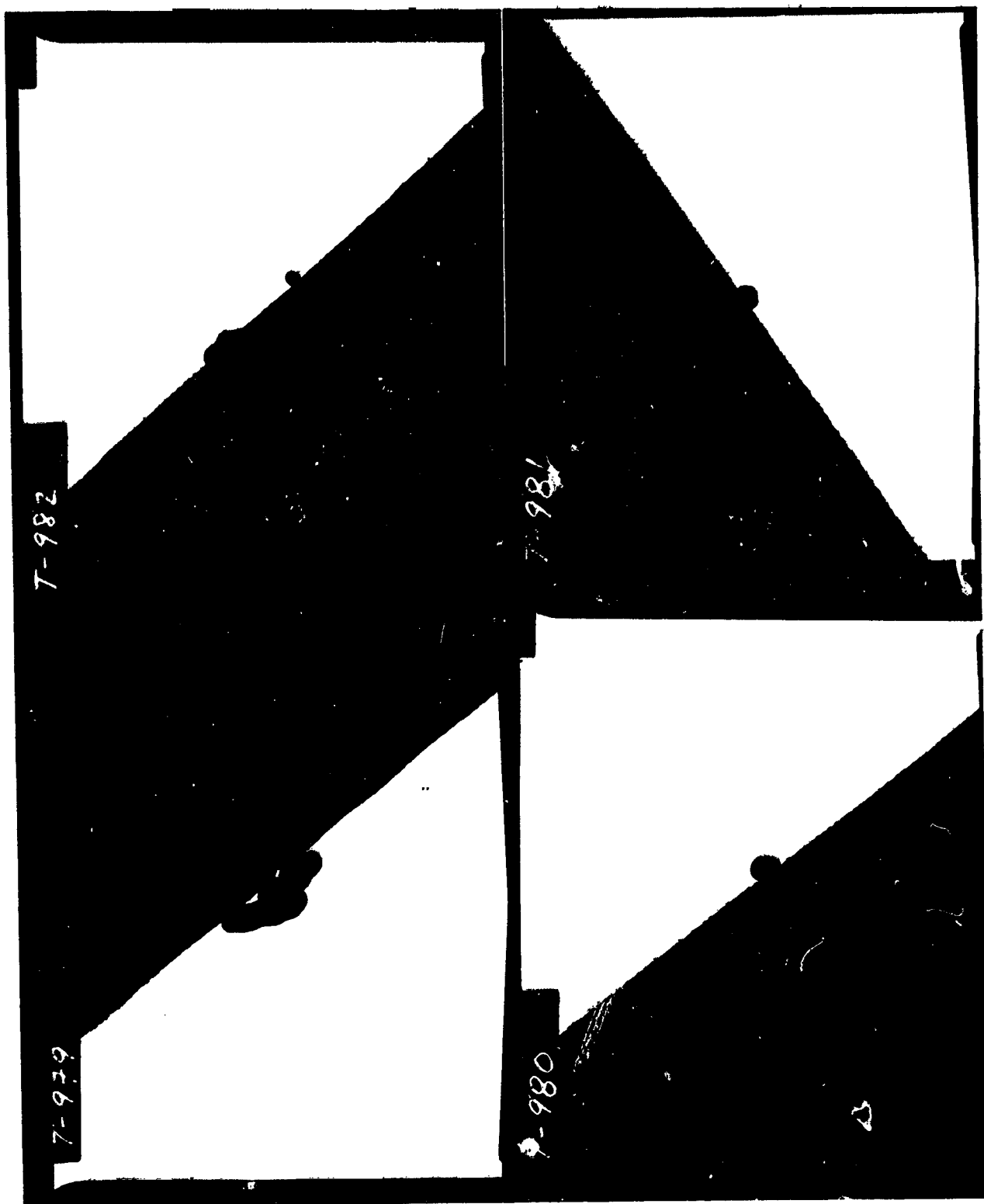


Figure AII-2 TEM Photograph of 1500<sup>o</sup>C Felt Sample Catalyzed by NASA-I Method, 12.5 $\mu$ g Au/cm<sup>2</sup>. (90,000 X Magnification; 1 mm = 11 nm.)

ORIGINAL PAGE IS  
OF POOR QUALITY

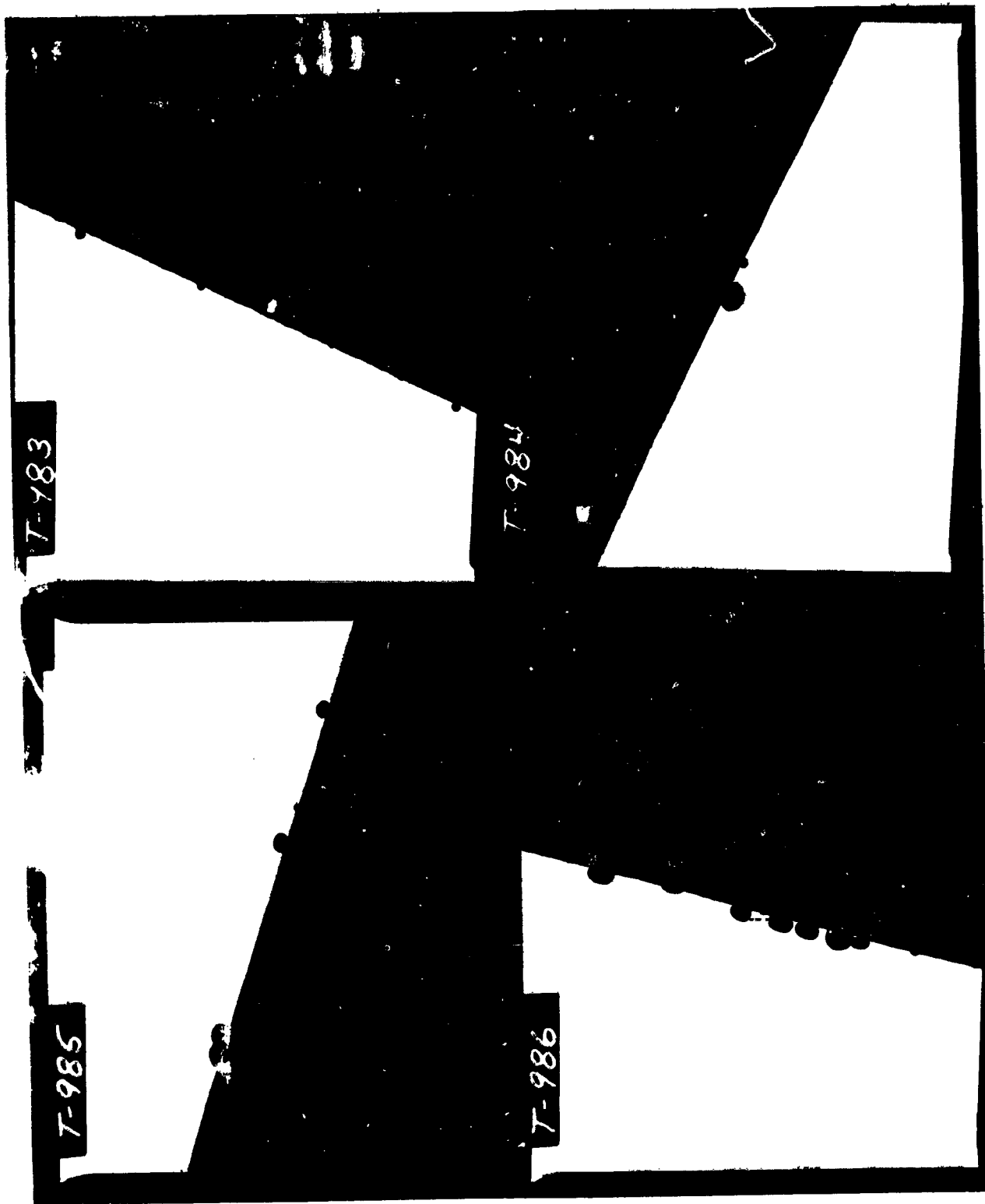


Figure AII-3 TEM Photograph of 1500°C Felt Sample Catalyzed by NASA-II  
Method; 12.5 $\mu$ g Au/cm<sup>2</sup>. (90,000 X Magnification; 1 mm = 11 nm.)

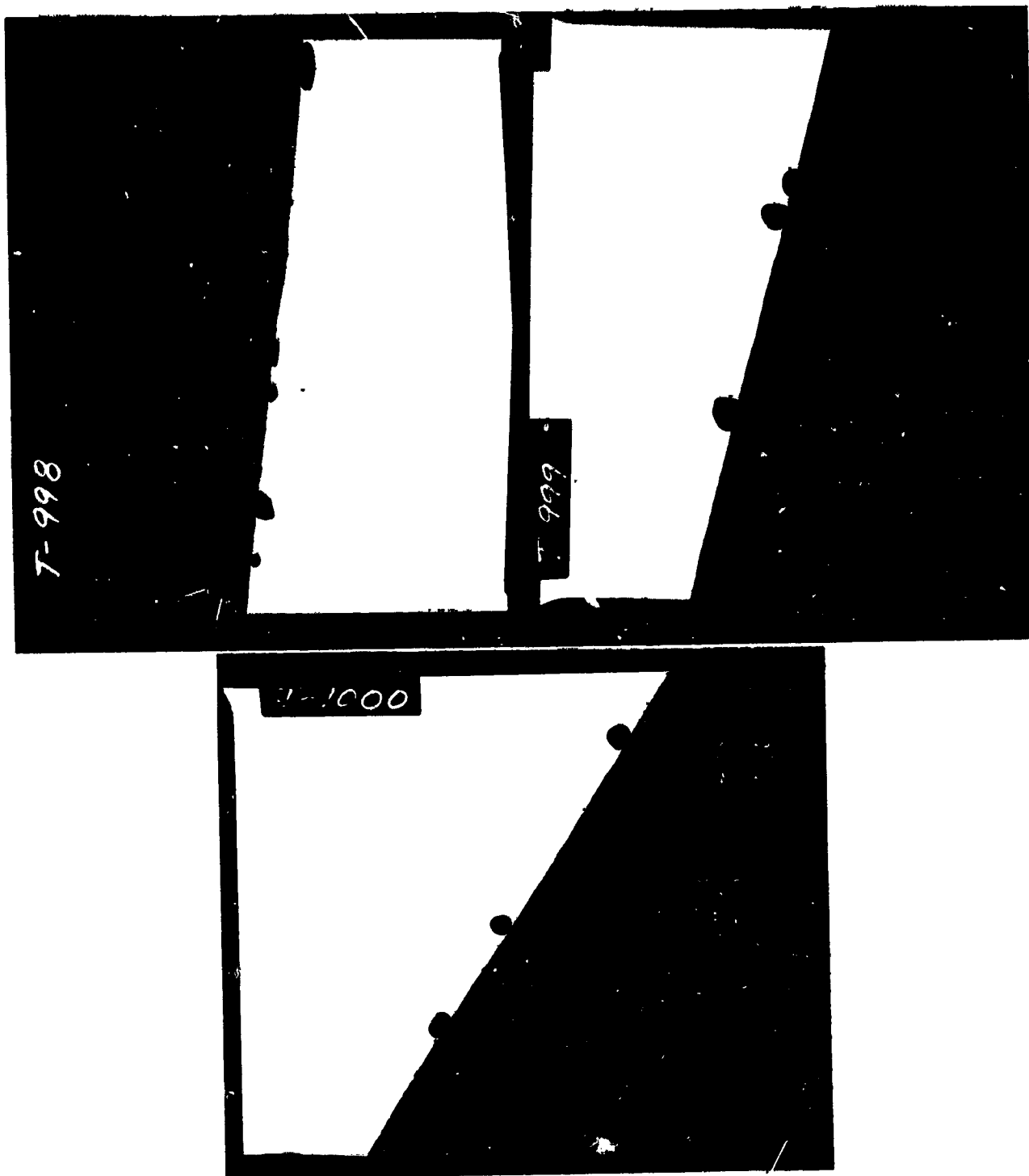


Figure AII-4 TEM Photograph of 1800°C Felt Sample Catalyzed by Double Immersion-Method, 12.5 $\mu$ g Au/cm<sup>2</sup>. (90,000 X Magnification; 1 mm = 11 nm.)

ORIGINAL PAGE IS  
OF POOR QUALITY

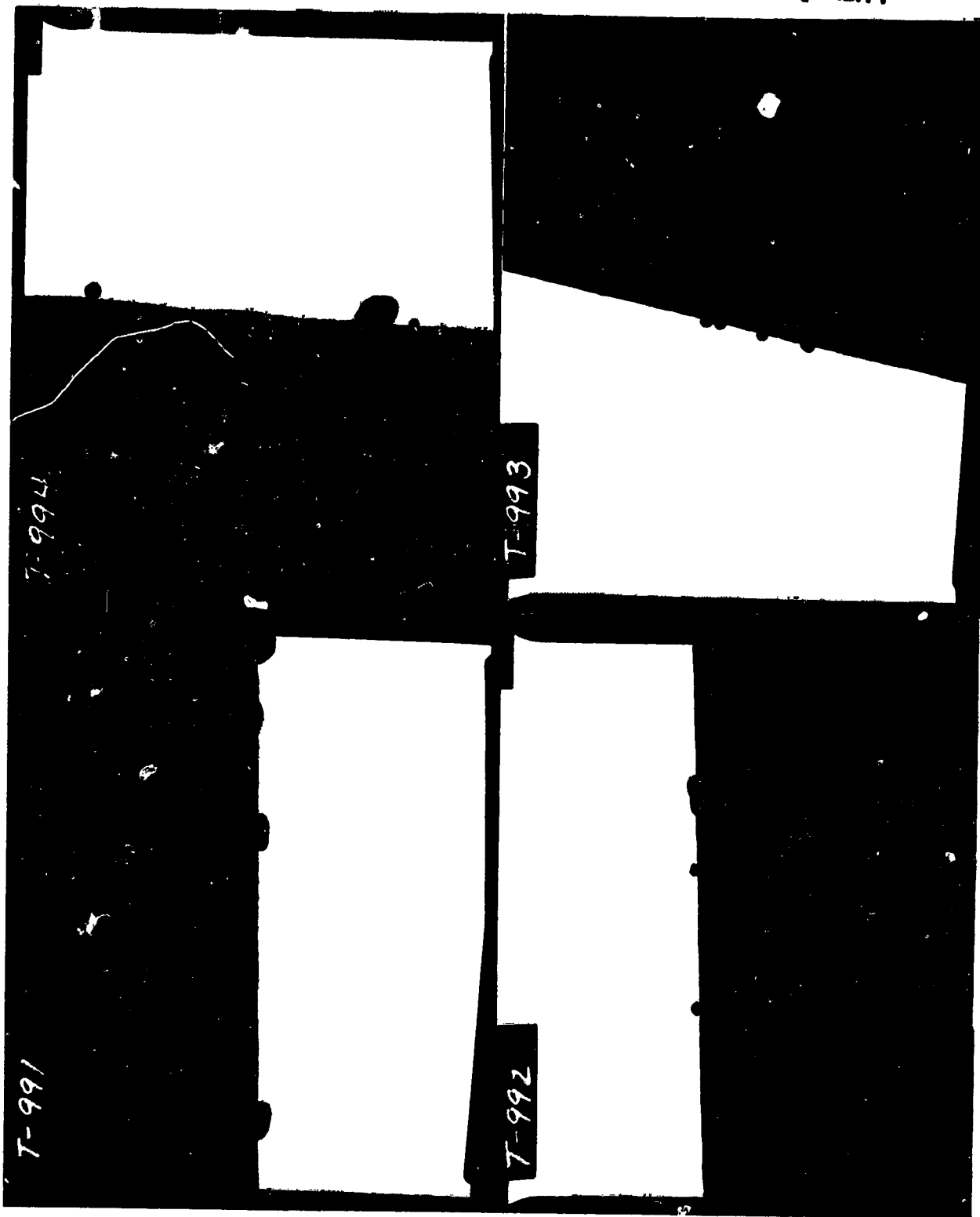


Figure AII-5 TEM Photograph of 1800°C Felt Sample Catalyzed by NASA-I  
Method, 12.5 $\mu$ g Au/cm<sup>2</sup>. (90,000 X Magnification; 1 mm = 11 nm.)

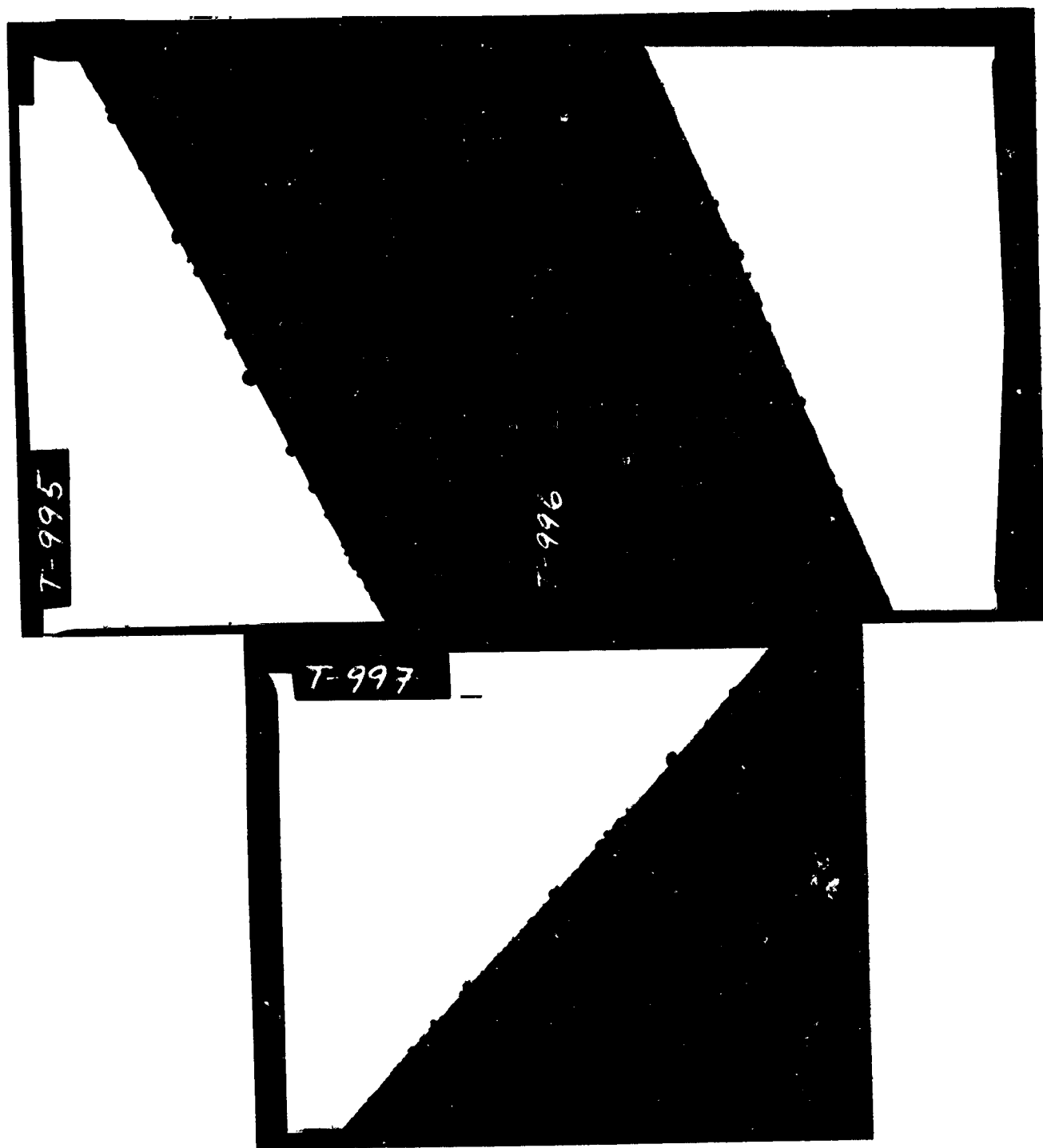


Figure AII-6 TEM Photograph of 1800°C Felt Sample Catalyzed by NASA-II Method, 12.5 $\mu$ g Au/cm<sup>2</sup>. (90,000 X Magnification; 1 mm = 11 nm.)

ORIGINAL PAGE IS  
OF POOR QUALITY

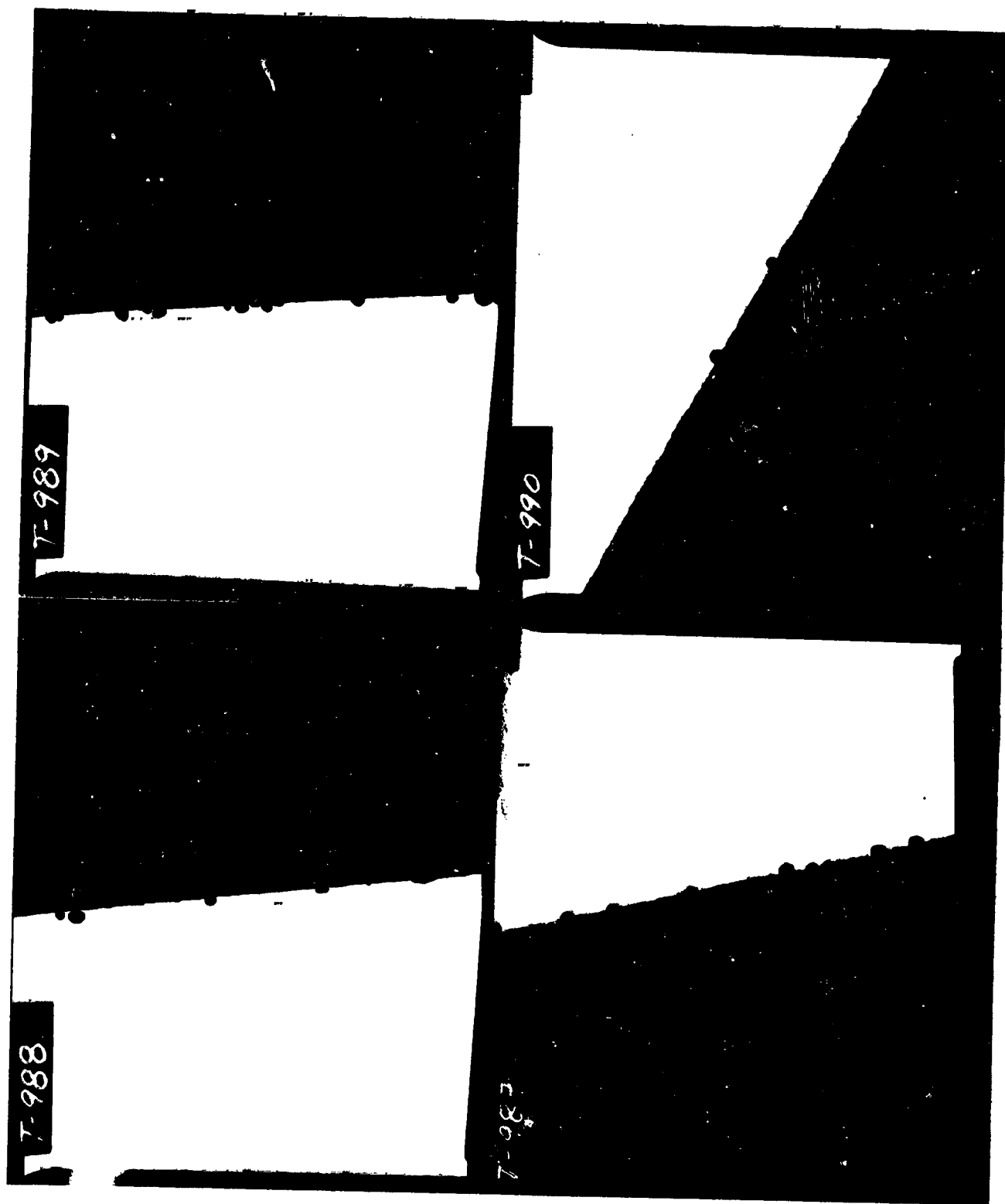


Figure AII-7 TEM Photograph of 2300°C Felt Sample Catalyzed by NASA-I Method, 12.5 $\mu$ g Au/cm<sup>2</sup>. (90,000 X Magnification; 1 mm = 11 nm.)

APPENDIX III. - CONTROLLED VARIATIONS OF CATALYZING PROCEDURE  
(SUPPLEMENTAL DATA)

TABLE A.III-I. CATALYZATION PARAMETER VARIATION: SUMMARY OF SELECTED CURRENT-DATA POINTS

ELECTRODE DESCRIPTION	Fig. Ref.	1. $I_{cH^+}$ at - 950 mV		3. $I_{cH^+}$ Cr <sup>3+</sup>	4. $I_{cH^+}$ Cr <sup>3+</sup> min.	5. $I_{cPb^{2+}}$		6. $I_{aPb}$		7. Cr <sup>3+</sup> Cath.		8. Cr <sup>2+</sup> Anod.
		Au/C (mA)	Pb/Au (mA)			Pb/Au (mA)	Au (mA)	Peak (mA)	Peak (mA)	I <sub>c</sub> (mA)	I <sub>a</sub> (mA)	
FMI-C-1/8 Lot 011882, 1650° C												
EVP-16	1	545	2	24	17		19	.31		100		107
DVP-16	2	76	1	21	15		20	32		85		91
EVA-5B	3	480	1	15	13		14	29		70		80
EVA-30B	4	350	6	35	21		23	38		110		123
EVA-180B	5	440	2	28	16		16	30		122		132
EVA-180B(R)	6	390	9	28	20		26	40		112		120
EVA-180	7	595	22	52	31		37	53		137		160
EVA-180(R)	8	450	19	70	53		38	55		106		141

ORIGINAL PAGE IS OF POOR QUALITY

ORIGINAL PAGE IS  
OF POOR QUALITY

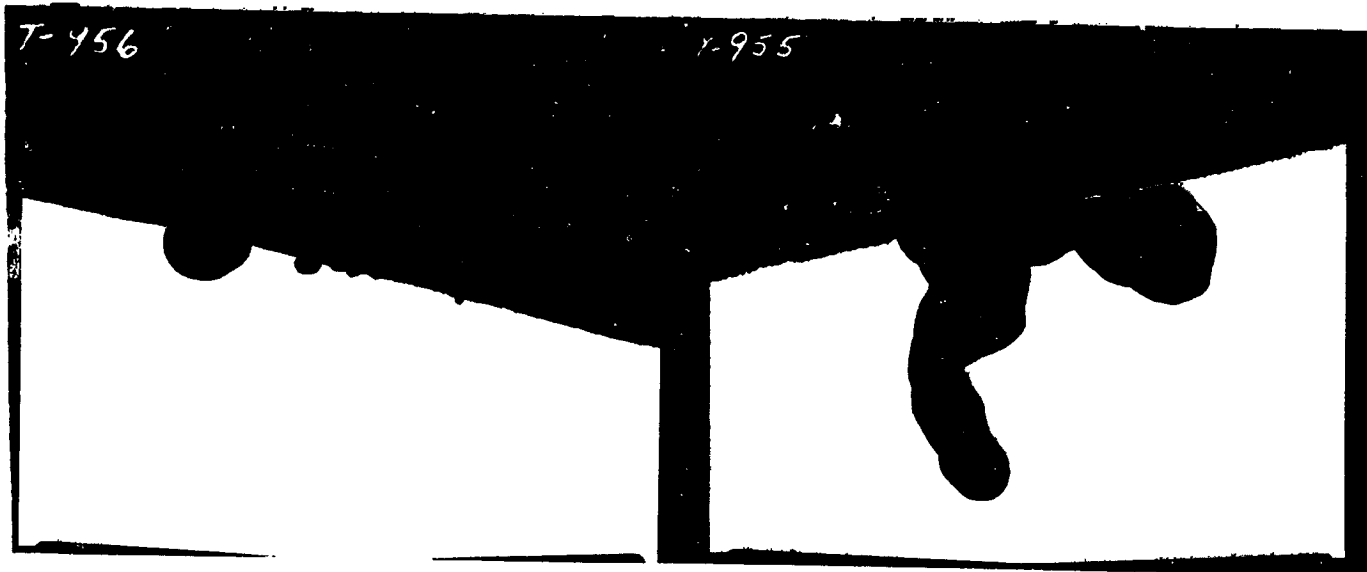


Figure AIII-1 Sample EVP-16; "Exact Volume", 16 Hours "Closed" Exposure.

**Substrate:**

Carbon felt Lot 011882-1650°C; Pretreatment 1 N KOH.

**Catalyzation:**

Target loading of  $12.5 \mu\text{gAu}/\text{cm}^2$  using aqueous/methanol solution.

Gold chloride solution used in exact volume for felt saturation.

-49cm<sup>2</sup> felt sample immersed in 16 ml of solution

-felt rotated in solution after 2 minutes.

-sample transferred directly to plastic bag after 5 minutes.

-removed from plastic bag after 16 hours, air dried for 1 hour.

-oven dried at 110°C for 2 hours.

-baked at 270° for 2 hours.

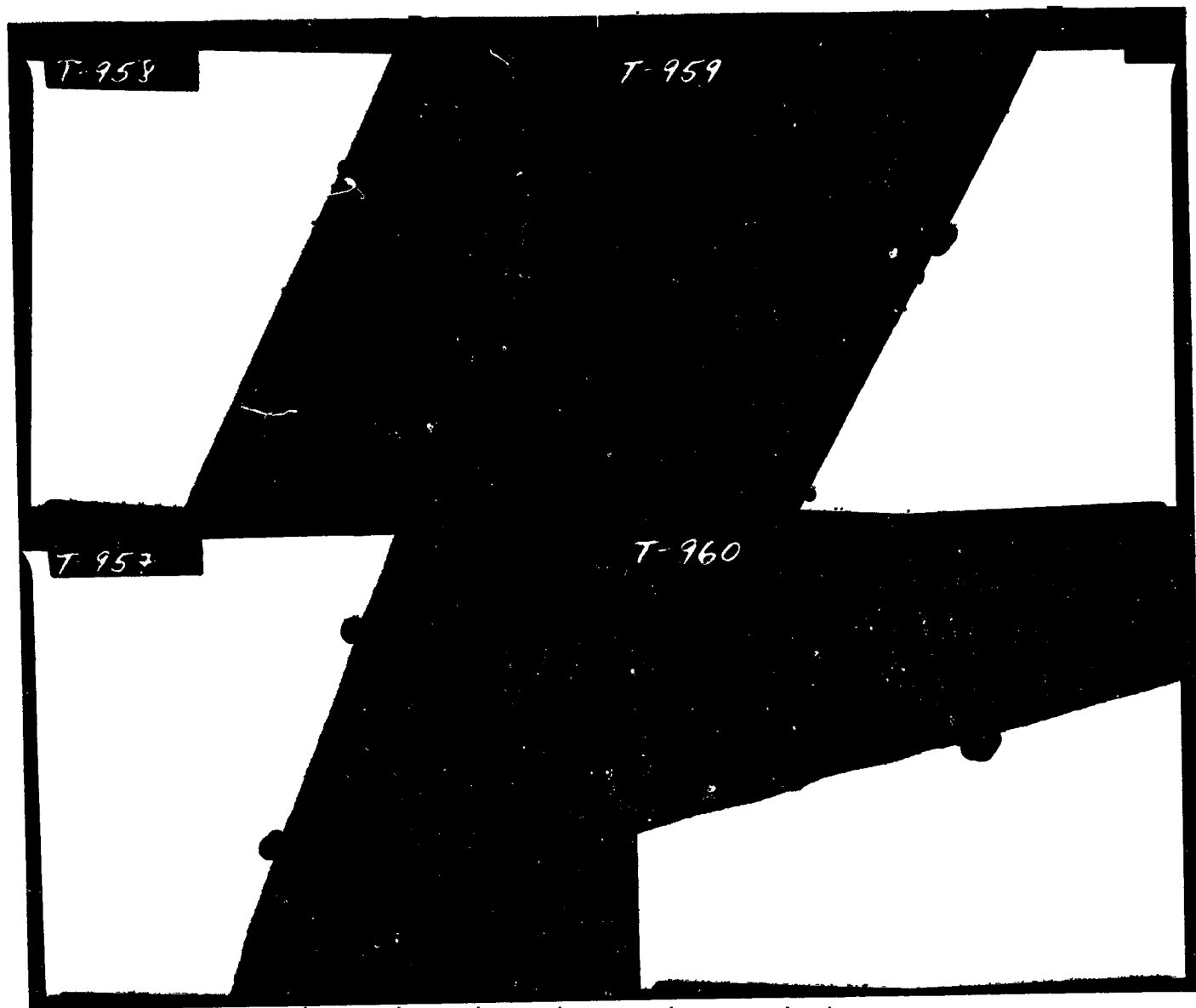


Figure AIII-2 Sample DVP-16; "Double Volume", 16 Hours "Closed" Exposure

Substrate:

Carbon felt Lot 011882-1650<sup>0</sup>G; Pretreatment 1 N KOH

Catalyzation:

- Target loading of  $12.5 \mu\text{gAu}/\text{cm}^2$  using aqueous/methanol solution.  
Gold chloride solution used in double volume for felt saturation.
- 49  $\text{cm}^2$  felt sample immersed in 32 ml of solution.
  - felt rotated in solution after 2 minutes.
  - sample transferred directly to plastic bag after 5 minutes.
  - removed from plastic bag after 16 hours, air dried for 1 hour.
  - oven dried at  $110^\circ\text{C}$  for 2 hours.
  - baked at  $270^\circ$  for 2 hours.

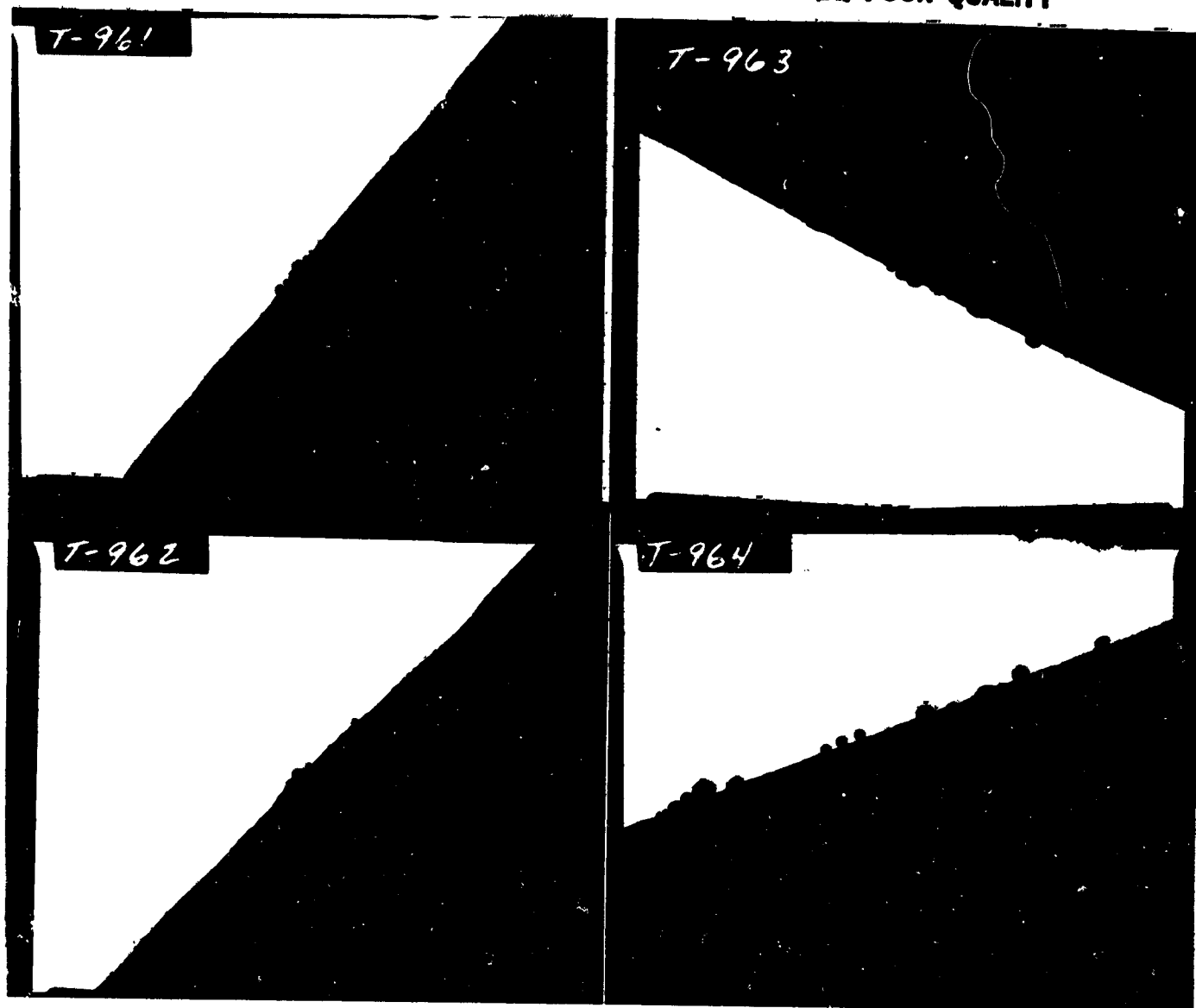


Figure AIII-3 Sample EVA-5B; "Exact Volume", 5 Minutes "Open" Exposure.

**Substrate:**

Carbon felt Lot 011882-1650<sup>0</sup>C; Pretreatment 1 N KOH.

**Catalyzation:**

Target loading of 12.5 $\mu$ gAu/cm<sup>2</sup> using aqueous/methanol solution.

Gold chloride solution used in exact volume for felt saturation.

-49cm<sup>2</sup> felt sample immersed in 16 ml of solution.

-felt rotated in solution after 2 minutes.

-sample transferred directly to 110<sup>0</sup>C oven after 5 minutes

-oven dried at 110<sup>0</sup>C for 2 hours.

-baked at 270<sup>0</sup> for 2 hours.

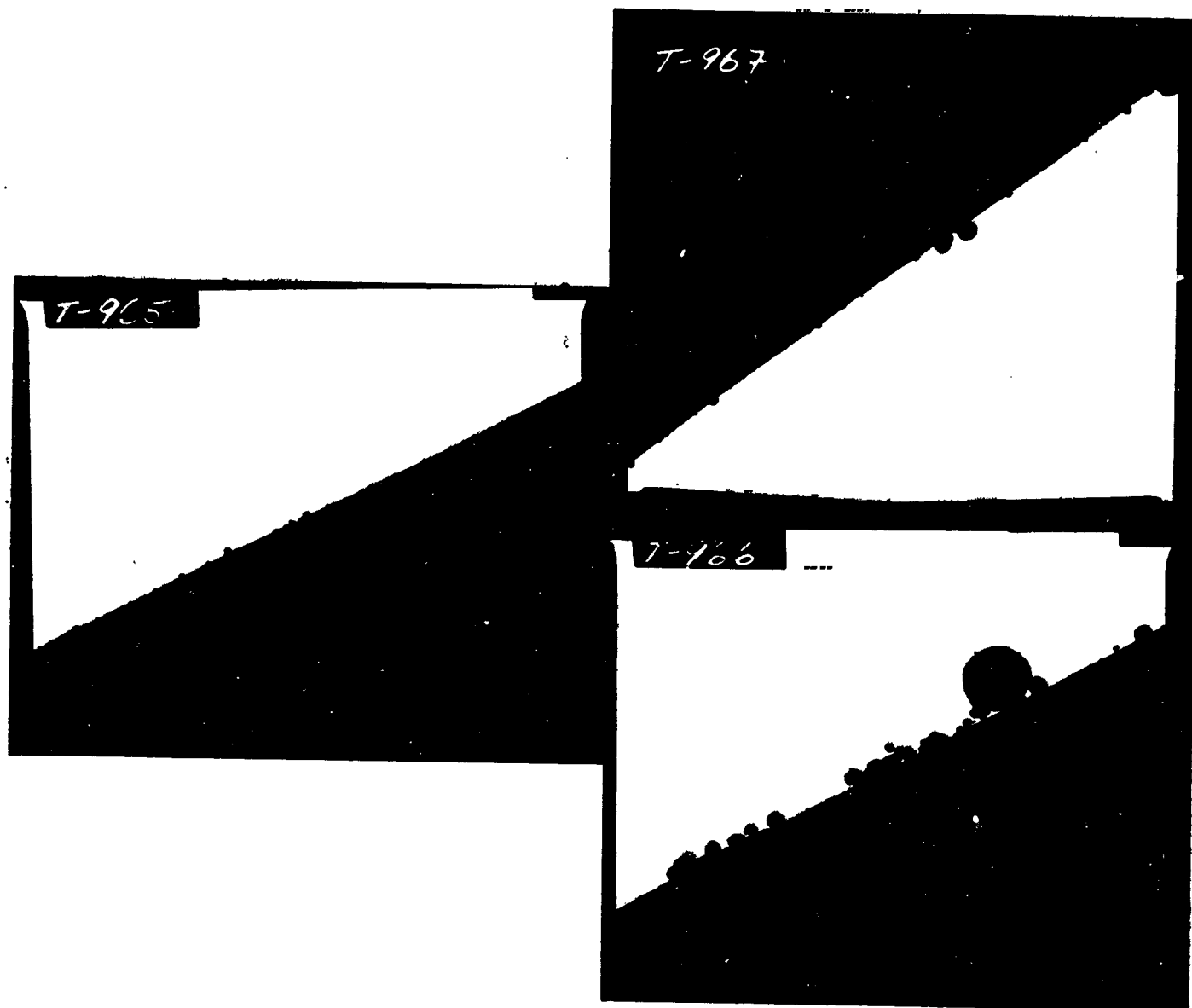


Figure AIII-4 Sample EVA 30B; "Exact Volume", 30 Minutes "Open" Exposure

Substrate:

Carbon felt Lot 011882-1650°C; Pretreatment 1 N KOH.

Catalyzation:

Target loading of  $12.5\mu\text{gAu}/\text{cm}^2$  using aqueous/methanol solution.

Gold chloride solution used in exact volume for felt saturation.

-49cm<sup>2</sup> felt sample immersed in 16 ml of solution.

-felt rotated in solution after 2 minutes.

-sample transferred directly to 110°C oven after 30 minutes

-oven dried at 110°C for 2 hours.

-baked at 270° for 2 hours.

ORIGINAL PAGE IS  
OF POOR QUALITY

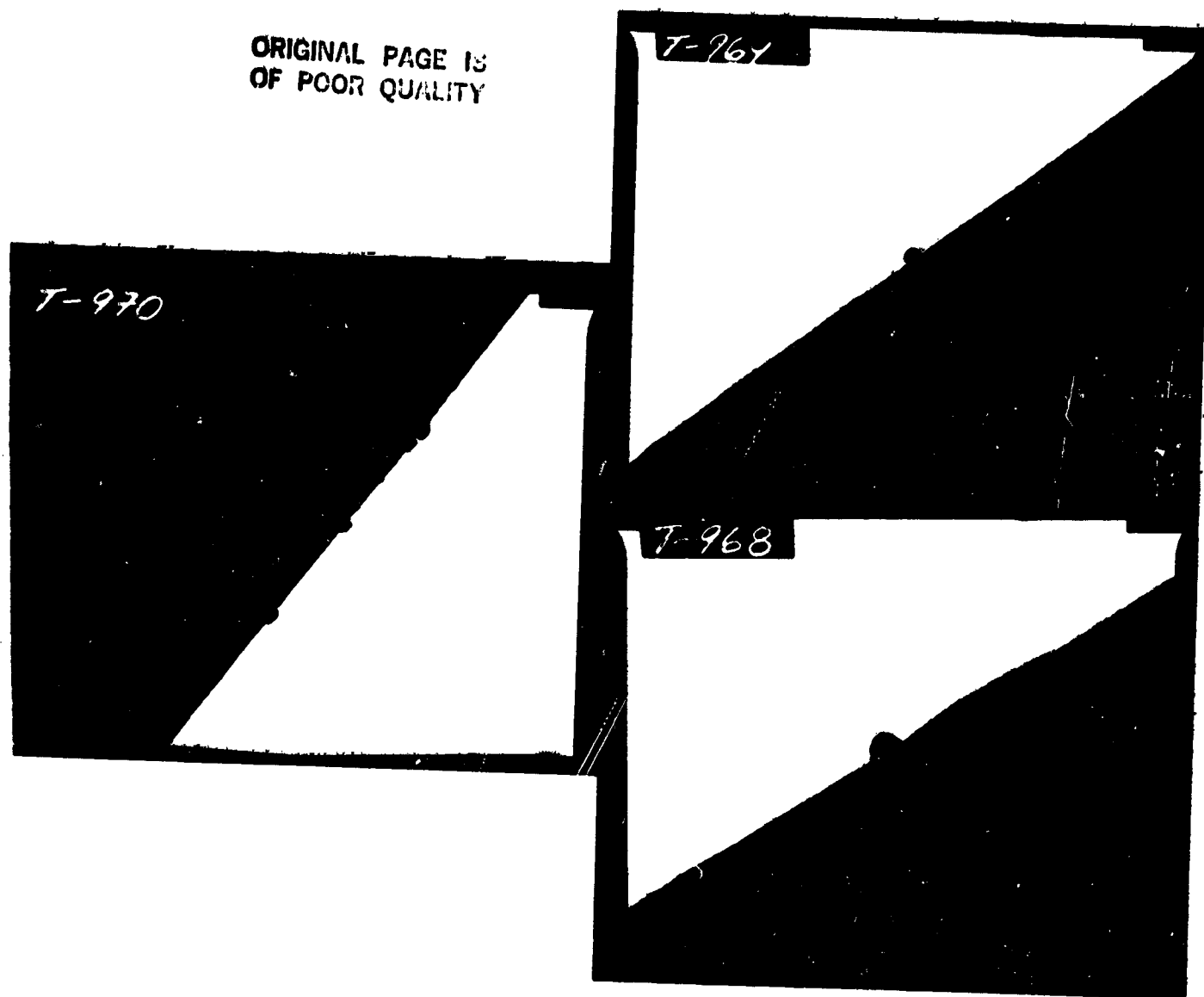


Figure AIII-5 Sample EVA-180P; "Exact Volume" 180 Minutes "Open" Exposure

Substrate:

Carbon felt Lot 011882-1650°C; Pretreatment 1 N KOH.

Catalyzation:

Target loading of 12.5 $\mu$ gAu/cm<sup>2</sup> using aqueous methanol solution.  
Gold chloride solution used in exact volume for felt saturation.

-4 cm<sup>2</sup> felt sample immersed in 16 ml of solution.

-felt rotated in solution after 2 minutes.

-sample transferred directly to 110° oven after 180 minutes.

-oven dried at 110°C for 2 hours.

-heated at 270° for 2 hours.

ORIGINAL PAGE IS  
OF POOR QUALITY

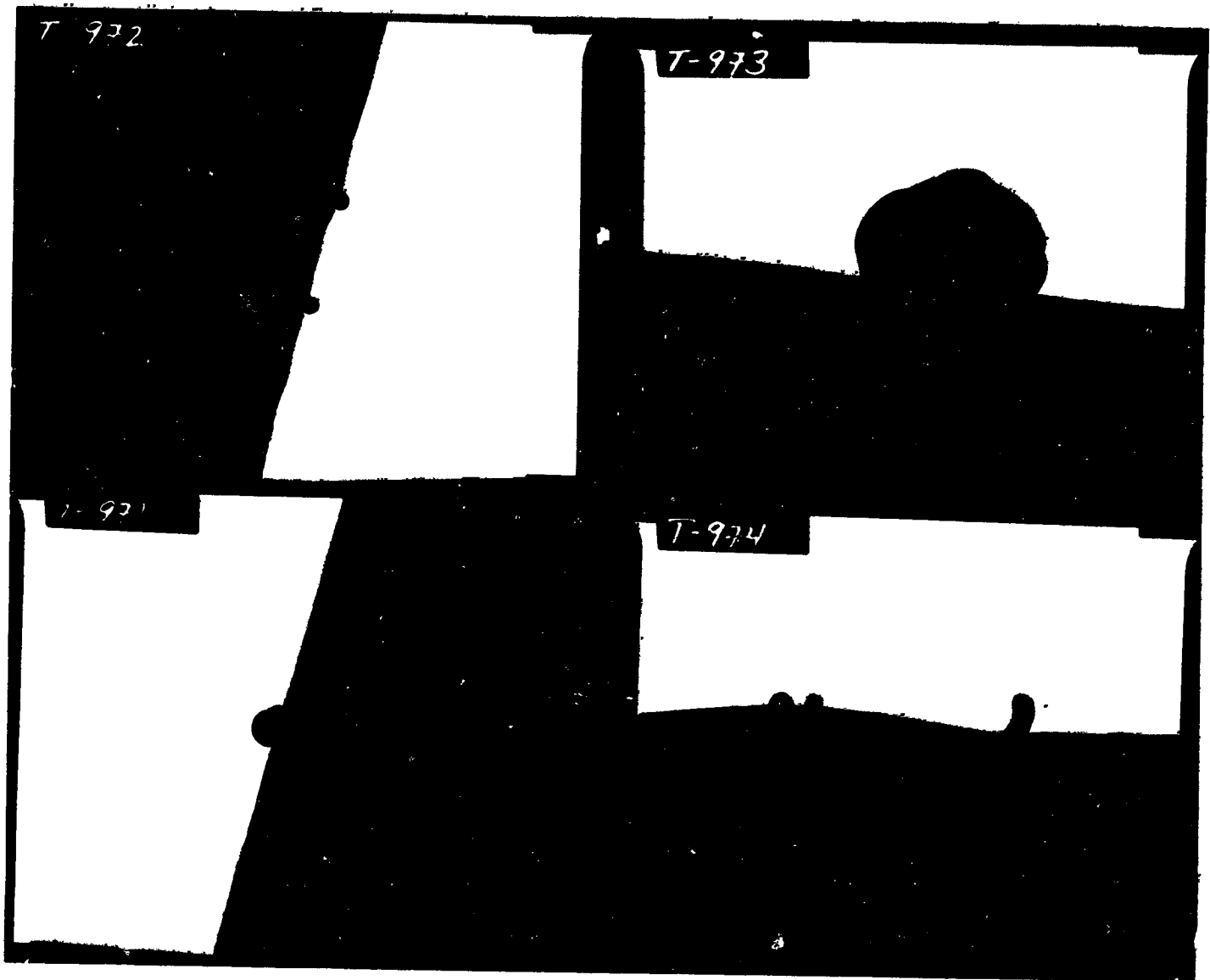


Figure AIII-6 Sample EVA-180; "Exact Volume", -180 Minutes "Open" Exposure

Substrate:

Carbon felt Lot 011882-1650°C; Pretreatment 1 N KOH.

Catalyzation:

Target loading of 12.5  $\mu\text{gAu}/\text{cm}^2$  using aqueous methanol solution.

Gold chloride solution used in exact volume for felt saturation.

-49  $\text{cm}^2$  felt sample immersed in 16 ml of solution.

-felt rotated in solution after 2 minutes.

-sample transferred directly to 110° oven after 180 minutes.

-oven dried at 110° for 2 hours.

-not baked at 270°C.

APPENDIX IV. - EFFECTS OF PRE-CATALYZATION STATE AND CATALYZATION TEMPERATURE  
(SUPPLEMENTAL DATA)

TABLE AIV-I. CATALYZATION OPTIMIZATION STUDY: SUMMARY OF SELECTED CURRENT-DATA POINTS

Electrode Description	Fig. Ref.	1		2		3		4		5		6		7		8	
		$I_c H^+$	$I_c H^+$ at -950 mV	Au/C	Pb/Au	Pb/Au	Cr <sup>3+</sup>	Cr <sup>3+</sup>	Cr <sup>3+</sup>	Cr <sup>3+</sup>	$I_c H^+$	Cr <sup>3+</sup>					
		(mA)	(mA)	(mA)	(mA)	(mA)	(mA)	(mA)	Min.	Peak	Peak	Peak	Peak	$I_c$	$I_c$	$I_a$	$I_a$
										(mA)	(mA)	(mA)	(mA)	(mA)	(mA)	(mA)	(mA)
FMI-C-1/8 Lot 051882																	
1650°, Optimization																	
Methanol Dry	15	580	4	16	15	12	22	66	70								
Methanol Damp	16	160	3	18	14	13	28	55	58								
Acetone Dry	17	610	6	23	16	17	30	95	102								
Acetone Damp	18	400	3	12	9	11	22	55	60								

ORIGINAL PAGE IS  
OF POOR QUALITY

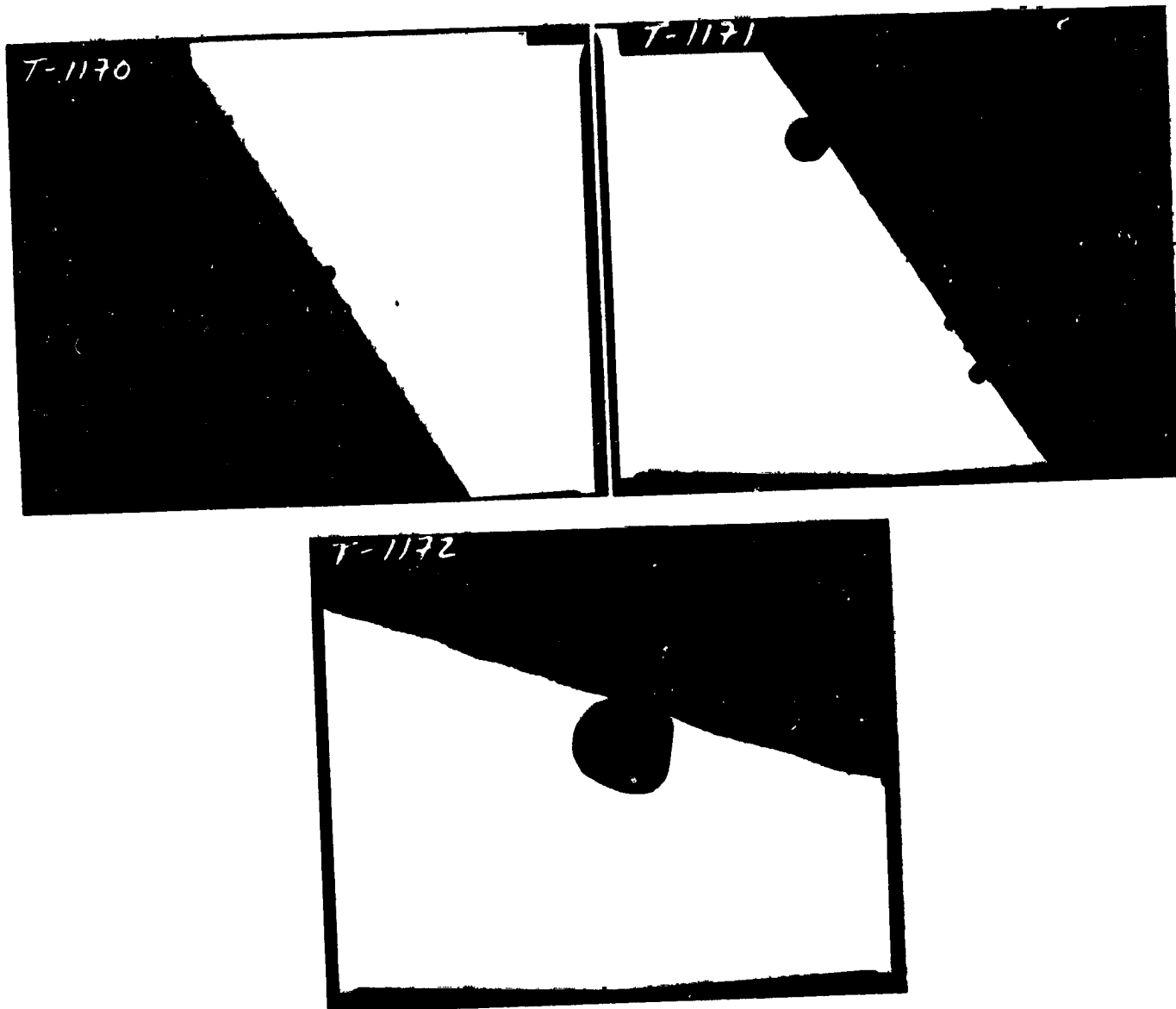


Figure AIV-1. Gold Particles on Carbon Fiber;  
Precatalyzation pH of Felt was 5, Sample A.  
Catalyzed at 25°C by NASA-I Method.  
(TEM 90,000X; 1 mm = 11 nm).

ORIGINAL PAGE IS  
OF POOR QUALITY

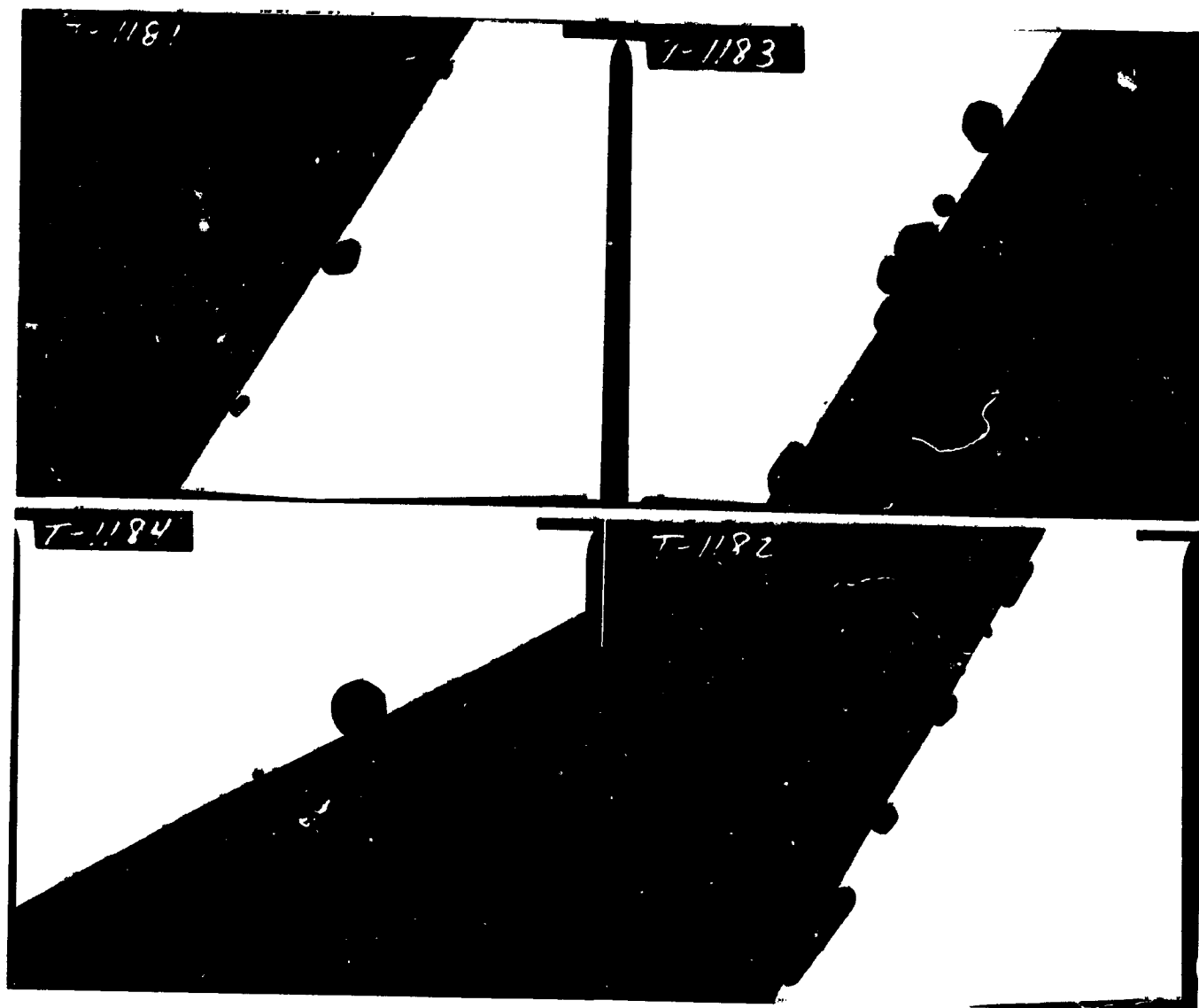


Figure AIV-2. Gold Particles on Carbon Fiber;  
Precatalyzation pH of Felt was 5, Sample B.  
Catalyzed at 25°C by NASA-I Method.  
(TEM 90,000X; 1 mm = 11 nm).

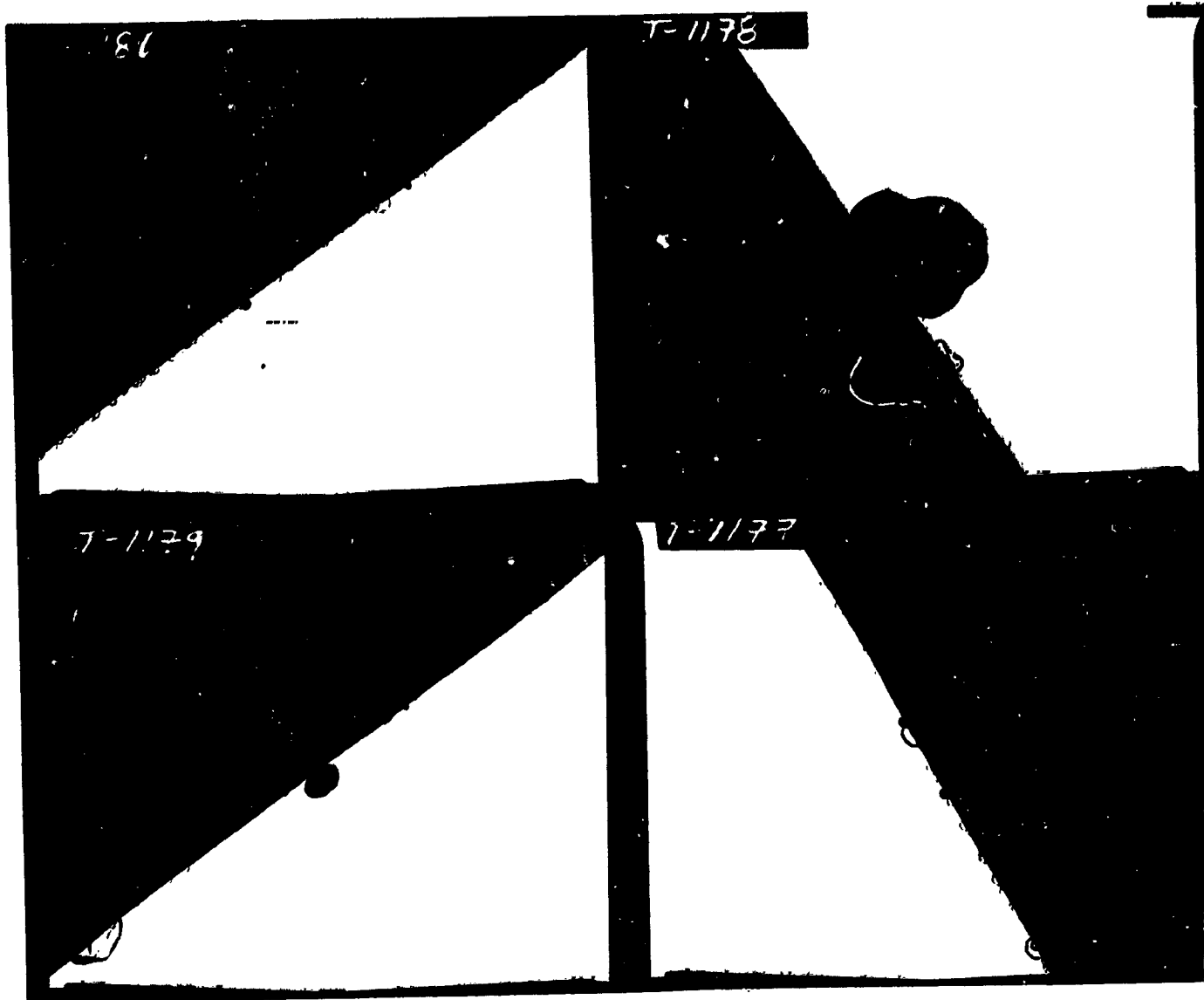


Figure AIV-3. Gold Particles on Carbon Fiber;  
Precatalyzation pH of Felt was 9, Sample A.  
Catalyzed at 25°C by NASA-I Method.  
(TEM 90,000X; 1 mm = 11 nm).

ORIGINAL PAGE IS  
OF POOR QUALITY

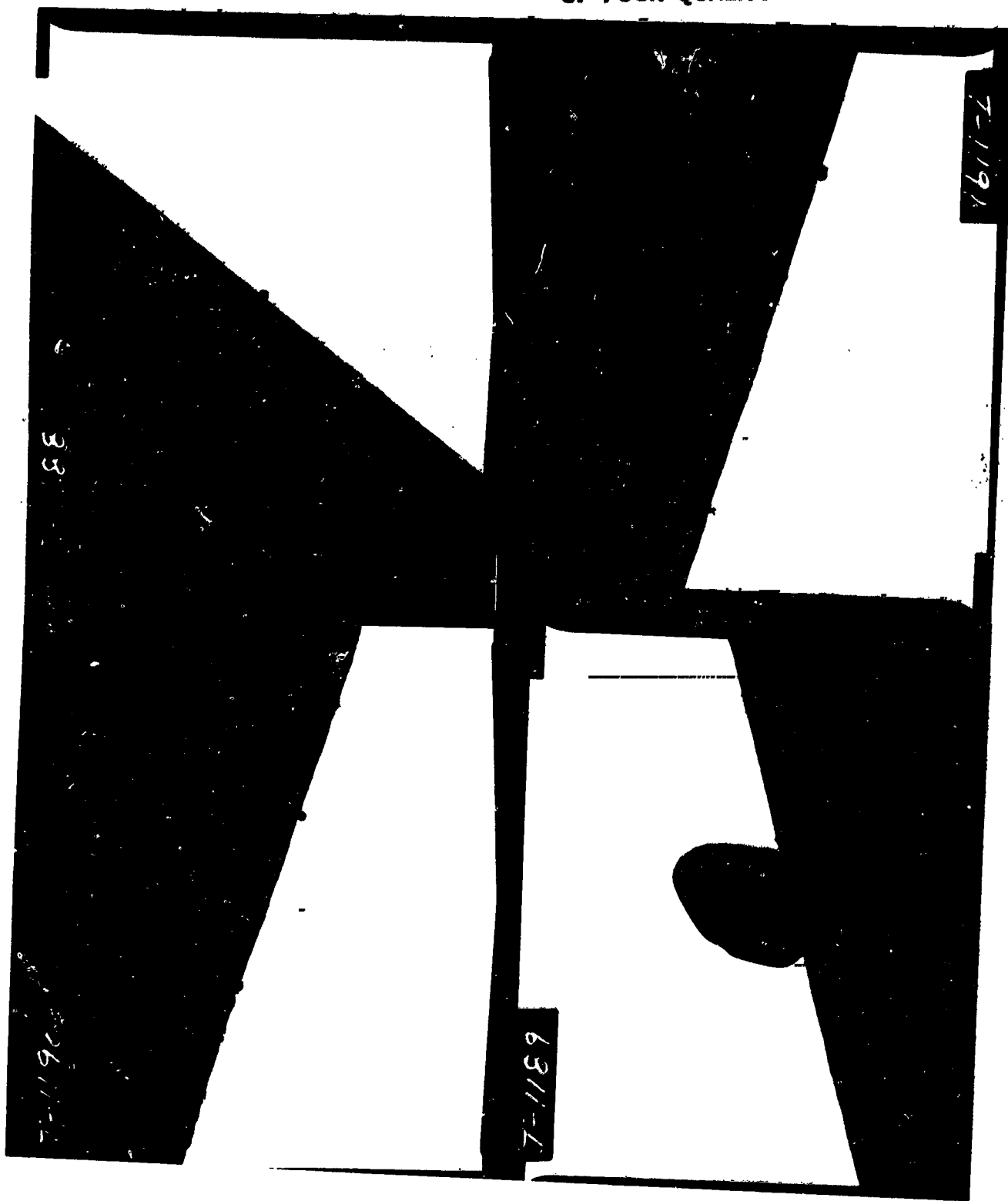


Figure AIV-4. Gold Particles on Carbon Fiber;  
Precatalyzation pH of Felt was 9, Sample B.  
Catalyzed at 25°C by NASA-1 Method.  
(TEM 90,000X; 1 mm = 11 nm).

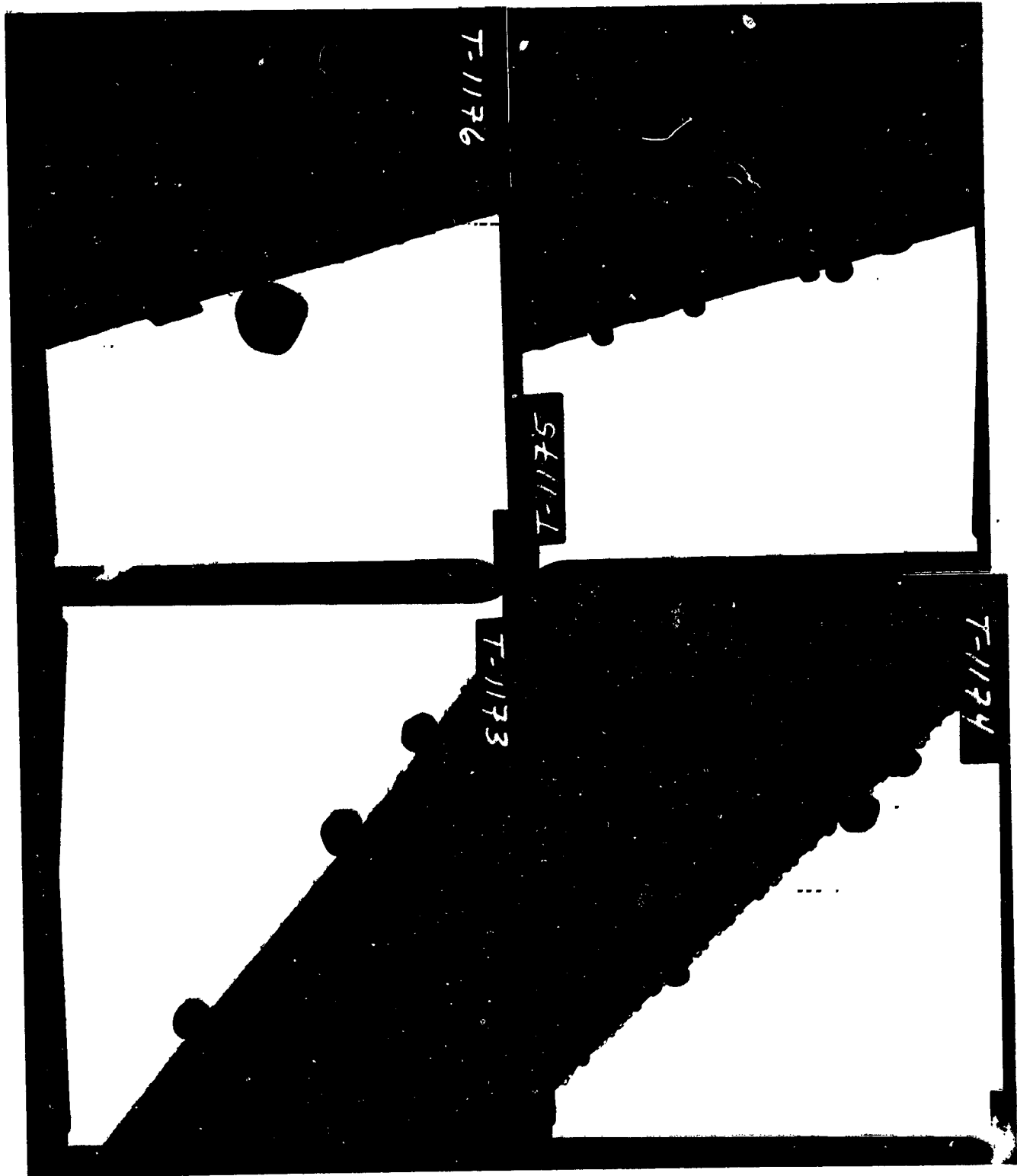


Figure AIV-5. Gold Particles on Carbon Fiber;  
Precatalyzation pH of Felt was 7, Sample A.  
Catalyzed at 25°C by NASA-I Method.  
(TEM 90,000X; 1 mm = 11 nm).

ORIGINAL PAGE IS  
OF POOR QUALITY

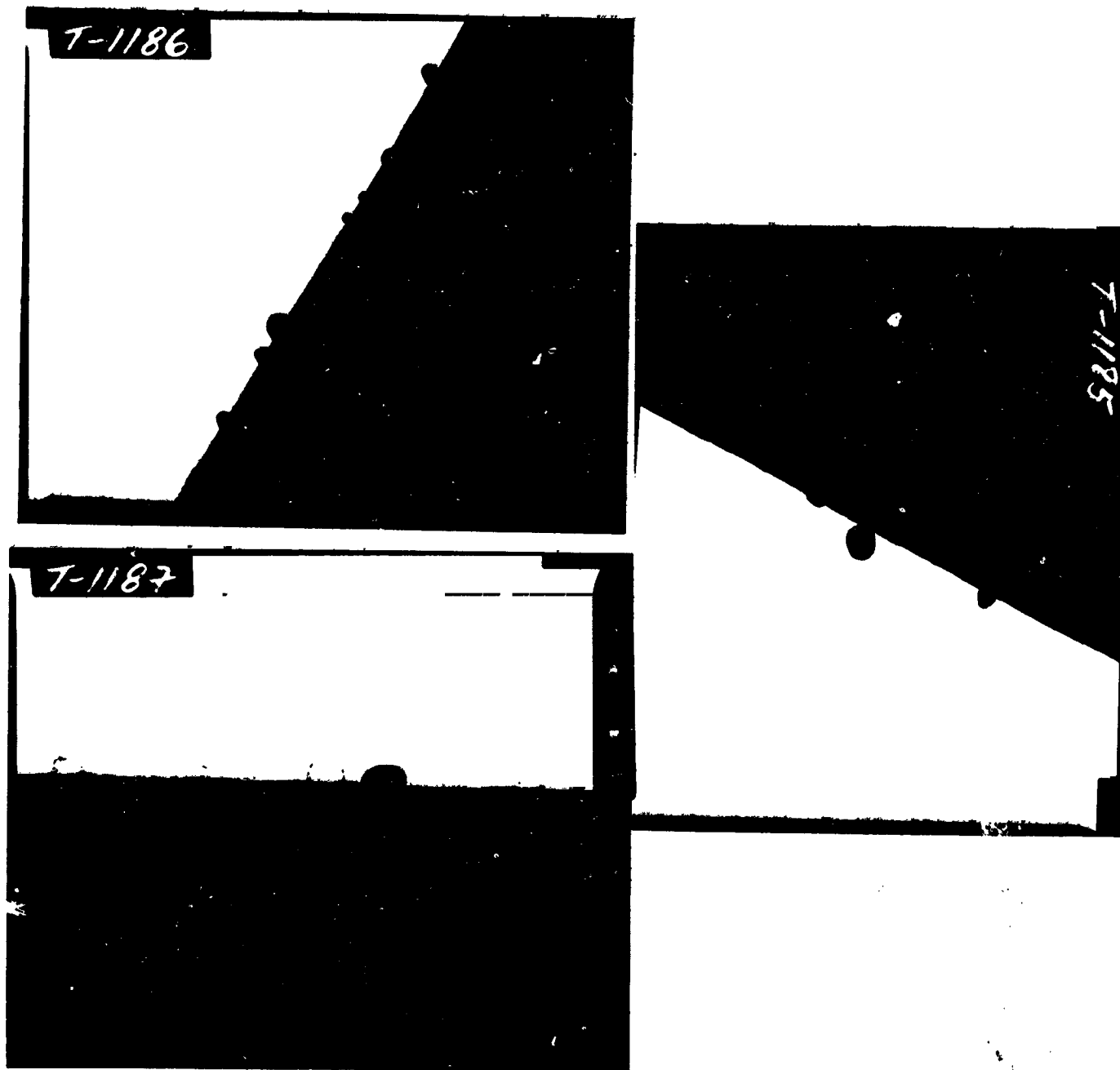


Figure AIV-6. Gold Particles on Carbon Fiber;  
Precatalyzation pH of Felt was 7, Sample B.  
Catalyzed at 25°C by NASA-I Method.  
(TEM 90,000X; 1 mm = 11 nm).



Figure AIV-7. Gold Particles on Carbon Fiber;  
Precatalyzation pH of Felt was 7;  
Catalyzed at 0°C by NASA-I Method.  
(TEM 90,000X; 1 mm = 11 nm).

ORIGINAL PAGE IS  
OF POOR QUALITY

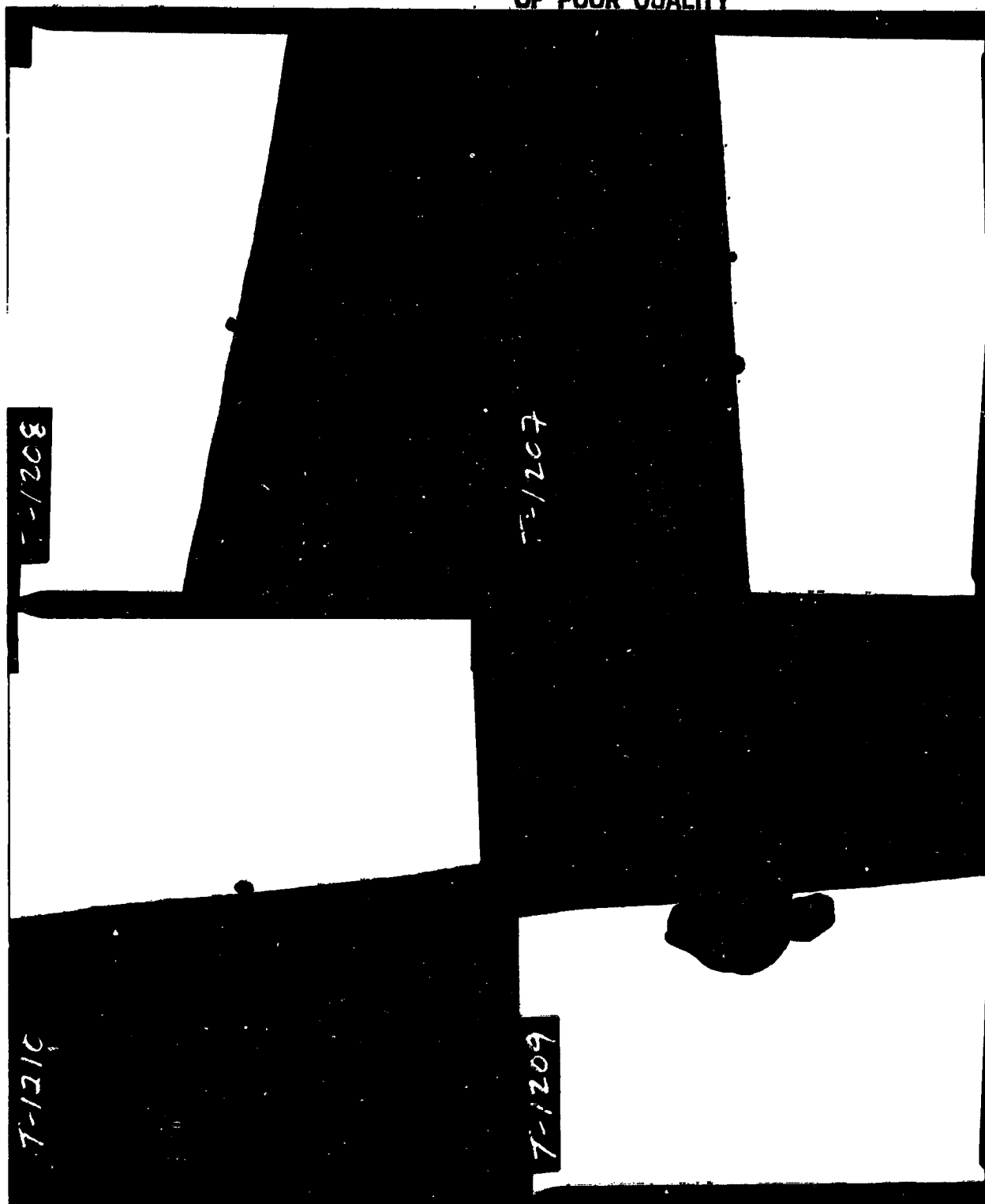


Figure AIV-8. Gold Particles on Carbon Fiber;  
Precatalyzation pH of Felt was 7;  
Catalyzed at 50°C by NASA-I Method.  
(TEM 90,000X; 1 mm = 11 nm).

APPENDIX V. - REPRODUCIBILITY OF ELECTROCHEMICAL PERFORMANCE  
(SUPPLEMENTAL DATA)

TABLE AV-I. REPRODUCIBILITY STUDY: SUMMARY OF SELECTED CURRENT-DATA POINTS

Electrode Description	Fig. Ref.	1		2		3		4		5		6		7		8	
		$I_{CH^+}$ (mA)	Au/C	$I_{CH^+}$ at -950 mV (mA)	Pb/Au	$I_{CH^+}$ Pb/Au (mA)	Cr <sup>3+</sup> Pb/Au (mA)	Cr <sup>3+</sup> Pb/Au (mA)	$I_{CH^+}Cr^{3+}$ Min. (mA)	$I_{CH^+}Cr^{3+}$ Peak (mA)							
FMI-C-1/8 Lot 011882/1650°C																	
SAMPLE																	
1A	18	550	3	45	24	28	46	149	159								
1B	19	310	1	17	13	14	30	61	65								
1C	20	300	2	14	13	14	28	44	46								
2A	21	380	2	20	18	12	25	79	79								
2B	22	250	2	18	14	12	32	58	62								
2C	23	510	5	29	21	29	44	105	111								
3A	24	250	2	17	15	13	27	47	48								
3B	25	220	1	13	11	13	25	47	50								
3C	26	235	1	14	12	13	28	49	51								

ORIGINAL PAGE IS  
OF POOR QUALITY

APPENDIX VI. -...STUDY OF LEAD DISTRIBUTION ON ELECTRODES  
(SUPPLEMENTAL DATA)

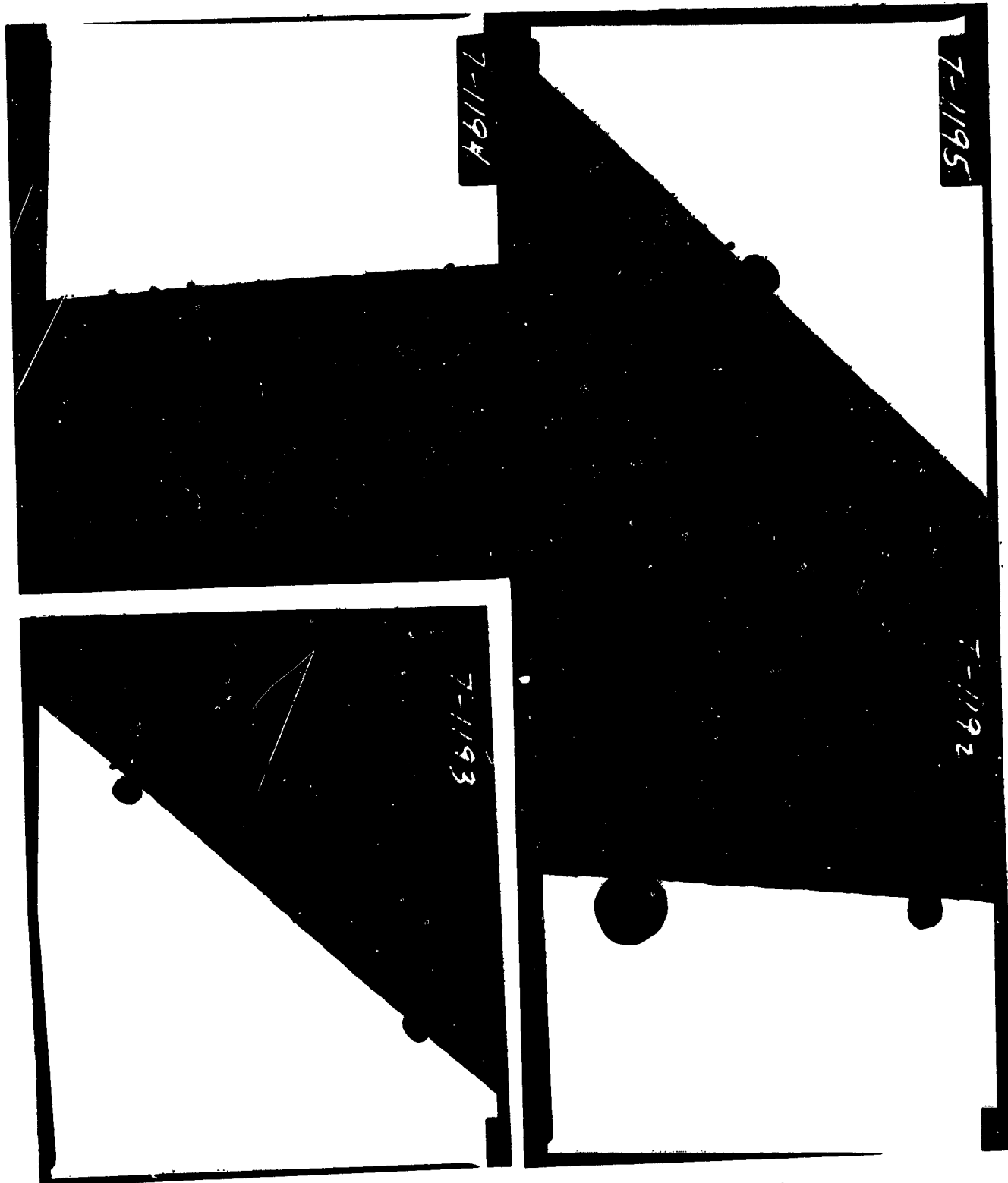


Figure AVI-1. Lead Plated Sample; Gold Particles on  
Carbon Fiber. Catalyzed from pH 5 Felt  
at 25°C by NASA-I Method.  
(TEM 90,000X; 1 mm = 11 nm).



Figure AVI-2. Lead Plated Sample; Gold Particles on Carbon Fiber. Catalyzed from pH 7 Felt at 25°C by NASA-I Method. (TEM 90,000X; 1 mm = 11 nm).

ORIGINAL PAGE IS  
OF POOR QUALITY

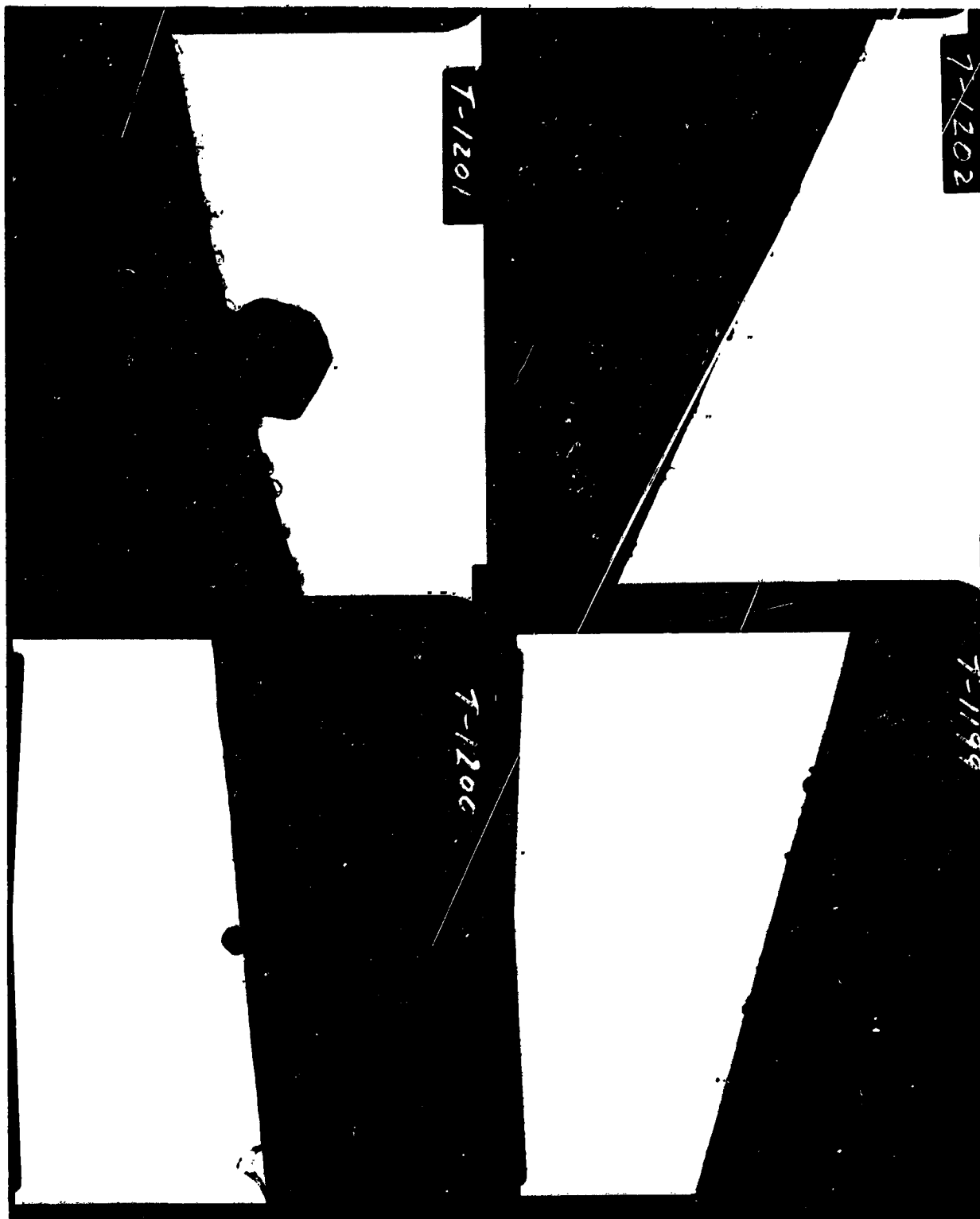


Figure AVI-3. Lead Plated Sample; Gold Particles on  
Carbon Fiber. Catalyzed from pH 9 Felt  
at 25°C by NASA-I Method.  
(TEM 90,000X; 1 mm = 11 nm).

APPENDIX VII. - EFFECTS OF ACIDITY LEVEL. (SUPPLEMENTAL DATA)

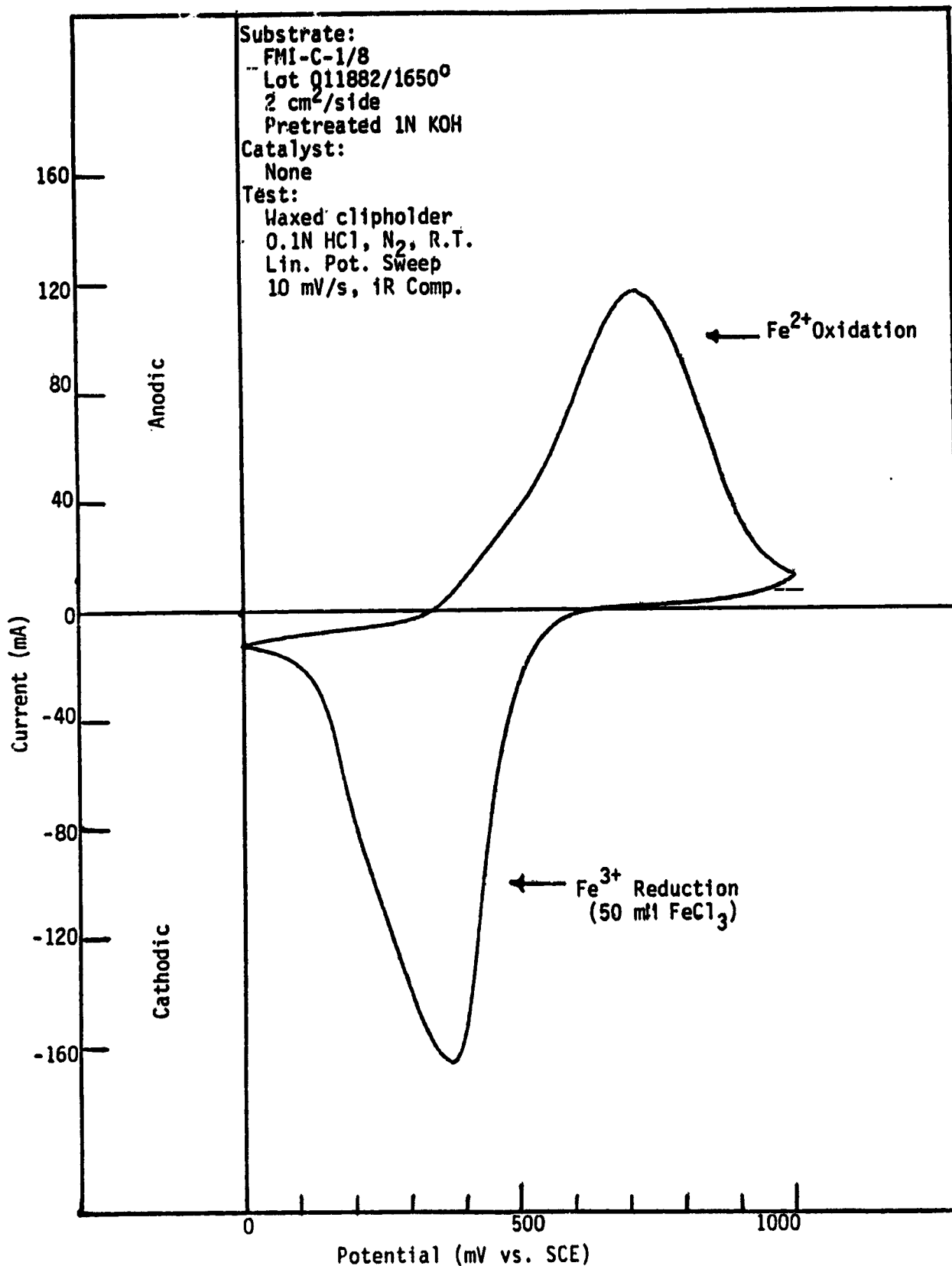


Figure A VII -1. Effect of Acidity Level: Fe<sup>3+</sup> in 0.1N HCl.

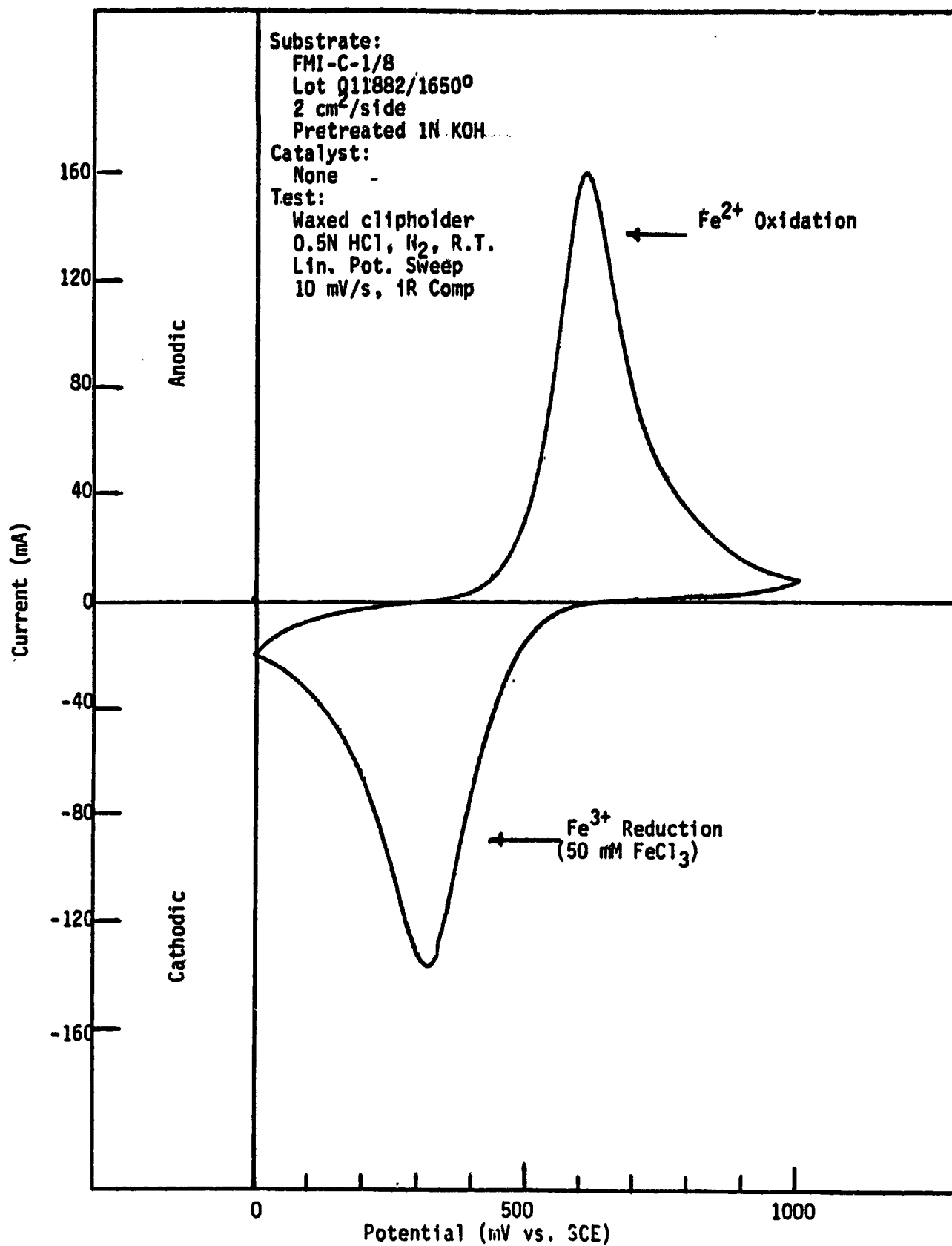


Figure A VII -2. Effect of Acidity Level: Fe<sup>3+</sup> in 0.5N HCl.

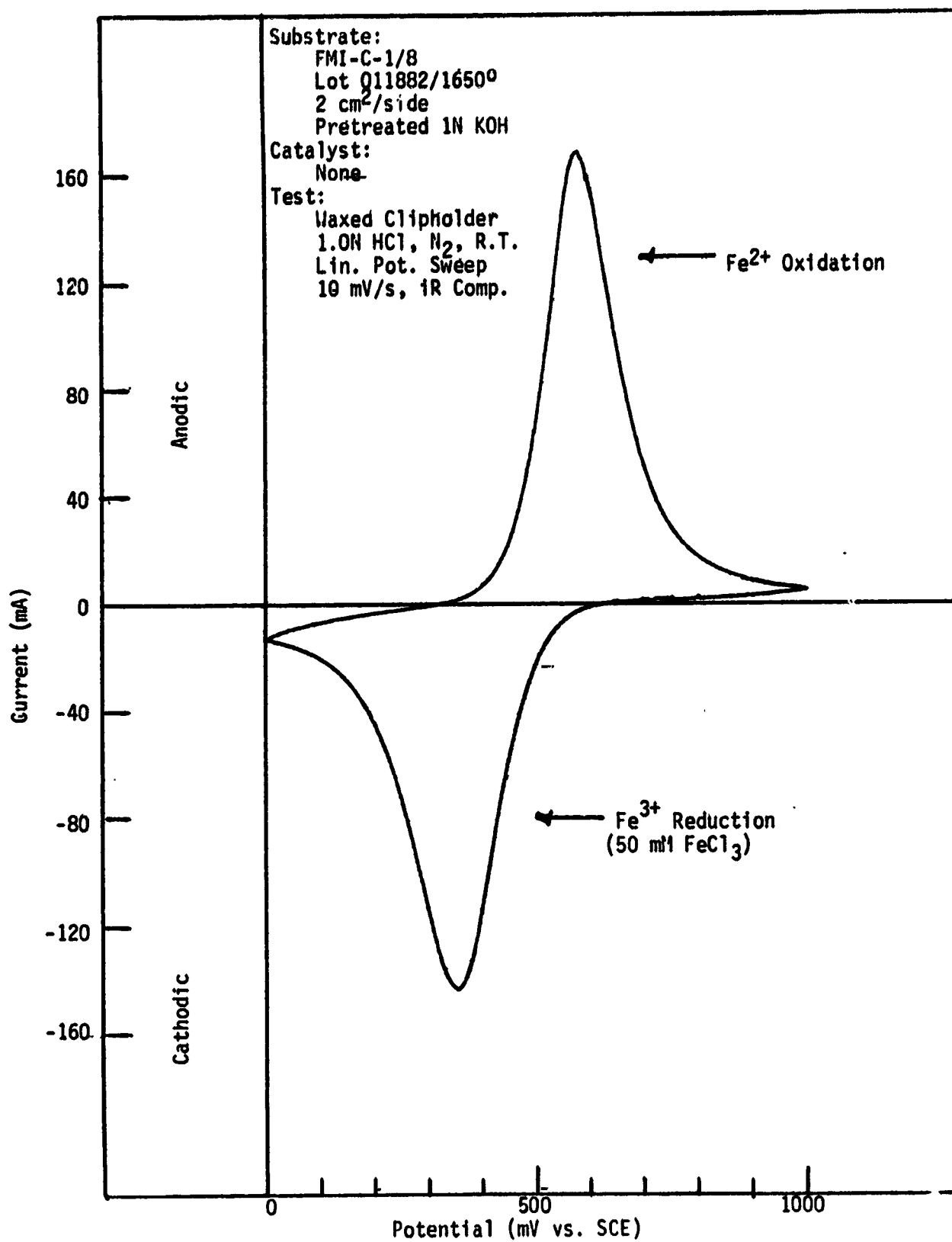


Figure A VII-3. Effect of Acidity Level: Fe<sup>3+</sup> in 1.0N HCl.

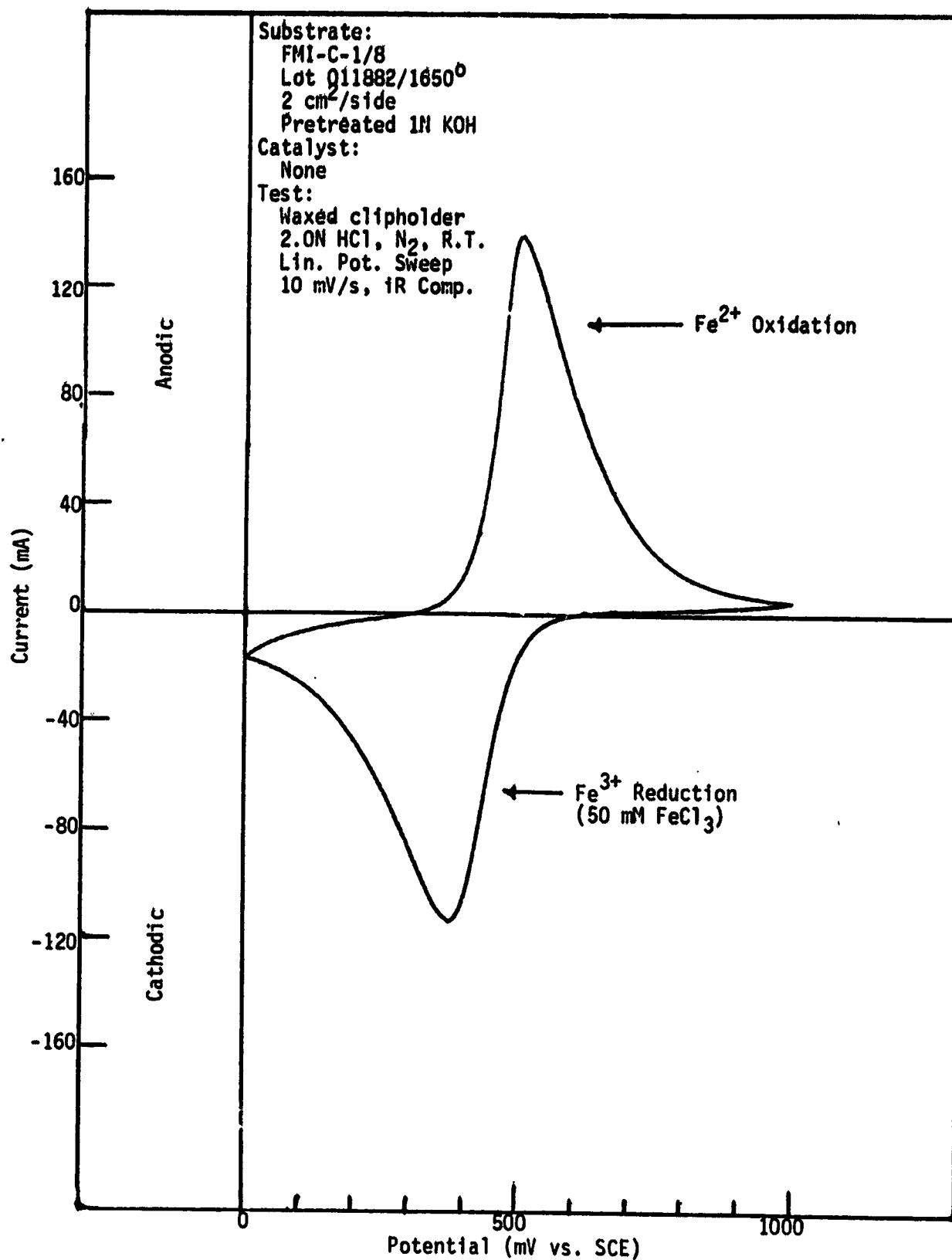


Figure A VII-4. Effect of Acidity Level: Fe<sup>3+</sup> in 2.0N HCl.

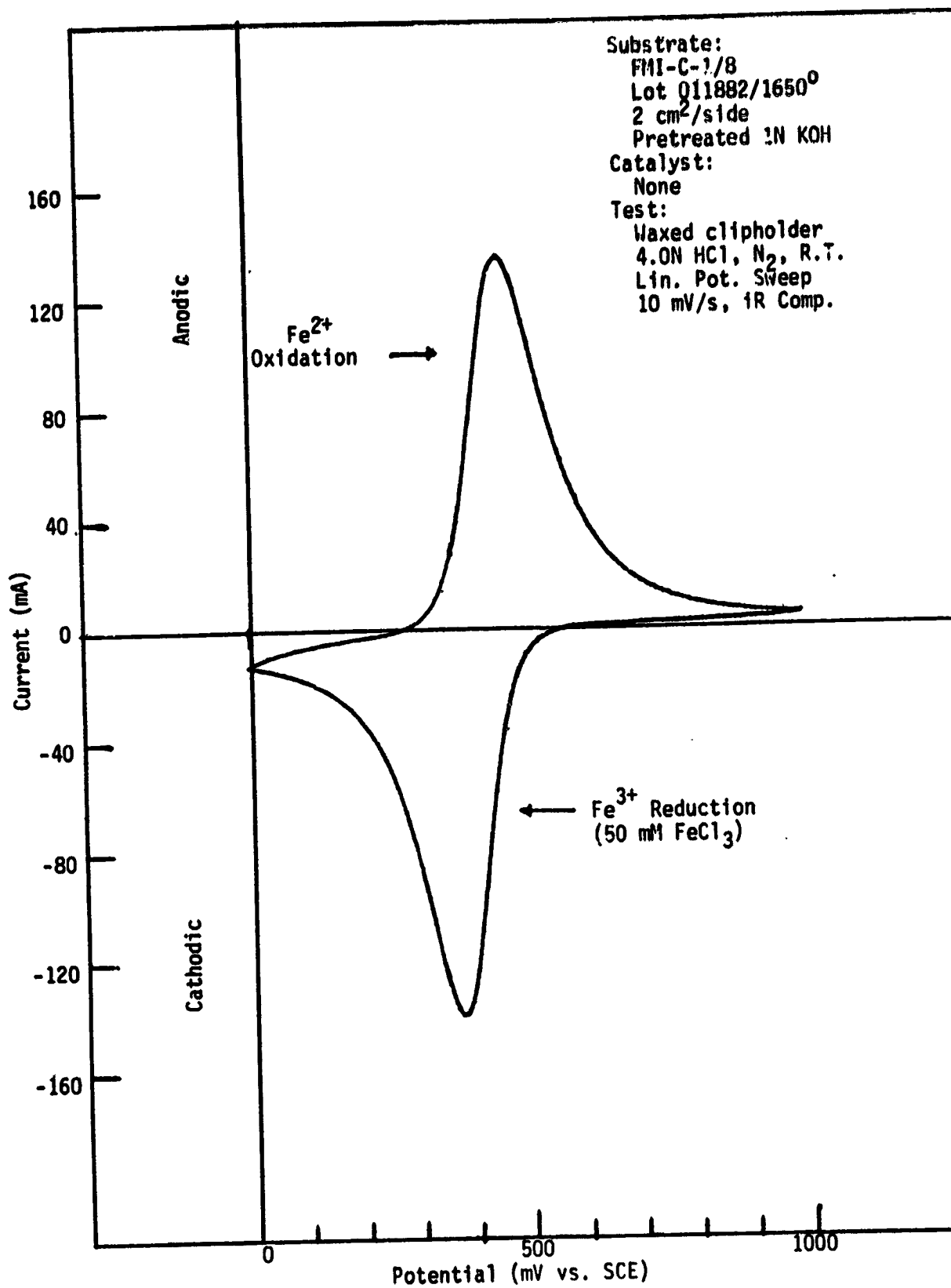


Figure A VII-5. Effect of Acidity Level: Fe<sup>3+</sup> in 4.0N HCl.

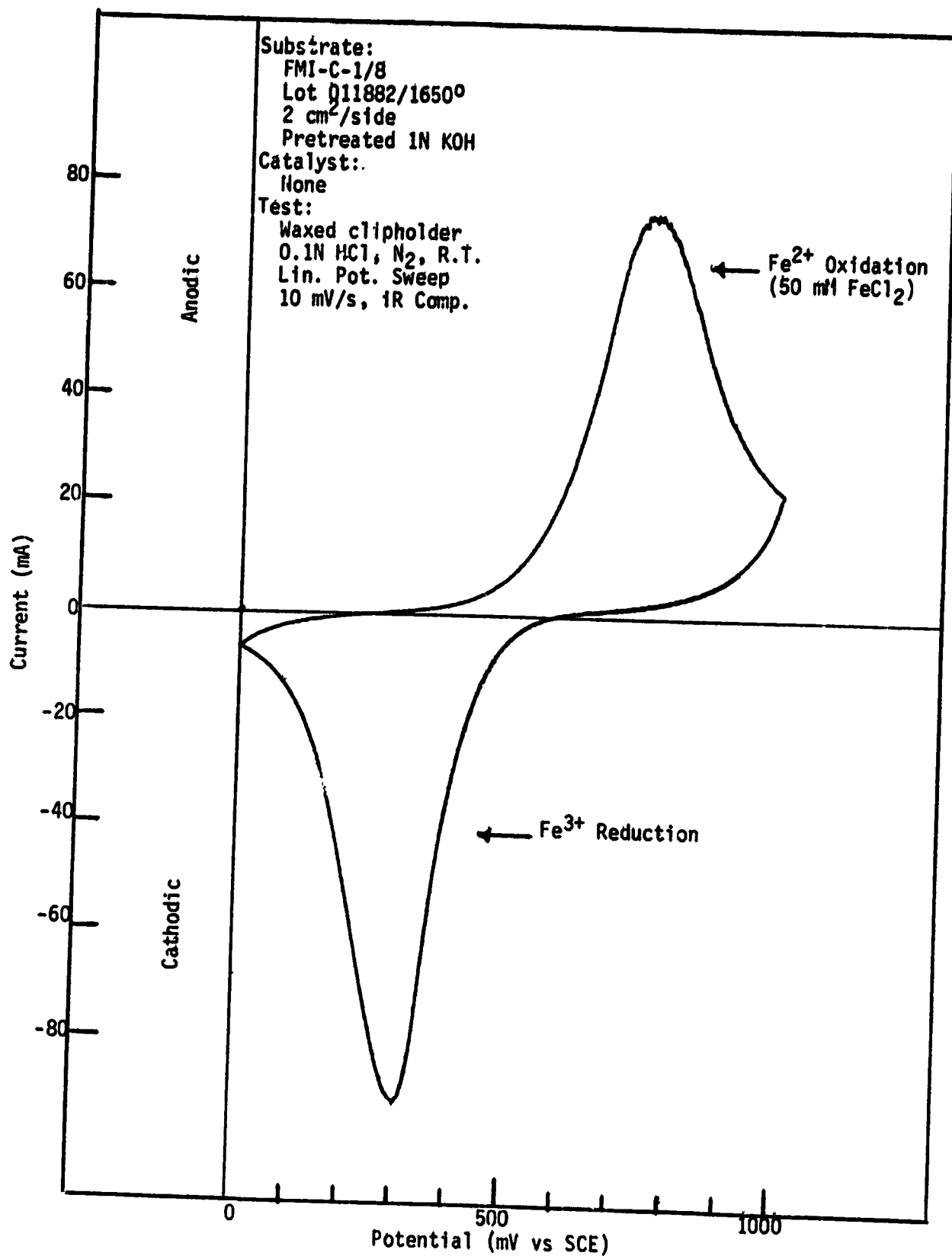


Figure A VII-6. Effect of Acidity Level: Fe<sup>2+</sup> in 0.1N HCl.

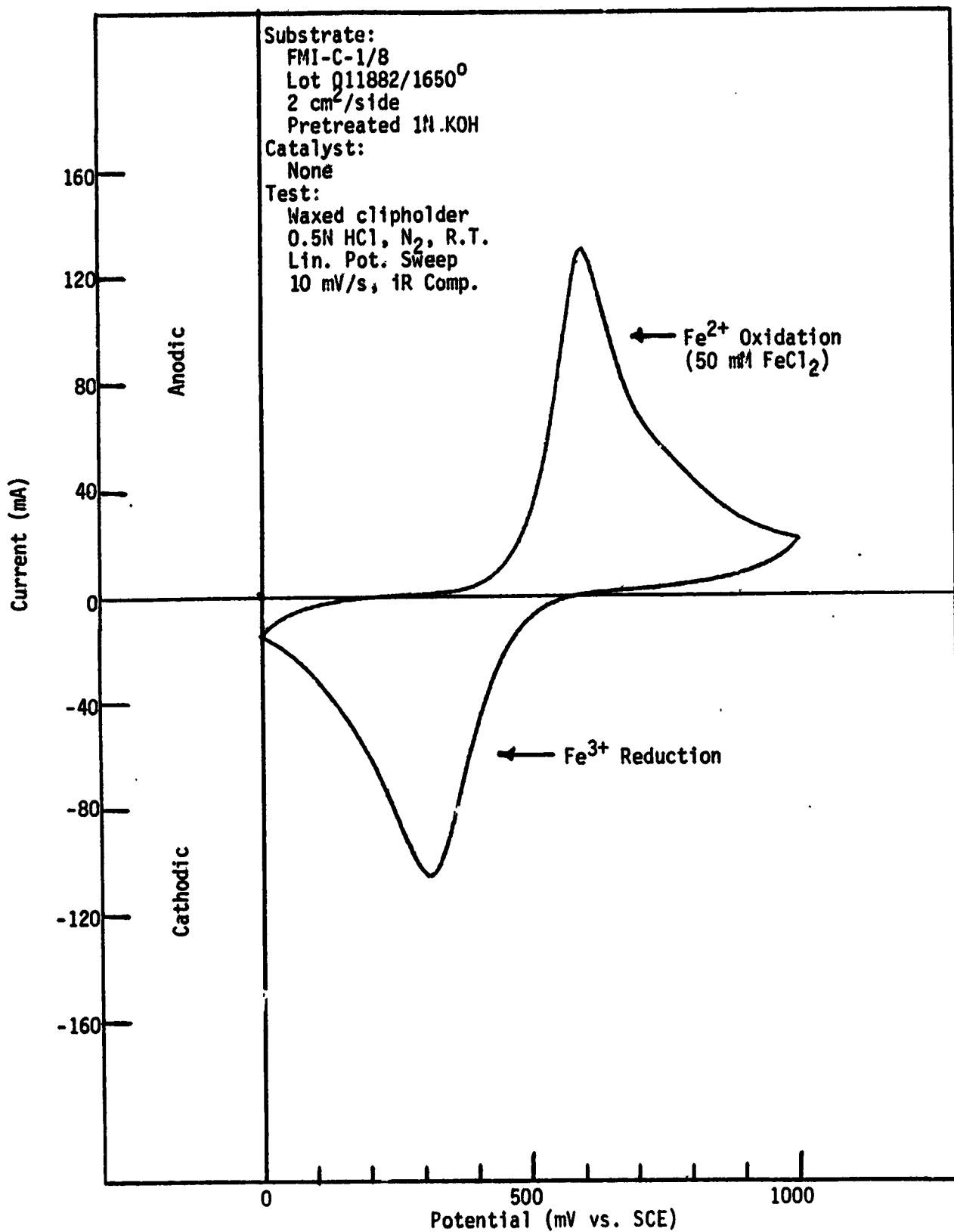


Figure A VII-7. Effect of Acidity Level: Fe<sup>2+</sup> in 0.5N HCl.

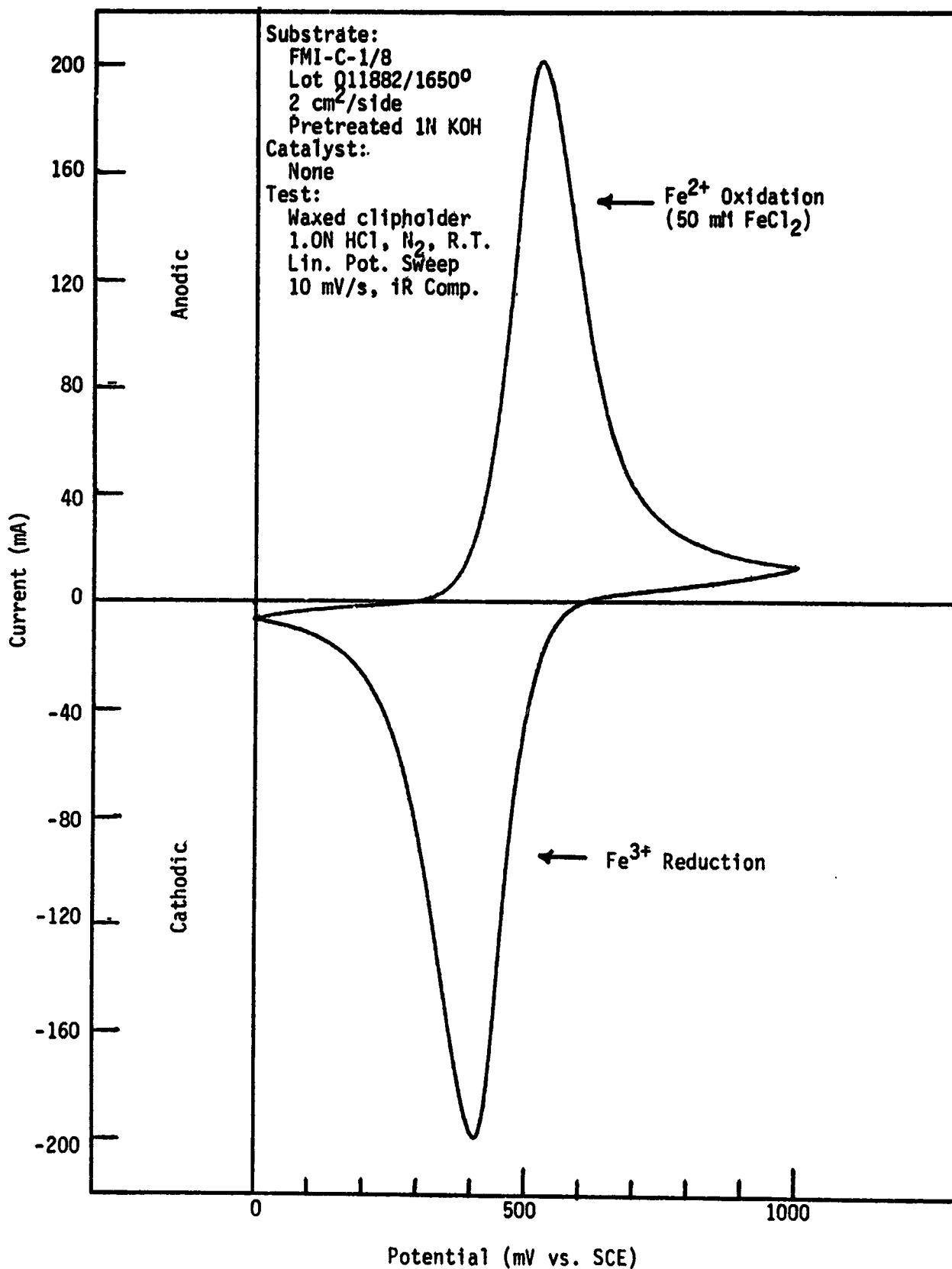


Figure A VII-8. Effect of Acidity Level: Fe<sup>2+</sup> in 1.0N HCl.

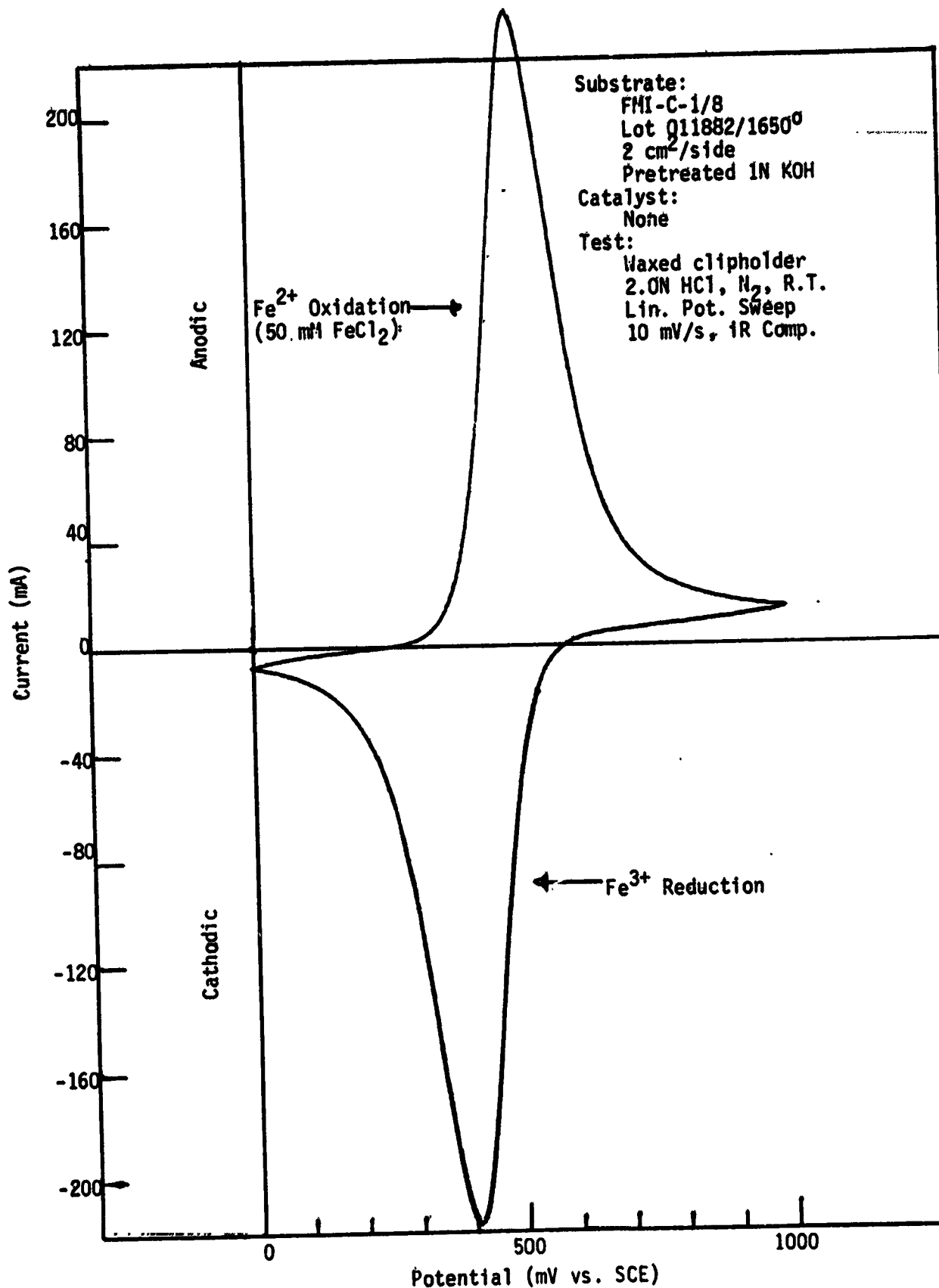


Figure A VII-9. Effect of Acidity Level: Fe<sup>2+</sup> in 2.0N HCl.

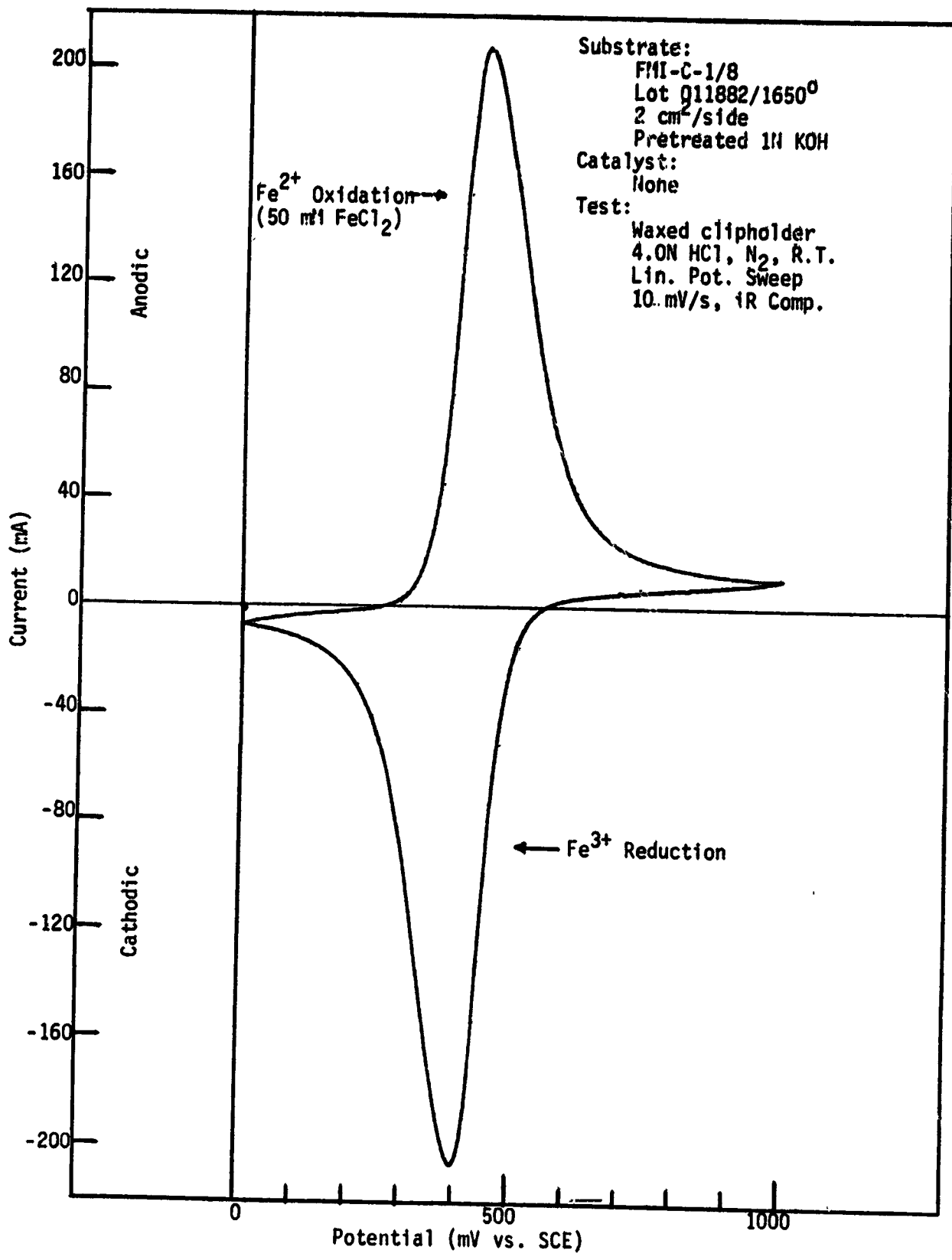


Figure A VII-10. Effect of Acidity Level: Fe<sup>2+</sup> in 4.0N HCl.

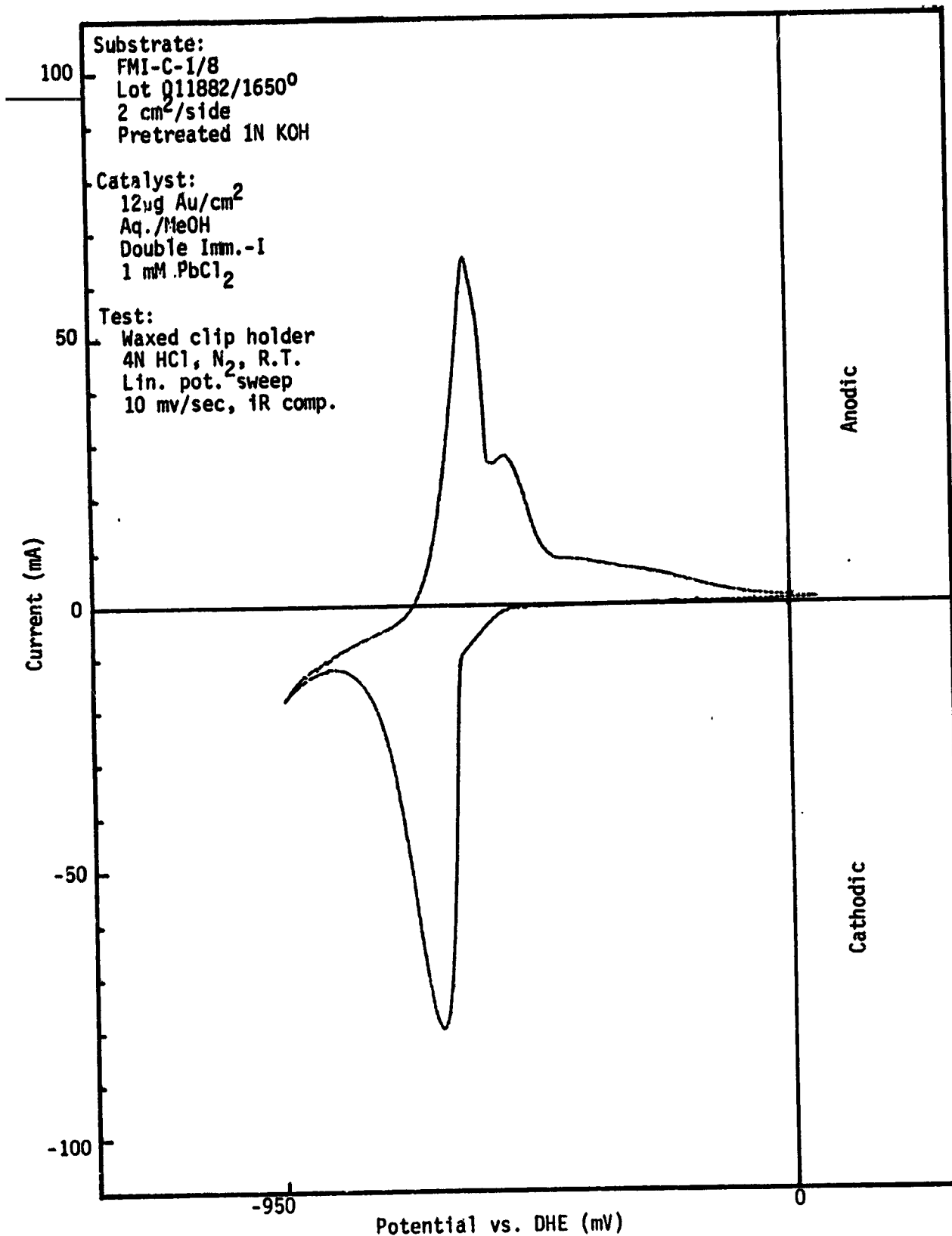


Figure A VII-11. Acidity Level Effects: Electrochemical Performance in 50 mM CrCl<sub>3</sub> in 4.0N HCl (aged).

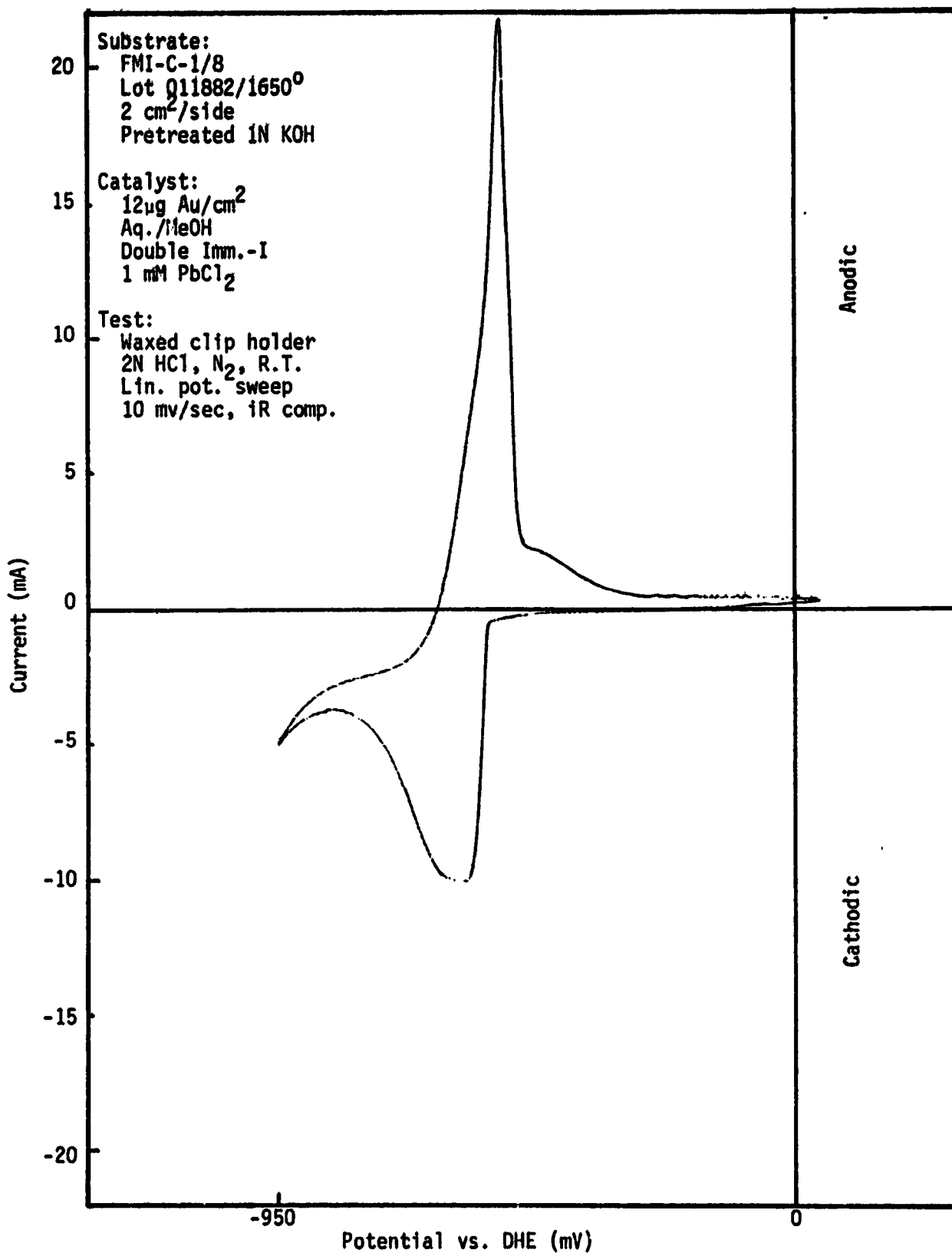


Figure A VII-12. Acidity Level Effects: Electrochemical Performance in 50 mM CrCl<sub>3</sub> in 2.0N HCl (aged).

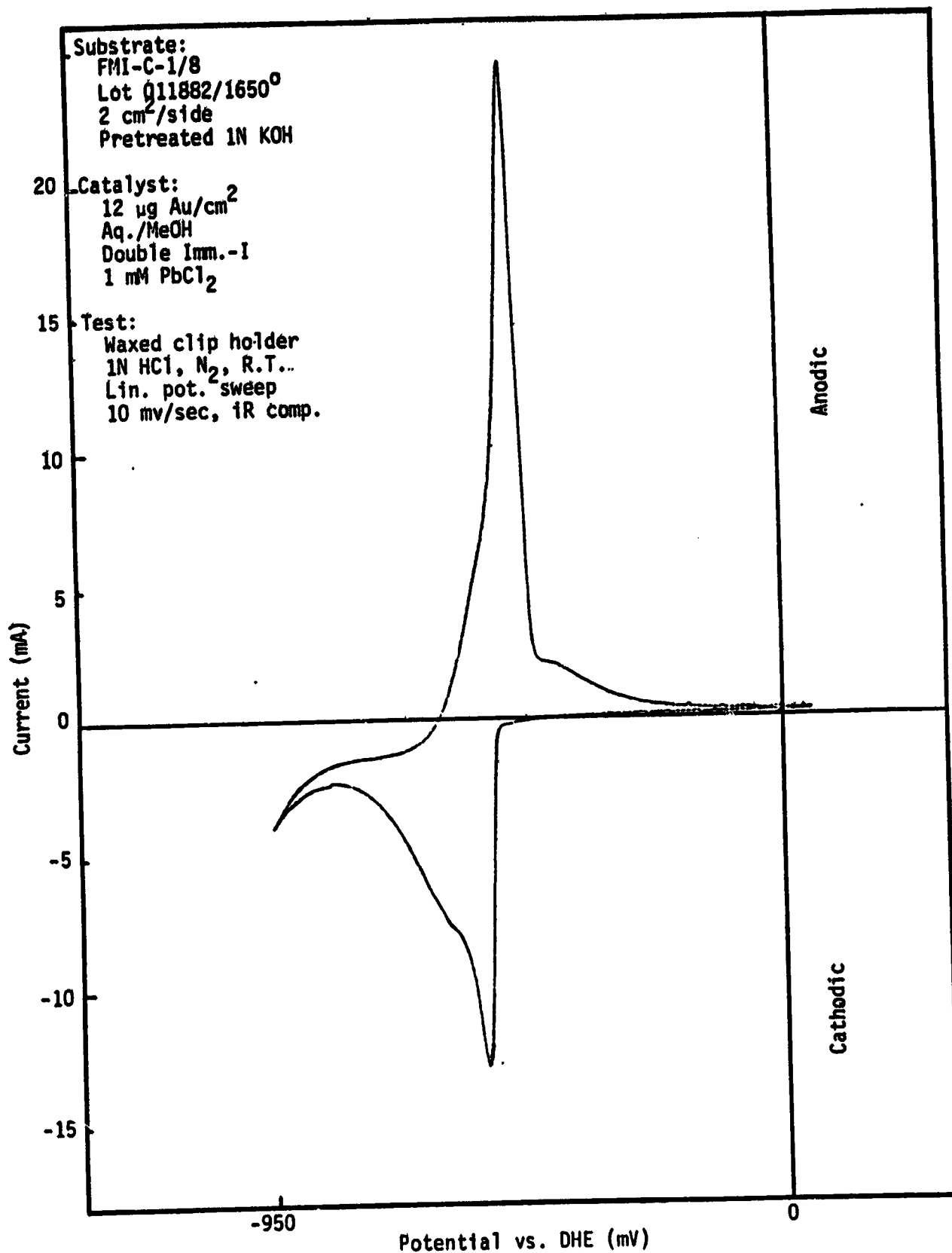


Figure A VII-13. Acidity Level Effects: Electrochemical Performance in 50 mM CrCl<sub>3</sub> in 1.0N HCl (aged).

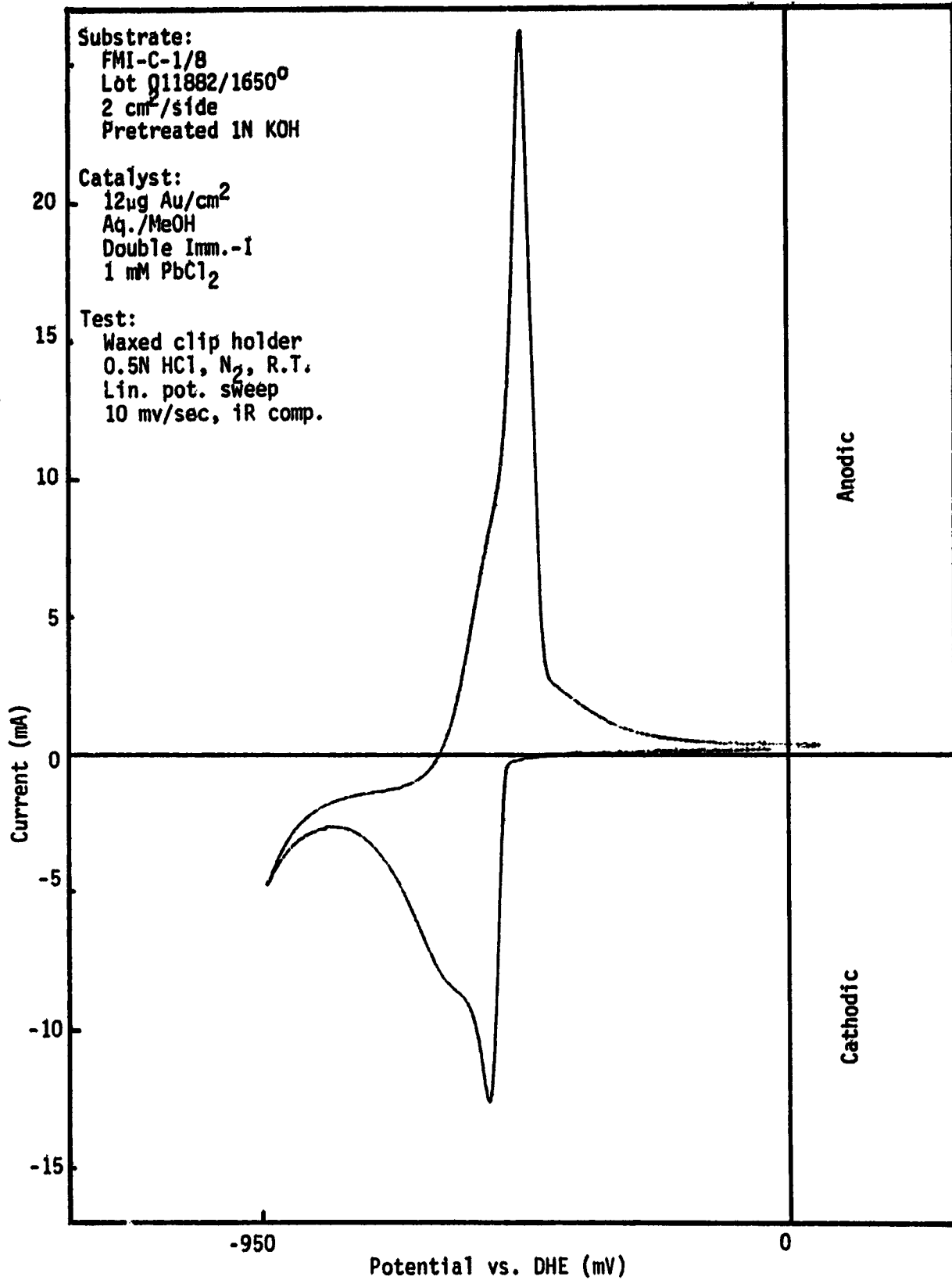


Figure A VII-14. Acidity Level Effects: Electrochemical Performance in 50 mM CrCl<sub>3</sub> in 0.5N HCl (aged).

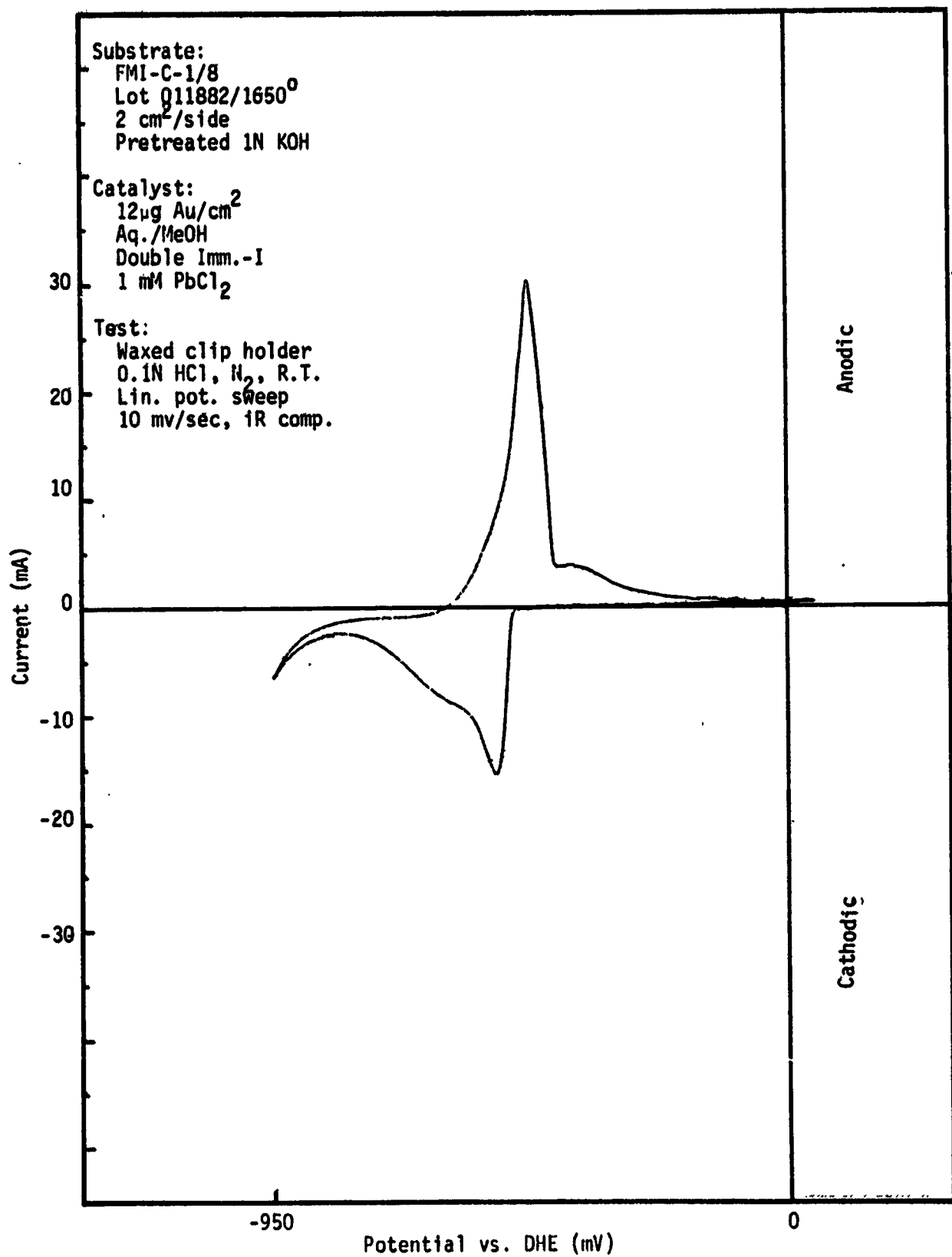


Figure A VII-15. Acidity Level Effects: Electrochemical Performance in 50 mM CrCl<sub>3</sub> in 0.1N HCl (aged).

APPENDIX VIII. -- TEMPERATURE DEPENDENCE (SUPPLEMENTAL DATA)

Figure A VIII-1.  $\text{Fe}^{3+}/\text{Fe}^{2+}$  Reaction at 25°C. in 1.0M  $\text{FeCl}_3$ .

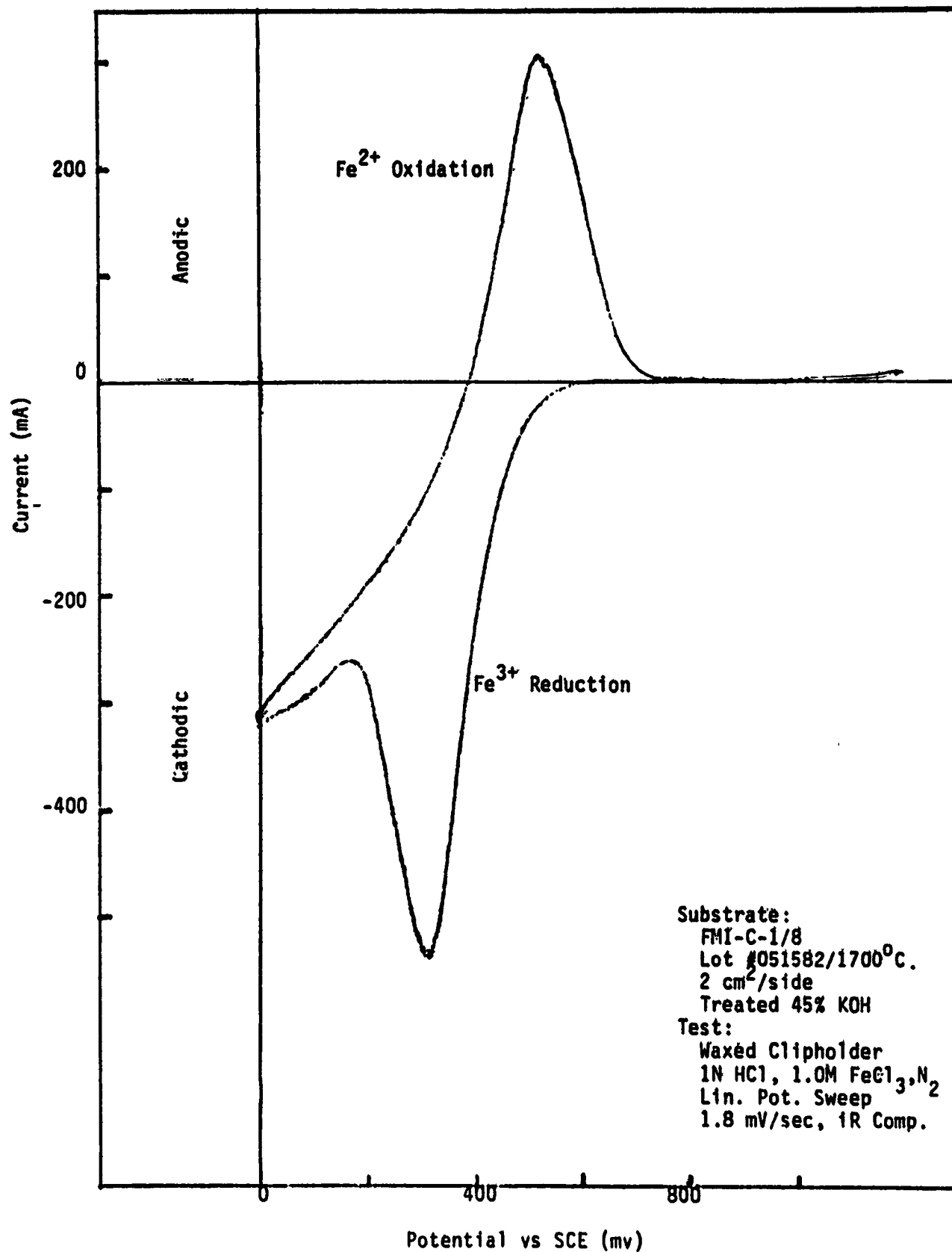


Figure A VIII-2.  $\text{Fe}^{3+}/\text{Fe}^{2+}$  Reaction at 45°C. in 1.0M  $\text{FeCl}_3$ .

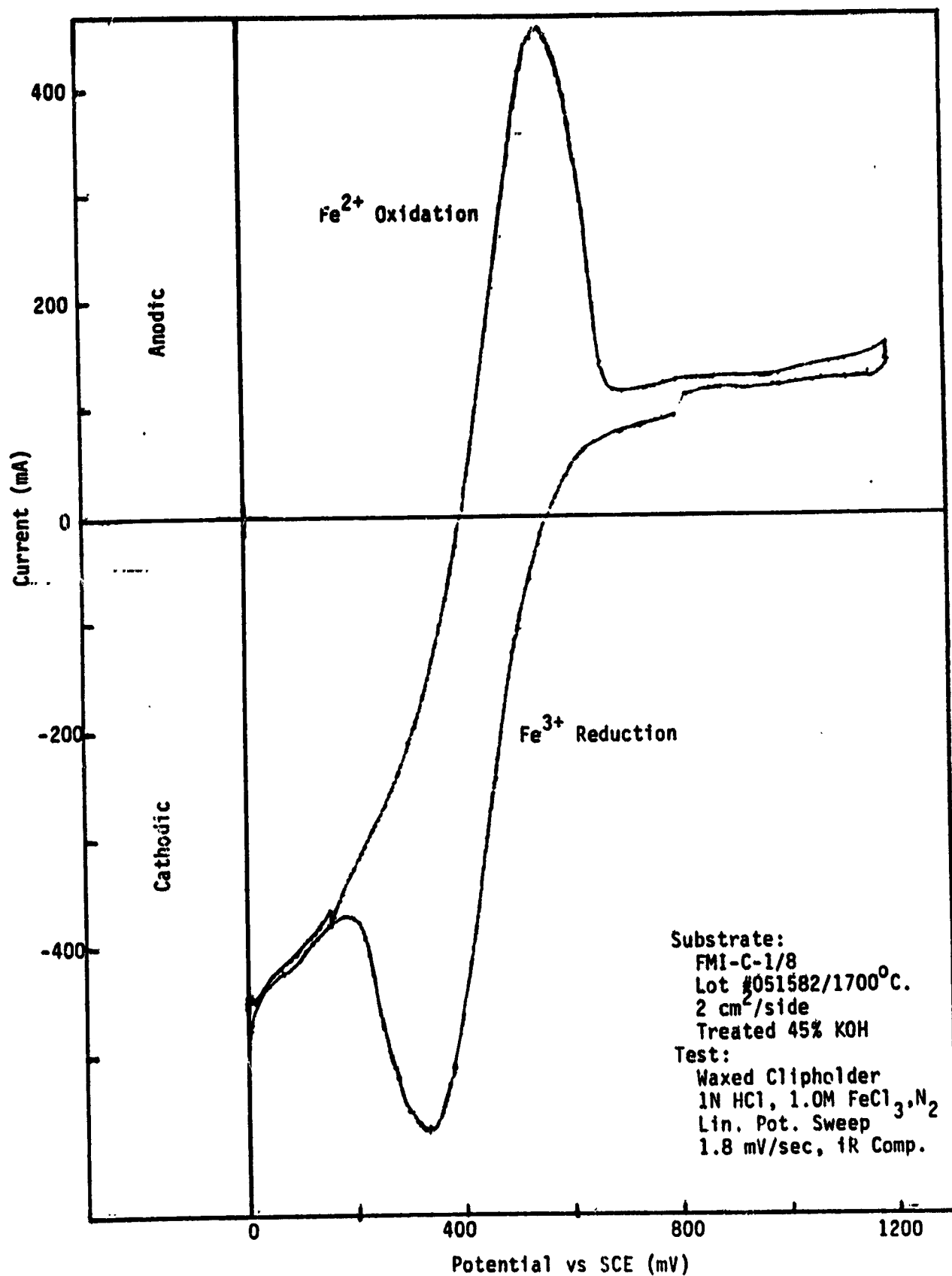


Figure A VIII-3.  $\text{Fe}^{3+}/\text{Fe}^{2+}$  Reaction at  $55^{\circ}\text{C}$ . in 1.0M  $\text{FeCl}_3$ .

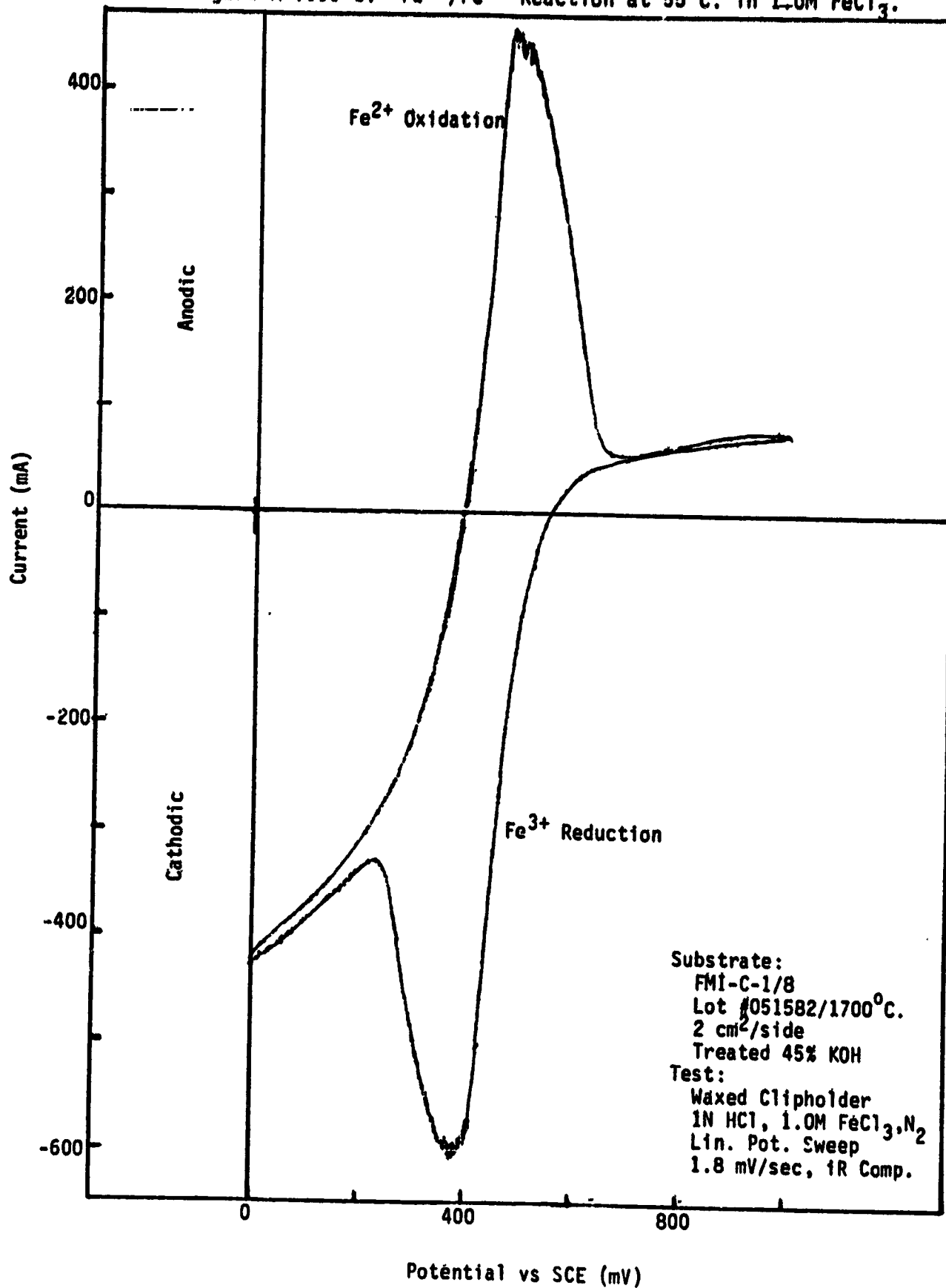


Figure A VIII-4.  $\text{Fe}^{3+}/\text{Fe}^{2+}$  Reaction at  $65^{\circ}\text{C}$ . in  $1.0\text{M FeCl}_3$ .

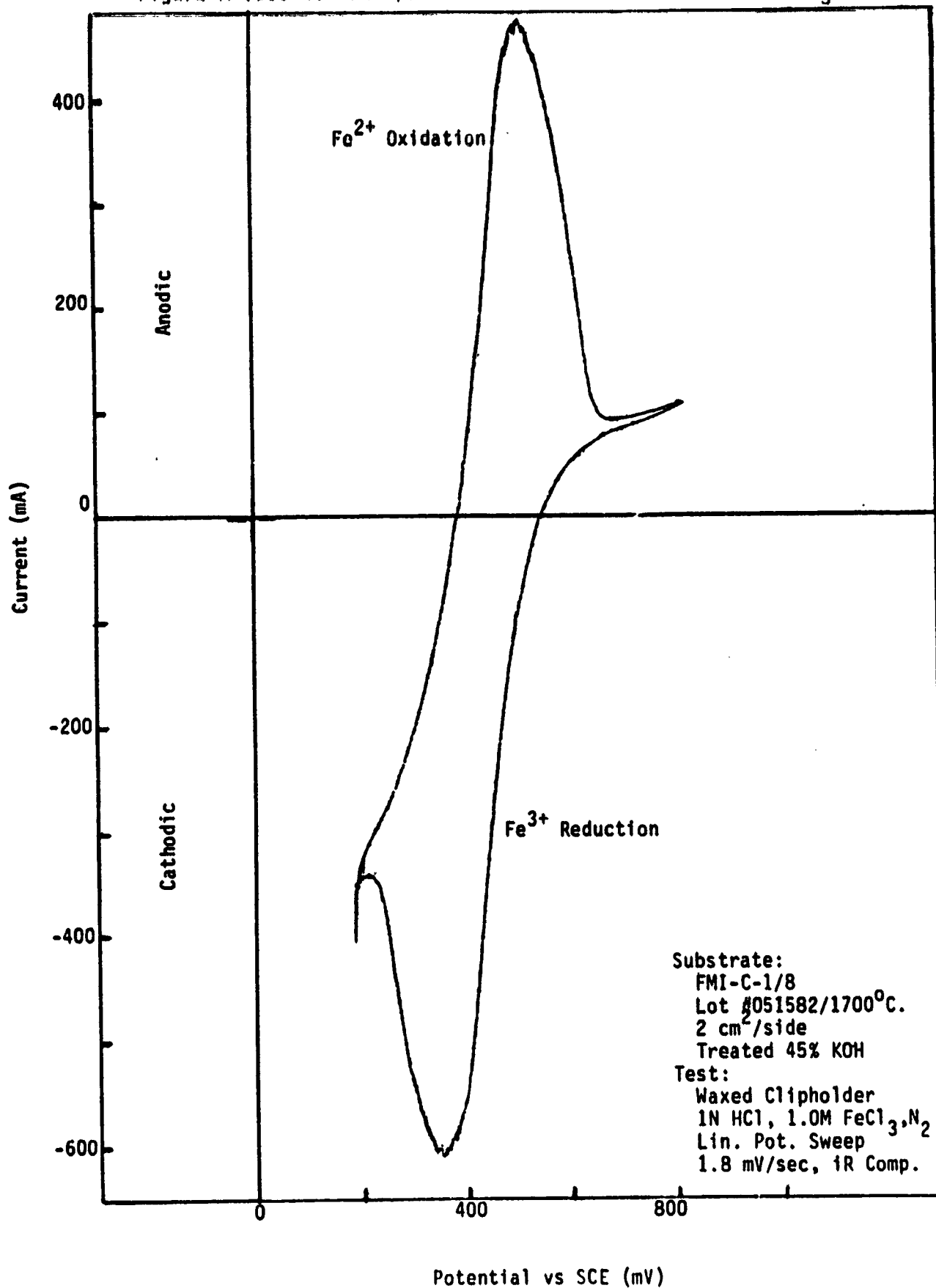


Figure A VIII-5.  $\text{Fe}^{3+}/\text{Fe}^{2+}$  Reaction at 25°C. in 1.5M  $\text{FeCl}_3$ .

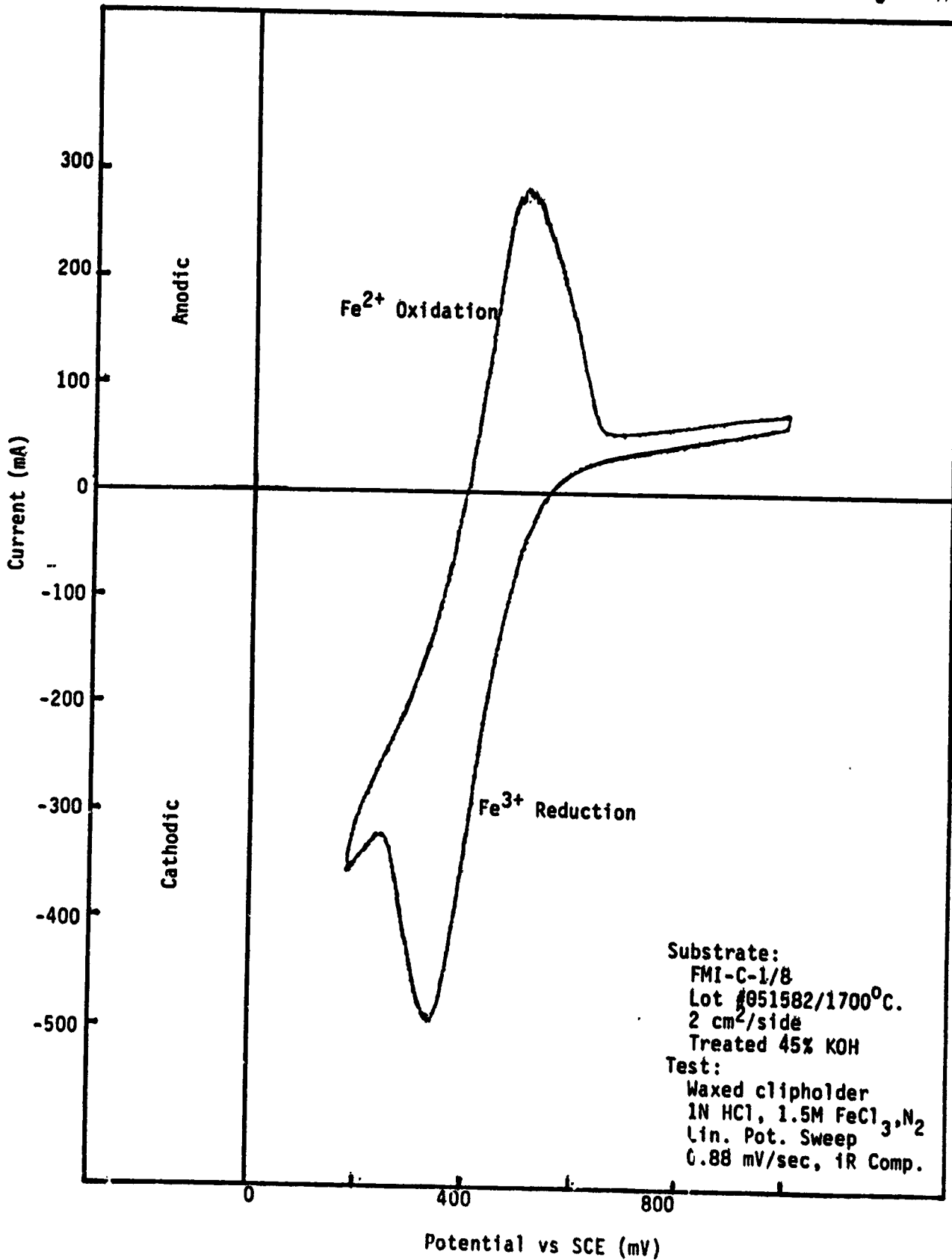


Figure A VIII-6.  $\text{Fe}^{3+}/\text{Fe}^{2+}$  Reaction at  $45^{\circ}\text{C}$ . in  $1.5\text{M FeCl}_3$ .

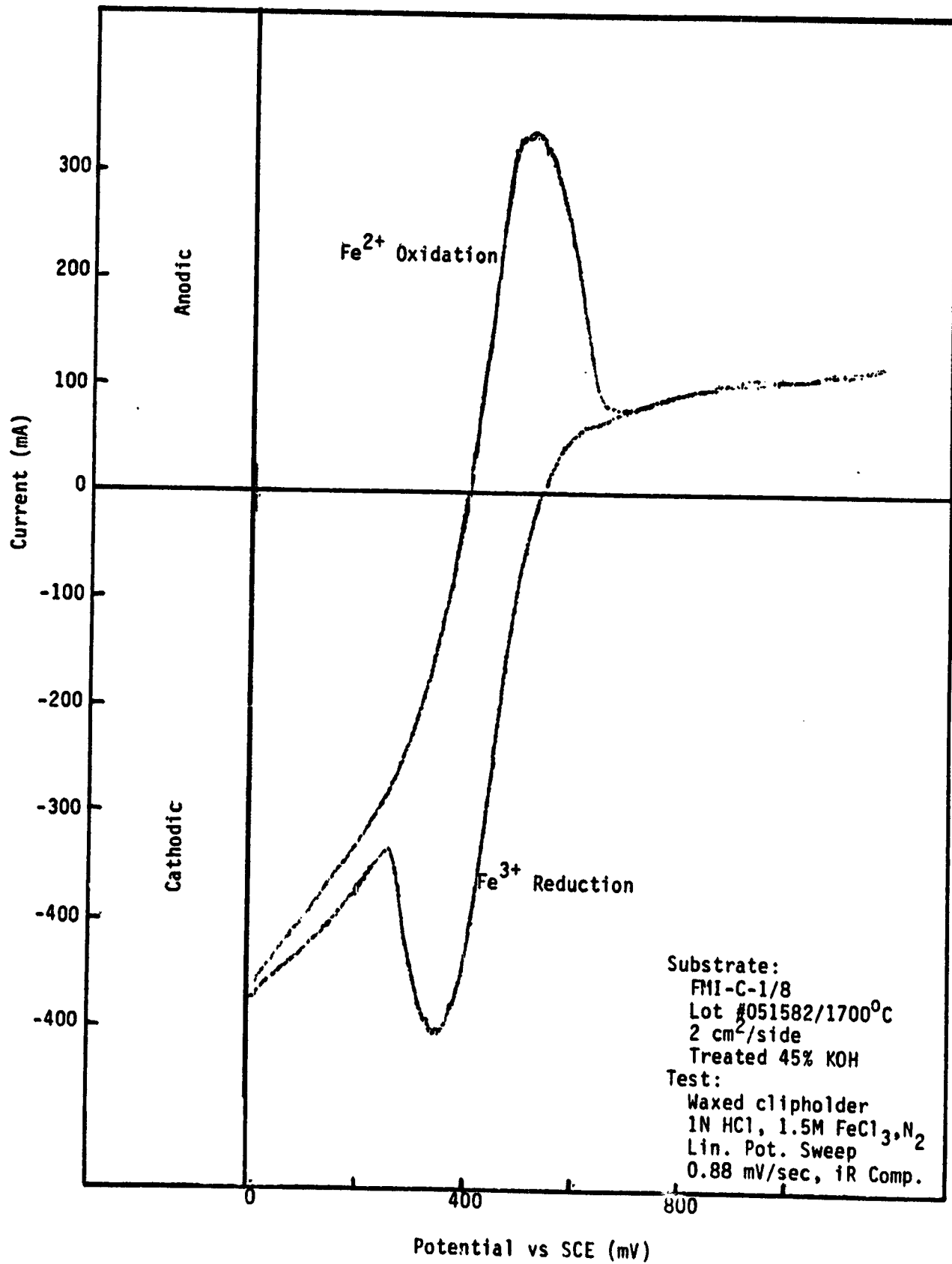


Figure A VIII-7.  $\text{Fe}^{3+}/\text{Fe}^{2+}$  Reaction at  $55^{\circ}\text{C}$ . in  $1.5\text{M FeCl}_3$ .

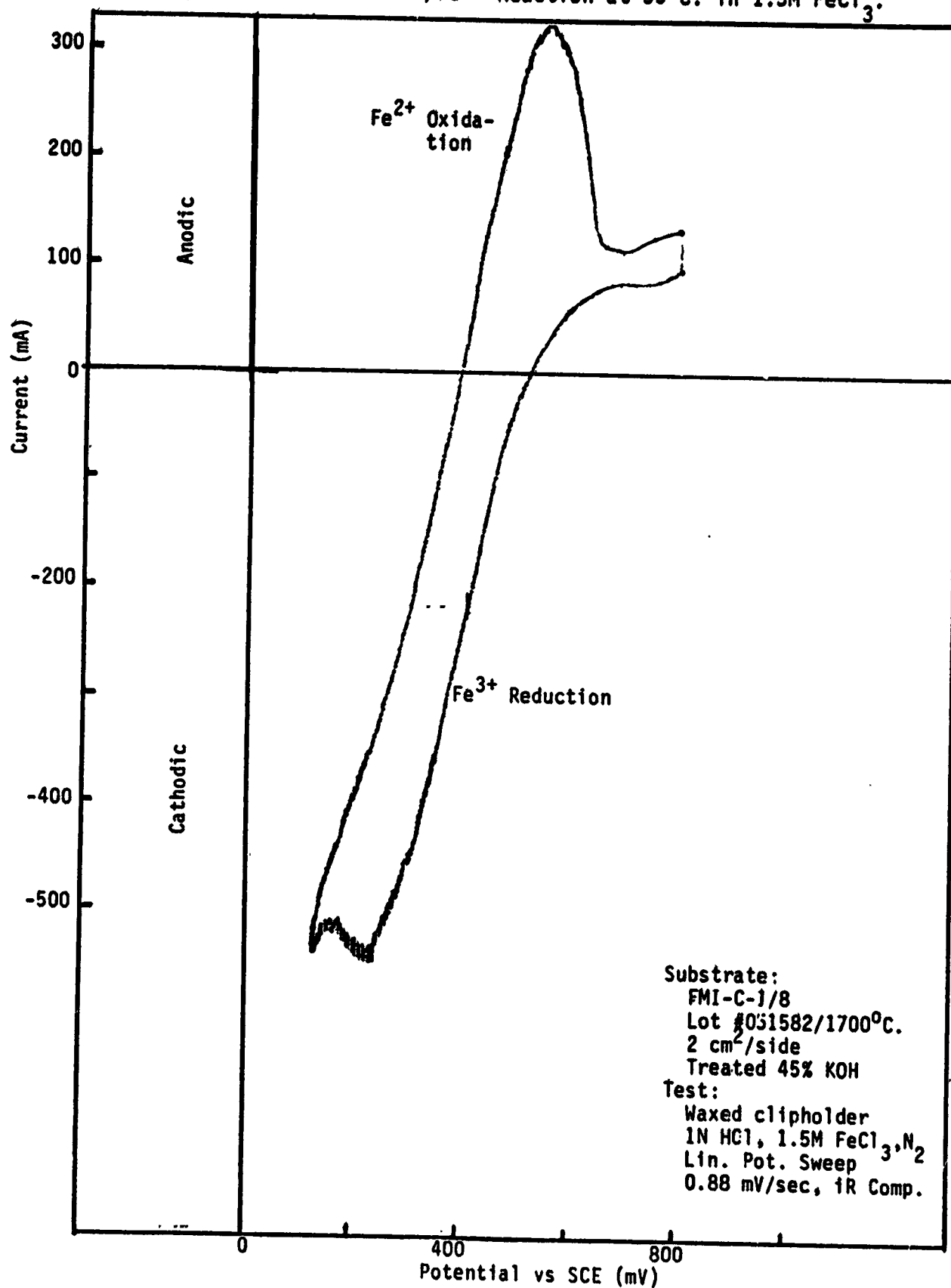


Figure A VIII-8.  $\text{Fe}^{3+}/\text{Fe}^{2+}$  Reaction at 65°C. in 1.5M  $\text{FeCl}_3$ .

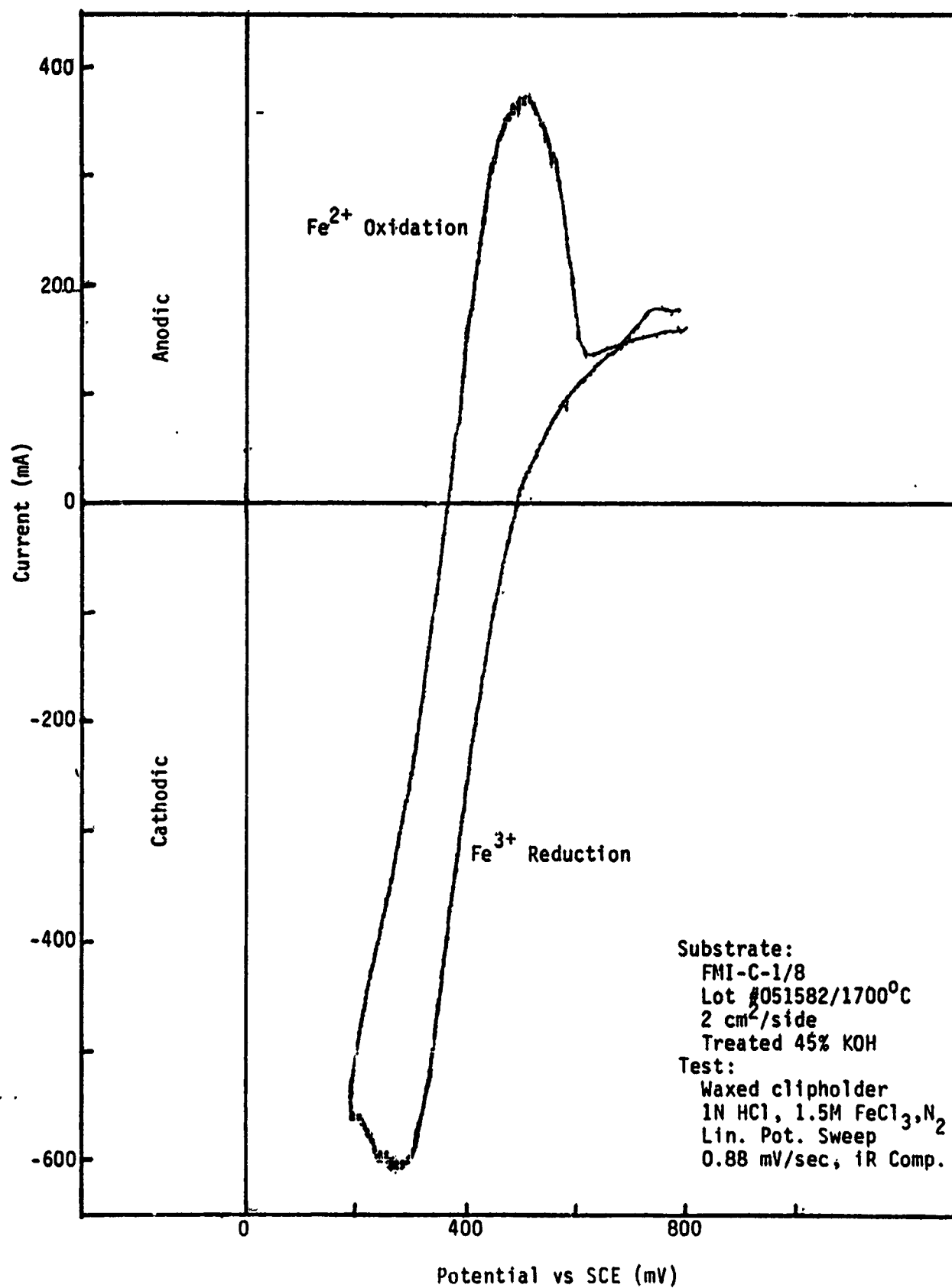


Figure A VIII-9.  $\text{Fe}^{3+}/\text{Fe}^{2+}$  Reaction at 25°C. in 2.0M  $\text{FeCl}_3$ .

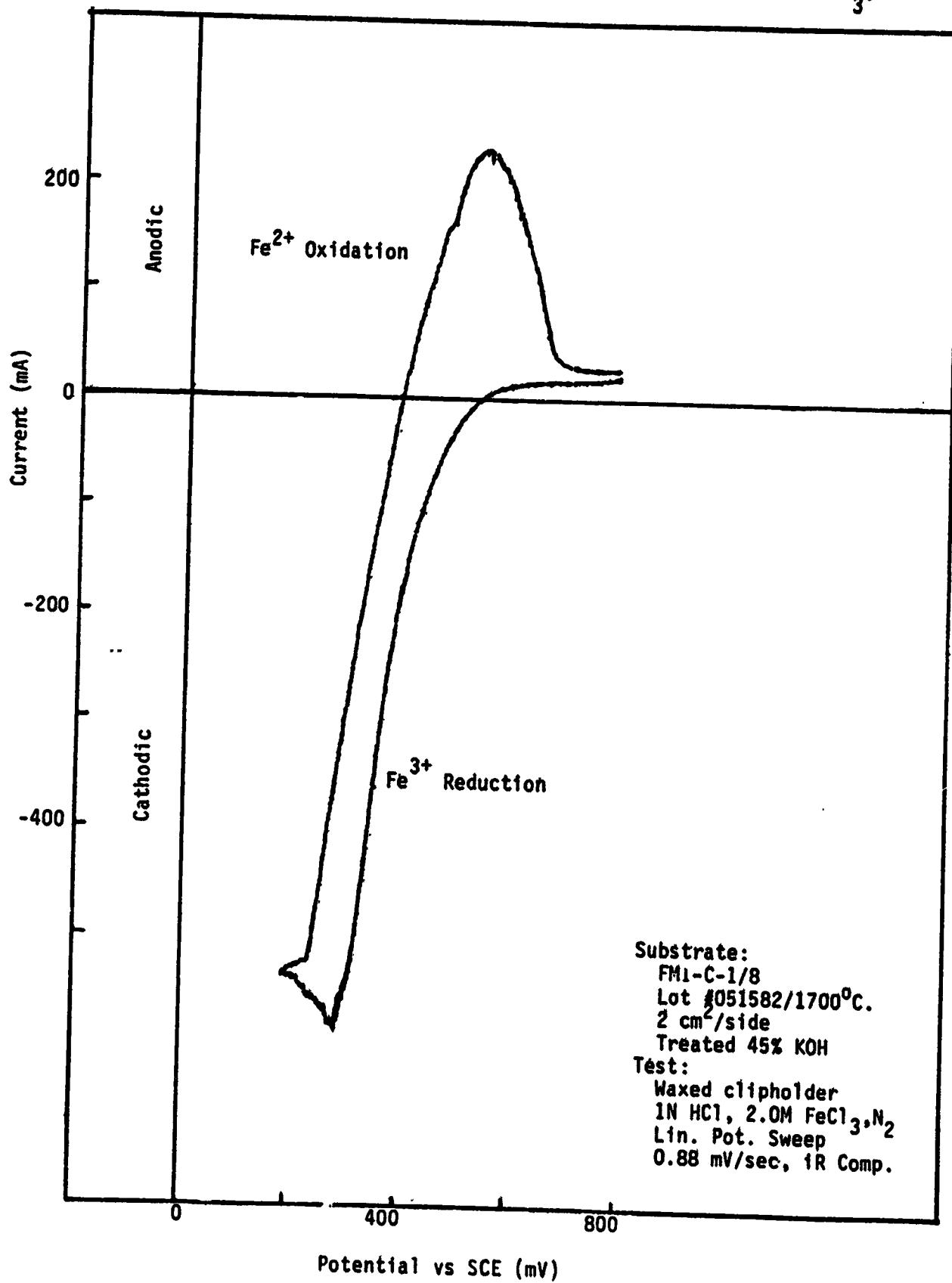


Figure A VIII-10.  $\text{Fe}^{3+}/\text{Fe}^{2+}$  Reaction at  $45^{\circ}\text{C}$ . in  $2.0\text{M FeCl}_3$ .

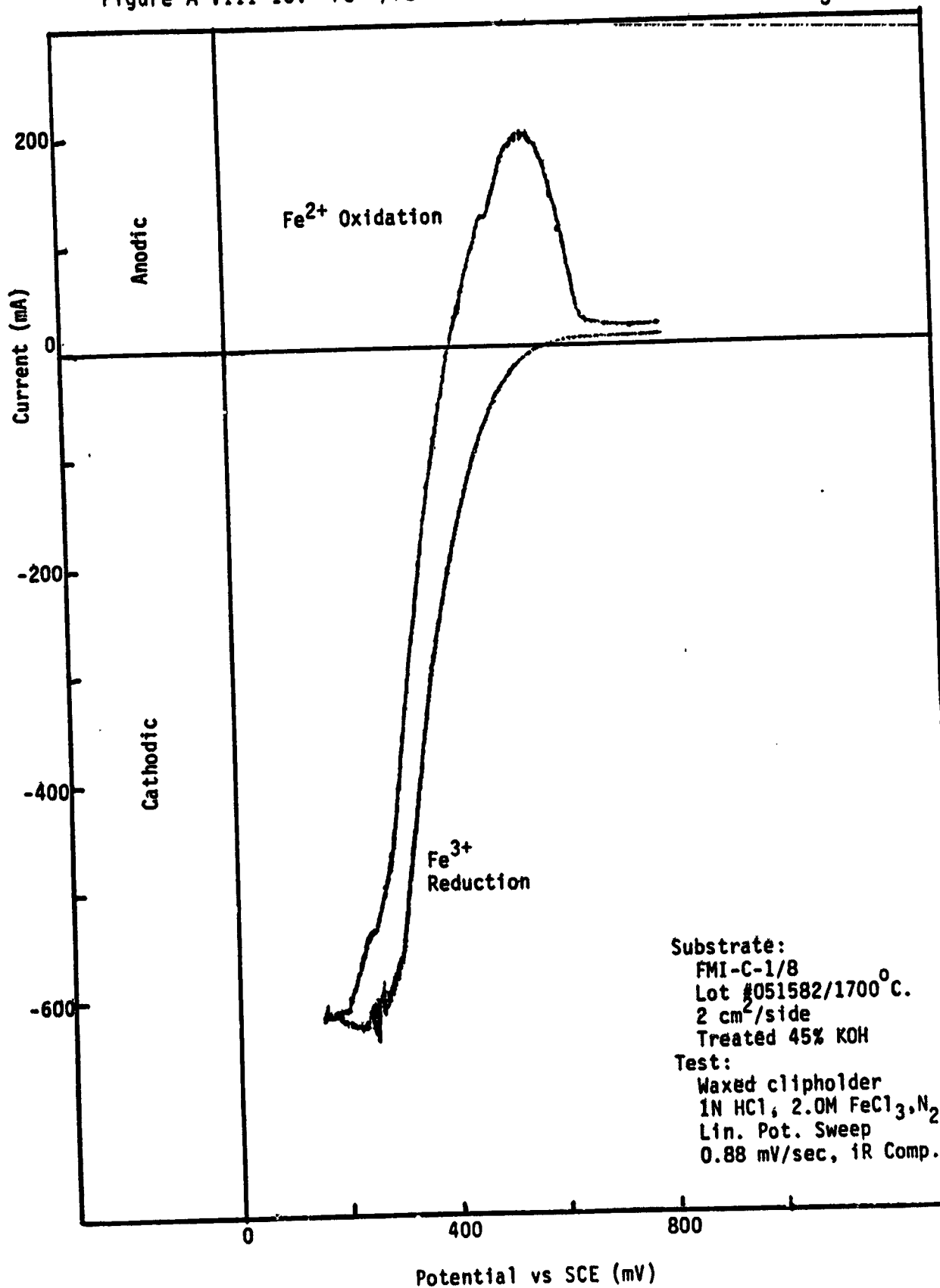


Figure A VIII-11.  $\text{Fe}^{3+}/\text{Fe}^{2+}$  Reaction at  $55^{\circ}\text{C}$ . in  $2.0\text{M FeCl}_3$ .

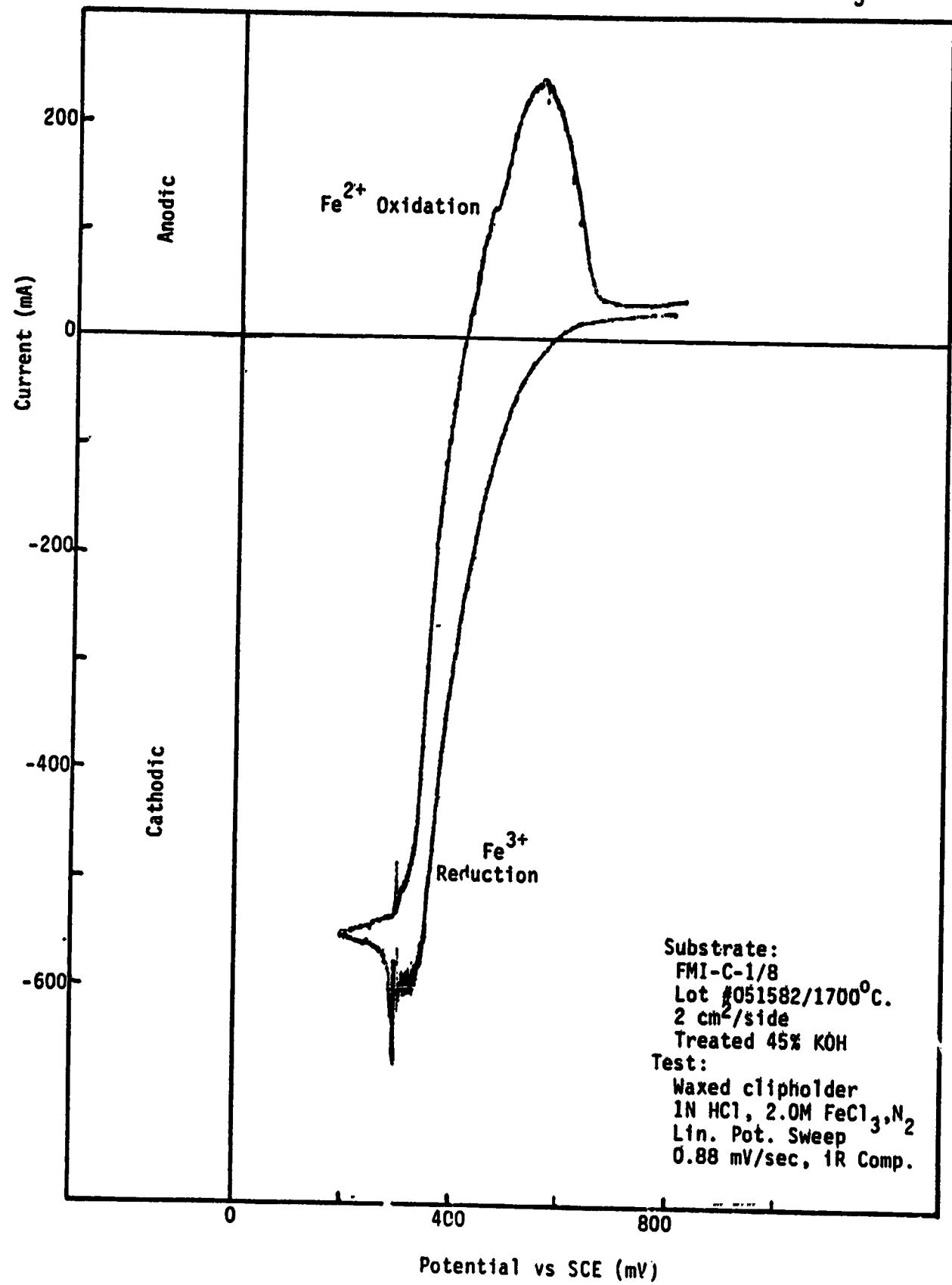


Figure A VIII-12.  $\text{Fe}^{3+}/\text{Fe}^{2+}$  Reaction at  $65^{\circ}\text{C}$ . in  $2.0\text{M FeCl}_3$ .

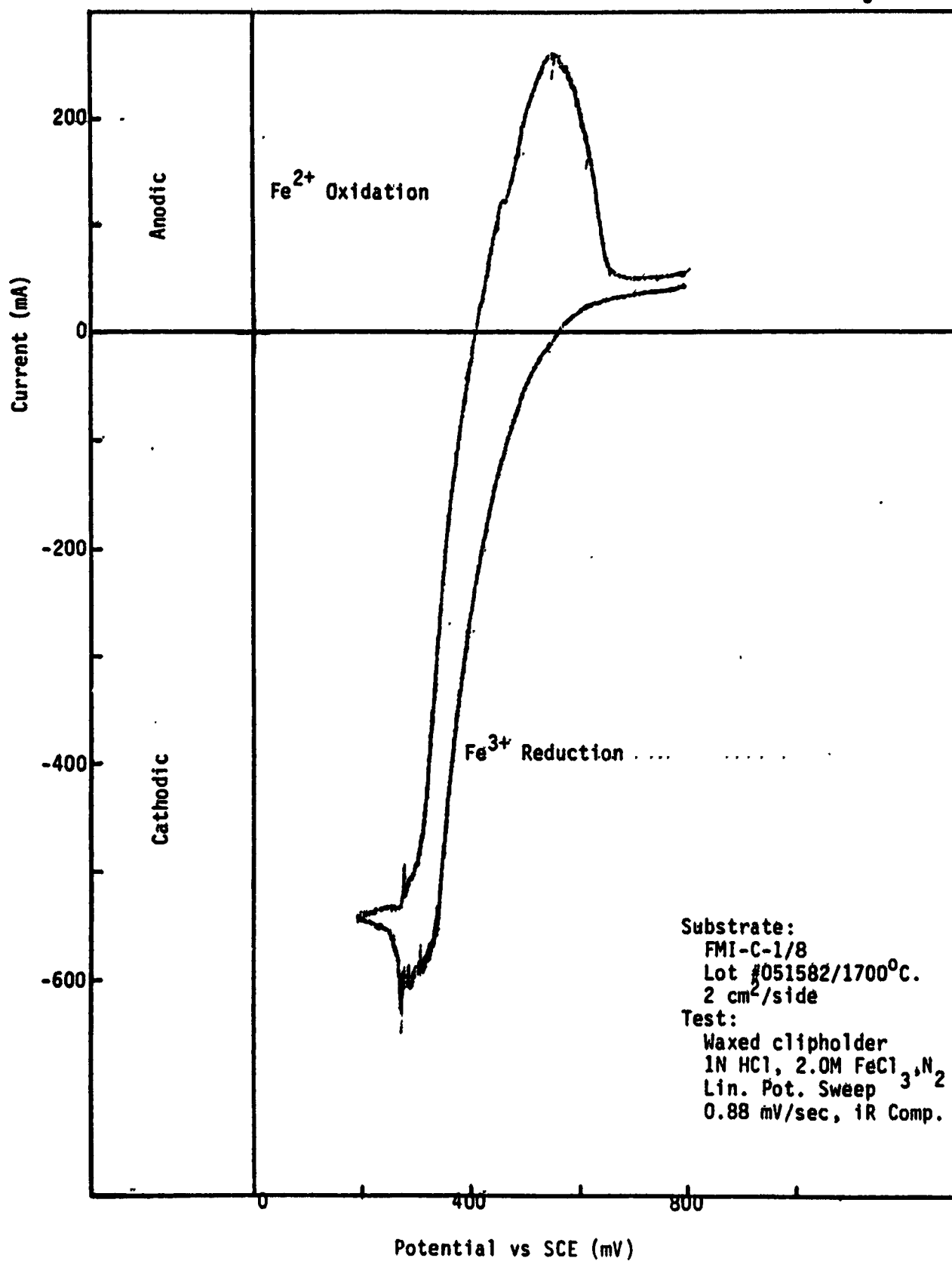


Figure A VIII-13.  $\text{Cr}^{3+}/\text{Cr}^{2+}$  Reaction at  $25^{\circ}\text{C}$ . in  $1.0\text{M CrCl}_3$ .

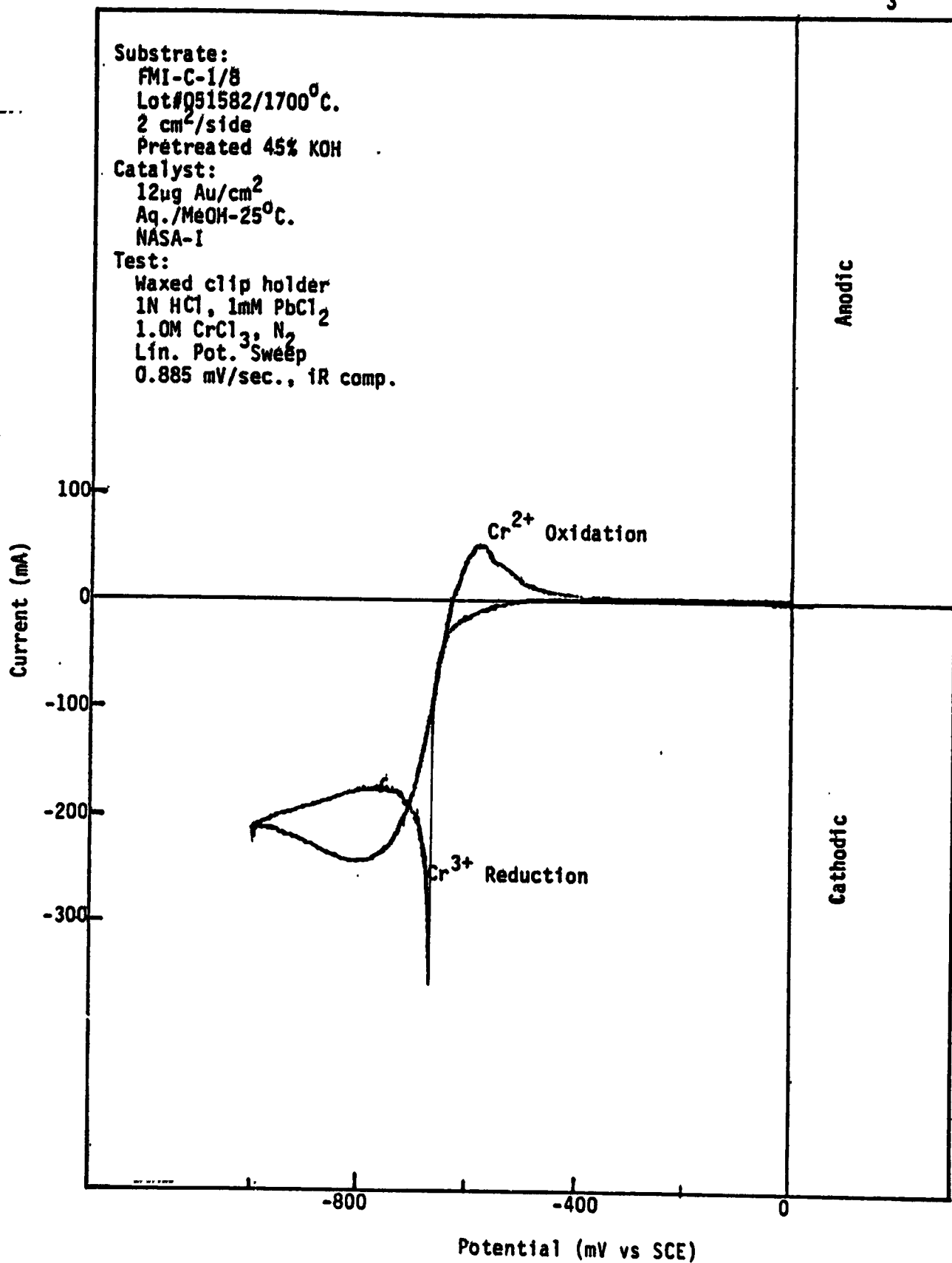


Figure A VIII-14.  $\text{Cr}^{3+}/\text{Cr}^{2+}$  Reaction at  $45^\circ\text{C}$  in  $1.0\text{M CrCl}_3$ .

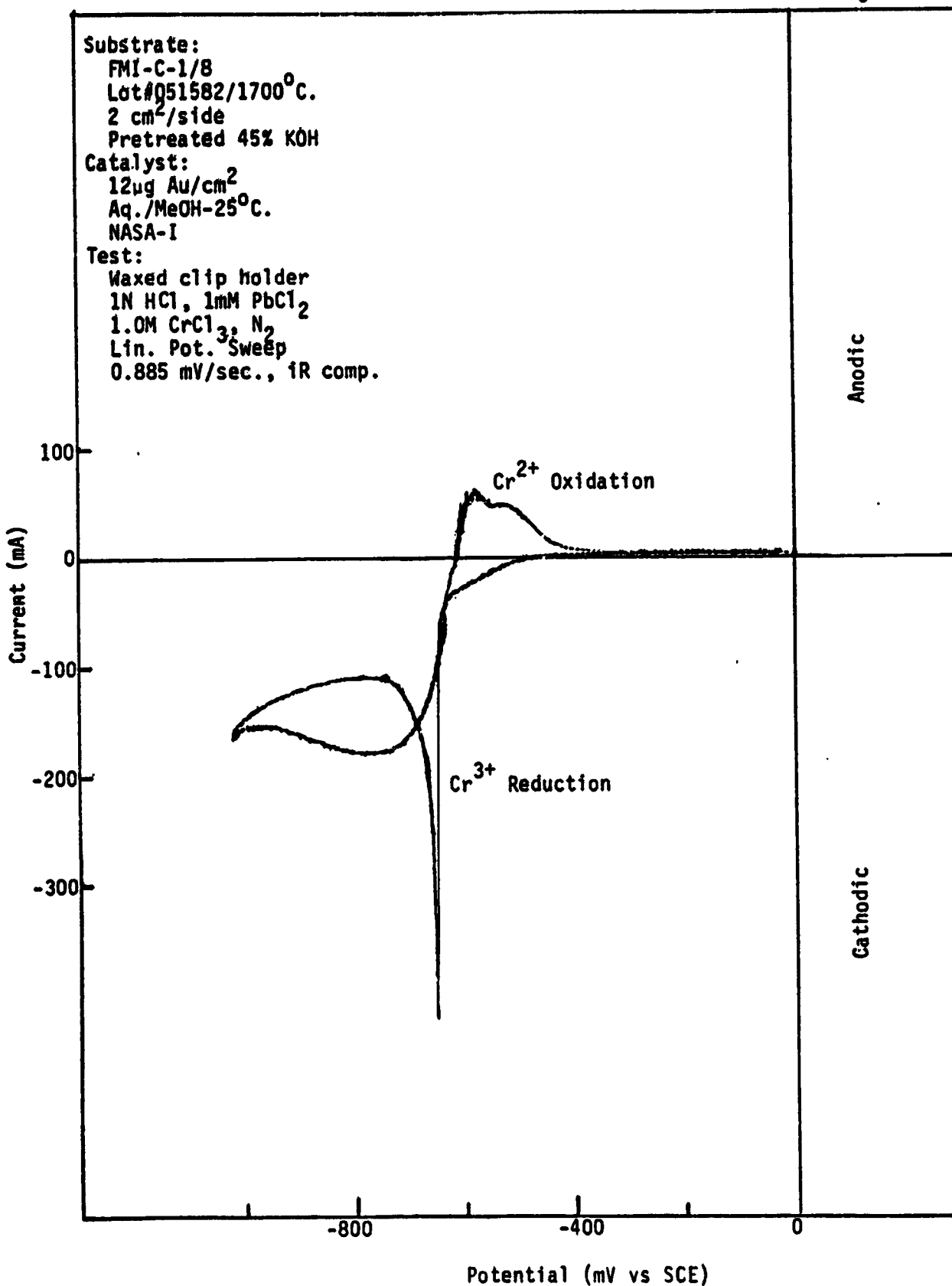


Figure A VIII-15.  $\text{Cr}^{3+}/\text{Cr}^{2+}$  Reaction at  $55^{\circ}\text{C}$ . in  $1.0\text{M}\text{-CrCl}_3$ .

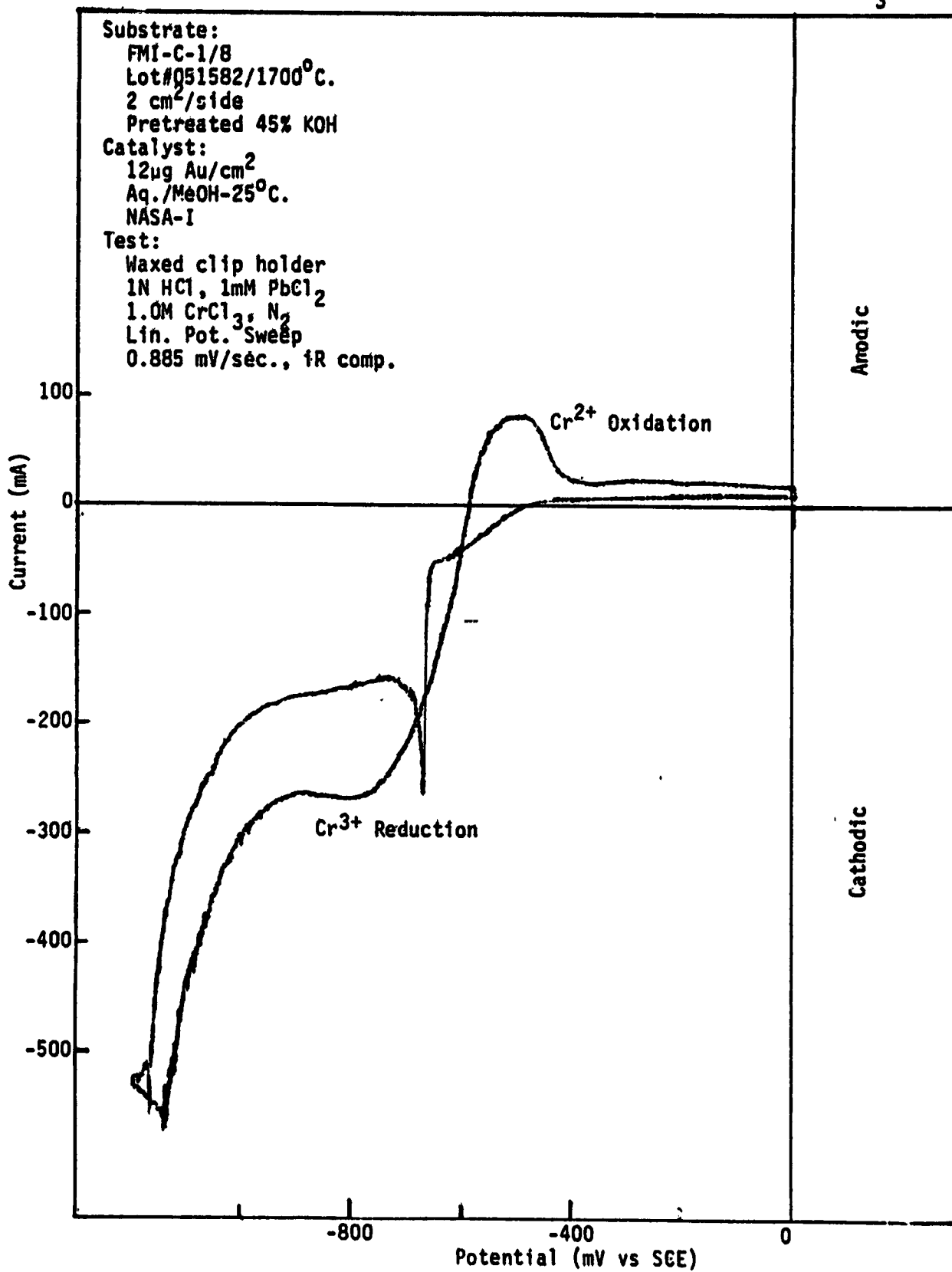


Figure A VIII-16.  $\text{Cr}^{3+}/\text{Cr}^{2+}$  Reaction at  $65^{\circ}\text{C}$ . in  $1.0\text{M CrCl}_3$ .

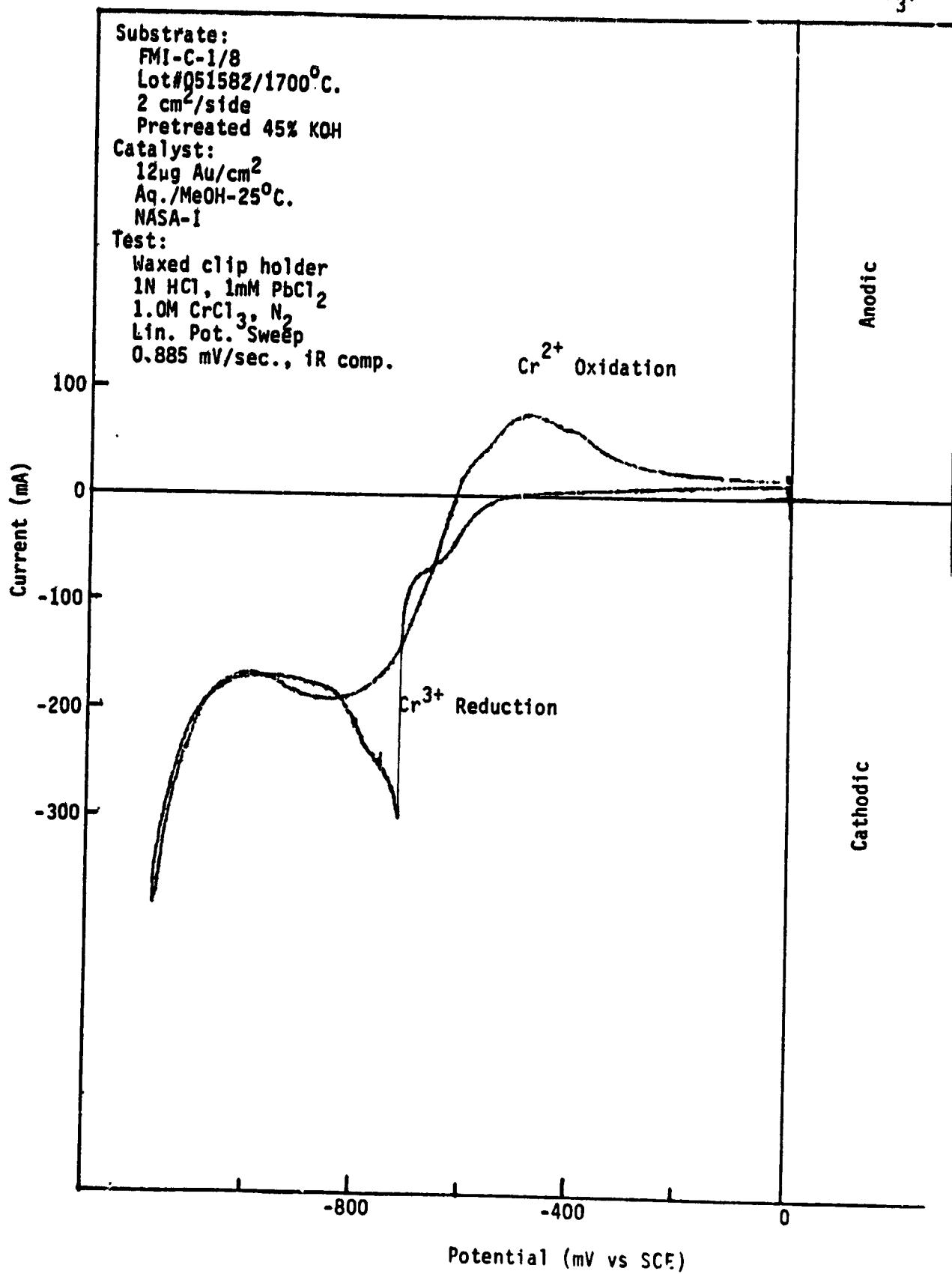


Figure A VIII-17.  $\text{Cr}^{3+}/\text{Cr}^{2+}$  Reaction at  $25^{\circ}\text{C}$ . in  $1.5\text{M CrCl}_3$ .

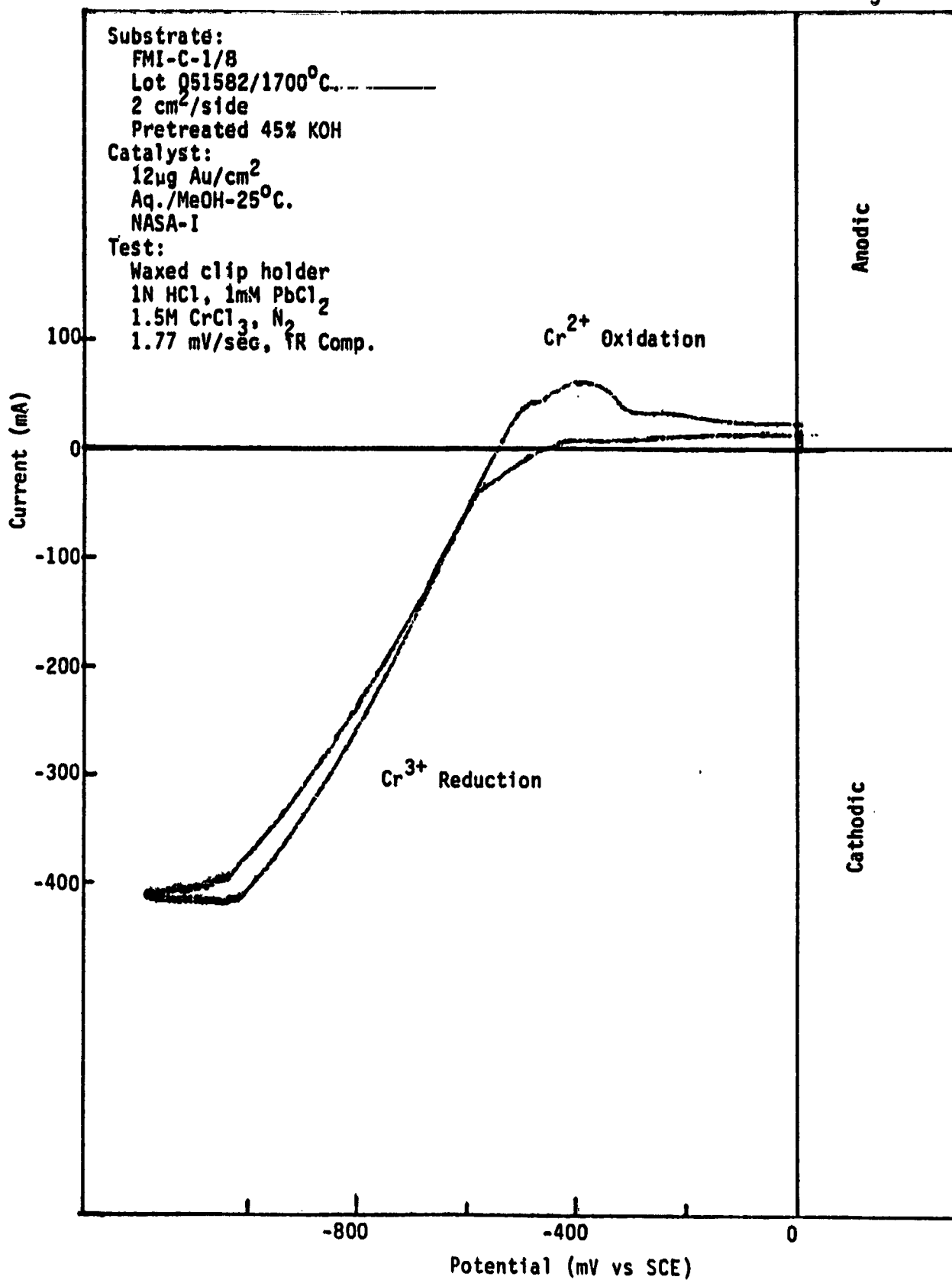


Figure A VIII-18.  $\text{Cr}^{3+}/\text{Cr}^{2+}$  Reaction at  $45^{\circ}\text{C}$ . in  $1.5\text{M CrCl}_3$ .

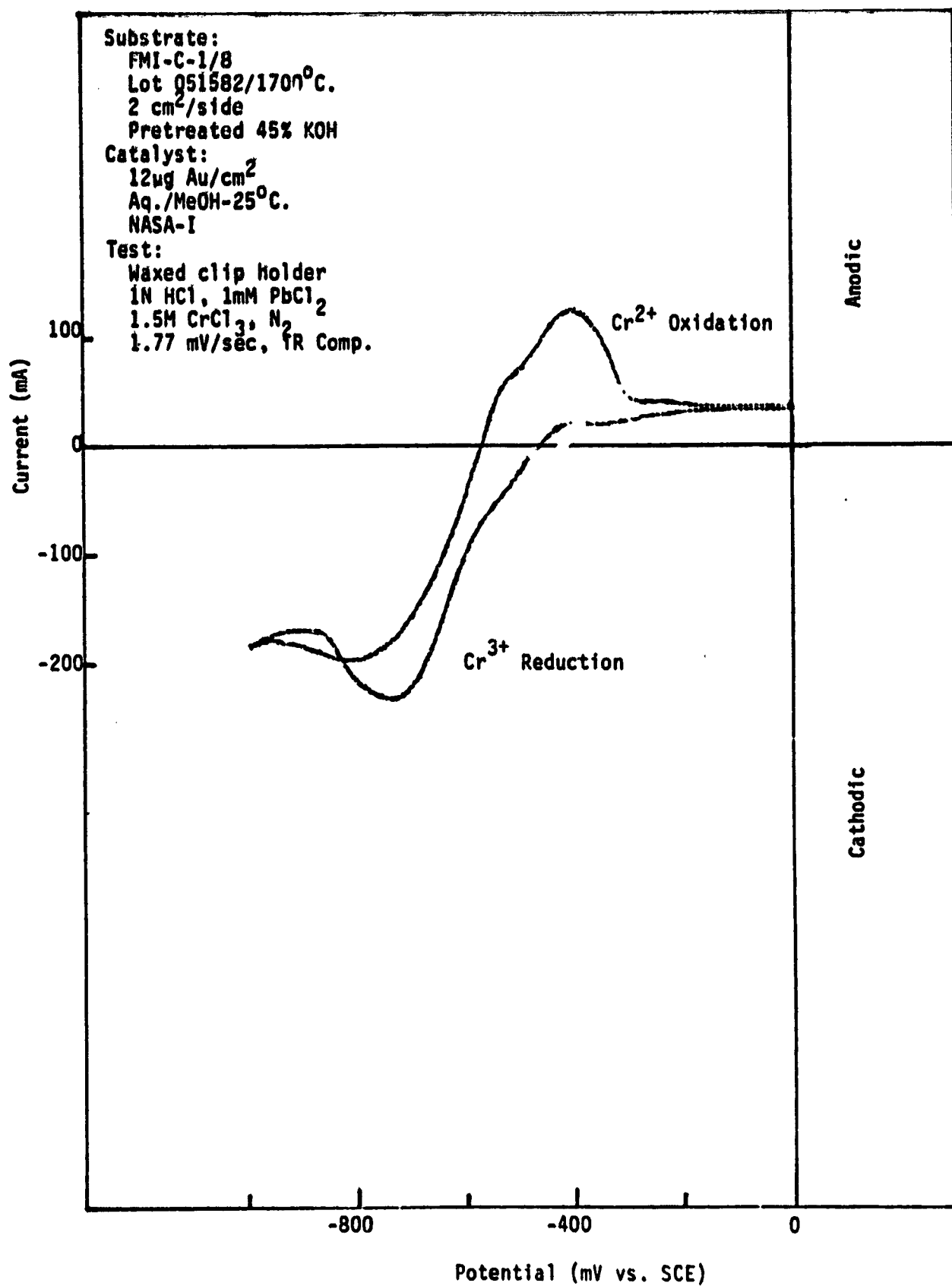


Figure A VIII-19.  $\text{Cr}^{3+}/\text{Cr}^{2+}$  Reaction at  $55^{\circ}\text{C}$ . in  $1.5\text{M CrCl}_3$ .

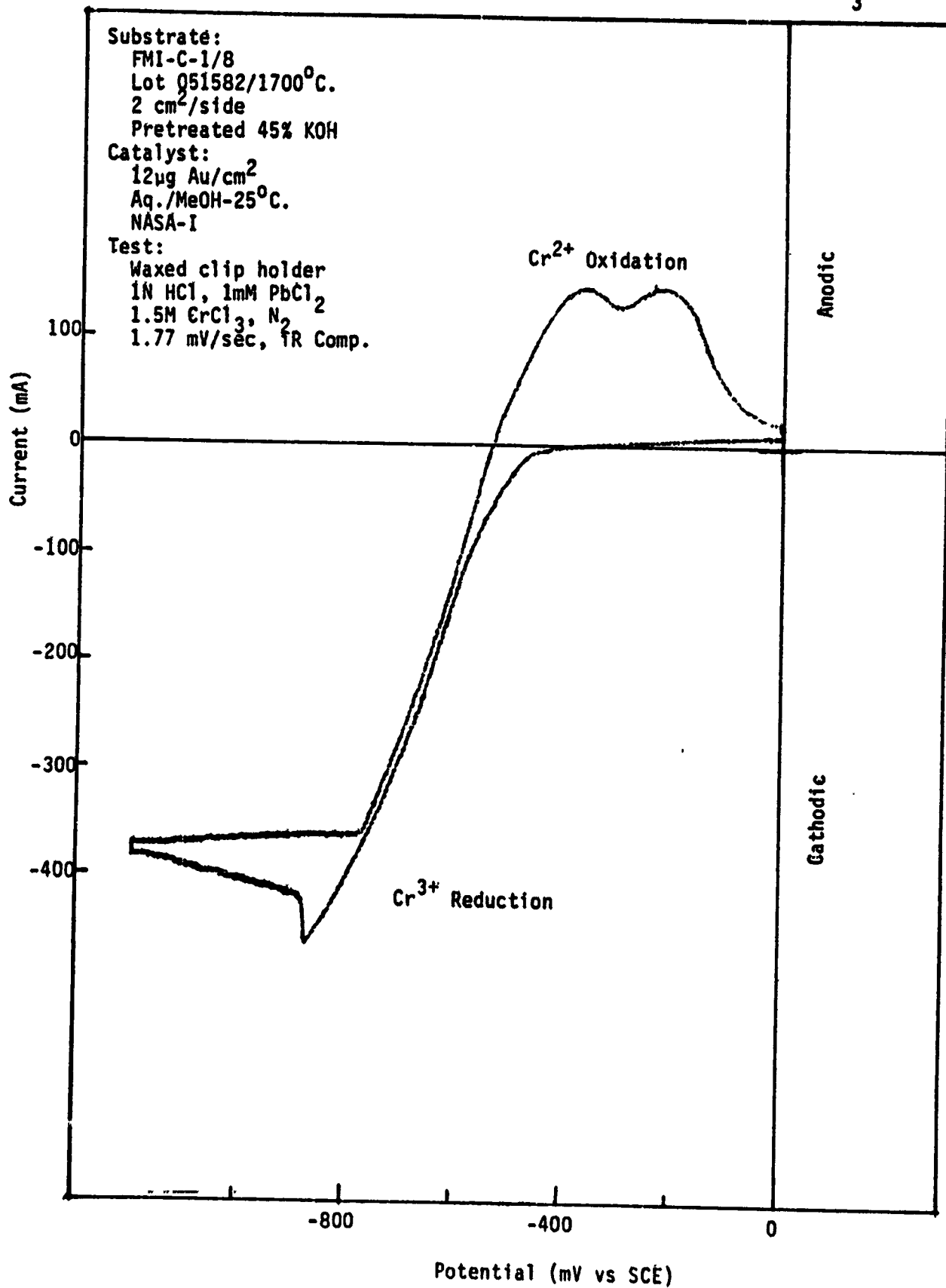


Figure A VIII-20.  $\text{Cr}^{3+}/\text{Cr}^{2+}$  Reaction at  $65^{\circ}\text{C}$  in  $1.5\text{M CrCl}_3$ .

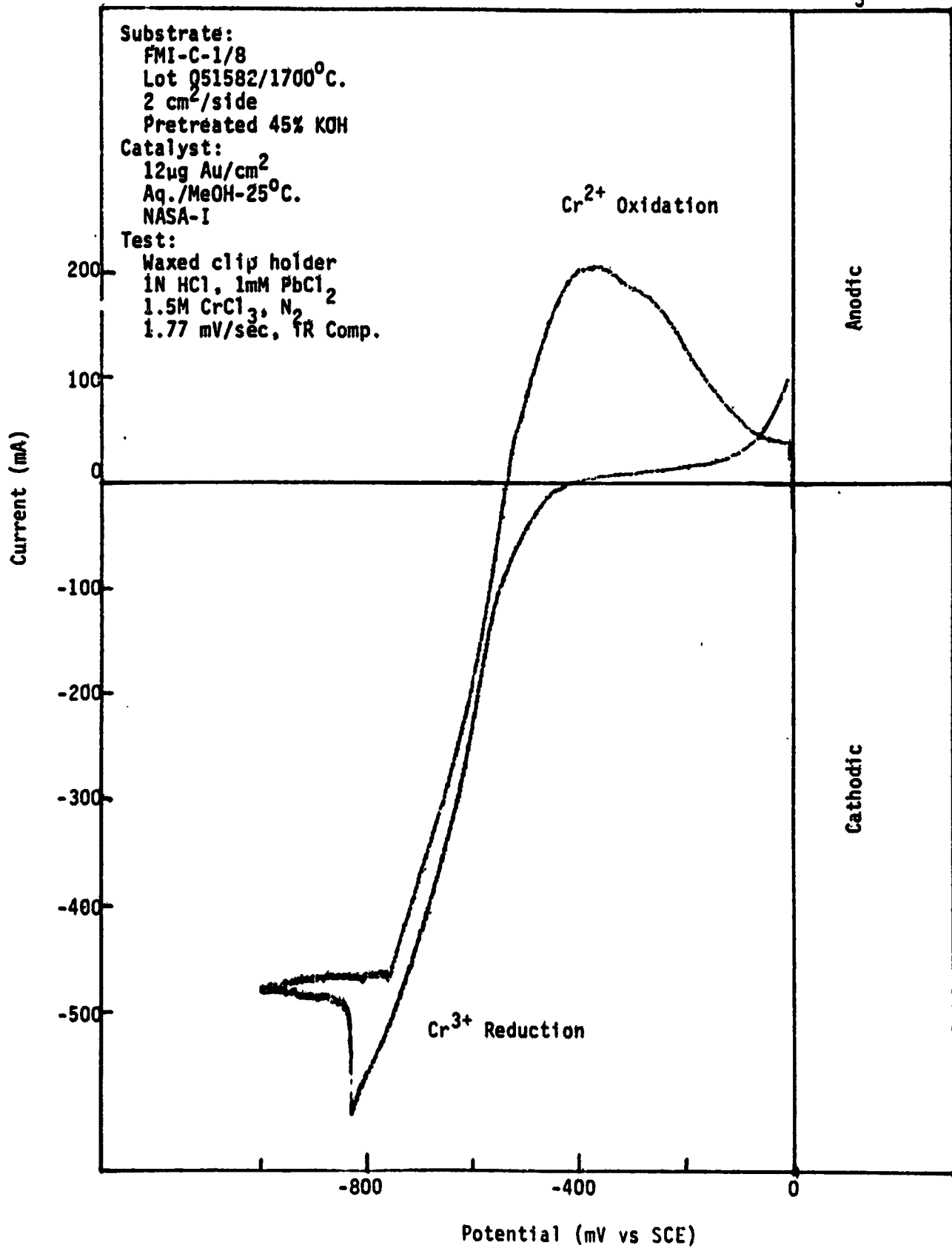


Figure A VIII-21...  $\text{Cr}^{3+}/\text{Cr}^{2+}$  Reaction at  $25^{\circ}\text{C}$ . in  $2.0\text{M CrCl}_3$ .

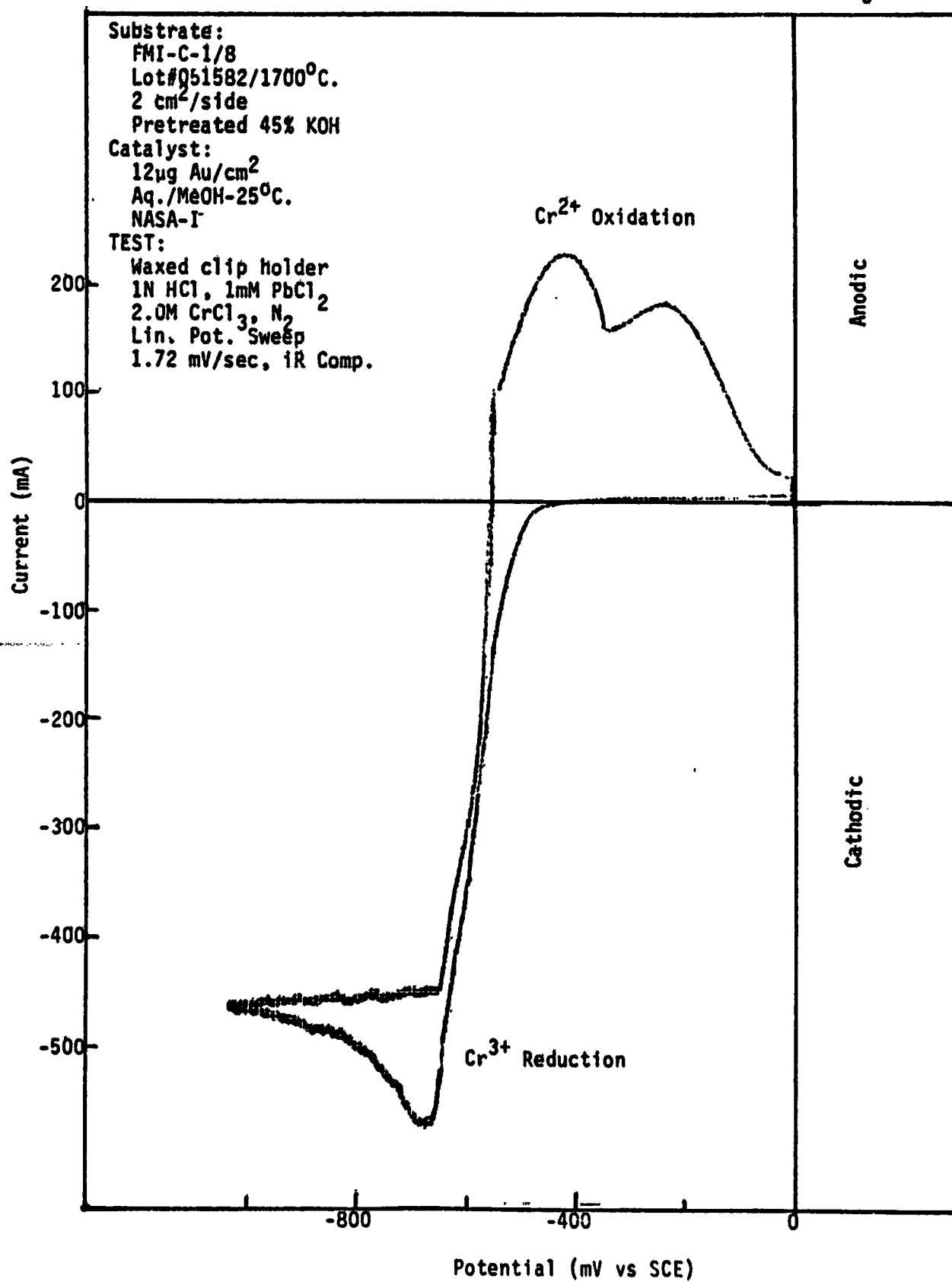


Figure A VIII-22.  $\text{Cr}^{3+}/\text{Cr}^{2+}$  Reaction at  $45^{\circ}\text{C}$ . in  $2.0\text{M CrCl}_3$ .

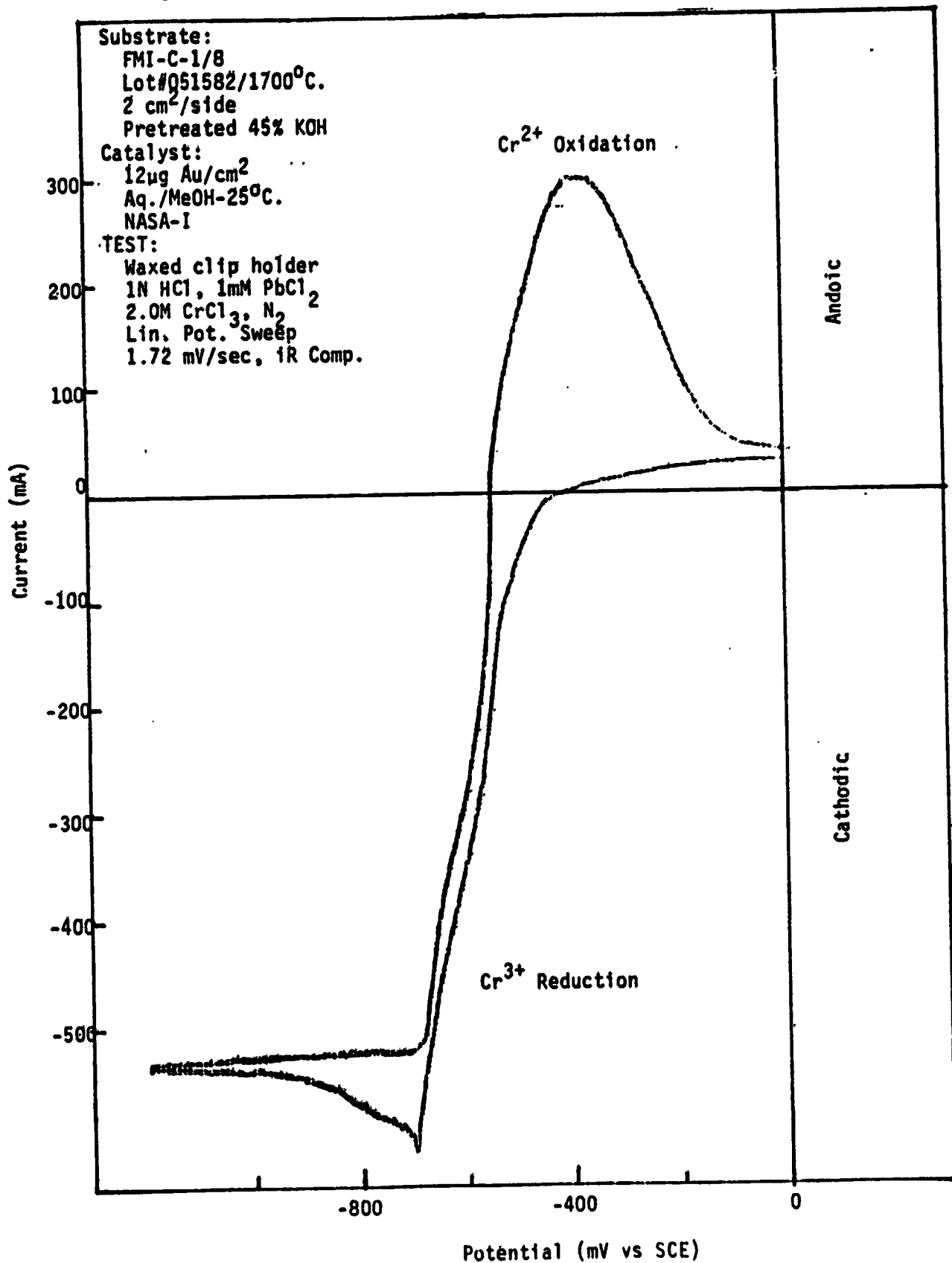


Figure A VIII-23.  $\text{Cr}^{3+}/\text{Cr}^{2+}$  Reaction at  $55^\circ\text{C}$ . in  $2.0\text{M CrCl}_3$ .

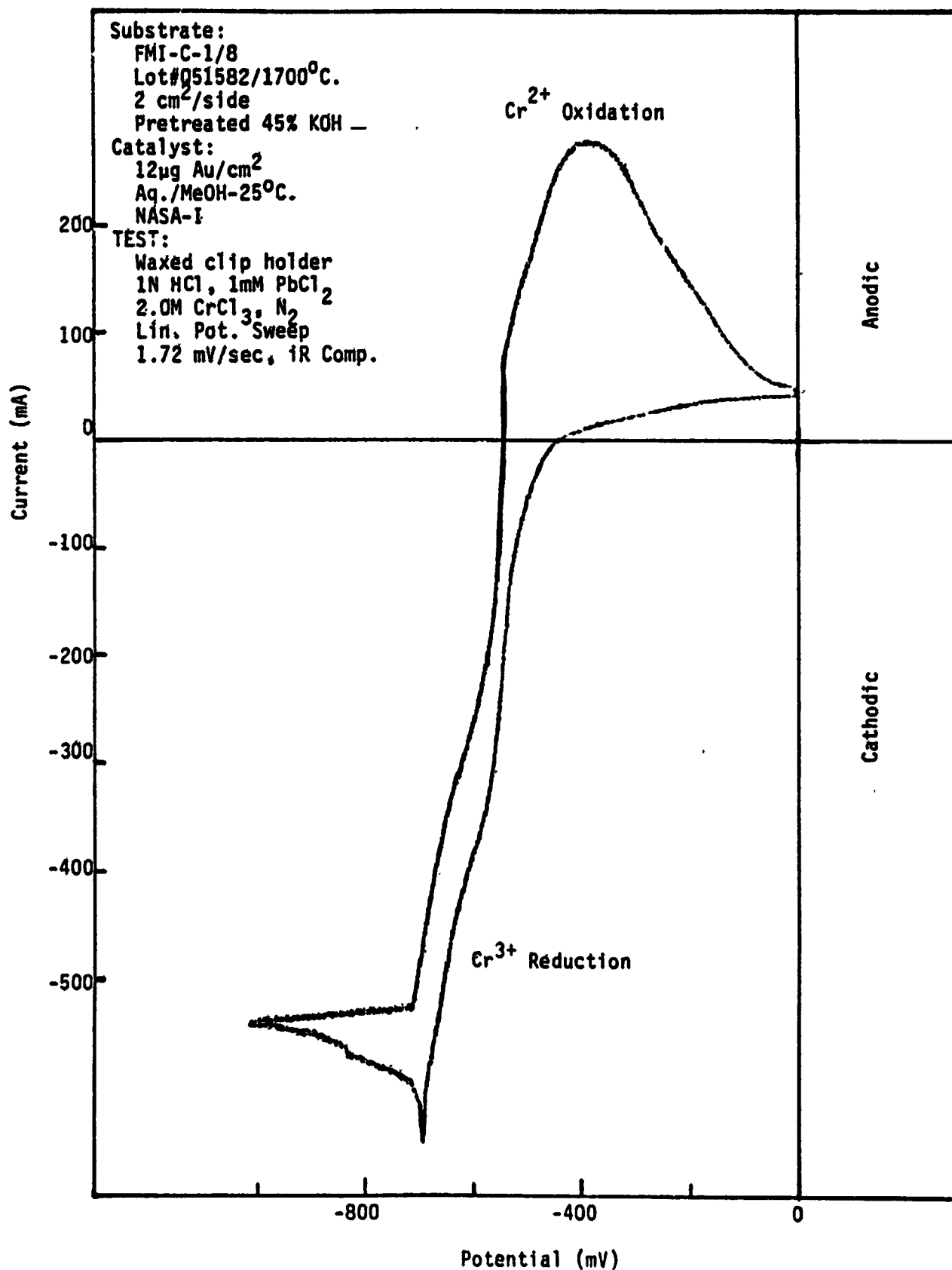
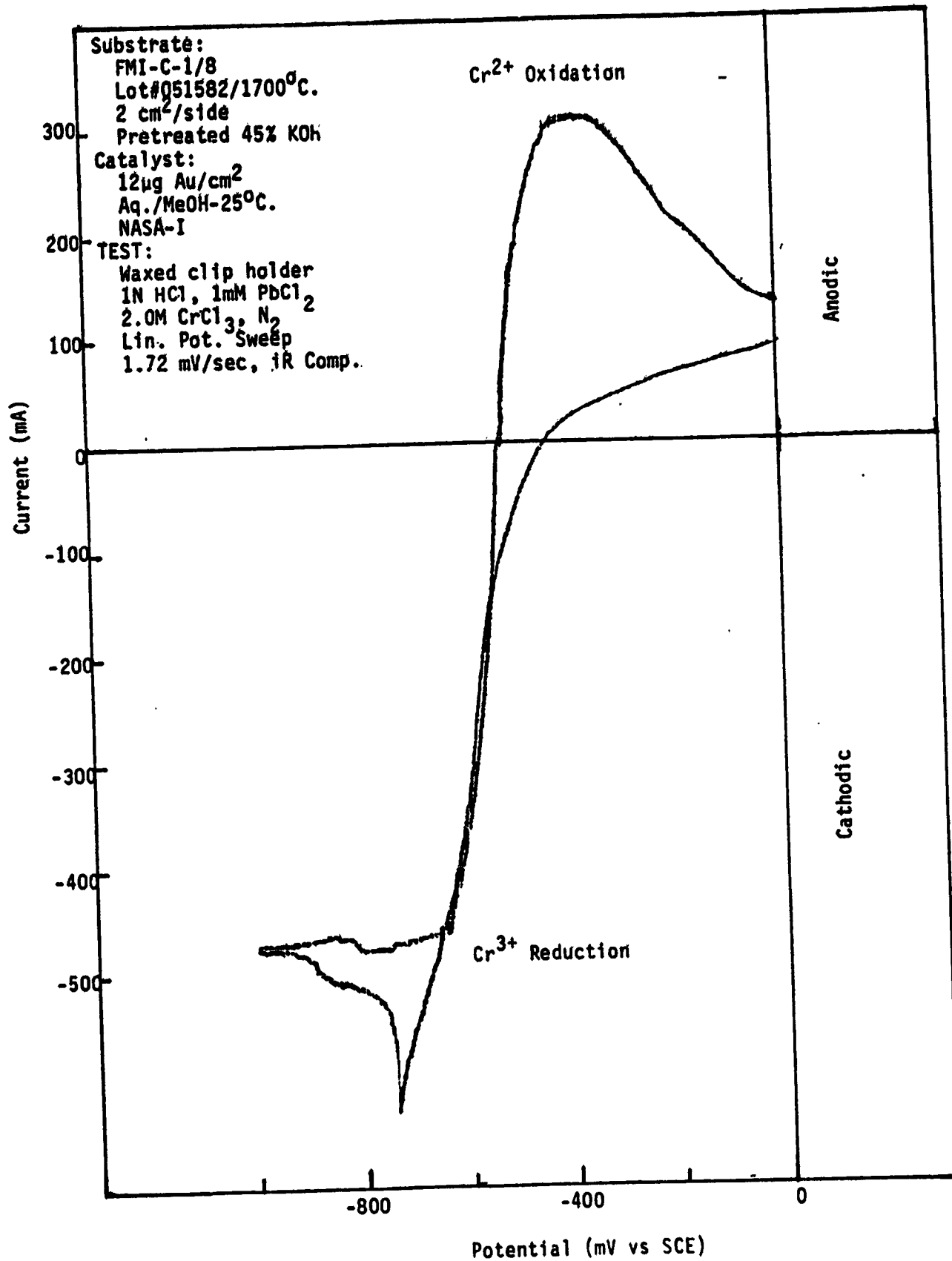


Figure A VIII-24.  $\text{Cr}^{3+}/\text{Cr}^{2+}$  Reaction at  $65^\circ\text{C}$ . in  $2.0\text{M CrCl}_3$ .



1. Report No. <b>NASA CR-174724</b>	2. Government Accession No.	3. Recipient's Catalog No.
4. Title and Subtitle <b>Development of Electrodes for the NASA Iron/Chromium Redox System and Factors Affecting Their Performance</b>		5. Report Date <b>June 1984</b>
7. Author(s) <b>Larry Swette and Vinod Jalan</b>		6. Performing Organization Code
9. Performing Organization Name and Address <b>GINER, INC. 14 Spring Street Waltham, Massachusetts 02154</b>		8. Performing Organization Report No.
12. Sponsoring Agency Name and Address <b>U.S. Department of Energy Division of Energy Storage Systems Washington, D.C. 20545</b>		10. Work Unit No.
		11. Contract or Grant No. <b>DEN 3-26Z</b>
		13. Type of Report and Period Covered <b>Contractor Report</b>
		14. Sponsoring Agency Code Report No. <b>DOE/NASA/0262-1</b>
15. Supplementary Notes <b>Final Report. Prepared under Interagency Agreement DE-AI04-80AL12726. Project Manager, Randall F. Gahn, Power Technology Division, NASA Lewis Research Center, Cleveland, Ohio 44135.</b>		
16. Abstract This program was directed primarily to the development of the negative ( $\text{Cr}^{3+}/\text{Cr}^{2+}$ ) electrode for the NASA chromous/ferric Redox battery. The investigation of the effects of substrate processing and gold/lead catalyzation parameters on electrochemical performance were continued in this phase. In addition, the effects of reactant cross-mixing, acidity level, and temperature were examined for both Redox couples. Finally, the performance of optimized electrodes was tested in system hardware (1/3 square foot single cell).  The major findings were as follows:  (1) The recommended processing temperature for the carbon felt, as a substrate for the negative electrode, is 1650° to 1750 °C.  (2) The recommended gold catalyzation procedure is essentially the published NASA procedure (NASA TM-82724, Nov. 1981) based on deposition from aqueous methanol solution, with the imposition of a few controls such as temperature (25 °C) and precatalyzation pH of the felt (7).  (3) Experimental observations of the gold catalyzation process and subsequent electron microscopy indicate that the gold is deposited from the colloidal state, induced by contact of the solution with the carbon felt.  (4) Electrodeposited lead appears to be present as a thin uniform layer over the entire surface of the carbon fibers, rather than as discrete particles.  (5) Cross-mixing of reactants ( $\text{Fe}^{2+}$ in negative electrode solution or $\text{Cr}^{3+}$ in positive electrode solution) did not appear to produce significant interference at either electrode.  (6) Increased temperature and acidity levels resulted in increased reversibility. Higher acidity levels and reactant concentrations tended to retard conversion to the nonreactive hexaquo chromium (III) complex.		
17. Key Words (Suggested by Author(s)) <b>Redox cell, energy storage, chromium, chromous-ferric, electrocatalysis, gold, lead, carbon felt</b>		18. Distribution Statement <b>Unclassified - unlimited STAR Category 44 DOE Category UC-94c</b>
19. Security Classif. (of this report) <b>Unclassified</b>	20. Security Classif. (of this page) <b>Unclassified</b>	21. No. of pages <b>285</b>
		22. Price* <b>A13</b>